⇓PRIVATE

DASBUCH

ohne Eigenschaften

Afschnit II: Halbclassiche Chaos

Gone with the Wind School
formerly known as the
Copenhagen School of Cycling

Unsung Heroes, too numerous to list
with a disclaimer by **Professor Gatto Nero**

BOYSCOUT EDITION

⇑PRIVATE

ChaosBook.org/version11.9.1, Apr 24 2007 printed June 17, 2007
ChaosBook.org/boyscouts comments to: predrag@nbi.dk

⇓PRIVATE
⇑PRIVATE
reproduce here the tableofcontents

Chapter 31

Prologue

> Anyone who uses words "quantum" and "chaos" in the same sentence should be hung by his thumbs on a tree in the park behind the Niels Bohr Institute.
> Joseph Ford

(G. Vattay, G. Tanner and P. Cvitanović) add Per sect 5.8.

You have read the first volume of this book. So far, so good – anyone can play a game of classical pinball, and a skilled neuroscientist can poke rat brains. We learned that information about chaotic dynamics can be obtained by calculating spectra of linear operators such as the evolution operator of sect. 10.2 or the associated partial differential equations such as the Liouville equation (9.36). The spectra of these operators can be expressed in terms of periodic orbits of the deterministic dynamics by means of trace formulas and cycle expansions.

But what happens quantum mechanically, i.e., if we scatter waves rather than point-like pinballs? Can we turn the problem round and study linear PDE's in terms of the underlying deterministic dynamics? And, is there a link between structures in the spectrum or the eigenfunctions of a PDE and the dynamical properties of the underlying classical flow? The answer is yes, but ... things are becoming somewhat more complicated when studying 2nd or higher order linear PDE's. We can find classical dynamics associated with a linear PDE, just take geometric optics as a familiar example. Propagation of light follows a second order wave equation but may in certain limits be well described in terms of geometric rays. A theory in terms of properties of the classical dynamics alone, referred to here as the *semiclassical theory*, will not be exact, in contrast to the classical periodic orbit formulas obtained so far. Waves exhibit new phenomena, such as interference, diffraction, and higher $\hbar$ corrections which will only be partially incorporated into the periodic orbit theory.

⇓PRIVATE
☞ chapter 43
☞ chapter 42
⇑PRIVATE

⇓PRIVATE

What is "Quantum Chaos"? The approaches tried fall roughly into four categories:

Keplerian orbit
orbit!Keplerian
Balmer spectrum
spectrum!Balmer
Bohr!-Sommerfeld quantization
Bohr!–˜de˜Broglie picture
quantization!Bohr-Sommerfeld

- semiclassics - quantum manifestations of dynamics that is classically chaotic. This is the operational definition of "Quantum Chaos" for purposes of this book.
- random matrix theory of spetral statistics and its connections to semiclassics
- statistical properties of quantum wavefunctions, scars due to underlying classical dynamics
- quantum suppresion of diffusion; localization, quantum incoherence

This book covers, rather incompletely, only the first topic: semiclassical manifestations of quantum chaos. Random matrix theory has its own rich methodology unrelated to the themes developed here. Physically the most profound (but not discussed here either) is the quantum suppresion of diffusion, observed in atomic systems and ultra cold gases.

The real issue here is the issue of "delocalization time" T_E, or the time of validity of semiclassics in describing quantum evolution. On intuitive grounds, this is often assumed to be the Ehrenfest time $T_E \approx \frac{1}{\lambda} \ln \frac{1}{\hbar}$, the time at which the finest classical fractal structure (typical length $e^{-\lambda T_E}$) becomes comparable to size of quantum phasespace cells: $N = \text{volume}/\hbar^D$, $ln(1/N^{1/D}) \approx ln\hbar$. The question of in which order one is allow to take the limits $t \to \infty$, $1/\hbar \to \infty$ is subtler than the Ehrenfest time estimate would imply.

replace ≈ by similar

⇑PRIVATE

31.1 Quantum pinball

In what follows, we will restrict the discussion to the non-relativistic Schrödinger equation. [1] The approach will be very much in the spirit of the early days of quantum mechanics, before its wave character has been fully uncovered by Schrödinger in the mid 1920's. Indeed, were physicists of the period as familiar with classical chaos as we are today, this theory could have been developed 80 years ago. It was the discrete nature of the hydrogen spectrum which inspired the Bohr - de Broglie picture of the old quantum theory: one places a wave instead of a particle on a Keplerian orbit around the hydrogen nucleus. The quantization condition is that only those orbits contribute for which this wave is stationary; from this followed the Balmer spectrum and the Bohr-Sommerfeld quantization which eventually led to the more sophisticated theory of Heisenberg, Schrödinger and others. Today we are very aware of the fact that elliptic orbits are an idiosyncracy of the Kepler problem, and that chaos is the rule; so can the Bohr quantization be generalized to chaotic systems?

The question was answered affirmatively by M. Gutzwiller, as late as 1971: a chaotic system can indeed be quantized by placing a wave on each

[1] Tanner: Reference to diffusion equation?

resonances!quantum
quantum!resonances

of the *infinity* of unstable periodic orbits. Due to the instability of the orbits the wave does not stay localized but leaks into neighborhoods of other periodic orbits. Contributions of different periodic orbits interfere and the quantization condition can no longer be attributed to a single periodic orbit: A coherent summation over the infinity of periodic orbit contributions gives the desired spectrum.

credit Brack

The pleasant surprise is that the zeros of the dynamical zeta function (1.9) derived in the context of classical chaotic dynamics,

☞ chapter 15

$$1/\zeta(z) = \prod_p (1 - t_p)\,,$$

also yield excellent estimates of *quantum* resonances, with the quantum amplitude associated with a given cycle approximated semiclassically by the weight

$$t_p = \frac{1}{|\Lambda_p|^{\frac{1}{2}}} e^{\frac{i}{\hbar}S_p - i\pi m_p/2}\,, \tag{31.1}$$

whose magnitude is the square root of the classical weight (15.11)

$$t_p = \frac{1}{|\Lambda_p|} e^{\beta\cdot A_p - sT_p}\,,$$

[2] and the phase is given by the Bohr-Sommerfeld action integral S_p, together with an additional topological phase m_p, the number of caustics along the periodic trajectory, points where the naive semiclassical approximation fails.

☞ chapter 34

In this approach, the quantal spectra of classically chaotic dynamical systems are determined from the zeros of dynamical zeta functions, defined by cycle expansions of infinite products of form

$$1/\zeta = \prod_p (1 - t_p) = 1 - \sum_f t_f - \sum_k c_k \tag{31.2}$$

with weight t_p associated to every prime (non-repeating) periodic orbit (or *cycle*) p.

The key observation is that the chaotic dynamics is often organized around a few *fundamental* cycles. These short cycles capture the skeletal topology of the motion in the sense that any long orbit can approximately be pieced together from the fundamental cycles. In chapter 18 it was

[2] Whelan: I am confused. The first weight is only the square root of the classical one if you set beta=s=0...

resonances!complex

shown that for this reason the cycle expansion (31.2) is a highly convergent expansion dominated by short cycles grouped into *fundamental* contributions, with longer cycles contributing rapidly decreasing *curvature* corrections. Computations with dynamical zeta functions are rather straightforward; typically one determines lengths and stabilities of a finite number of shortest periodic orbits, substitutes them into (31.2), and estimates the zeros of $1/\zeta$ from such polynomial approximations.

From the vantage point of the dynamical systems theory, the trace formulas (both the exact Selberg and the semiclassical Gutzwiller trace formula) fit into a general framework of replacing phase space averages by sums over periodic orbits. For classical hyperbolic systems this is possible since the invariant density can be represented by sum over all periodic orbits, with weights related to their instability. The semiclassical periodic orbit sums differ from the classical ones only in phase factors and stability weights; such differences may be traced back to the fact that in quantum mechanics the amplitudes rather than the probabilities are added.

☞ chapter 36

The type of dynamics has a strong influence on the convergence of cycle expansions and the properties of quantal spectra; this necessitates development of different approaches for different types of dynamical behavior such as, on one hand, the strongly hyperbolic and, on the other hand, the intermittent dynamics of chapters 18 and 21. For generic nonhyperbolic systems (which we shall not discuss here), with mixed phase space and marginally stable orbits, periodic orbit summations are hard to control, and it is still not clear that the periodic orbit sums should necessarily be the computational method of choice.

Where is all this taking us? The goal of this part of the book is to demonstrate that the cycle expansions, developed so far in classical settings, are also a powerful tool for evaluation of *quantum* resonances of classically chaotic systems.

First we shall warm up playing our game of pinball, this time in a quantum version. Were the game of pinball a closed system, quantum mechanically one would determine its stationary eigenfunctions and eigenenergies. For open systems one seeks instead complex resonances, where the imaginary part of the eigenenergy describes the rate at which the quantum wave function leaks out of the central scattering region. This will turn out to work well, except who truly wants to know accurately the resonances of a quantum pinball? [3]

☞ chapter 38

31.2 Quantization of helium

Once we have derived the semiclassical weight associated with the periodic orbit p (31.1), we will finally be in position to accomplish something altogether

[3] Whelan: Do you want to mention why you look at open systems: complete grammars and so on...

three body@3-body problem
collinear helium
helium!collinear
repeller
quantum!chaos

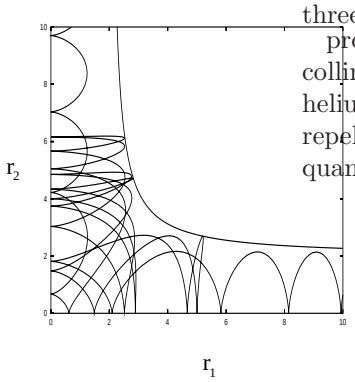

Figure 31.1: A typical collinear helium trajectory in the $r_1 - r_2$ plane; the trajectory enters along the r_1 axis and escapes to infinity along the r_2 axis.

remarkable. We are now able to put together all ingredients that make the game of pinball unpredictable, and compute a "chaotic" part of the helium spectrum to shocking accuracy. From the classical dynamics point of view, helium is an example of Poincaré's dreaded and intractable 3-body problem. Undaunted, we forge ahead and consider the *collinear* helium, with zero total angular momentum, and the two electrons on the opposite sides of the nucleus.

☞ chapter 41

thank Kai

We set the electron mass to 1, the nucleus mass to ∞, the helium nucleus charge to 2, the electron charges to -1. The Hamiltonian is

$$H = \frac{1}{2}p_1^2 + \frac{1}{2}p_2^2 - \frac{2}{r_1} - \frac{2}{r_2} + \frac{1}{r_1 + r_2}\,. \tag{31.3}$$

Due to the energy conservation, only three of the phase space coordinates (r_1, r_2, p_1, p_2) are independent. The dynamics can be visualized as a motion in the (r_1, r_2), $r_i \geq 0$ quadrant, figure 31.1, or, better still, by a well chosen 2-dimensional Poincaré section.

The motion in the (r_1, r_2) plane is topologically similar to the pinball motion in a 3-disk system, except that the motion is not free, but in the Coulomb potential. The classical collinear helium is also a repeller; almost all of the classical trajectories escape. Miraculously, the symbolic dynamics for the survivors turns out to be binary, just as in the 3-disk game of pinball, so we know what cycles need to be computed for the cycle expansion (1.10). A set of shortest cycles up to a given symbol string length then yields an estimate of the helium spectrum. This simple calculation yields surprisingly accurate eigenvalues; even though the cycle expansion was based on the *semiclassical approximation* (31.1) which is expected to be good only in the classical large energy limit, the eigenenergies are good to 1% all the way down to the ground state.

☞ chapter 41

Before we can get to this point, we first have to recapitulate some basic notions of quantum mechanics; after having defined the main quantum objects of interest, the quantum propagator and the Green's function, we

random matrix theory
quantum!chaos

will relate the quantum propagation to the classical flow of the underlying dynamical system. We will then proceed to construct semiclassical approximations to the quantum propagator and the Green's function. A rederivation of classical Hamiltonian dynamics starting from the Hamilton-Jacobi equation will be offered along the way. The derivation of the Gutzwiller trace formula and the semiclassical zeta function as a sum and as a product over periodic orbits will be given in chapter 36. In subsequent chapters we buttress our case by applying and extending the theory: a cycle expansion calculation of scattering resonances in a 3-disk billiard in chapter 38, the spectrum of helium in chapter 41, and the incorporation of diffraction effects in chapters 42 and 43.

⇓PRIVATE
⇑PRIVATE

Guide to literature

A key prerequisite to developing any theory of "quantum chaos" is solid understanding of Hamiltonian mechanics. For that, Arnol'd monograph [1.34] is the essential reference. Ozorio de Almeida's monograph [7.11] offers a compact introduction to the aspects of Hamiltonian dynamics required for the quantization of integrable and nearly integrable systems, with emphasis on periodic orbits, normal forms, catastrophy theory and torus quantization. The book by Brack and Bhaduri [31.1] is an excellent introduction to the semiclassical methods. Gutzwiller's monograph [31.2] is an advanced introduction focusing on chaotic dynamics both in classical Hamiltonian settings and in the semiclassical quantization. This book is worth browsing through for its many insights and erudite comments on quantum and celestial mechanics even if one is not working on problems of quantum chaos. More suitable as a graduate course text is Reichl's exposition [31.3].

include the Stöckmann experimental book

This book does not discuss the random matrix theory approach to chaos in quantal spectra; no randomness assumptions are made here, rather the goal is to milk the deterministic chaotic dynamics for its full worth. The book concentrates on the periodic orbit theory. For an introduction to "quantum chaos" that focuses on the random matrix theory the reader is referred to the excellent monograph by Haake [31.4], among others.

add Bluhmel

References

[31.1] M. Brack and R.K. Bhaduri, *Semiclassical Physics* (Addison-Wesley, New York 1997).

[31.2] M.C. Gutzwiller, *Chaos in Classical and Quantum Mechanics* (Springer, New York 1990).

[31.3] L.E. Reichl, *The Transition to Chaos in Conservative Classical Systems: Quantum Manifestations* (Springer-Verlag, New York 1992).

[31.4] F. Haake, *Quantum Signatures of Chaos*, 2. edition (Springer-Verlag, New York 2001).

quantum!mechanics
mechanics!quantum
Schr“”odinger!equation
Hamiltonian
Schr“”odinger!equation!time independent
eigenfunction!energy

Chapter 32

Quantum mechanics, briefly

We start with a review of standard quantum mechanical concepts prerequisite to the derivation of the semiclassical trace formula.

In coordinate representation the time evolution of a quantum mechanical wave function is governed by the Schrödinger equation

$$i\hbar\frac{\partial}{\partial t}\psi(q,t) = \hat{H}(q,\frac{\hbar}{i}\frac{\partial}{\partial q})\psi(q,t), \tag{32.1}$$

where the Hamilton operator $\hat{H}(q,-i\hbar\partial_q)$ is obtained from the classical Hamiltonian by substitution $p \to -i\hbar\partial_q$. Most of the Hamiltonians we shall consider here are of form

$$H(q,p) = T(p) + V(q)\,, \qquad T(p) = p^2/2m\,, \tag{32.2}$$

describing dynamics of a particle in a D-dimensional potential $V(q)$. For time independent Hamiltonians we are interested in finding stationary solutions of the Schrödinger equation of the form

$$\psi_n(q,t) = e^{-iE_n t/\hbar}\phi_n(q), \tag{32.3}$$

where E_n are the eigenenergies of the time-independent Schrödinger equation

$$\hat{H}\phi(q) = E\phi(q)\,. \tag{32.4}$$

If the kinetic term can be separated out as in (32.2), the time-independent Schrödinger equation

$$-\frac{\hbar^2}{2m}\partial^2\phi(q) + V(q)\phi(q) = E\phi(q) \tag{32.5}$$

Hilbert!space

can be rewritten in terms of a local wavenumber

$$(\partial^2 + k^2(q))\phi = 0\,, \qquad \hbar^2 k(q) = \sqrt{2m(E - V(q))}\,. \tag{32.6}$$

For bound systems the spectrum is discrete and the eigenfunctions form an orthonormal,

$$\int dq\, \phi_n(q)\phi_m^*(q) = \delta_{nm}\,, \tag{32.7}$$

and complete,

$$\sum_n \phi_n(q)\phi_n^*(q') = \delta(q - q')\,, \tag{32.8}$$

set of functions in a Hilbert space. Here and throughout the text,

$$\int dq = \int dq_1 dq_2 ... dq_D. \tag{32.9}$$

For simplicity we will assume that the system is bound, although most of the results will be applicable to open systems, where one has complex resonances instead of real energies, and the spectrum has continuous components.

☞ chapter 38

A given wave function can be expanded in the energy eigenbasis

$$\psi(q,t) = \sum_n c_n e^{-iE_n t/\hbar}\phi_n(q)\,, \tag{32.10}$$

where the expansion coefficient c_n is given by the projection of the initial wave function $\psi(q,0)$ onto the nth eigenstate

$$c_n = \int dq\, \phi_n^*(q)\psi(q,0). \tag{32.11}$$

By substituting (32.11) into (32.10), we can cast the evolution of a wave function into a multiplicative form

$$\psi(q,t) = \int dq' K(q,q',t)\psi(q',0)\,,$$

with the kernel

$$K(q,q',t) = \sum_n \phi_n(q)\, e^{-iE_n t/\hbar}\phi_n^*(q') \tag{32.12}$$

called the quantum evolution operator, or the *propagator*. Applied twice, first for time t_1 and then for time t_2, it propagates the initial wave function from q' to q'', and then from q'' to q

$$K(q,q',t_1+t_2) = \int dq''\, K(q,q'',t_2)K(q'',q',t_1) \tag{32.13}$$

forward in time, hence the name "propagator". In non-relativistic quantum mechanics the range of q'' is infinite, meaning that the wave can propagate at any speed; in relativistic quantum mechanics this is rectified by restricting the propagation to the forward light cone.

Since the propagator is a linear combination of the eigenfunctions of the Schrödinger equation, it also satisfies the Schrödinger equation

$$i\hbar\frac{\partial}{\partial t}K(q,q',t) = \hat{H}(q,\frac{i}{\hbar}\frac{\partial}{\partial q})K(q,q',t)\,, \tag{32.14}$$

and is thus a wave function defined for $t \geq 0$; from the completeness relation (32.8) we obtain the boundary condition at $t = 0$:

$$\lim_{t\to 0_+} K(q,q',t) = \delta(q-q')\,. \tag{32.15}$$

The propagator thus represents the time evolution of a wave packet which starts out as a configuration space delta-function localized in the point q' at the initial time $t = 0$.

For time independent Hamiltonians the time dependence of the wave functions is known as soon as the eigenenergies E_n and eigenfunctions ϕ_n have been determined. With time dependence rendered "trivial", it makes sense to focus on the *Green's function*, the Laplace transformation of the propagator

$$G(q,q',E+i\epsilon) = \frac{1}{i\hbar}\int_0^\infty dt\, e^{\frac{i}{\hbar}Et-\frac{\epsilon}{\hbar}t}K(q,q',t) = \sum_n \frac{\phi_n(q)\phi_n^*(q')}{E-E_n+i\epsilon}\,. \tag{32.16}$$

Here ϵ is a small positive number, ensuring the existence of the integral. The eigenenergies show up as poles in the Green's function with residues corresponding to the wave function amplitudes. If one is only interested in the spectrum, one may restrict the considerations to the (formal) trace of the Green's function,

$$\mathrm{tr}\, G(q,q',E) = \int dq\, G(q,q,E) = \sum_n \frac{1}{E-E_n}\,, \tag{32.17}$$

evolution!operator!quantum
quantum!evolution
quantum!propagator
propagator
delta function!Dirac
Green's function!energy dependent
Laplace!transform
Green's function!trace

⇓PRELIMINARY
??
page ??
⇑PRELIMINARY

IOP usage is: Green function
⇓PRELIMINARY
32.2
page 612
⇑PRELIMINARY

density of states!quantum
Green's function!density of states
density of states!Green's function

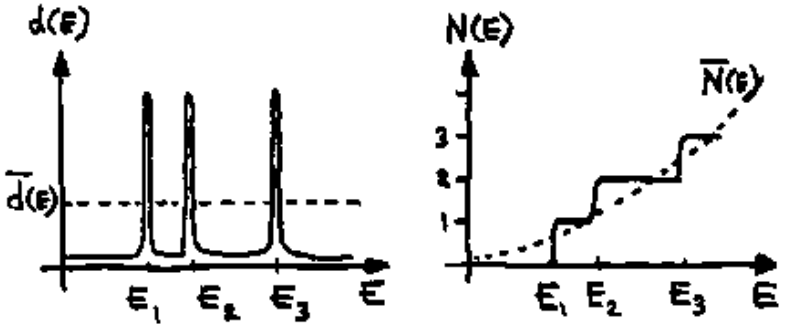

Figure 32.1: Schematic picture of **a)** the density of states $d(E)$, and **b)** the spectral staircase function $N(E)$. The dashed lines denote the mean density of states $\bar{d}(E)$ and the average number of states $\bar{N}(E)$ discussed in more detail in sect. 36.1.1.

where E is complex, with a positive imaginary part, and we have used the eigenfunction orthonormality (32.7). This trace is formal, since as it stands, the sum in (32.17) is often divergent. [1] We shall return to this point in sects. 36.1.1 and 36.1.2. [2]

A useful characterization of the set of eigenvalues is given in terms of the *density of states*, with a delta function peak at each eigenenergy, figure 32.1 (a),

$$d(E) = \sum_n \delta(E - E_n). \tag{32.18}$$

32.1
page 612

Using the identity

$$\delta(E - E_n) = -\lim_{\epsilon \to +0} \frac{1}{\pi} \mathrm{Im} \frac{1}{E - E_n + i\epsilon} \tag{32.19}$$

we can express the density of states in terms of the trace of the Green's function, that is

$$d(E) = \sum_n \delta(E - E_n) = -\lim_{\epsilon \to 0} \frac{1}{\pi} \mathrm{Im}\, \mathrm{tr}\, G(q, q', E + i\epsilon). \tag{32.20}$$

☞ sect. 36.1.1

As we shall see after "some" work, a semiclassical formula for right hand side of this relation will yield the quantum spectrum in terms of periodic orbits.

[1] Whelan: The convergence depends on the density of states. For a 1D infinite square well the energies are proportional to n^2 and the equation above would converge. I think (but may be wrong, I am going on memory) that there is a complementarity. If the trace of the propagator converges the trace of the Green's function does not and vice-versa. By the way, you may want to write down the trace of the propagator as $K(t) = \sum_{n} exp(-iE_n t/\hbar)$.

[2] Tanner: Cite Voros, Sieber ...

The density of states can be written as the derivative $d(E) = \mathrm{d}N(E)/\mathrm{d}E$ of the *spectral staircase* function

spectral!staircase
staircase!spectral
Heaviside function

$$N(E) = \sum_n \Theta(E - E_n) \tag{32.21}$$

which counts the number of eigenenergies below E, figure 32.1 (b). Here Θ is the Heaviside function

$$\Theta(x) = 1 \quad \text{if } x > 0; \quad \Theta(x) = 0 \quad \text{if } x < 0\,. \tag{32.22}$$

add spect determinant here

The spectral staircase is a useful quantity in many contexts, both experimental and theoretical. This completes our lightning review of quantum mechanics.

prepare refsQmech.tex exerQmech.tex, soluQmech.tex

Dirac delta function
Green's function

Exercises

(23.18) in edition 10?

Exercise 32.1 Dirac delta function, Lorentzian representation. *Derive the representation (32.19)*

$$\delta(E-E_n) = -\lim_{\epsilon\to+0}\frac{1}{\pi}\mathrm{Im}\,\frac{1}{E-E_n+i\epsilon}$$

of a delta function as imaginary part of $1/x$.

(Hint: read up on principal parts, positive and negative frequency part of the delta function, the Cauchy theorem in a good quantum mechanics textbook).

Exercise 32.2 Green's function. *Verify Green's function Laplace transform (32.16),*

$$\begin{aligned} G(q,q',E+i\varepsilon) &= \frac{1}{i\hbar}\int_0^\infty dt\; e^{\frac{i}{\hbar}Et-\frac{\varepsilon}{\hbar}t}K(q,q',t) \\ &= \sum\frac{\phi_n(q)\phi_n^*(q')}{E-E_n+i\varepsilon} \end{aligned}$$

argue that positive ϵ *is needed (hint: read a good quantum mechanics textbook).*

Wentzel-"-Kramers-
"-Brillouin
WKB!quantization
quantization!WKB

Chapter 33

WKB quantization

spelling Brillouin?

The wave function for a particle of energy E moving in a constant potential V is

$$\psi = Ae^{\frac{i}{\hbar}pq} \tag{33.1}$$

with a constant amplitude A, and constant wavelength $\lambda = 2\pi/k$, $k = p/\hbar$, and $p = \pm\sqrt{2m(E-V)}$ is the momentum. Here we generalize this solution to the case where the potential varies slowly over many wavelengths. This semiclassical (or WKB) approximate solution of the Schrödinger equation fails at classical turning points, configuration space points where the particle momentum vanishes. In such neighborhoods, where the semiclassical approximation fails, one needs to solve locally the exact quantum problem, in order to compute connection coefficients which patch up semiclassical segments into an approximate global wave function.

Two lessons follow. First, semiclassical methods can be very powerful - classical mechanics computations yield suprisingly accurate estimates of quantal spectra, without solving the Schrödinger equation. Second, semiclassical quantization does depend on a purely wave-mechanical phenomena, the coherent addition of phases accrued by all fixed energy phase space trajectories that connect pairs of coordinate points, and the topological phase loss at every turning point, a topological property of the classical flow that plays no role in classical mechanics.

33.1 WKB ansatz

Consider a time-independent Schrödinger equation in 1 spatial dimension:

$$-\frac{\hbar^2}{2m}\psi''(q) + V(q)\psi(q) = E\psi(q)\,, \tag{33.2}$$

action

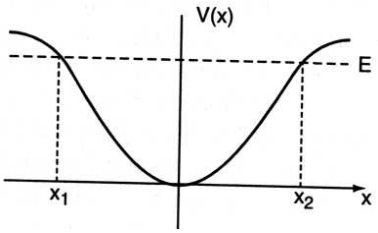

Figure 33.1: A 1-dimensional potential, location of the two turning points at fixed energy E.

with potential $V(q)$ growing sufficiently fast as $q \to \pm\infty$ so that the classical particle motion is confined for any E. Define the local momentum $p(q)$ and the local wavenumber $k(q)$ by

$$p(q) = \pm\sqrt{2m(E - V(q))}, \quad p(q) = \hbar k(q)\,. \tag{33.3}$$

The variable wavenumber form of the Schrödinger equation

$$\psi'' + k^2(q)\psi = 0 \tag{33.4}$$

sugests that the wave function be written as $\psi = Ae^{\frac{i}{\hbar}S}$, A and S real functions of q. Substitution yields two equations, one for the real and other for the imaginary part:

$$(S')^2 = p^2 + \hbar^2\frac{A''}{A} \tag{33.5}$$

$$S''A + 2S'A' = \frac{1}{A}\frac{d}{dq}(S'A^2) = 0\,. \tag{33.6}$$

The Wentzel-Kramers-Brillouin *(WKB)* or *semiclassical* approximation consists of dropping the $\hbar^2$ term in (33.5). Recalling that $p = \hbar k$, this amounts to assuming that $k^2 \gg \frac{A''}{A}$, which in turn implies that the phase of the wave function is changing much faster than its overall amplitude. So the WKB approximation can interpreted either as a short wavelength/high frequency approximation to a wave-mechanical problem, or as the semiclassical, $\hbar \ll 1$ approximation to quantum mechanics.

redraw figure 33.1, or ask Brack for premission!

Setting $\hbar = 0$ and integrating (33.5) we obtain the phase increment of a wave function initially at q, at energy E

$$S(q, q', E) = \int_{q'}^{q} dq'' p(q'')\,. \tag{33.7}$$

This integral over a particle trajectory of constant energy, called the *action*, will play a key role in all that follows. The integration of (33.6) is even easier

$$A(q) = \frac{C}{|p(q)|^{\frac{1}{2}}}, \qquad C = |p(q')|^{\frac{1}{2}}\psi(q')\,, \tag{33.8}$$

where the integration constant C is fixed by the value of the wave function at the initial point q'. The *WKB* (or *semiclassical*) *ansatz* wave function is given by

degree of freedom

$$\psi_{sc}(q,q',E) = \frac{C}{|p(q)|^{\frac{1}{2}}} e^{\frac{i}{\hbar}S(q,q',E)}\,. \tag{33.9}$$

In what follows we shall supress dependence on the initial point and energy in such formulas, $(q,q',E) \to (q)$.

The WKB ansatz generalizes the free motion wave function (33.1), with the probability density $|A(q)|^2$ for finding a particle at q now inversely proportional to the velocity at that point, and the phase $\frac{1}{\hbar}q\,p$ replaced by $\frac{1}{\hbar}\int dq\,p(q)$, the integrated action along the trajectory. This is fine, except at any turning point q_0, figure 33.1, where all energy is potential, and

$$p(q) \to 0 \quad \text{as} \quad q \to q_0\,, \tag{33.10}$$

fix up $A \to \infty$

so that the assumption that $k^2 \gg \frac{A''}{A}$ fails. What can one do in this case?

⇓PRIVATE

The answer, in the form given in standard quantum mechanics textbooks, will be reviewed in sect. 33.4. However, for the task at hand, a simple physical picture, due to Maslov, does the job. In the q coordinate, the turning points are defined by the zero kinetic energy condition (see figure 33.1), and the motion appears singular. This is not so in the full phase space: the trajectory in a smooth confining 1-dimensional potential is always a smooth loop, with the "special" role of the turning points q_L, q_R seen to be an artifact of a particular choice of the (q,p) coordinate frame. Maslov's idea was to proceed from the initial point (q',p') to a point (q_A,p_A) preceeding the turning point in the $\psi(q)$ representation, then switch to the momentum representation

⇑PRIVATE

redraw the figure 33.2!

$$\widetilde{\psi}(p) = \frac{1}{\sqrt{2\pi\hbar}} \int dq\, e^{-\frac{i}{\hbar}qp}\psi(q)\,, \tag{33.11}$$

continue from (q_A,p_A) to (q_B,p_B), switch back to the coordinate representation,

$$\psi(q) = \frac{1}{\sqrt{2\pi\hbar}} \int dp\, e^{\frac{i}{\hbar}qp}\,\widetilde{\psi}(p)\,, \tag{33.12}$$

and so on.

define dof

The only rub is that one usually cannot evaluate these transforms exactly. But, as the WKB wave function (33.9) is approximate anyway, it suffices to estimate these transforms to leading order in $\hbar$ accuracy. This is accomplished by the method of stationary phase.

stationary!phase approximation
extremal point
Fresnel integral

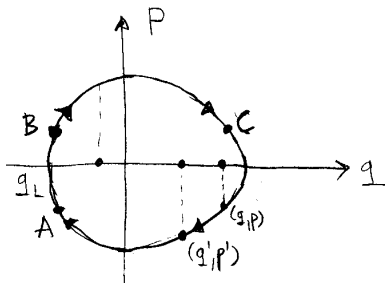

Figure 33.2: A 1-dof phase space trajectory of a particle moving in a bound potential.

33.2 Method of stationary phase

All "semiclassical" approximations are based on saddlepoint evaluations of integrals of the type [1]

$$I = \int dx\, A(x)\, e^{is\Phi(x)}\,, \qquad x, \Phi(x) \in \mathbb{R}\,, \tag{33.13}$$

where s is assumed to be a large, real parameter, and $\Phi(x)$ is a real-valued function. In our applications $s = 1/\hbar$ will always be assumed large.

For large s, the phase oscillates rapidly and "averages to zero" everywhere except at the *extremal points* $\Phi'(x_0) = 0$. The method of approximating an integral by its values at extremal points is called the *method of stationary phase*. Consider first the case of a 1-dimensional integral, and expand $\Phi(x_0 + \delta x)$ around x_0 to second order in δx,

$$I = \int dx\, A(x)\, e^{is(\Phi(x_0)+\frac{1}{2}\Phi''(x_0)\delta x^2+\ldots)}\,. \tag{33.14}$$

Assume (for time being) that $\Phi''(x_0) \neq 0$, with either sign, $\mathrm{sgn}[\Phi''] = \Phi''/|\Phi''| = \pm 1$. If in the neighborhood of x_0 the amplitude $A(x)$ varies slowly over many oscillations of the exponential function, we may retain the leading term in the Taylor expansion of the amplitude, and approximate the integral up to quadratic terms in the phase by

$$I \approx A(x_0) e^{is\Phi(x_0)} \int dx\, e^{\frac{1}{2}is\Phi''(x_0)(x-x_0)^2}\,. \tag{33.15}$$

Using the *Fresnel integral formula*

33.1 page 624

$$\frac{1}{\sqrt{2\pi}} \int_{-\infty}^{\infty} dx\, e^{-\frac{x^2}{2ia}} = \sqrt{ia} = |a|^{1/2}\, e^{i\frac{\pi}{4}\frac{a}{|a|}} \tag{33.16}$$

recheck the i factor in (33.16)

we obtain

$$I \approx A(x_0) \left| \frac{2\pi}{s\Phi''(x_0)} \right|^{1/2} e^{is\Phi(x_0)\pm i\frac{\pi}{4}}\,, \tag{33.17}$$

[1] Mason: explain "saddlepoint"

where $\pm$ corresponds to the positive/negative sign of $s\Phi''(x_0)$.

WKB!quantization
quantization!WKB

33.3 WKB quantization

We can now evaluate the Fourier transforms (33.11), (33.12) to the same order in $\hbar$ as the WKB wave function using the stationary phase method,

$$\begin{aligned}\widetilde{\psi}_{sc}(p) &= \frac{C}{\sqrt{2\pi\hbar}}\int \frac{dq}{|p(q)|^{\frac{1}{2}}}\, e^{\frac{i}{\hbar}(S(q)-qp)} \\ &\approx \frac{C}{\sqrt{2\pi\hbar}}\frac{e^{\frac{i}{\hbar}(S(q^*)-q^*p)}}{|p(q^*)|^{\frac{1}{2}}}\int dq\, e^{\frac{i}{2\hbar}S''(q^*)(q-q^*)^2}\,, \end{aligned} \tag{33.18}$$

where q^* is given implicitly by the stationary phase condition

$$0 = S'(q^*) - p = p(q^*) - p$$

and the sign of $S''(q^*) = p'(q^*)$ determines the phase of the Fresnel integral (33.16)

$$\widetilde{\psi}_{sc}(p) = \frac{C}{|p(q^*)p'(q^*)|^{\frac{1}{2}}} e^{\frac{i}{\hbar}[S(q^*)-q^*p]+\frac{i\pi}{4}\mathrm{sgn}[S''(q^*)]}\,. \tag{33.19}$$

As we continue from (q_A, p_A) to (q_B, p_B), nothing problematic occurrs - $p(q^*)$ is finite, and so is the acceleration $p'(q^*)$. Otherwise, the trajectory would take infinitely long to get across. We recognize the exponent as the Legendre transform

$$\tilde{S}(p) = S(q(p)) - q(p)p$$

which can be used to expresses everything in terms of the p variable,

$$q^* = q(p), \quad \frac{d}{dq}q = 1 = \frac{dp}{dq}\frac{dq(p)}{dp} = q'(p)p'(q^*)\,. \tag{33.20}$$

As the classical trajectory crosses q_L, the weight in (33.19),

$$\frac{d}{dq}p^2(q_L) = 2p(q_L)p'(q_L) = -2mV'(q)\,, \tag{33.21}$$

is finite, and $S''(q^*) = p'(q^*) < 0$ for any point in the lower left quadrant, including (q_A, p_A). Hence, the phase loss in (33.19) is $-\frac{\pi}{4}$. To go back from the p to the q representation, just turn figure 33.2 90^o anticlockwise.

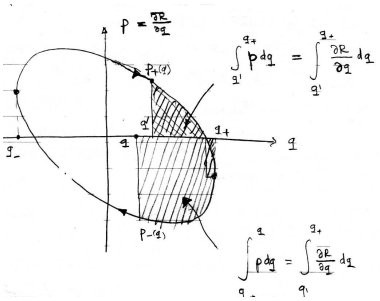

Figure 33.3: $S_p(E)$, the action of a periodic orbit p at energy E, equals the area in the phase space traced out by the 1-dof trajectory.

Everything is the same if you replace $(q,p) \to (-p,q)$; so, without much ado we get the semiclassical wave function at the point (q_B, p_B),

$$\psi_{sc}(q) = \frac{e^{\frac{i}{\hbar}(\tilde{S}(p^*)+qp^*)-\frac{i\pi}{4}}}{|q^*(p^*)|^{\frac{1}{2}}}\,\widetilde{\psi}_{sc}(p^*) = \frac{C}{|p(q)|^{\frac{1}{2}}}e^{\frac{i}{\hbar}S(q)-\frac{i\pi}{2}}\,. \tag{33.22}$$

The extra $|p'(q^*)|^{1/2}$ weight in (33.19) is cancelled by the $|q'(p^*)|^{1/2}$ term, by the Legendre relation (33.20).

The message is that going through a smooth potential turning point the WKB wave function phase slips by $-\frac{\pi}{2}$. This is equally true for the right and the left turning points, as can be seen by rotating figure 33.2 by 180^o, and flipping coordinates $(q,p) \to (-q,-p)$. While a turning point is not an invariant concept (for a sufficiently short trajectory segment, it can be undone by a 45^o turn), for a complete period $(q,p) = (q',p')$ the total phase slip is always $-2\cdot\pi/2$, as a loop always has $m = 2$ turning points. [2]

The *WKB quantization condition* follows by demanding that the wave function computed after a complete period be single-valued. With the normalization (33.8), we obtain

$$\psi(q') = \psi(q) = \left|\frac{p(q')}{p(q)}\right|^{\frac{1}{2}} e^{i(\frac{1}{\hbar}\oint p(q)dq-\pi)}\psi(q')\,.$$

The prefactor is 1 by the periodic orbit condition $q = q'$, so the phase must be a multiple of 2π,

$$\frac{1}{\hbar}\oint p(q)dq = 2\pi\left(n+\frac{m}{4}\right)\,, \tag{33.23}$$

where m is the number of turning points along the trajectory - for this 1-dof problem, $m = 2$.

[2] Whelan: It is also possible to have $+\pi/2$ phase slips if the trajectory plotted in p-q space has concave dimples and is not purely convex. In that case $S'' > 0$ although it may not be very pedagogical to get into that... PC: forget this comment unless there is an example of interest.

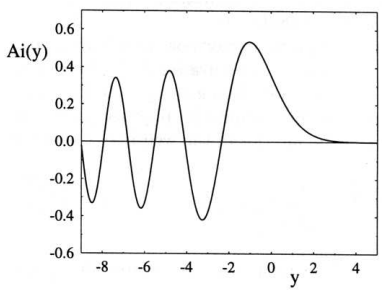

Figure 33.4: Airy function $Ai(q)$.

The action integral in (33.23) is the area (see figure 33.3) enclosed by the classical phase space loop of figure 33.2, and the quantization condition says that eigenenergies correspond to loops whose action is an integer multiple of the unit quantum of action, Planck's constant $\hbar$. The extra topological phase, which, although it had been discovered many times in centuries past, had to wait for its most recent quantum chaotic (re)birth until the 1970's. Despite its derivation in a noninvariant coordinate frame, the final result involves only canonically invariant classical quantities, the periodic orbit action S, and the topological index m.

⇓PRELIMINARY
☞ appendix A.7
⇑PRELIMINARY

33.3.1 Harmonic oscillator quantization

Let us check the WKB quantization for one case (the only case?) whose quantum mechanics we fully understand: the harmonic oscillator

$$E = \frac{1}{2m}\left(p^2 + (m\omega q)^2\right) .$$

The loop in figure 33.2 is now a circle in the $(m\omega q, p)$ plane, the action is its area $S = 2\pi E/\omega$, and the spectrum in the WKB approximation

$$E_n = \hbar\omega(n + 1/2) \tag{33.24}$$

turns out to be the *exact* harmonic oscillator spectrum. The stationary phase condition (33.18) keeps $V(q)$ accurate to order q^2, which in this case is the whole answer (but we were simply lucky, really). For many 1-dof problems the WKB spectrum turns out to be very accurate all the way down to the ground state. Surprisingly accurate, if one interprets dropping the $\hbar^2$ term in (33.5) as a short wavelength approximation.

33.4 Beyond the quadratic saddle point

We showed, with a bit of Fresnel/Maslov voodoo, that in a smoothly varying potential the phase of the WKB wave function slips by a $\pi/2$ for each turning point. This $\pi/2$ came from a $\sqrt{i}$ in the Fresnel integral (33.16), one

Airy integral
Airy!equation
WKB!connection formulas
connection formulas
Airy!function
RECHECK

such factor for every time we switched representation from the configuration space to the momentum space, or back. Good, but what does this mean?

The stationary phase approximation (33.14) fails whenever $\Phi''(x) = 0$, or, in our the WKB ansatz (33.18), whenever the momentum $p'(q) = S''(q)$ vanishes. In that case we have to go beyond the quadratic approximation (33.15) to the first nonvanishing term in the Taylor expansion of the exponent. If $\Phi'''(x_0) \neq 0$, then

$$I \approx A(x_0) e^{is\Phi(x_0)} \int_{-\infty}^{\infty} dx\, e^{is\Phi'''(x_0)\frac{(x-x_0)^3}{6}} . \tag{33.25}$$

Airy functions can be represented by integrals of the form

$$Ai(x) = \frac{1}{2\pi} \int_{-\infty}^{+\infty} dy\, e^{i(xy-\frac{y^3}{3})} . \tag{33.26}$$

Derivations of the WKB quantization condition given in standard quantum mechanics textbooks rely on expanding the potential close to the turning point

$$V(q) = V(q_0) + (q - q_0)V'(q_0) + \cdots ,$$

solving the Airy equation

$$\psi'' = q\psi , \tag{33.27}$$

and matching the oscillatory and the exponentially decaying "forbidden" region wave function pieces by means of the *WKB connection formulas*. That requires staring at Airy functions and learning about their asymptotics - a challenge that we will have to eventually overcome, in order to incorporate diffraction phenomena into semiclassical quantization.

⇓PRELIMINARY
☞ chapter ??
⇑PRELIMINARY

2) what does the wave function look like?

3) generically useful when Gaussian approximations fail

The physical origin of the topological phase is illustrated by the shape of the Airy function, figure 33.4. For a potential with a finite slope $V'(q)$ the wave function pentrates into the forbidden region, and accomodates a bit more of a stationary wavelength then what one would expect from the classical trajectory alone. For infinite walls (i.e., billiards) a different argument applies: the wave function must vanish at the wall, and the phase slip due to a specular reflection is $-\pi$, rather than $-\pi/2$.

⇓PRELIMINARY

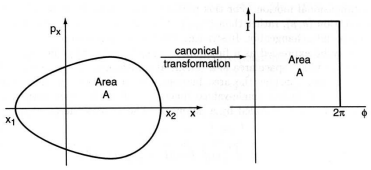

Figure 33.5: EBK quantization.

body@3-body problem
eigenvalue
value!zero
function
Wentzel-Kramers-Brillouin
WKB!quantization
quantization!WKB
Bohr-Sommerfeld quantization

33.5 EBK quantization

> If there exist fewer than ℓ integrals of type (14), as is the case, for example, according to POINCARÉ in the three-body problem, then the p_i are not expressible by the q_i and the quantum condition of SOMMERFELD-EPSTEIN fails also in the slightly generalized form that has been given here.
>
> A. Einstein, *Zum Quantensatz von Sommerfeld und Epstein* (1917)

All 1-dimensional Hamiltonian problems are integrable (see sect. 5.1).

refer to figure 33.5

D-dimensional version of eqs. (33.3) and (33.4) will be given below, in (34.3) and (34.4).

⇑PRELIMINARY

Commentary

3

Remark 33.1 Airy function. The stationary phase approximation is all that is needed for the semiclassical approximation, with the proviso that D in (34.36) has no zero eigenvalues. The zero eigenvalue case would require going beyond the Gaussian saddle-point approximation, which typically leads to approximations of the integrals in terms of Airy functions [33.10].

33.4
page 624

⇓PRELIMINARY

Remark 33.2 WKB quantization.

refs. [20.12, 33.1] and Mark Holmer? Sakuarai QM book?

4

⇑PRELIMINARY

Remark 33.3 Bohr-Sommerfeld quantization. Bohr-Sommerfeld quantization condition was the key result of the old quantum theory, in which the electron trajectories were purely classical. They were lucky - the symmetries of the Kepler problem work out in such a way that the total topological index $m = 4$ amount

find the Bohr-Sommerfeld reference

[3] Whelan: You are referring to a formula that is yet to come. That might be confusing for readers.

[4] Mason: I volunteer to write a chapter on the Berry phase

effectively to numbering the energy levels starting with $n = 1$. They were unlucky - because the hydrogen $m = 4$ masked the topological index, they could never get the helium spectrum right - the semiclassical calculation had to wait for until 1980, when Leopold and Percival [A.6] added the topological indices.

[5]

⇓PRELIMINARY

Remark 33.4 EBK quantization. Review: Percival [33.11].

blab about Einstein [34.1], Poincaré, Keller

⇑PRELIMINARY

Résumé

The WKB ansatz wave function for 1-degree of freedom problems fails at the turning points of the classical trajectory. While in the q-representation the WKB ansatz a turning point is singular, along the p direction the classical trajectory in the same neighborhood is smooth, as for any smooth bound potential the classical motion is topologically a circle around the origin in the (q, p) space. The simplest way to deal with such singularities is as follows; follow the classical trajectory in q-space until the WKB approximation fails close to the turning point; then insert $\int dp|p\rangle\langle p|$ and follow the classical trajectory in the p-space until you encounter the next p-space turning point; go back to the q-space representation, an so on. Each matching involves a Fresnel integral, yielding an extra $e^{-i\pi/4}$ phase shift, for a total of $e^{-i\pi}$ phase shift for a full period of a semiclassical particle moving in a soft potential. The condition that the wave-function be single-valued then leads to the 1-dimensional WKB quantization, and its lucky cousin, the Bohr-Sommerfeld quantization.

Alternatively, one can linearize the potential around the turning point a, $V(q) = V(a) + (q - a)V'(a) + \cdots$, and solve the quantum mechanical constant linear potential $V(q) = qF$ problem exactly, in terms of an Airy function. An approximate wave function is then patched together from an Airy function at each turning point, and the WKB ansatz wave-function segments inbetween via the WKB connection formulas. The single-valuedness condition again yields the 1-dimensional WKB quantization. This a bit more work than tracking the classical trajectory in the full phase space, but it gives us a better feeling for shapes of quantum eigenfunctions, and exemplifies the general strategy for dealing with other singularities, such as wedges, bifurcation points, creeping and tunneling: patch together the WKB segments by means of exact QM solutions to local approximations to singular points.

⇓PRELIMINARY

[5] Mason: I never understood why Duffing quantization was not solved completely, in terms of elliptic functions

then instead of doing an integral over $e^{iq^2S''/2}$, one has to keep the cubic term, and do an integral of form $\int dp e^{i(p^3/3-qp)}$. As this integral has no simple analytic solution, it has a name: Airy function.

⇑PRELIMINARY

References

[33.1] D. J. Griffiths, *Introduction to Quantum Mechanics* (Prentice-Hall, Englewood Cliffs, New Jersey, 1994).

[33.2] J.W.S. Rayleigh, *The Theory of Sound* (Macmillan, London 1896; reprinted by Dover, New York 1945).

[33.3] J.B. Keller, *Ann. Phys. (N.Y.)* **4**, 180 (1958).

[33.4] J.B. Keller and S.I. Rubinow, *Ann. Phys. (N.Y.)* **9**, 24 (1960).

[33.5] J.B. Keller, "A geometrical theory of diffraction", in *Calculus of variations and its applications*, *Proc. of Symposia in appl. math.* **8**, (McGraw-Hill, New York, 1958).

[33.6] J.B. Keller, *Calculus of Variations* **27**, (1958).

[33.7] V.P. Maslov, *Théorie des Perturbations et Métodes Asymptotiques* (Dunod, Paris, 1972).

[33.8] V.P. Maslov and M.V. Fedoriuk, *Semi-Classical Approximation in Quantum Mechanics* (Reidel, Boston 1981).

[33.9] V.I. Arnold, *Functional Anal. Appl.* **1**, 1 (1967).

[33.10] N. Bleistein and R.A. Handelsman, *Asymptotic Expansions of Integrals* (Dover, New York 1986).

[33.11] I.C. Percival, *Adv. Chem. Phys.* **36**, 1 (1977).

Fresnel integral
Sterling formula
stationary!phase approximation
Airy function
bifurcation!Airy function approximation
Airy function!at a bifurcation

Exercises

Exercise 33.1 WKB ansatz. *Try to show that no other ansatz other than (34.1) gives a meaningful definition of the momentum in the $\hbar \to 0$ limit.* [6]

Exercise 33.2 Fresnel integral. *Derive the Fresnel integral*

$$\frac{1}{\sqrt{2\pi}} \int_{-\infty}^{\infty} dx\, e^{-\frac{x^2}{2ia}} = \sqrt{ia} = |a|^{1/2} e^{i\frac{\pi}{4}\frac{a}{|a|}} .$$

Exercise 33.3 Sterling formula for $n!$. *Compute an approximate value of $n!$ for large n using the stationary phase approximation. Hint: $n! = \int_0^\infty dt\, t^n e^{-t}$.*

Rytis fixed $t^{n-1} \to t^n$

Exercise 33.4 Airy function for large arguments. *Important contributions as stationary phase points may arise from extremal points where the first non-zero term in a Taylor expansion of the phase is of third or higher order. Such situations occur, for example, at bifurcation points or in diffraction effects, (such as waves near sharp corners, waves creeping around obstacles, etc.).* [7] *In such calculations, one meets Airy functions integrals of the form*

$$Ai(x) = \frac{1}{2\pi} \int_{-\infty}^{+\infty} dy\, e^{i(xy - \frac{y^3}{3})} . \tag{33.28}$$

Calculate the Airy function $Ai(x)$ using the stationary phase approximation. What happens when considering the limit $x \to 0$. Estimate for which value of x [8] *the stationary phase approximation breaks down.*

[6] Tanner: Predrag: It is not quite clear to me what you are up to; give more guidance ...

[7] Tanner: Is this true. PC: Remarks to additional chapters

[8] Dorte: ulaeseligt

de Broglie wavelength
quantum!interference

Chapter 34

Semiclassical evolution

find the full reference

> William Rowan Hamilton was born in 1805. At three he could read English; by four he began to read Latin, Greek and Hebrew, by ten he read Sanskrit, Persian, Arabic, Chaldee, Syrian and sundry Indian dialects. At age seventeen he began to think about optics, and worked out his great principle of "Characteristic Function".
>
> Turnbull, *Lives of Mathematicians*

(G. Vattay, G. Tanner and P. Cvitanović)

Semiclassical approximations to quantum mechanics are valid in the regime where the de Broglie wavelength $\lambda \sim \hbar/p$ of a particle with momentum p is much shorter than the length scales across which the potential of the system changes significantly. In the short wavelength approximation the particle is a point-like object bouncing off potential walls, the same way it does in the classical mechanics. The novelty of quantum mechanics is the interference of the point-like particle with other versions of itself traveling along different classical trajectories, a feat impossible in classical mechanics. The short wavelength – or semiclassical – formalism is developed by formally taking the limit $\hbar \to 0$ in quantum mechanics in such a way that quantum quantities go to their classical counterparts. [1]

Brack has a nice discussion

☞ remark 34.1

34.1 Hamilton-Jacobi theory

We saw in chapter 33 that for a 1-dof particle moving in a slowly varying potential, it makes sense to generalize the free particle wave function (33.1) to a wave function

include qm.tex remarks

$$\psi(q,t) = A(q,t)e^{iR(q,t)/\hbar}\,, \tag{34.1}$$

[1] Tanner: Debatable; this limit is quite tricky in general ....

WKB
Wentzel-Kramers-Brillouin
Hamilton!-Jacobi equation
semiclassical!approximation
Hamilton!equations

with slowly varying (real) amplitude $A(q,t)$ and rapidly varying (real) phase $R(q,t)$. its phase and magnitude. The time evolution of the phase and the magnitude of ψ follows from the Schrödinger equation (32.1)

$$\left(i\hbar\frac{\partial}{\partial t}+\frac{\hbar^2}{2m}\frac{\partial^2}{\partial q^2}-V(q)\right)\psi(q,t)=0\,. \tag{34.2}$$

Assume $A\neq 0$, and separate out the real and the imaginary parts. We get two equations: The real part governs the time evolution of the phase

$$\frac{\partial R}{\partial t}+\frac{1}{2m}\left(\frac{\partial R}{\partial q}\right)^2+V(q)-\frac{\hbar^2}{2m}\frac{1}{A}\frac{\partial^2}{\partial q^2}A=0\,, \tag{34.3}$$

and the imaginary part the time evolution of the amplitude

$$\frac{\partial A}{\partial t}+\frac{1}{m}\sum_{i=1}^{D}\frac{\partial A}{\partial q_i}\frac{\partial R}{\partial q_i}+\frac{1}{2m}A\frac{\partial^2 R}{\partial q^2}=0\,. \tag{34.4}$$

In this way a linear PDE for a complex wave function is converted into a set of coupled non-linear PDE's for real-valued functions R and A. The coupling term in (34.3) is, however, of order $\hbar^2$ and thus small in the semiclassical limit $\hbar\to 0$.

Now we generalize the *Wentzel-Kramers-Brillouin* (WKB) *ansatz* for 1-dof dynamics to the Van Vleck *ansatz* in arbitrary dimension: we assume the magnitude $A(q,t)$ varies slowly compared to the phase $R(q,t)/\hbar$, so we drop the $\hbar$-dependent term. In this approximation the phase $R(q,t)$ and the corresponding "momentum field" $\frac{\partial R}{\partial q}(q,t)$ can be determined from the amplitude independent equation

$$\frac{\partial R}{\partial t}+H\left(q,\frac{\partial R}{\partial q}\right)=0\,. \tag{34.5}$$

In classical mechanics this equation is known as the *Hamilton-Jacobi equation*. We will refer to this step (as well as all leading order in $\hbar$ approximations to follow) as the *semiclassical approximation* to wave mechanics, and from now on work only within this approximation.

add Artuso lects. p.29 density, semicl. momentum

34.1.1 Hamilton's equations

We now solve the nonlinear partial differential equation (34.5) in a way the 17 year old Hamilton might have solved it. The main step is the step leading from the nonlinear PDE (34.9) to Hamilton's ODEs (34.10). If you already understand the Hamilton-Jacobi theory, you can safely skip this section.

Hamiltonian

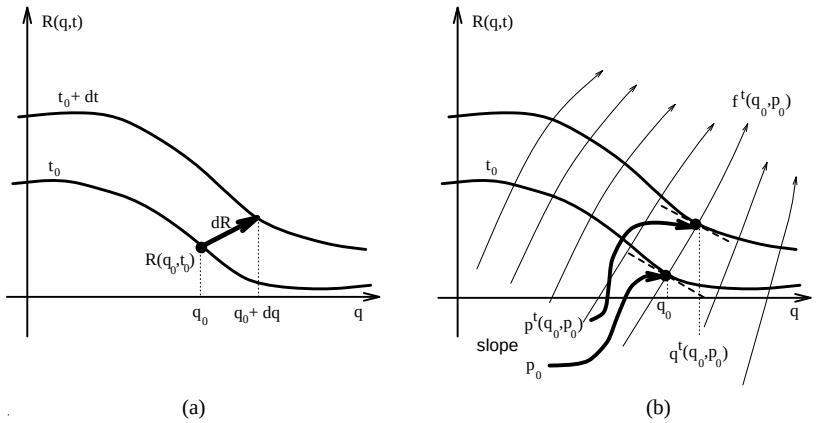

Figure 34.1: (a) A phase $R(q,t)$ plotted as a function of the position q for two infinitesimally close times. (b) The phase $R(q,t)$ transported by a swarm of "particles"; The Hamilton's equations (34.10) construct $R(q,t)$ by transporting $q_0 \to q(t)$ and the slope of $R(q_0,t_0)$, that is $p_0 \to p(t)$.

fast track:
sect. 34.1.3, p. 630

The wave equation (32.1) describes how the wave function ψ evolves with time, and if you think of ψ as an (infinite dimensional) vector, position q plays a role of an index. In one spatial dimension the phase R plotted as a function of the position q for two different times looks something like figure 34.1 (a): The phase $R(q,t_0)$ deforms smoothly with time into the phase $R(q,t)$ at time t. Hamilton's idea was to let a swarm of particles transport R and its slope $\partial R/\partial q$ at q at initial time $t=t_0$ to a corresponding $R(q,t)$ and its slope at time t, figure 34.1 (b). For notational convenience, define

$$p_i = p_i(q,t) := \frac{\partial R}{\partial q_i}\,, \quad i = 1,2,\ldots,D\,. \tag{34.6}$$

We saw earlier that (34.3) reduces in the semiclassical approximation to the Hamilton-Jacobi equation (34.5). To make life simple, we shall assume throughout this chapter that the Hamilton's function $H(q,p)$ does not depend explicitly on time t, i.e., the energy is conserved.

To start with, we also assume that the function $R(q,t)$ is smooth and well defined for every q at the initial time t. This is true for sufficiently short times; as we will see later, R develops folds and becomes multi-valued as t progresses. Consider now the variation of the function $R(q,t)$ with respect to independent infinitesimal variations of the time and space coordinates dt and dq, figure 34.1 (a)

$$dR = \frac{\partial R}{\partial t}dt + \frac{\partial R}{\partial q}dq\,. \tag{34.7}$$

Dividing through by dt and substituting (34.5) we obtain the total derivative

of $R(q,t)$ with respect to time *along the as yet arbitrary direction* $\dot{q}$, that is,

$$\frac{dR}{dt}(q,\dot{q},t) = -H(q,p) + \dot{q}\cdot p\,. \tag{34.8}$$

Note that the "momentum" $p = \partial R/\partial q$ is a well defined function of q and t. In order to integrate $R(q,t)$ with the help of (34.8) we also need to know how $p = \partial R/\partial q$ changes along $\dot{q}$. Varying p with respect to independent infinitesimal variations dt and dq and substituting the Hamilton-Jacobi equation (34.5) yields

$$d\frac{\partial R}{\partial q} = \frac{\partial^2 R}{\partial q \partial t}dt + \frac{\partial^2 R}{\partial q^2}dq = -\left(\frac{\partial H}{\partial q} + \frac{\partial H}{\partial p}\frac{\partial p}{\partial q}\right)dt + \frac{\partial p}{\partial q}dq\,.$$

Note that $H(q,p)$ depends on q also through $p(q,t) = \partial R/\partial q$, hence the $\frac{\partial H}{\partial p}$ term in the above equation. Dividing again through by dt we get the time derivative of $\partial R/\partial q$, that is,

$$\dot{p}(q,\dot{q},t) + \frac{\partial H}{\partial q} = \left(\dot{q} - \frac{\partial H}{\partial p}\right)\frac{\partial p}{\partial q}\,. \tag{34.9}$$

Time variation of p depends not only on the yet unknown $\dot{q}$, but also on the second derivatives of R with respect to q with yet unknown time dependence. However, if we *choose* $\dot{q}$ (which was arbitrary, so far) such that the right hand side of the above equation vanishes, we can calculate the function $R(q,t)$ along a specific trajectory $(q(t),p(t))$ given by integrating the ordinary differential equations

$$\dot{q} = \frac{\partial H(q,p)}{\partial p}, \qquad \dot{p} = -\frac{\partial H(q,p)}{\partial q} \tag{34.10}$$

with initial conditions

$$q(t_0) = q', \qquad p(t_0) = p' = \frac{\partial R}{\partial q}(q',t_0). \tag{34.11}$$

☞ sect. 5.1

We recognize (34.10) as Hamilton's equations of motion of classical mechanics. The miracle happens in the step leading from (34.5) to (34.9) – if you missed it, you have missed the point. Hamilton derived his equations contemplating optics - it took him three more years to realize that all of Newtonian dynamics can be profitably recast in this form.

$\dot{q}$ is no longer an independent function, and the phase $R(q,t)$ can now be computed by integrating equation (34.8) along the trajectory $(q(t),p(t))$

$$\begin{aligned} R(q,t) &= R(q',t_0) + R(q,t;q',t_0) \\ R(q,t;q',t_0) &= \int_{t_0}^{t} d\tau\,[\dot{q}(\tau)\cdot p(\tau) - H(q(\tau),p(\tau))]\,, \end{aligned} \tag{34.12}$$

with the initial conditions (34.11). In this way the Hamilton-Jacobi *partial* differential equation (34.3) is solved by integrating a set of *ordinary* differential equations, Hamilton's equations. In order to determine $R(q,t)$ for arbitrary q and t we have to find a q' such that the trajectory starting in $(q', p' = \partial_q R(q', t_0))$ reaches q in time t and then compute R along this trajectory, see figure 34.1 (b). The integrand of (34.12) is known as the *Lagrangian*,

Lagrangian
Hamilton!principal function
Legendre transform
action

$$L(q, \dot{q}, t) = \dot{q} \cdot p - H(q, p, t)\,. \tag{34.13}$$

A variational principle lurks here, but we shall not make much fuss about it as yet.

Throughout this chapter we assume that the energy is conserved, and that the only time dependence of $H(q,p)$ is through $(q(\tau), p(\tau))$, so the value of $R(q,t;q',t_0)$ does not depend on t_0, but only on the elapsed time $t - t_0$. To simplify notation we will set $t_0 = 0$ and write

$$R(q, q', t) = R(q, t; q', 0)\,.$$

The initial momentum of the particle must coincide with the initial momentum of the trajectory connecting q' and q:

rethink

$$p' = \frac{\partial}{\partial q'} R(q', 0) = -\frac{\partial}{\partial q'} R(q, q', t). \tag{34.14}$$

The function $R(q, q', t)$ is known as *Hamilton's principal function*.

34.7 page 649
34.11 page 649

To summarize: Hamilton's achievement was to trade in the Hamilton-Jacobi *partial* differential equation (34.5) describing the evolution of a wave front for a finite number of *ordinary* differential equations of motion, with the initial phase $R(q,0)$ incremented by the integral (34.12) evaluated along the phase space trajectory $(q(\tau), p(\tau))$.

34.1.2 Action

Before proceeding, we note in passing a few facts about Hamiltonian dynamics that will be needed for the construction of semiclassical Green's functions. If the energy is conserved, the $\int H(q,p)d\tau$ integral in (34.12) is simply Et. The first term, or the *action*

$$S(q, q', E) = \int_0^t d\tau\, \dot{q}(\tau) \cdot p(\tau) = \int_{q'}^{q} dq \cdot p \tag{34.15}$$

is integrated along a trajectory from q' to q with a fixed energy E. By (34.12) the action is a Legendre transform of Hamilton's principal function

$$S(q, q', E) = R(q, q', t) + Et\,. \tag{34.16}$$

Lagrangian!manifold
Stokes theorem

The time of flight t along the trajectory connecting $q' \to q$ with fixed energy E is given by

$$\frac{\partial}{\partial E} S(q, q', E) = t \,. \tag{34.17}$$

The way to think about the formula (34.16) for action is that the time of flight is a function of the energy, $t = t(q, q', E)$. The left hand side is explicitly a function of E; the right hand side is an implicit function of E through energy dependence of the flight time t.

Going in the opposite direction, the energy of a trajectory $E = E(q, q', t)$ connecting $q' \to q$ with a given time of flight t is given by the derivative of Hamilton's principal function

$$\frac{\partial}{\partial t} R(q, q', t) = -E \,, \tag{34.18}$$

and the second variations of R and S are related in the standard way of Legendre transforms:

$$\frac{\partial^2}{\partial t^2} R(q, q', t) \frac{\partial^2}{\partial E^2} S(q, q', E) = -1 \,. \tag{34.19}$$

A geometric visualization of what the phase evolution looks like is very helpful in understanding the origin of topological indices to be introduced in what follows. Given an initial phase $R(q, t_0)$, the gradient $\partial_q R$ defines a D-dimensional *Lagrangian manifold* $(q,\ p = \partial_q R(q))$ in the full $2d$ dimensional phase space (q, p). The defining property of this manifold is that any contractible loop γ in it has zero action,

☞ sect. 34.1.5

$$0 = \oint_\gamma dq \cdot p,$$

a fact that follows from the definition of p as a gradient, and the Stokes theorem. Hamilton's equations of motion preserve this property and map a Lagrangian manifold into a Lagrangian manifold at a later time. t

Returning back to the main line of our argument: so far we have determined the wave function phase $R(q, t)$. Next we show that the velocity field given by the Hamilton's equations together with the continuity equation determines the amplitude of the wave function.

34.1.3 Density evolution

To obtain the full solution of the Schrödinger equation (32.1), we also have to integrate (34.4).

$$\rho(q, t) := A^2 = \psi^* \psi$$

plays the role of a density. To the leding order in $\hbar$, the gradient of R may be interpreted as the semiclassical momentum density

continuity equation

$$\psi(q,t)^*(-i\hbar\frac{\partial}{\partial q})\psi(q,t) \;=\; -i\hbar A\frac{\partial A}{\partial q} + \rho\frac{\partial R}{\partial q}\,.$$

Evaluated along the trajectory $(q(t),p(t))$, the amplitude equation (34.4) is equivalent to the continuity equation (9.35) after multiplying (34.4) by $2A$, that is

⇓PRELIMINARY
34.12
page 649
⇑PRELIMINARY

$$\frac{\partial\rho}{\partial t} + \frac{\partial}{\partial q_i}(\rho v_i) = 0\,. \tag{34.20}$$

Here, $v_i = \dot{q}_i = p_i/m$ denotes a velocity field, which is in turn determined by the gradient of $R(q,t)$, or the *Lagrangian manifold* $(q(t),p(t)=\partial_q R(q,t))$,

$$v = \frac{1}{m}\frac{\partial}{\partial q}R(q,t).$$

As we already know how to solve the Hamilton-Jacobi equation (34.5), we can also solve for the density evolution as follows:

The density $\rho(q)$ can be visualized as the density of a configuration space flow $q(t)$ of a swarm of hypothetical particles; the trajectories $q(t)$ are solutions of Hamilton's equations with initial conditions given by $(q(0) = q', p(0) = p' = \partial_q R(q',0))$.

If we take a small configuration space volume d^Dq around some point q at time t, then the number of particles in it is $\rho(q,t)d^Ddq$. They started initially in a small volume d^Dq' around the point q' of the configuration space. For the moment, we assume that there is only one solution, the case of several paths will be considered below. The number of particles at time t in the volume is the same as the number of particles in the initial volume at $t = 0$,

$$\rho(q(t),t)d^Dq = \rho(q',0)d^Dq'\,,$$

see figure 34.2. [2] The ratio of the initial and the final volumes can be expressed as

$$\rho(q(t),t) = \left|\det\frac{\partial q'}{\partial q}\right|\rho(q',0)\,. \tag{34.21}$$

☞ sect. 9.2

As we know how to compute trajectories $(q(t),p(t))$, we know how to compute this Jacobian and, by (34.21), the density $\rho(q(t),t)$ at time t.

⇓PRELIMINARY

semiclassical!wave function
wave function!semiclassical

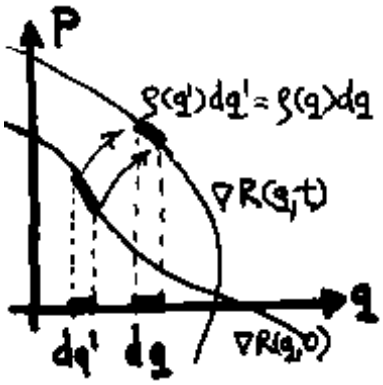

Figure 34.2: Density evolution of an initial surface $(q', p' = \partial_q R(q', 0)$ into $(q(t), p(t))$ surface time t later, sketched in 1 dimension. While the number of trajectories and the phase space Liouville volume are conserved, the density of trajectories projected on the q coordinate varies; trajectories which started in dq' at time zero end up in the interval dq.

34.1.4 Topological index

more part of previous here!

34.1.5 Semiclassical wave function

⇑PRELIMINARY

Now we have all ingredients to write down the semiclassical wave function at time t. Consider first the case when our initial wave function can be written in terms of single-valued functions $A(q', 0)$ and $R(q', 0)$. For sufficiently short times, $R(q, t)$ will remain a single-valued function of q, and every $d^D q$ configuration space volume element keeps its orientation. The evolved wave function is in the semiclassical approximation then given by

$$\begin{aligned} \psi_{sc}(q,t) &= A(q,t)e^{iR(q,t)/\hbar} = \sqrt{\det \frac{\partial q'}{\partial q}}\, A(q',0)e^{i(R(q',0)+R(q,q',t))/\hbar} \\ &= \sqrt{\det \frac{\partial q'}{\partial q}}\, e^{iR(q,q',t)/\hbar}\, \psi(q',0)\,. \end{aligned}$$

As the time progresses the Lagrangian manifold $\partial_q R(q, t)$ can develop folds, so for longer times the value of the phase $R(q, t)$ is not necessarily unique; in general more than one trajectory will connect points q and q' with different phases $R(q, q', t)$ accumulated along these paths, see figure 34.3.

We thus expect in general a collection of different trajectories from q' to q which we will index by j, with different phase increments $R_j(q, q', t)$. The hypothetical particles of the density flow at a given configuration space point can move with different momenta $p = \partial_q R_j(q, t)$. This is not an ambiguity, since in the full (q, p) phase space each particle follows its own trajectory with a unique momentum.

Whenever the Lagrangian manifold develops a fold, the density of the phase space trajectories in the fold projected on the configuration coordinates diverges. As illustrated in figure 34.3, when the Lagrangian manifold develops a fold at $q = q_1$; the volume element dq_1 in the neighborhood of the folding point is proportional to $\sqrt{dq'}$ instead of dq'. The Jacobian $\partial q'/\partial q$ diverges like $1/\sqrt{q_1 - q(t)}$ when computed along the trajectory

finish editing

[2] Tanner: Better picture needed

going trough the folding point at q_1. After the folding the orientation of the interval dq' has changed when being mapped into dq_2; in addition the function R, as well as its derivative which defines the Lagrangian manifold, becomes multi-valued. Distinct trajectories starting from different initial points q' can now reach the same final point q_2. (That is, the point q' may have more than one pre-image.) The projection of a simple fold, or of an envelope of a family of phase space trajectories, is called a *caustic*; this expression comes from the Greek word for "capable of burning", evoking the luminous patterns that one observes swirling across the bottom of a swimming pool.

caustic
topological!index
WKB!wave function
wave function!WKB
semiclassical!propagator
propagator!semiclassical

The folding also changes the orientation of the pieces of the Lagrangian manifold $(q, \partial_q R(q,t))$ with respect to the initial manifold, so the eigenvalues of the Jacobian determinant change sign at each fold crossing. We can keep track of the signs by writing the Jacobian determinant as

$$\det \left.\frac{\partial q'}{\partial q}\right|_j = e^{-i\pi m_j(q,q',t)} \left|\det \left.\frac{\partial q'}{\partial q}\right|_j\right| ,$$

where $m_j(q,q',t)$ counts the number of sign changes of the Jacobian determinant on the way from q' to q along the trajectory indexed with j, see figure 34.3. [3] We shall refer to the integer $m_j(q,q',t)$ as the *topological* of the trajectory. [4] So in general the semiclassical approximation to the wave function is thus a sum over possible trajectories that start at any inital q' and end in q in time t

Morse index into Keller remark

$$\psi_{sc}(q,t) = \int dq' \sum_j \left|\det \left.\frac{\partial q'}{\partial q}\right|_j\right|^{1/2} e^{iR_j(q,q',t)/\hbar - i\pi m_j(q,q',t)/2} \psi(q'_j, 0) \,, \quad (34.22)$$

each contribution weighted by corresponding density, phase increment and the topological index. [5]

That the correct topological index is obtained by simply counting the number of eigenvalue sign changes and taking the square root is not obvious - the careful argument requires that quantum wave functions evaluated across the folds remain single valued. [6]

this argument is worse than the earlier version

draw multiple initial conditions in figure 34.3

34.2 Semiclassical propagator

We saw in chapter 32 that the evolution of an initial wave function $\psi(q,0)$ is completely determined by the propagator (32.12). As $K(q,q',t)$ itself satisfies the Schrödinger equation (32.14), we can treat it as a wave function

[3] Tanner: Better picture is needed
[4] Tanner: Check topological index
[5] Bartsch: need $||\partial q' \partial q||$, not $||\partial p' \partial q||$
[6] Tanner: Include littlejohn reference refref Litt92

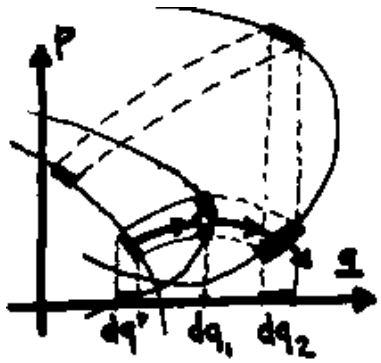

Figure 34.3: Folding of the Lagrangian surface $(q, \partial_q R(q,t))$.

parameterized by the configuration point q'. In order to obtain a semiclassical approximation to the propagator we follow now the ideas developed in the last section. There is, however, one small complication: the initial condition (32.15) demands that the propagator at $t = 0$ is a δ-function at $q = q'$, that is, the amplitude is infinite at q' and the phase is not well defined. Our hypothetical cloud of particles is thus initially localized at $q = q'$ with *any* initial velocity. This is in contrast to the situation in the previous section where we assumed that the particles at a given point q have well defined velocity (or a discrete set of velocities) given by $\dot{q} = \partial_p H(q,p)$. We will now derive at a semiclassical expression for $K(q,q',t)$ by considering the propagator for short times first, and extrapolating from there to arbitrary times t.

34.2.1 Short time propagator

For infinitesimally short times δt away from the singular point $t = 0$ we assume that it is again possible to write the propagator in terms of a well defined phase and amplitude, that is

$$K(q,q',\delta t) = A(q,q',\delta t)e^{\frac{i}{\hbar}R(q,q',\delta t)}\,.$$

As all particles start at $q = q'$, $R(q,q',\delta t)$ will be of the form (34.12), that is

$$R(q,q',\delta t) = p\dot{q}\delta t - H(q,p)\delta t\,, \tag{34.23}$$

with $\dot{q} \approx (q-q')/\delta t$. For Hamiltonians of the form (32.2) we have $\dot{q} = p/m$, which leads to

$$R(q,q',\delta t) = \frac{m(q-q')^2}{2\delta t} - V(q)\delta t\,.$$

Here V can be evaluated any place along the trajectory from q to q', for example at the midway point $V((q+q')/2)$. Inserting this into our ansatz for the propagator we obtain

$$K_{sc}(q,q',\delta t) \approx A(q,q',\delta t)e^{\frac{i}{\hbar}\left(\frac{m}{2\delta t}(q-q')^2 - V(q)\delta t\right)}\,. \tag{34.24}$$

Gaussian!integral, d-dimensional
Dirac delta function
propagator!short time

For infinitesimal times we can neglect the term $V(q)\delta t$, so $K_{sc}(q,q',\delta t)$ is a d-dimensional Gaussian with width $\sigma^2 = i\hbar\delta t/m$. This Gaussian is a finite width approximation to the Dirac delta function

$$\delta(z) = \lim_{\sigma\to 0} \frac{1}{\sqrt{2\pi\sigma^2}} e^{-z^2/2\sigma^2} \tag{34.25}$$

if $A = (m/2\pi i\hbar\delta t)^{D/2}$, with $A(q,q',\delta t)$ fixed by the Dirac delta function normalization condition. The correctly normalized propagator for infinitesimal times δt is therefore

34.2
page 648

$$K_{sc}(q,q',\delta t) \approx \left(\frac{m}{2\pi i\hbar\delta t}\right)^{D/2} e^{\frac{i}{\hbar}\left(\frac{m(q-q')^2}{2\delta t} - V(q)\delta t\right)} . \tag{34.26}$$

The short time dynamics of the Lagrangian manifold $(q, \partial_q R)$ which corresponds to the quantum propagator can now be deduced from (34.23); one obtains

$$\frac{\partial R}{\partial q} = p \approx \frac{m}{\delta t}(q-q') ,$$

i.e., is the particles start for short times on a Lagrangian manifold which is a plane in phase space, see figure 34.4. [7] Note, that for $\delta t \to 0$, this plane is given by the condition $q = q'$, that is, particles start on a plane parallel to the momentum axis. As we have already noted, all particles start at $q = q'$ but with different velocities for $t = 0$. The inital surface $(q', p' = \partial_q R(q', 0))$ is mapped into the surface $(q(t), p(t))$ some time t later. The slope of the Lagrangian plane for a short finite time is given as

$$\frac{\partial p_i}{\partial q_j} = -\frac{\partial^2 R}{\partial q_j \partial q'_i} = -\frac{\partial p'_i}{\partial q_j} = \frac{m}{\delta t}\delta_{ij} .$$

The prefactor $(m/\delta t)^{D/2}$ in (34.26) can therefore be interpreted as the determinant of the Jacobian of the transformation from final position coordinates q to initial momentum coordinates p', that is

$$K_{sc}(q,q',\delta t) = \frac{1}{(2\pi i\hbar)^{D/2}} \left(\det \frac{\partial p'}{\partial q}\right)^{1/2} e^{iR(q,q',\delta t)/\hbar}, \tag{34.27}$$

where

$$\left.\frac{\partial p'_i}{\partial q_j}\right|_{t,q'} = \frac{\partial^2 R(q,q',\delta t)}{\partial q_j \partial q'_i} \tag{34.28}$$

The subscript $\cdots|_{t,q'}$ indicates that the partial derivatives are to be evaluated with t, q' fixed.

propagator!Van Vleck
Van Vleck!propagator

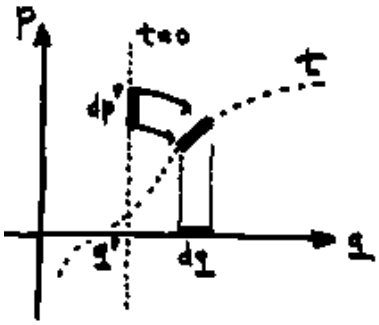

Figure 34.4: Evolution of the semiclassical propagator. The configuration which corresponds to the initial conditions of the propagator is a Lagrangian manifold $q = q'$, that is, a plane parallel to the p axis. The hypothetical particles are thus initially all placed at q' but take on all possible momenta p'. The Jacobian matrix C (34.29) relates an initial volume element in momentum space dp' to a final configuration space volume dq.

figure 34.4

The propagator in (34.27) has been obtained for short times. It is, however, already more or less in its final form. We only have to evolve our short time approximation of the propagator according to (34.22) [8]

$$K_{sc}(q'', q', t' + \delta t) = \sum_j \left| \det \frac{\partial q}{\partial q''} \right|_j^{1/2} e^{iR_j(q'',q,t')/\hbar - i\pi m_j(q'',q,t')/2} K(q, q'_j, \delta t)\,,$$

and we included here already the possibility that the phase becomes multi-valued, that is, that there is more than one path from q' to q''. The topological index $m_j = m_j(q'', q', t)$ is the number of singularities in the Jacobian along the trajectory j from q' to q''. We can write $K_{sc}(q'', q', t'+\delta t)$ in closed form using the fact that $R(q'', q, t') + R(q, q', \delta t) = R(q'', q', t' + \delta t)$ and the multiplicativity of Jacobian determinants, that is

$$\det \left. \frac{\partial q}{\partial q''} \right|_t \det \left. \frac{\partial p'}{\partial q} \right|_{q',\delta t} = \det \left. \frac{\partial p'}{\partial q''} \right|_{q',t'+\delta t} . \tag{34.29}$$

The final form of the semiclassical or *Van Vleck propagator*, is thus [9]

$$K_{sc}(q, q', t) = \sum_j \frac{1}{(2\pi i\hbar)^{D/2}} \left| \det \frac{\partial p'}{\partial q} \right|^{1/2} e^{iR_j(q,q',t)/\hbar - im_j\pi/2} . \tag{34.30}$$

This Van Vleck propagator is the essential ingredient of the semiclassical quantization to follow.

The apparent simplicity of the semiclassical propagator is deceptive. The wave function is not evolved simply by multiplying by a complex number of magnitude $\sqrt{\det \partial p'/\partial q}$ and phase $R(q, q', t)$; the more difficult task in general is to find the trajectories connecting q' and q in a given time t.

[7] Tanner: make a figure here
[8] Bartsch: cheat! need to do a saddlepoint integral here
[9] Tanner: Reference in the remarks

In addition, we have to treat the approximate propagator (34.30) with some care. Unlike the full quantum propagator, which satisfies the group property (32.13) exactly, the semiclassical propagator performs this only approximately, that is

stationary!phase approximation
Feynman path integral

$$K_{sc}(q,q',t_1+t_2) \approx \int dq''\, K_{sc}(q,q'',t_2)K_{sc}(q'',q',t_1)\,. \tag{34.31}$$

The connection can be made explicit by the stationary phase approximation, sect. 33.2. Approximating the integral in (34.31) by integrating only over regions near points q'' at which the phase is stationary, leads to the stationary phase condition

$$\frac{\partial R(q,q'',t_2)}{\partial q_i''} + \frac{\partial R(q'',q',t_1)}{\partial q_i''} = 0. \tag{34.32}$$

Classical trajectories contribute whenever the final momentum for a path from q' to q'' and the initial momentum for a path from q'' to q coincide. Unlike the classical evolution of sect. 10.2, the semiclassical evolution is not an evolution by linear operator multiplication, but evolution supplemented by a stationary phase condition $p_{out} = p_{in}$ that matches up the classical momenta at each evolution step.

crosslink with sect. 33.2

⇓PRELIMINARY
34.16
page 650
⇑PRELIMINARY

for notes: written in 1928; topological phase introduced by Gutzwiller

34.2.2 Free particle propagator

To develop some intuition about the above formalism, consider the case of a free particle. For a free particle the potential energy vanishes, the kinetic energy is $\frac{m}{2}\dot{q}^2$, and the Hamilton's principal function (34.12) is

$$R(q,q',t) = \frac{m(q-q')^2}{2t}\,. \tag{34.33}$$

The weight $\det \frac{\partial p'}{\partial q}$ from (34.28) can be evaluated explicitly, and the Van Vleck propagator is

$$K_{sc}(q,q',t) = \left(\frac{m}{2\pi i\hbar t}\right)^{D/2} e^{im(q-q')^2/2\hbar t}\,, \tag{34.34}$$

identical to the short time propagator (34.26), with $V(q) = 0$. This case is rather exceptional: for a free particle the semiclassical propagator turns out to be the exact quantum propagator $K(q,q',t)$, as can be checked by substitution in the Schrödinger equation (34.2). The Feynman path integral formalism uses this fact to construct an exact quantum propagator by integrating the free particle propagator (with $V(q)$ treated as constant for short times) along all possible (not necessarily classical) paths from q' to q.

☞ remark 34.4

migh move this to a remark
34.13
page 650
34.14
page 650
34.15

34.3 Semiclassical Green's function

So far we have derived semiclassical formulas for the time evolution of wave functions, that is, we obtained approximate solutions to the time dependent Schrödinger equation (32.1). Even though we assumed in the calculation a time independent Hamiltonian of the special form (32.2), the derivation would lead to the same final result (34.30) were one to consider more complicated or explicitly time dependent Hamiltonians. The propagator is thus important when we are interested in finite time quantum mechanical effects. For time independent Hamiltonians, the time dependence of the propagator as well as of wave functions is, however, essentially given in terms of the energy eigen-spectrum of the system, as in (32.10). It is therefore advantageous to switch from a time representation to an energy representation, that is from the propagator (32.12) to the energy dependent Green's function (32.16). A semiclassical approximation of the Green's function $G_{sc}(q,q',E)$ is given by the Laplace transform (32.16) of the Van Vleck propagator $K_{sc}(q,q',t)$:

$$G_{sc}(q,q',E) = \frac{1}{i\hbar}\int_0^\infty dt\, e^{iEt/\hbar} K_{sc}(q,q',t)\,. \tag{34.35}$$

The expression as it stands is not very useful; in order to evaluate the integral, at least to the leading order in $\hbar$, we need to turn to the method of stationary phase again.

34.3.1 Stationary phase in higher dimensions

33.1
page 624

Generalizing the method of sect. 33.2 to d dimensions, consider stationary phase points fulfilling

$$\frac{d}{dx_i}\Phi(x)\Big|_{x=x_0} = 0 \quad \forall i = 1,\dots d\,.$$

An expansion of the phase up to second order involves now the symmetric matrix of second derivatives of $\Phi(x)$, that is

$$D_{ij}(x_0) = \frac{\partial^2}{\partial x_i \partial x_j}\Phi(x)\Big|_{x=x_0}\,.$$

After choosing a suitable coordinate system which diagonalizes D, we can approximate the d-dimensional integral by d one-dimensional Fresnel integrals; the stationary phase estimate of (33.13) is then

$$I \approx \sum_{x_0} (2\pi i/s)^{d/2}\, |\det D(x_0)|^{-1/2} A(x_0)\, e^{is\Phi(x_0) - \frac{i\pi}{2}m(x_0)}\,, \tag{34.36}$$

where the sum runs over all stationary phase points x_0 of $\Phi(x)$ and $m(x_0)$ counts the number of negative eigenvalues of $D(x_0)$.

zero eigenvalue
eigenvalue!zero

34.3 648

The stationary phase approximation is all that is needed for the semiclassical approximation, with the proviso that D in (34.36) has no zero eigenvalues.

34.4 648

33.3 624

⇓PRELIMINARY

34.3.2 Topological index

How do we actually *determine* the topological index? The argument goes something like this:

An interpretation is that as the trajectory went through a turning point, the d^2R/dq^2 has changed sign.

In D-dof the argument is that this folding of the Lagrangian manifold (trajectory reversing direction) happens generically separately for each (q_i, p_i) pair, $i = 1, 2, ..., d$. Exceptions are classified by the catastrophe theory and do not concern us here and now. Hence at a turning point in the ith direction the remaining directions can be integrated in the Gaussian way as usual, and the ith one picks up $e^{-i\pi/2}$ phase shift; one interpretation is that the ith eigenvalue of d^2R/dq_jdq_k has changed sign.

There is another claim - that one is counting the number of times the neighborhood of the classical periodic trajectory twists around before reconnecting after one period, but I do not know how to make that a simple argument.

⇑PRELIMINARY

34.3.3 Long trajectories

When evaluating the integral (34.35) approximately we have to distinguish between two types of contributions: those coming from stationary points of the phase and those coming from infinitesimally short times. The first type of contributions can be obtained by the stationary phase approximation and will be treated in this section. The latter originate from the singular behavior of the propagator for $t \to 0$ where the assumption that the amplitude changes slowly compared to the phase is not valid. The short time contributions therefore have to be treated separately, which we will do in sect. 34.3.4.

The stationary phase points t^* of the integrand in (34.35) are given by the condition

$$\frac{\partial}{\partial t} R(q, q', t^*) + E = 0\,. \tag{34.37}$$

We recognize this condition as the solution of (34.18), the time $t^* = t^*(q, q', E)$ in which a particle of energy E starting out in q' reaches q. Taking into

action

account the second derivative of the phase evaluated at the stationary phase point,

$$R(q,q',t)+Et = R(q,q',t^*)+Et^*+\frac{1}{2}(t-t^*)^2\frac{\partial^2}{\partial t^2}R(q,q',t^*)+\cdots$$

the stationary phase approximation of the integral corresponding to a classical trajectory j in the Van Vleck propagator sum (34.30) yields

$$G_j(q,q',E) = \frac{1}{i\hbar(2i\pi\hbar)^{(D-1)/2}}\left|\det C_j\left(\frac{\partial^2 R_j}{\partial t^2}\right)^{-1}\right|^{1/2} e^{\frac{i}{\hbar}S_j-\frac{i\pi}{2}m_j}\,, \quad (34.38)$$

where $m_j = m_j(q,q',E)$ now includes a possible additional phase arising from the time stationary phase integration (33.16), and $C_j = C_j(q,q',t^*)$, $R_j = R_j(q,q',t^*)$ are evaluated at the transit time t^*. We re-express the phase in terms of the energy dependent action (34.16)

$$S(q,q',E) = R(q,q',t^*)+Et^*\,, \qquad \text{with} \quad t^* = t^*(q,q',E)\,, \quad (34.39)$$

the Legendre transform of Hamilton's principal function. Note that the partial derivative of the action (34.39) with respect to q_i

$$\frac{\partial S(q,q',E)}{\partial q_i} = \frac{\partial R(q,q',t^*)}{\partial q_i}+\left(\frac{\partial R(q,q',t)}{\partial t^*}+E\right)\frac{\partial t}{\partial q_i}.$$

is equal to

$$\frac{\partial S(q,q',E)}{\partial q_i} = \frac{\partial R(q,q',t^*)}{\partial q_i}, \quad (34.40)$$

due to the stationary phase condition (34.37), so the definition of momentum as a partial derivative with respect to q remains unaltered by the Legendre transform from time to energy domain.

34.17
page 650

Next we will simplify the amplitude term in (34.38) and rewrite it as an explicit function of the energy. Consider the $[(D+1)\times(D+1)]$ matrix

$$D(q,q',E) = \begin{pmatrix} \frac{\partial^2 S}{\partial q'\partial q} & \frac{\partial^2 S}{\partial q'\partial E} \\ \frac{\partial^2 S}{\partial q\partial E} & \frac{\partial^2 S}{\partial E^2} \end{pmatrix} = \begin{pmatrix} -\frac{\partial p'}{\partial q} & -\frac{\partial p'}{\partial E} \\ \frac{\partial t}{\partial q} & \frac{\partial t}{\partial E} \end{pmatrix}, \quad (34.41)$$

where $S = S(q,q',E)$ and we used (34.14–34.17) here to obtain the left hand side of (34.41). The minus signs follow from observing from the definition of (34.15) that $S(q,q',E) = -S(q',q,E)$. Note that D is nothing but the Jacobian matrix of the coordinate transformation $(q,E)\to(p',t)$

for fixed q'. We can therefore use the multiplication rules of determinants of Jacobians, which are just ratios of volume elements, to obtain

ELIMINARY
34.19
650
ELIMINARY

$$\begin{aligned}\det D &= (-1)^{D+1}\left(\det\frac{\partial(p',t)}{\partial(q,E)}\right)_{q'} = (-1)^{D+1}\left(\det\frac{\partial(p',t)}{\partial(q,t)}\frac{\partial(q,t)}{\partial(q,E)}\right)_{q'}\\ &= (-1)^{D+1}\left(\det\frac{\partial p'}{\partial q}\right)_{t,q'}\left(\det\frac{\partial t}{\partial E}\right)_{q',q} = \det C\left(\frac{\partial^2 R}{\partial t^2}\right)^{-1}.\end{aligned}$$

We use here the notation $(\det .)_{q',t}$ for a Jacobian determinant with partial derivatives evaluated at t, q' fixed, and likewise for other subscripts. Using the relation (34.19) which relates the term $\frac{\partial t}{\partial E}$ to $\partial_t^2 R$ we can write the determinant of D as a product of the Van Vleck determinant (34.28) and the amplitude factor arising from the stationary phase approximation. The amplitude in (34.38) can thus be interpreted as the determinant of a Jacobian of a coordinate transformation which includes time and energy as independent coordinates. This causes the increase in the dimensionality of the matrix D relative to the Van Vleck determinant (34.28).

We can now write down the semiclassical approximation of the contribution of the jth trajectory to the Green's function (34.38) in explicitly energy dependent form:

$$G_j(q,q',E) = \frac{1}{i\hbar(2i\pi\hbar)^{(D-1)/2}}\left|\det D_j\right|^{1/2} e^{\frac{i}{\hbar}S_j - \frac{i\pi}{2}m_j}\,. \qquad (34.42)$$

However, this is still not the most convenient form of the Green's function.

The trajectory contributing to $G_j(q,q',E)$ is constrained to a given energy E, and will therefore be on a phase space manifold of constant energy, that is $H(q,p) = E$. Writing this condition as a partial differential equation for $S(q,q',E)$, that is

$$H(q,\frac{\partial S}{\partial q}) = E\,,$$

one obtains

$$\begin{aligned}\frac{\partial}{\partial q'_i}H(q,p) &= 0 = \frac{\partial H}{\partial p_j}\frac{\partial p_j}{\partial q'_i} = \dot q_j\frac{\partial^2 S}{\partial q_j\partial q'_i}\\ \frac{\partial}{\partial q_i}H(q',p') &= 0 = \frac{\partial^2 S}{\partial q_i\partial q'_j}\dot q'_j\,,\end{aligned} \qquad (34.43)$$

that is the sub-matrix $\partial^2 S/\partial q_i\partial q'_j$ has (left- and right-) eigenvectors corresponding to an eigenvalue 0. Rotate the local coordinate system at the either end of the trajectory

$$(q_1, q_2, q_3, \cdots, q_d) \to (q_\parallel, q_{\perp 1}, q_{\perp 2}, \cdots, q_{\perp(D-1)})$$

longitudinal!coordinate
coordinate!longitudinal
transverse!stability

so that one axis points along the trajectory and all others are perpendicular to it

$$(\dot{q_1}, \dot{q_2}, \dot{q_3}, \cdots, \dot{q_d}) \to (\dot{q}, 0, 0, \cdots, 0)\,.$$

With such local coordinate systems at both ends, with the longitudinal coordinate axis $q_\parallel$ pointing along the velocity vector of magnitude $\dot{q}$, the stability matrix of $S(q, q', E)$ has a column and a row of zeros as (34.43) takes form

$$\dot{q}\frac{\partial^2 S}{\partial q_\parallel \partial q'_i} = \frac{\partial^2 S}{\partial q_i \partial q'_\parallel}\dot{q'} = 0\,.$$

The initial and final velocities are non-vanishing except for points $|\dot{q}| = 0$. These are the turning points (where all energy is potential), and we assume that neither q nor q' is a turning point (in our application - periodic orbits - we can always chose $q = q'$ not a turning point). In the local coordinate system with one axis along the trajectory and all other perpendicular to it the determinant of (34.41) is of the form

$$\det D(q, q', E) = (-1)^{D+1} \begin{pmatrix} & 0 & 0 & \frac{\partial^2 S}{\partial E \partial q'_\parallel} \\ \det & 0 & \frac{\partial^2\ S}{\partial q_\perp \partial q'_\perp} & * \\ & \frac{\partial^2 S}{\partial q_\parallel \partial E} & * & * \end{pmatrix}\,. \quad (34.44)$$

The corner entries can be evaluated using (34.17)

$$\frac{\partial^2 S}{\partial q_\parallel \partial E} = \frac{\partial}{\partial q_\parallel} t = \frac{1}{\dot{q}}\,, \qquad \frac{\partial^2 S}{\partial E \partial q'_\parallel} = \frac{1}{\dot{q'}}\,.$$

As the $q_\parallel$ axis points along the velocity direction, velocities $\dot{q}$, $\dot{q}'$ are by construction almost always positive non-vanishing numbers. In this way the determinant of the $[(D+1)\times(D+1)]$ dimensional matrix $D(q, q', E)$ can be reduced to the determinant of a $[(D-1)\times(D-1)]$ dimensional *transverse* matrix $D_\perp(q, q', E)$

$$\begin{aligned} \det D(q, q', E) &= \frac{1}{\dot{q}\dot{q}'} \det D_\perp(q, q', E) \\ D_\perp(q, q', E)_{ik} &= -\frac{\partial^2 S(q, q', E)}{\partial q_{\perp i} \partial q'_{\perp k}}\,. \end{aligned} \quad (34.45)$$

Putting everything together we obtain the jth trajectory contribution to the semiclassical Green's function

34.20
page 650

$$G_j(q, q', E) = \frac{1}{i\hbar(2\pi i\hbar)^{(D-1)/2}} \frac{1}{|\dot{q}\dot{q}'|^{1/2}} \left|\det D_\perp^j\right|^{1/2} e^{\frac{i}{\hbar}S_j - \frac{i\pi}{2}m_j}\,, \quad (34.46)$$

where the topological index $m_j = m_j(q, q', E)$ now counts the number of changes of sign of $\det D_\perp^j$ along the trajectory j which connects q' to q at energy E.

The endpoint velocities $\dot{q}$, $\dot{q}'$ also depend on (q, q', E) and the trajectory j. [10]

Green's function!trace!long orbits
Green's function!short distance
propagator!short time
Hankel function
Green's function!short distance

34.3.4 Short trajectories

The stationary phase method cannot be used when t^* is small, both because we cannot extend the integration in (33.16) to $-\infty$, and because the amplitude of $K(q, q', t)$ is divergent. In this case we have to evaluate the integral involving the short time form of the exact quantum mechanical propagator (34.26)

$$G_0(q, q', E) = \frac{1}{i\hbar} \int_0^\infty dt \left(\frac{m}{2\pi i\hbar t}\right)^{D/2} e^{\frac{i}{\hbar}\left(\frac{m(q-q')^2}{2t} - V(q)t + Et\right)} . \quad (34.47)$$

handwritten insert "A" here

By introducing a dimensionless variable $\tau = t\sqrt{2m(E - V(q))}/m|q - q'|$, the integral can be rewritten as

simplify $\hbar k(q) = \sqrt{2m(E - V(q))}$

$$G_0(q, q', E) = \frac{m}{i\hbar^2(2\pi i)^{D/2}} \left(\frac{\sqrt{2m(E-V)}}{\hbar|q-q'|}\right)^{\frac{D}{2}-1} \int_0^\infty \frac{d\tau}{\tau^{D/2}} e^{\frac{i}{2\hbar}S_0(q,q',E)(\tau+1/\tau)},$$

where $S_0(q, q', E) = \sqrt{2m(E - V)}|q - q'|$ is the short distance form of the action. Using the integral representation of the Hankel function of first kind

$$H_\nu^+(z) = -\frac{i}{\pi} e^{-i\nu\pi/2} \int_0^\infty e^{\frac{1}{2}iz(\tau+1/\tau)} \tau^{-\nu-1} d\tau$$

we can write the short distance form of the Green's function as

$$G_0(q, q', E) \approx -\frac{im}{2\hbar^2} \left(\frac{\sqrt{2m(E-V)}}{2\pi\hbar|q-q'|}\right)^{\frac{D-2}{2}} H^+_{\frac{D-2}{2}}(S_0(q, q', E)/\hbar) . \quad (34.48)$$

Hankel functions are stabdard, and their the short wavelength asymptotics is described in standard reference books. The short distance Green's function approximation is valid when $S_0(q, q', E) \leq \hbar$.

[10] Bartsch: omit this: " While in the case of the propagator the initial momentum variations $\delta p'$ are unrestricted, for the Green's function the $(\delta q', \delta p')$ variations are restricted to the constant energy shell; the appearance of the $1/\dot{q}\dot{q}'$ weights in the Green's function can be traced to this constraint.

quantum!potential
hydrodynamical!interpretation of QM

Commentary

Remark 34.1 Limit $\hbar \to 0$. The semiclassical limit "$\hbar \to 0$" discussed in sect. 34 is a shorthand notation for the limit in which typical quantities like the actions R or S in semiclassical expressions for the propagator or the Green's function become large compared to $\hbar$. In the world that we live in the quantity $\hbar$ is a fixed physical constant whose value [34.8] is $1.054571596(82)\ 10^{-34}$ Js.

Remark 34.2 Madelung's fluid dynamics. Already Schrödinger [34.3] noted that

$$\rho = \rho(q,t) := A^2 = \psi^* \psi$$

plays the role of a density, and that the gradient of R may be interpreted as a local semiclassical momentum, as the momentum density is

$$\psi(q,t)^*(-i\hbar\frac{\partial}{\partial q})\psi(q,t) \ = \ -i\hbar A\frac{\partial A}{\partial q} + \rho\frac{\partial R}{\partial q}\,.$$

A very different interpretation of (34.3–34.4) has been given by Madelung [34.2], and then built upon by Bohm [34.6] and others [34.3, 34.7]. Keeping the $\hbar$ dependent term in (34.3), the ordinary differential equations driving the flow (34.10) have to be altered; if the Hamiltonian can be written as kinetic plus potential term $V(q)$ as in (32.2), the $\hbar^2$ term modifies the p equation of motion as

$$\dot{p_i} = -\frac{\partial}{\partial q_i}\left(V(q) + Q(q,t)\right)\,, \tag{34.49}$$

where, for the example at hand,

$$Q(q,t) = -\frac{\hbar^2}{2m}\frac{1}{\sqrt{\rho}}\frac{\partial^2}{\partial q^2}\sqrt{\rho} \tag{34.50}$$

interpreted by Bohm [34.6] as the "quantum potential". Madelung observed that Hamilton's equation for the momentum (34.49) can be rewritten as

$$\frac{\partial v_i}{\partial t} + \left(v\cdot\frac{\partial}{\partial q}\right)v_i = -\frac{1}{m}\frac{\partial V}{\partial q_i} - \frac{1}{m\rho}\frac{\partial}{\partial q_j}\sigma_{ij}\,, \tag{34.51}$$

where $\sigma_{ij} = \frac{\hbar^2\rho}{4m}\frac{\partial^2 \ln\rho}{\partial q_i \partial q_j}$ is the "pressure" stress tensor, $v_i = p_i/m$, and $\rho = A^2$ as defined [34.3] in sect. 34.1.3. We recall that the Eulerian $\frac{\partial}{\partial t} + \frac{\partial q_i}{\partial t}\frac{\partial}{\partial q_i}$ is the ordinary derivative of Lagrangian mechanics, that is $\frac{d}{dt}$. For comparison, the Euler equation for classical hydrodynamics is

$$\frac{\partial v_i}{\partial t} + \left(v\cdot\frac{\partial}{\partial q}\right)v_i = -\frac{1}{m}\frac{\partial V}{\partial q_i} - \frac{1}{m\rho}\frac{\partial}{\partial q_j}(p\delta_{ij})\,,$$

where $p\delta_{ij}$ is the pressure tensor.

The classical dynamics corresponding to quantum evolution is thus that of an "hypothetical fluid" experiencing $\hbar$ and ρ dependent stresses. The "hydrodynamic" interpretation of quantum mechanics has, however, not been very fruitful in practice.

Poincaré!-Cartan theorem
Morse index
index!Morse
Dirac path integral
Feynman path integral
Gutzwiller path integral
⇓PRELIMINARY
catastrophe theory

Remark 34.3 Lagrangian manifolds. Hamilton's equations of motion map a Lagrangian manifold into a Lagrangian manifold time t later. This fact is called the Poincaré-Cartan theorem. [11] V.P. Maslov [33.7] derived the topological index by the Lagrangian manifold technique in 1965-1967, apparently unaware at the time of Keller's work. V.I. Arnol'd knew Keller's papers, but when he showed that there exist a connection between the Morse index and the topological index in his 1967 article [33.9], the Lagrangian manifold formalism was more to his taste, and he chose to name the index after Maslov. The name "Maslov index" stuck.

☞ appendix A.7

⇑PRELIMINARY

Remark 34.4 Path integrals. The semiclassical propagator (34.30) can also be derived from Feynman's path integral formalism. Dirac was the first to discover that in the short-time limit the quantum propagator (34.34) is exact. Feynman noted in 1946 that one can construct the exact propagator of the quantum Schrödinger equation by formally summing over all possible (and emphatically not classical) paths from q' to q , i.e.,

⇓PRIVATE

$$\textit{Feynman path integral here}\,. \tag{34.52}$$

⇑PRIVATE

Gutzwiller started from the path integral to rederive Van Vleck's semiclassical expression for the propagator; Van Vleck's original derivation is very much in the spirit of what has presented in this chapter. He did, however, not consider the possibility of the formation of caustics or folds of Lagrangian manifolds and thus did not include the topological phases in his semiclassical expression for the propagator. Some 40 years later Gutzwiller [36.4] added the topological indices when deriving the semiclassical propagator from Feynman's path integral by stationary phase conditions. [12]

⇓PRELIMINARY

Remark 34.5 More general Hamiltonians. GT: Maybe remark here on non kinetic+potential Hamiltonians?

Remark 34.6 Catastrophe theory. In more exceptional cases when several eigenvalues diverge simultaneously one encounters higher order caustics, whose classification is the subject of *catastrophe theory*, see for example refref ?? for details.

⇑PRELIMINARY

[11] Tanner: Reference here

[12] Tanner: Could add some blah-blah about Morse, Keller and Maslov here; I would have to read that up, though. Bummer.

Green's function!semiclassical
semiclassical!Green's function
Laplace!transform

Résumé

The aim of the semiclassical or short-wavelength methods is to approximate a solution of the Schrödinger equation with a semiclassical wave function

$$\psi_{sc}(q,t) = \sum_j A_j(q,t) e^{iR_j(q,t)/\hbar} ,$$

accurate to the leading order in $\hbar$. Here the sum is over all classical trajectories that connect the initial point q' to the final point q in time t. "Semi–" refers to $\hbar$, the quantum unit of phase in the exponent. The quantum mechanics enters only through this atomic scale, in units of which the variation of the phase across the classical potential is assumed to be large. "–classical" refers to the rest - both the amplitudes $A_j(q,t)$ and the phases $R_j(q,t)$ - which are determined by the classical Hamilton-Jacobi equations.

In the semiclassical approximation the quantum time evolution operator is given by the *semiclassical propagator*

$$K_{sc}(q,q',t) = \frac{1}{(2\pi i\hbar)^{D/2}} \sum_j \left| \det \frac{\partial p'}{\partial q} \right|_j^{1/2} e^{\frac{i}{\hbar}R_j - \frac{i\pi}{2}m_j} ,$$

where the topological index $m_j(q,q',t)$ counts the number of the direction reversal along the jth classical trajectory that connects $q' \to q$ in time t. Until very recently it was not possible to resolve quantum evolution on quantum time scales (such as one revolution of electron around a nucleus) - physical measurements are almost always done at time scales asymptotically large compared to the intrinsic quantum time scale. Formally this information is extracted by means of a Laplace transform of the propagator which yields the energy dependent *semiclassical Green's function*

$$\begin{aligned} G_{sc}(q,q',E) &= G_0(q,q',E) + \sum_j G_j(q,q',E) \\ G_j(q,q',E) &= \frac{1}{i\hbar(2\pi i\hbar)^{\frac{(D-1)}{2}}} \left| \frac{1}{\dot{q}\dot{q}'} \det \frac{\partial p'_\perp}{\partial q_\perp} \right|_j^{1/2} e^{\frac{i}{\hbar}S_j - \frac{i\pi}{2}m_j} \end{aligned} \qquad (34.53)$$

where $G_0(q,q',E)$ is the contribution of short trajectories with $S_0(q,q',E) \leq \hbar$, while the sum is over the contributions of long trajectories (34.46) going from q' to q with fixed energy E, with $S_j(q,q',E) \gg \hbar$.

References

[34.1] A. Einstein, "On the Quantum Theorem of Sommerfeld and Epstein," p. 443, English translation of "Zum Quantensatz von Sommerfeld und Epstein",

Verh. Deutsch. Phys. Ges. **19**, 82 (1917), in *The Collected Papers of Albert Einstein*, Volume **6**: *The Berlin Years: Writings, 1914-1917*, A. Engel, transl. and E. Schucking, (Princeton University Press, Princeton, New Jersey 1997).

[34.2] E. Madelung, *Zeitschr. fr Physik* **40**, 332 (1926).

[34.3] E. Schrödinger, *Annalen der Physik* **79**, 361, 489; **80**, 437, **81**, 109 (1926).

[34.4] J. H. van Vleck, *Quantum Principles and the Line Spectra*, Bull. Natl. Res. Council **10**, 1 (1926).

[34.5] J. H. van Vleck, *Proc. Natl. Acad. Sci.* **14**, 178 (1928).

[34.6] D. Bohm, *Phys. Rev.* **85**, 166 (1952).

[34.7] P.R. Holland, *The quantum theory of motion - An account of the de Broglie-Bohm casual interpretation of quantum mechanics* (Cambridge Univ. Press, Cambridge 1993).

[34.8] `physics.nist.gov/cgi-bin/cuu`

Gaussian!integral
Dirac delta function
Gaussian!integral
Gaussian!integral, d-dimensional
stationary!phase approximation

Exercises

Exercise 34.1 **Who ordered $\sqrt{\pi}$?** *Derive the Gaussian integral*

$$\frac{1}{\sqrt{2\pi}}\int_{-\infty}^{\infty} dx\, e^{-\frac{x^2}{2a}} = \sqrt{a}\,, \qquad a>0\,.$$

assuming only that you know to integrate the exponential function e^{-x}. Hint, hint: x^2 is a radius-squared of something. π is related to the area or circumference of something.

Exercise 34.2 **Dirac delta function, Gaussian representation.** *Consider the Gaussian distribution function*

$$\delta_\sigma(z) = \frac{1}{\sqrt{2\pi\sigma^2}} e^{-z^2/2\sigma^2}\,.$$

Show that in $\sigma \to 0$ limit this is the Dirac delta function

$$\int_{\mathcal{M}} dx\, \delta(x) = 1 \text{ if } 0\in\mathcal{M}\,, \text{ zero otherwise}\,.$$

Exercise 34.3 **D-dimensional Gaussian integrals.** *Show that the Gaussian integral in D-dimensions is given by*

$$\frac{1}{(2\pi)^{d/2}}\int d^d\phi e^{-\frac{1}{2}\phi^T\cdot M^{-1}\cdot\phi+\phi\cdot J} \;=\; |\det M|^{\frac{1}{2}}\, e^{\frac{1}{2}J^T\cdot M\cdot J}\,, \qquad (34.54)$$

where M is a real positive definite $[d\times d]$ matrix, that is a matrix with strictly positive eigenvalues. x, J are D-dimensional vectors, and x^T is the transpose of x.

Exercise 34.4 **Stationary phase approximation in higher dimensions.** *All semiclassical approximations are based on saddlepoint evaluations of integrals of type*

$$I = \int d^D x A(x) e^{i\Phi(x)/\hbar} \qquad (34.55)$$

for small values of $\hbar$. Obtain the stationary phase estimate

$$I \approx \sum_n A(x_n) e^{i\Phi(x_n)/\hbar} \frac{(2\pi i\hbar)^{D/2}}{\sqrt{\det \mathbf{D}^2\Phi(x_n)}},$$

where $\mathbf{D}^2\Phi(x_n)$ denotes the second derivative matrix.

Exercise 34.5 **Schrödinger equation in the Madelung form.** *Verify the decomposition of Schrödinger equation into real and imaginary parts, eqs. (34.3) and (34.4).*

Exercise 34.6 **Transport equations.** *Write the wave-function in the asymptotic form*

$$\psi(q,t) = e^{\frac{i}{\hbar}R(x,t)+\frac{i}{\hbar}\varepsilon t}\sum_{n\geq 0}(i\hbar)^n A_n(x,t)\,.$$

Derive the transport equations for the A_n by substituting this into the Schrödinger equation and then collecting terms by orders of $\hbar$. Notice that equation for $\dot{A}_n$ only requires knowledge of A_{n-1} and R.

Exercise 34.7 **Easy examples of the Hamilton's principal function.** *Calculate $R(q,q',t)$ for*

a) a D-dimensional free particle

b) a 3-dimensional particle in constant magnetic field

c) a 1-dimensional harmonic oscillator.

(Continuation: exercise 34.17.)

Exercise 34.8 **1-dimensional harmonic oscillator.** *Take a 1-dimensional harmonic oscillator $U(q) = \frac{1}{2}kq^2$. Take a WKB wave function of form $A(q,t) = a(t)$ and $R(q,t) = r(t)+b(t)q+c(t)q^2$, where $r(t), a(t), b(t)$ and $c(t)$ are time dependent coefficients. Derive ordinary differential equations by using (34.3) and (34.4) and solve them. (Continuation: exercise 34.11.)*

rethink - what is the point of this exercise?

Exercise 34.9 **1-dimensional linear potential.** *Take a 1-dimensional linear potential $U(q) = -Fq$. Take a WKB wave function of form $A(q,t) = a(t)$ and $R(q,t) = r(t)+b(t)q+c(t)q^2$, where $r(t), a(t), b(t)$ and $c(t)$ are time dependent coefficients. Derive and solve the ordinary differential equations from (34.3) and (34.4).*

Exercise 34.10 **D-dimensional quadratic potentials.** *Generalize the above method to general D-dimensional quadratic potentials.* [13]

Exercise 34.11 **Time evolution of R.** *(Continuation of exercise 34.8). Calculate the time evolution of $R(q,0) = a+bq+cq^2$ for a 1-dimensional harmonic oscillator using (34.12) and (34.14).*

⇓PRELIMINARY

Exercise 34.12 **Checking text - continuity equation.** *Check (34.20)*

[13] Mason: what's the point? exercise 34.8 and exercise 34.9 are the same?

⇑PRELIMINARY

Green's function!semiclassical
semiclassical!Green's function

Exercise 34.13 D**-dimensional free particle propagator.** *Verify the results in sect. 34.2.2; show explicitely that (34.34), the semiclassical Van Vleck propagator in D dimensions, solves the Schrödinger's equation.*

Exercise 34.14 **Propagator, charged particle in constant magnetic field.** *Calculate the semiclassical propagator for a charged particle in constant magnetic field in 3 dimensions. Verify that the semiclassical expression coincides with the exact solution.*

Exercise 34.15 **1-dimensional harmonic oscillator propagator.** *Calculate the semiclassical propagator for a 1-dimensional harmonic oscillator and verify that it is identical to the exact quantum propagator.*

⇓PRELIMINARY

Exercise 34.16 **Exact vs. semiclassical propagator.** *What is the difference between the exact and the semiclassical propagator?* [14]

⇑PRELIMINARY

[15]

Exercise 34.17 **Free particle action.** *Calculate the energy dependent action for a free particle, a charged particle in a constant magnetic field and for the harmonic oscillator.*

Exercise 34.18 **Zero length orbits.** *Derive the classical trace (14.1) rigorously and either add the $t \to 0_+$ zero length contribution to the trace formula, or show that it vanishes. Send us a reprint of* Phys. Rev. Lett. *with the correct derivation.*

⇓PRELIMINARY

Exercise 34.19 **A usefull determinant identity.** *Show that the following two determinants equal each other:*
[16] $A[(n+1)\times(n+1)]determinant$

$$\det\left(M'_n\right) = \begin{matrix} \\ \\ \\ \\ n+1 \end{matrix} \overset{\begin{matrix} n+1 \end{matrix}}{\begin{bmatrix} x_{1,1} & \dots & x_{1,n} & y_1 \\ \vdots & \ddots & \vdots & \vdots \\ x_{n,1} & \dots & x_{n,n} & y_n \\ z_1 & \dots & z_n & E \end{bmatrix}} \tag{34.56}$$

and the $[n\times n]$ determinant:

$$E\det\left(M_n\right) = E \overset{\begin{matrix} n \end{matrix}}{\begin{bmatrix} x_{1,1}-y_1z_1E^{-1} & \dots & x_{1,n}-y_1z_nE^{-1} \\ \vdots & \ddots & \vdots \\ x_{n,1}-y_nz_1E^{-1} & \dots & x_{n,n}-y_nz_nE^{-1} \end{bmatrix}} \begin{matrix} \\ \\ n \end{matrix} \tag{34.57}$$

⇑PRELIMINARY

Exercise 34.20 **Free particle semiclassical Green's functions.** *Calculate the semiclassical Green's functions for the systems of exercise 34.17.*

[14] Tanner: Predrag: Question very unspecific; don't know what you are up to. Not included in text yet
[15] Dorte: PC fills in systems of exercises....
[16] Dorte: ulaeseligt

Chapter 35

Noise

> He who establishes his argument by noise and command shows that his reason is weak.
> M. de Montaigne

(G. Vattay and P. Cvitanović)

This chapter (which reader can safely skip on the first reading) is about noise, how it affects classical dynamics, and the ways it mimicks quantum dynamics.

fast track:
chapter 36, p. 663

Why - in a study of deterministic and quantum chaos - start discussing noise? First, in physical settings any dynamics takes place against a noisy background, and whatever prediction we might have, we have to check its robustness to noise. Second, as we show in this chapter, to the leading order in noise strength the semiclassical Hamilton-Jacobi formalism carries over to weakly stochastic flows in totto. As classical noisy dynamics is more intuitive than quantum dynamics, this exercise helps demistify some of the formal machinery of semiclassical quantization. Surprisingly, symplectic structure emerges here not as a deep principle of mechanics, but an artifact of the leading approximation to quantum/noisy dynamics, not respected by higher order corrections. The same is true of semiclasical quantum dynamics; higher corrections do not respect canonical invariance. Third, the variational principle derived here will be refashioned into a powerful tool for determining periodic orbits in chapter 37.

We start by deriving the continuity equation for purely deterministic, noiseless flow, and then incorporate noise in stages: diffusion equation, Langevin equation, Fokker-Planck equation, Hamilton-Jacobi formulation, stochastic path integrals.

material invariant
passive scalar
conservation!equation
density
continuity equation

35.1 Deterministic transport

(E.A. Spiegel and P. Cvitanović)

Fluid dynamics is about physical flows of media with continuous densities. On the other hand, the flows in state spaces of dynamical systems frequently require more abstract tools. To sharpen our intuition about those, it is helpful to outline the more tangible fluid dynamical vision.

Consider first the simplest property of a fluid flow called *material invariant*. A material invariant $I(x)$ is a property attached to each point x that is preserved by the flow, $I(x) = I(f^t(x))$; for example, at this point a green particle (more formally: a *passive scalar*) is embedded into the fluid. As $I(x)$ is invariant, its total time derivative vanishes, $\dot{I}(x) = 0$. Written in terms of partial derivatives this is the *conservation equation* for the material invariant

$$\partial_t I + v \cdot \partial I = 0\,. \tag{35.1}$$

Let the *density* of representative points be $\rho(x,t)$. The manner in which the flow redistributes $I(x)$ is governed by a partial differential equation whose form is relatively simple because the representative points are neither created nor destroyed. This conservation property is expressed in the integral statement

$$\partial_t \int_V dx\, \rho I = -\int_{\partial V} d\sigma\, \hat{n}_i v_i \rho I\,,$$

where V is an arbitrary volume in the state space $\mathcal{M}$, ∂V is its surface, $\hat{n}$ is its outward normal, and repeated indices are summed over throughout. The divergence theorem turns the surface integral into a volume integral,

$$\int_V [\partial_t(\rho I) + \partial_i(v_i \rho I)]\, dx = 0\,,$$

where ∂_i is the partial derivative operator with respect to x_i. Since the integration is over an arbitrary volume, we conclude that

$$\partial_t(\rho I) + \partial_i(\rho I v_i) = 0\,. \tag{35.2}$$

The choice $I \equiv 1$ yields the *continuity equation* for the density:

$$\partial_t \rho + \partial_i(\rho v_i) = 0\,. \tag{35.3}$$

We have used here the language of fluid mechanics to ease the visualization, but, as we already saw in the discussion of infinitesimal action of the Perron-Frobenius operator (9.24), continuity equation applies to any deterministic state space flow.

35.2 Brownian difussion

Fick law
diffusion!equation
Dirac delta function
Einstein!diffusion formula

Consider tracer molecules, let us say green molecules, embedded in a denser gas of transparent molecules. Assume that the density of tracer molecules ρ compared to the background gas density is low, so we can neglect green-green collisions. Each green molecule, jostled by frequent collisions with the background gas, executes its own Brownian motion. The molecules are neither created nor destroyed, so their number within an arbitrary volume V changes with time only by the current density j_i flow through its surface ∂V (with $\hat{n}$ its outward normal):

$$\partial_t \int_V dx\, \rho = -\int_{\partial V} d\sigma\, \hat{n}_i j_i \,. \tag{35.4}$$

The divergence theorem turns this into the conservation law for tracer density:

$$\partial_t \rho + \partial_i j_i = 0 \,. \tag{35.5}$$

The tracer density ρ is defined as the average density of a "material particle", averaged over a subvolume large enough to contain many green (and still many more background) molecules, but small compared to the macroscopic observational scales. What is j? If the density is constant, on the average as many molecules leave the material particle volume as they enter it, so a reasonable phenomenological assumption is that the *average* current density (*not* the individual particle current density ρv_i in (35.3)) is driven by the density gradient

$$j_i = -D\frac{\partial \rho}{\partial x_i} \,. \tag{35.6}$$

This is the *Fick law*, with the diffusion constant D a phenomenological parameter. For simplicity here we assume that D is a scalar; in general $D \to D_{ij}(x,t)$ is a space- and time-dependent tensor. Substituting this j into (35.5) yields the *diffusion equation*

$$\frac{\partial}{\partial t}\rho(x,t) = D\frac{\partial^2}{\partial x^2}\rho(x,t) \,. \tag{35.7}$$

This linear equation has an exact solution in terms of an initial Dirac delta density distribution, $\rho(x,0) = \delta(x - x_0)$,

$$\rho(x,t) = \frac{1}{(4\pi D t)^{d/2}} e^{-\frac{(x-x_0)^2}{4Dt}} = \frac{1}{(4\pi D t)^{d/2}} e^{-\frac{\dot{x}^2}{4D}t} \,, \tag{35.8}$$

check factor of 4 here

noise!Gaussian
Gaussian!probability density
probability density!Gaussian
white noise
noise!white
Langevin equation

in the spirit of the quantum free particle propagation of sect. 34.2.2. The average distance covered in time t obeys the Einstein diffusion formula

change this - Ein is specific to Brow diffusion

$$\left\langle (x-x_0)^2 \right\rangle_t = \int dx\, \rho(x,t)(x-x_0)^2 = 2Dt\,. \tag{35.9}$$

35.3 Weak noise

> The connection between path integration and Brownian motion is so close that they are nearly indistingushable. Unfortunately though, like a body and its mirror image, the sum over paths for Brownian motion is a theory having substance, while its path integral image exists mainly in the eye of the beholder.
>
> L. S. Schulman

So far we have considered tracer molecule dynamics which is purely Brownian, with no deterministic "drift". Consider next a deterministic flow $\dot{x} = v(x)$ perturbed by a stochastic term $\xi(t)$,

$$\dot{x} = v(x) + \xi(t)\,. \tag{35.10}$$

check factor of 4

Assume that $\xi(t)$'s fluctuate around $[\dot{x} - v(x)]$ with a Gaussian probability density

$$p(\xi, \delta t) = \left(\frac{\delta t}{4\pi D}\right)^{d/2} e^{-\frac{\xi^2}{4D}\delta t}\,, \tag{35.11}$$

explain what average?

and are uncorrelated in time (white noise)

$$\left\langle \xi(t)\xi(t') \right\rangle = 2dD\delta(t-t')\,. \tag{35.12}$$

The normalization factors in (35.8) and (35.11) differ, as $p(\xi, \delta t)$ is a probability density for velocity ξ, and $\rho(x,t)$ is a probability density for position x. The material particle now drifts along the trajectory $x(t)$, so the velocity diffusion follows (35.8) for infinitesimal time δt only. As $D \to 0$, the distribution tends to the (noiseless, deterministic) Dirac delta function.

An example is the Langevin equation for a Brownian particle, in which one replaces the Newton's equation for force by two counter-balancing forces: random accelerations $\xi(t)$ which tend to smear out a particle trajectory, and a damping term which drives the velocity to zero.

explain what $|v(x)| > |\xi|$ means

The phenomenological Fick law current (35.6) is now a sum of two components, the material particle center-of-mass deterministic drift $v(x)$ and the weak noise term

$$j_i = \rho v_i - D\frac{\partial \rho}{\partial x_i}\,, \tag{35.13}$$

Substituting this j into (35.5) yields the *Fokker-Planck equation*

Fokker-Planck equation
continuity equation

$$\partial_t \rho + \partial_i(\rho v_i) = D\,\partial^2 \rho. \tag{35.14}$$

The left hand side, $d\rho/dt = \partial_t \rho + \partial \cdot (\rho v)$, is deterministic, with the continuity equation (35.3) recovered in the weak noise limit $D \to 0$. The right hand side describes the diffusive transport in or out of the material particle volume. If the density is lower than in the immediate neighborhood, the local curvature is positive, $\partial^2 \rho > 0$, and the density grows. Conversely, for negative curvature diffusion lowers the local density, thus smoothing the variability of ρ. Where is the density going globally?

If the system is bound, the probability density vanishes sufficiently fast outside the central region, $\rho(x,t) \to 0$ as $|x| \to \infty$, and the total probability is conserved

$$\int dx\, \rho(x,t) = 1\,.$$

Any initial density $\rho(x,0)$ is smoothed by diffusion and with time tends to the invariant density

$$\rho_0(x) = \lim_{t\to\infty} \rho(x,t)\,, \tag{35.15}$$

an eigenfunction $\rho(x,t) = e^{st}\,\rho_0(x)$ of the time-independent Fokker-Planck equation

$$\left(\partial_i v_i - D\,\partial^2 + s_\alpha\right)\rho_\alpha = 0\,, \tag{35.16}$$

with vanishing eigenvalue $s_0 = 0$. Provided the noiseless classical flow is hyperbolic, in the vanishing noise limit the leading eigenfunction of the Fokker-Planck equation tends to natural measure (9.16) of the corresponding deterministic flow, the leading eigenvector of the Perron-Frobenius operator.

If the system is open, there is a continuous outflow of probability from the region under study, the leading eigenvalue is contracting, $s_0 < 0$, and the density of the system tends to zero. In this case the leading eigenvalue s_0 of the time-independent Fokker-Planck equation (35.16) can be interpreted by saying that a finite density can be maintained by pumping back probability into the system at a constant rate $\gamma = -s_0$. The value of γ for which any initial probability density converges to a finite equilibrium density is called the *escape rate*. In the noiseless limit this coincides with the deterministic escape rate (10.15).

We have introduced noise phenomenologically, and used the weak noise assumption in retaining only the first derivative of ρ in formulating the Fick law (35.6) and including noise additively in (35.13). A full theory of stochastic ODEs is much subtler, but this will do for our purposes.

Hamilton!principal function
matrix!stability
stability!matrix

35.4 Weak noise approximation

In the spirit of the WKB approximation, we shall now study the evolution of the probability distribution by rewriting it as

$$\rho(x,t) = e^{\frac{1}{2D}R(x,t)}\,. \tag{35.17}$$

The time evolution of R is given by

$$\partial_t R + v\partial R + (\partial R)^2 = D\partial v + D\partial^2 R\,.$$

Consider now the weak noise limit and drop the terms proportional to D. The remaining equation

$$\partial_t R + H(x,\partial R) = 0$$

is the Hamilton-Jacobi equation (34.5). The function R can be interpreted as the Hamilton's principal function, corresponding to the Hamiltonian

$$H(x,p) = p\,v(x) + p^2/2\,,$$

with the Hamilton's equations of motion

$$\begin{aligned} \dot{x} &= \partial_p H = v + p \\ \dot{p} &= -\partial_x H = -A^T p\,, \end{aligned} \tag{35.18}$$

where A is the stability matrix (4.3)

$$A_{ij}(x) = \frac{\partial v_i(x)}{\partial x_j}\,.$$

The noise Lagrangian (34.13) is then

$$L(x,\dot{x}) = \dot{x}\cdot p - H = \frac{1}{2}\left[\dot{x} - v(x)\right]^2\,. \tag{35.19}$$

We have come the full circle - the Lagrangian is the exponent of our assumed Gaussian distribution (35.11) for noise $\xi^2 = [\dot{x} - v(x)]^2$. What is the meaning of this Hamiltonian, Lagrangian? Consider two points x_0 and x. Which noisy path is the most probable path that connects them in time t? The probability of a given path $\mathcal{P}$ is given by the probability of the noise sequence $\xi(t)$ which generates the path. This probability is proportional to the product of the noise probability functions (35.11) along the path, and

eck factors of 2

Wiener integral
variational principle

the total probability for reaching x from x_0 in time t is given by the sum over all paths, or the stochastic path integral (Wiener integral)

$$\begin{aligned} P(x,x_0,t) &\sim \sum_{\mathcal{P}} \prod_j p(\xi(\tau_j),\delta\tau_j) = \int \prod_j d\xi_j \left(\frac{\delta\tau_j}{2\pi D}\right)^{d/2} e^{-\frac{\xi(\tau_j)^2}{2D}\delta\tau_i} \\ &\to \frac{1}{Z}\sum_{\mathcal{P}} \exp\left(-\frac{1}{2D}\int_0^t d\tau\, \xi^2(\tau)\right) , \end{aligned} \tag{35.20}$$

where $\delta\tau_i = \tau_i - \tau_i$, and the normalization constant is

$$\frac{1}{Z} = \lim \prod_i \left(\frac{\delta\tau_i}{2\pi D}\right)^{d/2} .$$

The most probable path is the one maximizing the integral inside the exponential. If we express the noise (35.10) as

$$\xi(t) = \dot{x}(t) - v(x(t)) ,$$

the probability is maximized by the variational principle

$$\min \int_0^t d\tau [\dot{x}(\tau) - v(x(\tau))]^2 = \min \int_0^t L(x(\tau),\dot{x}(\tau)) d\tau .$$

By the standard arguments, for a given x, x' and t the the probability is maximized by a solution of Hamilton's equations (35.18) that connects the two points $x_0 \to x'$ in time t.

⇓PRIVATE

35.5 Straying from the True Path: the cost

Penalizing deviations from the True Path?

Newton descent derived from path integral for a weakly stochastic Langevin flow

stepwise error

$$F_i = \tilde{x}_{i+1} - f^{\Delta t_i}(\tilde{x}_i)$$

where $\tilde{x}_{i+1}$ is the next path point, and $f^{\Delta t_i}(\tilde{x}_i)$ is the point to which the flow transports $\tilde{x}_i$.

Cost function

$$F^2 = \sum_{i=0}^{N} \frac{1}{\Delta t_i} \left(\tilde{x}_{i+1} - f^{\Delta t_i}(\tilde{x}_i)\right)^2$$

Dimensionally $F^2 = [\text{lenght}]^2/[\text{time}] = \textit{diffusion}$

rewrite as

$$\begin{aligned} F^2 &= \sum_{i=0}^{N} \frac{1}{\Delta t_i} \left(\tilde{x}_{i+1} - \tilde{x}_i - f^{\Delta t_i}(\tilde{x}_i) - \tilde{x}_i\right)^2 \\ &= \sum_{i=0}^{N} \Delta t_i \left(\frac{\tilde{x}_{i+1} - \tilde{x}_i}{\Delta t_i} - \frac{f^{\Delta t_i}(\tilde{x}_i) - \tilde{x}_i}{\Delta t_i}\right)^2 \end{aligned}$$

$\Delta t_i \to 0$ limit:

$$F^2 = \int_0^T dt \left(\frac{d\tilde{x}}{dt} - v(\tilde{x})\right)^2$$

where T = cycle period

$$F^2 = \int_0^T dt \left(\frac{d\tilde{x}}{dt} - v(\tilde{x})\right)^2$$

$$= = \int_0^T dt \left(\frac{ds}{dt}\right)^2 \left(\tilde{v}(\tilde{x}) - v(\tilde{x})\frac{dt}{ds}\right)^2, \quad (35.21)$$

where T = cycle period

to relate time t and the path parameter s consider the euclidean lengths

True Path: $dx = vdt$
Strayed: $d\tilde{x} = \tilde{v}ds$

related by projecting path step $\tilde{v}ds$ onto the true trajectory step vdt

$$\frac{|v|dt}{|\tilde{v}|ds} = \cos\theta\,, \quad (35.22)$$

where θ is the angle between v to $\tilde{v}$

$$\cos\theta = \frac{\tilde{v}\cdot v}{|\tilde{v}||v|} \quad (35.23)$$

and thus

$$\frac{dt}{ds} = \frac{\tilde{v}\cdot v}{v^2}\,. \quad (35.24)$$

$$F^2 = \int_{t_i=0}^{T} dt \left(\frac{v^2}{\tilde{v}\cdot v}\right)^2 \left(\tilde{v}(\tilde{x}) - v(\tilde{x})\frac{\tilde{v}\cdot v}{v^2}\right)^2 . \tag{35.25}$$

Langevin equation
Onsager-Machlup
van Kampen, N. G.

decomposing

$$\begin{aligned} \tilde{v} &= (1 - \frac{v\otimes v}{v^2} + \frac{v\otimes v}{v^2})\tilde{v} \\ &= = P_\perp v + v\frac{v\cdot\tilde{v}}{v^2} \end{aligned} \tag{35.26}$$

where

$$P_\perp = 1 - \frac{v\otimes v}{v^2}$$

projects any vector components transverse to v

Parametrized by the Euclidean length s measured along the guess path L the cost function is

$$F^2 = \int_{s_i}^{s_f} ds\, \frac{v^2}{v\cdot\tilde{v}}\,(P_\perp\tilde{v})^2 \tag{35.27}$$

The projection operator $P_\perp$ in the cost function penalizes the local misorientation of the path by projecting on the directions perpendicular to the dynamical flow vector.

⇑PRIVATE

Commentary

Remark 35.1 Literature. The theory of stochastic processes is a vast subject, spanning over centuries and over disciplines ranging from pure mathematics to impure finance. We enjoyed reading van Kampen classic [35.1], especially his railings against those who blunder carelessly into nonlinear landscapes (with this chapter we join the list of van Kampen's sinners). A more specialized monograph like Risken's [35.2] will do just as well. The "Langevin equation" introduces noise and damping only into the acceleration of Newton's equations; here we are considering more general stochastic differential equations in the weak noise limit. Onsager-Machlup seminal paper [35.18] was the first to introduce a variational method - the "principle of least dissipation" - based on the Lagrangian of form (35.19). This paper deals only with a finite set of linearly damped thermodynamic variables. Here the setting is much more general: we study fluctuations over a state space varying velocity field $v(x)$. Schulman's monograph [35.11] contains a very readable summary of Kac's [35.12] exposition of Wiener's integral over stochastic paths.

⇓PRELIMINARY

Remark 35.2 Operator ordering. The Itó and Stratanovich operator ordering issues arise in the order beyond the leading approximation considered here. [1]

not true? rethink

⇑PRELIMINARY

[1] Mason: make sure no ref. refer to volume 1

noise!Gaussian

Résumé

When a deterministic trajectory is smeared out under the influence of Gaussian noise of strength D, the deterministic dynamics is recovered in the weak noise limit $D \to 0$. The effect of the noise can be taken into account by adding noise corrections to the classical trace formula. [2]

Add Foged by reference

recheck whether something can be used from chapter/refsQmnoise

References

[35.1] N. G. van Kampen, *Stochastic Processes in Physics and Chemistry* (North Holland, Amsterdam, 1981).

[35.2] H. Risken, *The Fokker-Planck equation: Methods of solution and applications* (Springer-Verlag, New York, 1989).

[35.3] W. Dittrich and M. Reuter, *Classical and Quantum Dynamics: From Classical Paths to Path Integrals* (Springer-Verlag, Berlin 1994).

[35.4] E. M. Lifshitz and L. P. Pitaevskii, *Physical Kinetics* (Pergamon, London 1981).

[35.5] C. Itzykson and J.-M. Drouffe, *Statistical field theory* (Cambridge U. Press, 1991).

[35.6] V. Ambegaokar, *Reasoning about luck; probability and its uses in physics* (Cambridge Univ. Press, Cambridge 1996).

[35.7] B. Sakita, *Quantum theory of many variable systems and fields* (World Scientific, Singapore 1985).

[35.8] G. E. Uhlenbeck, G. W. Ford and E. W. Montroll, *Lectures in Statistical Mechanics* (Amer. Math. Soc., Providence R.I., 1963).

[35.9] M. Kac, "Random walk and the theory of Brownian motion", (1946), reprinted in ref. [35.10].

[35.10] N. Wax, ed., *Selected Papers on Noise and Stochastic Processes* (Dover, New York 1954).

[35.11] L. S. Schulman, *Techniques and Applications of Path Integration* (Wiley-Interscience, New York 1981).

[35.12] M. Kac, *Probability and Related Topics in Physical Sciences* (Wiley-Interscience, New York 1959).

[35.13] E. Nelson, *Quantum Fluctuations* (Princeton Univ. Press 1985).

[35.14] H. Kunita, *Stochastic Flows and Stochastic Differential Equations* (Cambridge Univ. Press, 1990).

[35.15] H. Haken and G. Mayer-Kress, *Z. f. Physik* **B 43**, 185 (1981).

[35.16] M. Roncadelli, *Phys. Rev.* **E 52**, 4661 (1995).

[35.17] G. Ryskin, *Phys. Rev.* **E 56**, 5123 (1997).

ref. [35.19]

[35.18] L. Onsager and S. Machlup, *Phys. Rev.* **91**, 1505, 1512 (1953).

[35.19] Lord Rayleigh, *Phil. Mag.* **26**, 776 (1913).

[35.20] E. Gozzi, M. Reuter and W. D. Thacker, *Phys. Rev.* **D 40**, 3363 (1989).

[35.21] E. Gozzi and M. Reuter, *Phys. Lett.* **233B**, 383 (1989); **238B**, 451 (1990); **240B**, 137 (1990).

[35.22] E. Gozzi, M. Reuter and W. D. Thacker, *Phys. Rev.* **D 46**, 757 (1992).

[35.23] E. Gozzi, M. Reuter and W. D. Thacker, *Chaos, Solitons and Fractals* **2**, 441 (1992).

[35.24] Benzi et al., *Jour. Phys.* **A 18**, 2157 (1985).

[35.25] R. Graham, *Europhys. Lett.* **5**, 101 (1988).

[35.26] R. Graham and T. Tél, *Phys. Rev. A* **35**, 1382 (1987).

[35.27] R. Benzi, G. Paladin, G. Parisi and A. Vulpiani, *J. Phys.* **A 18**, 2157 (1985).

[35.28] L. Arnold and V. Wihstutz, *Lyapunov exponents*, *Lecture Notes in Math.* **1186** (Springer-Verlag, New York 1986).

[35.29] M. V. Feigelman and A. M. Tsvelik, *Sov. Phys. JETP* **56**, 823 (1982).

[35.30] G. Parisi and N. Sourlas, *Nucl. Phys.* **B206**, 321 (1982).

[35.31] F. Langouche et al., *Functional integration and semiclassical expansion* (Reidel, Dordrecht 1982).

[35.32] O. Cepas and J. Kurchan, "Canonically invariant formulation of Langevin and Fokker-Planck equations", *European Phys. J.* **B 2**, 221 (1998), `cond-mat/9706296`.

[35.33] S. Tanase-Nicola and J. Kurchan, "Statistical-mechanical formulation of Lyapunov exponents", `cond-mat/0210380`. update

[2] Mason: expand

semiclassical!quantization
quantization!semiclassical
orbit!returning
returning orbit

Chapter 36

Semiclassical quantization

(G. Vattay, G. Tanner and P. Cvitanović)

We derive here the Gutzwiller trace formula and the semiclassical zeta function, the central results of the semiclassical quantization of classically chaotic systems. In chapter 38 we will rederive these formulas for the case of scattering in open systems. Quintessential wave mechanics effects such as creeping, diffraction and tunneling will be taken up in chapters 42 and 43. If you still feel you got no satisfaction, we derive the trace formulas one more time in appendix O, this time both for quantum and stochastic flows.

⇓PRIVATE

⇑PRIVATE

36.1 Trace formula

Our next task is to evaluate the Green's function trace (32.17) in the semiclassical approximation. The trace

$$\operatorname{tr} G_{sc}(E) = \int d^D q\, G_{sc}(q,q,E) = \operatorname{tr} G_0(E) + \sum_j \int d^D q\, G_j(q,q,E)$$

receives contributions from "long" classical trajectories labeled by j which start and end in q after finite time, and the "zero length" trajectories whose lengths approach zero as $q' \to q$.

First we work out the contributions coming from the finite time *returning* classical orbits, i.e., trajectories that originate and end at a given configuration point q. As we are identifying q with q', taking of a trace involves (still another!) stationary phase condition in the $q' \to q$ limit,

add periodic trajectory to figure 36.1

$$\left.\frac{\partial S_j(q,q',E)}{\partial q_i}\right|_{q'=q} + \left.\frac{\partial S_j(q,q',E)}{\partial q'_i}\right|_{q'=q} = 0\,,$$

periodic!orbit
orbit!periodic
stationary!phase approximation

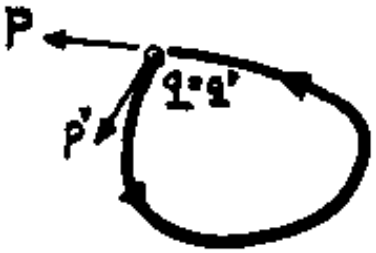

Figure 36.1: A returning trajectory in the configuration space. The orbit is periodic in the full phase space only if the initial and the final momenta of a returning trajectory coincide as well.

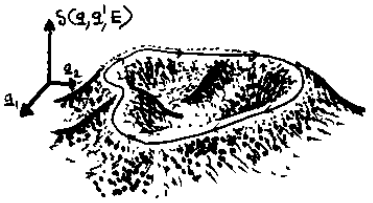

Figure 36.2: A romanticized sketch of $S_p(E) = S(q,q,E) = \oint p(q,E)dq$ landscape orbit. Unstable periodic orbits traverse isolated ridges and saddles of the mountainous landscape of the action $S(q_\parallel, q_\perp, E)$. Along a periodic orbit $S_p(E)$ is constant; in the transverse directions it generically changes quadratically.

meaning that the initial and final momenta (34.40) of contributing trajectories should coincide

$$p_i(q,q,E) - p'_i(q,q,E) = 0\,, \qquad q \in j\text{th periodic orbit}\,, \tag{36.1}$$

so the trace receives contributions only from those long classical trajectories which are *periodic* in the full phase space.

For a periodic orbit the natural coordinate system is the intrinsic one, with $q_\parallel$ axis pointing in the $\dot{q}$ direction along the orbit, and $q_\perp$, the rest of the coordinates transverse to $\dot{q}$. The jth periodic orbit contribution to the trace of the semiclassical Green's function in the intrinsic coordinates is

$$\mathrm{tr}\, G_j(E) = \frac{1}{i\hbar(2\pi\hbar)^{(d-1)/2}} \oint_j \frac{dq_\parallel}{\dot{q}} \int_j d^{d-1}q_\perp |\det D^j_\perp|^{1/2} e^{\frac{i}{\hbar}S_j - \frac{i\pi}{2}m_j},$$

where the integration in $q_\parallel$ goes from 0 to L_j, the geometric length of small tube around the orbit in the configuration space. As always, in the stationary phase approximation we worry only about the fast variations in the phase $S_j(q_\parallel, q_\perp, E)$, and assume that the density varies smoothly and is well approximated by its value $D^j_\perp(q_\parallel, 0, E)$ on the classical trajectory, $q_\perp = 0$. The topological index $m_j(q_\parallel, q_\perp, E)$ is an integer which does not depend on the initial point $q_\parallel$ and not change in the infinitesimal neighborhood of an isolated periodic orbit, so we set $m_j(E) = m_j(q_\parallel, q_\perp, E)$.

The transverse integration is again carried out by the stationary phase method, with the phase stationary on the periodic orbit, $q_\perp = 0$. The result of the transverse integration can depend only on the parallel coordinate

additional phase accrued?

$$\mathrm{tr}\, G_j(E) = \frac{1}{i\hbar} \oint \frac{dq_\parallel}{\dot{q}} \left| \frac{\det D_{\perp j}(q_\parallel, 0, E)}{\det D'_{\perp j}(q_\parallel, 0, E)} \right|^{1/2} e^{\frac{i}{\hbar}S_j - \frac{i\pi}{2}m_j},$$

where the new determinant in the denominator, $\det D'_{\perp j} =$

periodic!orbit
orbit!periodic

$$\det\left(\frac{\partial^2 S(q,q',E)}{\partial q_{\perp i}\partial q_{\perp j}}+\frac{\partial^2 S(q,q',E)}{\partial q'_{\perp i}\partial q_{\perp j}}+\frac{\partial^2 S(q,q',E)}{\partial q_{\perp i}\partial q'_{\perp j}}+\frac{\partial^2 S(q,q',E)}{\partial q'_{\perp i}\partial q'_{\perp j}}\right),$$

is the determinant of the second derivative matrix coming from the stationary phase integral in transverse directions. Mercifully, this integral also removes most of the $2\pi\hbar$ prefactors in (??). [1]

refers to refeq(22.64)

Credit Creagh, Brack, Stockmann

The ratio $\det D_{\perp j}/\det D'_{\perp j}$ is here to enforce the periodic boundary condition for the semiclassical Green's function evaluated on a periodic orbit. It can be given a meaning in terms of the monodromy matrix of the periodic orbit by following observations

recheck signs

$$\begin{aligned}\det D_\perp &= \left\|\frac{\partial p'_\perp}{\partial q_\perp}\right\| = \left\|\frac{\partial(q'_\perp,p'_\perp)}{\partial(q_\perp,q'_\perp)}\right\| \\ \det D'_\perp &= \left\|\frac{\partial p_\perp}{\partial q_\perp}-\frac{\partial p'_\perp}{\partial q_\perp}+\frac{\partial p_\perp}{\partial q'_\perp}-\frac{\partial p'_\perp}{\partial q'_\perp}\right\| = \left\|\frac{\partial(p_\perp-p'_\perp,q_\perp-q'_\perp),}{\partial(q_\perp,q'_\perp)}\right\| .\end{aligned}$$

Defining the $2(D-1)$-dimensional transverse vector $x_\perp=(q_\perp,p_\perp)$ in the full phase space we can express the ratio

$$\begin{aligned}\frac{\det D'_\perp}{\det D_\perp} &= \left\|\frac{\partial(p_\perp-p'_\perp,q_\perp-q'_\perp)}{\partial(q'_\perp,p'_\perp)}\right\| = \left\|\frac{\partial(x_\perp-x'_\perp)}{\partial x'_\perp}\right\| \\ &= \det\,(M-\mathbf{1})\ , \qquad (36.2)\end{aligned}$$

in terms of the monodromy matrix M for a surface of section transverse to the orbit within the constant energy $E=H(q,p)$ shell, discussed already in sect. ??.

⇓PRIVATE
⇑PRIVATE

The classical periodic orbit action $S_j(E)=\oint p(q_\parallel,E)dq_\parallel$ is an integral around a loop defined by the periodic orbit, and does not depend on the starting point $q_\parallel$ along the orbit, see figure 36.2. The eigenvalues of the monodromy matrix are also independent of where M_j is evaluated along the orbit, so $\det(1-M_j)$ can also be taken out of the the $q_\parallel$ integral

$$\mathrm{tr}\,G_j(E)=\frac{1}{i\hbar}\sum_j\frac{1}{|\det(1-M_j)|^{1/2}}e^{r(\frac{i}{\hbar}S_j-\frac{i\pi}{2}m_j)}\oint\frac{dq_\parallel}{\dot q_\parallel}\,.$$

Here we have assumed that M_j has no marginal eigenvalues. The determinant of the monodromy matrix, the action $S_p(E)=\oint p(q_\parallel,E)dq_\parallel$ and the topological index are all classical invariants of the periodic orbit. The integral in the parallel direction we now do exactly.

[1] Whelan: Don't forget to add the equation reference.

Gutzwiller!trace formula
trace!formula!Gutzwiller
topological index@"maslov" index

First we take into account the fact that any repeat of a periodic orbit is also a periodic orbit. The action and the topological index are additive along the trajectory, so for rth repeat they simply get multiplied by r. The monodromy matrix of the rth repeat of a prime cycle p is (by the chain rule for derivatives) M_p^r, where M_p is the prime cycle monodromy matrix. Let us denote the time period of the prime cycle p, the single, shortest traversal of a periodic orbit by T_p. The remaining integral can be carried out by change of variables $dt = dq_\parallel/\dot{q}(t)$

$$\int_0^{L_p} \frac{dq_\parallel}{\dot{q}(t)} = \int_0^{T_p} dt = T_p \,.$$

Note that the spatial integral corresponds to a *single* traversal. If you do not see why this is so, rethink the derivation of the classical trace formula (14.21) - that derivation takes only three pages of text. Regrettably, in the quantum case we do not know of an honest derivation that takes less than 30 pages. The final result, the *Gutzwiller trace formula*

$$\operatorname{tr} G_{sc}(E) = \operatorname{tr} G_0(E) + \frac{1}{i\hbar} \sum_p T_p \sum_{r=1}^{\infty} \frac{1}{|\det\left(1 - M_p^r\right)|^{1/2}} e^{r\left(\frac{i}{\hbar} S_p - \frac{i\pi}{2} m_p\right)} \,, \quad (36.3)$$

an expression for the trace of the semiclassical Green's function in terms of periodic orbits, is beautiful in its simplicity and elegance.

The topological index $m_p(E)$ counts the number of changes of sign of the matrix of second derivatives evaluated along the prime periodic orbit p. By now we have gone through so many stationary phase approximations that you have surely lost track of what the total $m_p(E)$ actually is. The rule is this: The topological index of a closed curve in a $2D$ phase space is the sum of the number of times the partial derivatives $\frac{\partial p_i}{\partial q_i}$ for each dual pair (q_i, p_i), $i = 1, 2, \ldots, D$ (no sum on i) change their signs as one goes once around the curve.

36.1.1 Average density of states

keep "tr" here

We still have to evaluate $\operatorname{tr} G_0(E)$, the contribution coming from the infinitesimal trajectories. The real part of $\operatorname{tr} G_0(E)$ is infinite in the $q' \to q$ limit, so it makes no sense to write it down explicitly here. However, the imaginary part is finite, and plays an important role in the density of states formula, which we derive next.

The semiclassical contribution to the density of states (32.17) is given by the imaginary part of the Gutzwiller trace formula (36.3) multiplied with $-1/\pi$. The contribution coming from the zero length trajectories is the imaginary part of (34.48) for $q' \to q$ integrated over the configuration space

$$d_0(E) = -\frac{1}{\pi} \int d^D q \, \operatorname{Im} G_0(q, q, E),$$

The resulting formula has a pretty interpretation; it estimates the number of quantum states that can be accomodated up to the energy E by counting the available quantum cells in the phase space. This number is given by the *Weyl rule* , as the ratio of the phase space volume bounded by energy E divided by h^D, the volume of a quantum cell,

density of states!average
Weyl rule
refer to the harm. oscill. to motivate this Thomas-Fermi formula?

$$N_{sc}(E) = \frac{1}{h^D} \int d^D p d^D q \, \Theta(E - H(q,p)) \,. \tag{36.4}$$

where $\Theta(x)$ is the Heaviside function (32.22). $N_{sc}(E)$ is an estimate of the spectral staircase (32.21), so its derivative yields the average density of states

$$d_0(E) = \frac{d}{dE} N_{sc}(E) = \frac{1}{h^D} \int d^D p d^D q \, \delta(E - H(q,p)) \,, \tag{36.5}$$

precisely the semiclassical result (36.6). For Hamiltonians of type $p^2/2m + V(q)$, the energy shell volume in (36.5) is a sphere of radius $\sqrt{2m(E - V(q))}$. The surface of a d-dimensional sphere of radius r is $\pi^{d/2} r^{d-1}/\Gamma(d/2)$, so the average density of states is given by

redirect the (36.6) reference

36.3 page 679

$$d_0(E) = \frac{2m}{\hbar^D 2^d \pi^{D2} \Gamma(D/2)} \int_{V(q)<E} d^D q \, [2m(E - V(q))]^{D/2-1} \,, \tag{36.6}$$

and

$$N_{sc}(E) = \frac{1}{h^D} \frac{\pi^{D/2}}{\Gamma(1 + D/2)} \int_{V(q)<E} d^D q \, [2m(E - V(q))]^{D/2} \,. \tag{36.7}$$

Physically this means that at a fixed energy the phase space can support $N_{sc}(E)$ distinct eigenfunctions; anything finer than the quantum cell h^D cannot be resolved, so the quantum phase space is effectively finite dimensional. The average density of states is of a particularly simple form in one spatial dimension

36.4 page 679

$$d_0(E) = \frac{T(E)}{2\pi\hbar} \,, \tag{36.8}$$

where $T(E)$ is the period of the periodic orbit of fixed energy E. In two spatial dimensions the average density of states is

$$d_0(E) = \frac{m\mathcal{A}(E)}{2\pi\hbar^2} \,, \tag{36.9}$$

where $\mathcal{A}(E)$ is the classically allowed area of configuration space for which $V(q) < E$.

36.5 page 679

⇓PRELIMINARY

into appendix? or into a remark?

density of states!average
semiclassical!density of states
ultraviolet divergence
divergence ultraviolet
Green's function!regularized

$$\mathrm{Im}\, G_0(q,q,E) = -\lim_{q'\to q} \frac{m}{2\hbar^2}\left(\frac{\sqrt{2m(E-V)}}{2\pi\hbar|q-q'|}\right)^{\frac{d-2}{2}} J^+_{\frac{d-2}{2}}(S_0(q,q',E)/\hbar).$$

where $G_0(q,q',E)$ is the short time Green's function (34.48). Using the Bessel function $J^+_\nu = \mathrm{Im}\, H^+_\nu$ asymptotic estimate

$$J_\nu(z) \approx \frac{1}{\Gamma(\nu+1)}\left(\frac{z}{2}\right)^\nu \text{ for } |z| << 1.$$

we obtain the zero length trajectories contribution to the density of states

$$d_0(E) = \frac{m}{\hbar^D 2^{d-1}\pi^{D/2}\Gamma(D/2)}\int_{V(q)<E} d^D q\,[2m(E-V(q))]^{(d-2)/2}\,. \quad (36.10)$$

rescue the original argument, say it is called "Weyl term"

⇑PRELIMINARY

The result is the same as (36.6), the average density estimate $d_0(E)$. The initial wild guess is indeed correct, and

The semiclassical density of states is a sum of the average density of states and the oscillation of the density of states around the average, $d_{sc}(E) = d_0(E) + d_{osc}(E)$, where

$$d_{osc}(E) = \frac{1}{\pi\hbar}\sum_p T_p \sum_{r=1}^{\infty} \frac{\cos(rS_p(E)/\hbar - rm_p\pi/2)}{|\det(1-M_p^r)|^{1/2}} \quad (36.11)$$

follows from the trace formula (36.3).

36.1.2 Regularization of the trace

The real part of the $q' \to q$ zero length Green's function (34.48) is ultraviolet divergent in dimensions $d > 1$, and so is its formal trace (32.17). The short distance behavior of the real part of the Green's function can be extracted from the real part of (34.48) by using the Bessel function expansion for small z

$$Y_\nu(z) \approx \begin{cases} -\frac{1}{\pi}\Gamma(\nu)\left(\frac{z}{2}\right)^{-\nu} & \text{for } \nu \neq 0 \\ \frac{2}{\pi}(\ln(z/2)+\gamma) & \text{for } \nu = 0 \end{cases},$$

where $\gamma = 0.577...$ is the Euler constant. The real part of the Green's function for short distance is dominated by the singular part

$$G_{sing}(|q-q'|,E) = \begin{cases} -\frac{m}{2\hbar^2\pi^{\frac{d}{2}}}\Gamma((d-2)/2)\frac{1}{|q-q'|^{d-2}} & \text{for } d \neq 2 \\ \frac{m}{2\pi\hbar^2}(\ln(2m(E-V)|q-q'|/2\hbar)+\gamma) & \text{for } d = 2 \end{cases}.$$

The *regularized* Green's function

regularization!Green's function
Green's function!regularized
quantum!chaos
Hadamard product regularization

there is no finite leftover?

$$G_{reg}(q,q',E) = G(q,q',E) - G_{sing}(|q-q'|,E)$$

is obtained by subtracting the $q' \to q$ ultraviolet divergence. For the regularized Green's function the Gutzwiller trace formula is

$$\mathrm{tr}\, G_{reg}(E) = -i\pi d_0(E) + \frac{1}{i\hbar}\sum_p T_p \sum_{r=1}^{\infty} \frac{e^{r(\frac{i}{\hbar}S_p(E) - \frac{i\pi}{2}m_p(E))}}{|\det\,(1-M_p^r)|^{1/2}}\,. \quad (36.12)$$

Now you stand where Gutzwiller stood in 1990. You hold the trace formula in your hands. You have no clue how good is the $\hbar \to 0$ approximation, how to take care of the sum over an infinity of periodic orbits, and whether the formula converges at all.

36.2 Semiclassical spectral determinant

The problem with trace formulas is that they diverge where we need them, at the individual energy eigenvalues. What to do? Much of the quantum chaos literature responds to the challenge of wrestling the trace formulas by replacing the delta functions in the density of states (32.18) by Gaussians. But there is no need to do this - we can compute the eigenenergies without any further ado by remembering that the smart way to determine the eigenvalues of linear operators is by determining zeros of their spectral determinants.

A sensible way to compute energy levels is to construct the spectral determinant whose zeroes yield the eigenenergies, $\det\,(\hat{H}-E)_{sc} = 0$. A first guess might be that the spectral determinant is the Hadamard product of form

$$\det\,(\hat{H}-E) = \prod_n (E-E_n),$$

finger here to appendix 23.1: tosect

but this product is not well defined, since for fixed E we multiply larger and larger numbers $(E-E_n)$. This problem is dealt with by *regularization*, discussed below in appendix 36.1.2. Here we offer an impressionistic sketch of regularization.

The logarithmic derivative of $\det\,(\hat{H}-E)$ is the (formal) trace of the Green's function

$$-\frac{d}{dE}\ln\det\,(\hat{H}-E) = \sum_n \frac{1}{E-E_n} = \mathrm{tr}\, G(E).$$

semiclassical!zeta function@"qS cycle!expansion

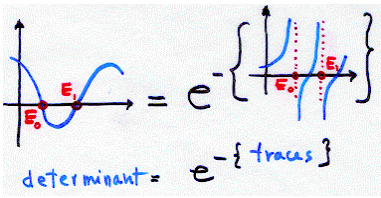

Figure 36.3: A sketch of how spectral determinants convert poles into zeros: The trace shows $1/(E-E_n)$ type singularities at the eigenenergies while the spectral determinant goes smoothly through zeroes.

This quantity, not surprisingly, is divergent again. The relation, however, opens a way to derive a convergent version of $\det(\hat{H}-E)_{sc}$, by replacing the trace with the regularized trace

$$-\frac{d}{dE}\ln\det(\hat{H}-E)_{sc} = \mathrm{tr}\, G_{reg}(E).$$

The regularized trace still has $1/(E-E_n)$ poles at the semiclassical eigenenergies, poles which can be generated only if $\det(\hat{H}-E)_{sc}$ has a zero at $E=E_n$, see figure 36.3. By integrating and exponentiating we obtain

$$\det(\hat{H}-E)_{sc} = \exp\left(-\int^E dE'\,\mathrm{tr}\, G_{reg}(E')\right)$$

Now we can use (36.12) and integrate the terms coming from periodic orbits, using the relation (34.17) between the action and the period of a periodic orbit, $dS_p(E) = T_p(E)dE$, and the relation (32.21) between the density of states and the spectral staircase, $dN_{sc}(E) = d_0(E)dE$. We obtain the *semiclassical zeta function*

$$\det(\hat{H}-E)_{sc} = e^{i\pi N_{sc}(E)}\exp\left(-\sum_p\sum_{r=1}^{\infty}\frac{1}{r}\frac{e^{ir(S_p/\hbar-m_p\pi/2)}}{|\det(1-M_p^r)|^{1/2}}\right). \quad (36.13)$$

☞ chapter 18

We already know from the study of classical evolution operator spectra of chapter 15 that this can be evaluated by means of cycle expansions. The beauty of this formula is that everything on the right side – the cycle action S_p, the topological index m_p and monodromy matrix M_p determinant – is intrinsic, coordinate-choice independent property of the cycle p.

We also neglected the slow energy dependence of the Jacobian determinant

36.3 One-dof systems

It has been a long trek, a stationary phase upon stationary phase. Let us check whether the result makes sense even in the simplest case, for quantum mechanics in one spatial dimension.

In one dimension the average density of states follows from the one-dof form of the oscillating density (36.11) and of the average density (36.8)

$$d(E) = \frac{T_p(E)}{2\pi\hbar} + \sum_r \frac{T_p(E)}{\pi\hbar}\cos(rS_p(E)/\hbar - rm_p(E)\pi/2). \quad (36.14)$$

Bohr!-Sommerfeld quantization
spectral!determinant@"fd!1-"dof

The classical particle oscillates in a single potential well with period $T_p(E)$. There is no monodromy matrix to evaluate, as in one dimension there is only the parallel coordinate, and no transverse directions. The r repetition sum in (36.14) can be rewritten by using the Fourier series expansion of a delta spike train

$$\sum_{n=-\infty}^{\infty} \delta(x-n) = \sum_{k=-\infty}^{\infty} e^{i2\pi kx} = 1 + \sum_{k=1}^{\infty} 2\cos(2\pi kx).$$

We obtain

$$d(E) = \frac{T_p(E)}{2\pi\hbar} \sum_n \delta(S_p(E)/2\pi\hbar - m_p(E)/4 - n). \tag{36.15}$$

This expression can be simplified by using the relation (34.17) between T_p and S_p, and the identity (9.7) $\delta(x-x^*) = |f'(x)|\delta(f(x))$, where x^* is the only zero of the function $f(x^*) = 0$ in the interval under consideration. We obtain

$$d(E) = \sum_n \delta(E - E_n),$$

where the energies E_n are the zeroes of the arguments of delta functions in (36.15)

$$S_p(E_n)/2\pi\hbar = n - m_p(E)/4\,,$$

where $m_p(E) = m_p = 2$ for smoth potential at both turning points, and $m_p(E) = m_p = 4$ for two billiard (infinite potential) walls. These are precisely the *Bohr-Sommerfeld quantized energies* E_n, defined by the condition

WKB eq ref here

$$\oint p(q, E_n)dq = h\left(n - \frac{m_p}{4}\right). \tag{36.16}$$

In this way the trace formula recovers the well known 1-dof quantization rule. In one dimension, the average of states can be expressed from the quantization condition. At $E = E_n$ the exact number of states is n, while the average number of states is $n - 1/2$ since the staircase function $N(E)$ has a unit jump in this point

$$N_{sc}(E) = n - 1/2 = S_p(E)/2\pi\hbar - m_p(E)/4 - 1/2. \tag{36.17}$$

spectral!determinant@"fd!2 "dof

The 1-dof spectral determinant follows from (36.13) by dropping the monodromy matrix part and using (36.17)

$$\det\left(\hat{H}-E\right)_{sc} = \exp\left(-\frac{i}{2\hbar}S_p + \frac{i\pi}{2}m_p\right)\exp\left(-\sum_r \frac{1}{r}e^{\frac{i}{\hbar}rS_p - \frac{i\pi}{2}rm_p}\right) . \quad (36.18)$$

Summation yields a logarithm by $\sum_r t^r/r = -\ln(1-t)$ and we get

$$\begin{aligned}\det\left(\hat{H}-E\right)_{sc} &= e^{-\frac{i}{2\hbar}S_p + \frac{im_p}{4} + \frac{i\pi}{2}}\left(1 - e^{\frac{i}{\hbar}S_p - i\frac{m_p}{2}}\right) \\ &= 2\sin\left(S_p(E)/\hbar - m_p(E)/4\right) .\end{aligned}$$

So in one dimension, where there is only one periodic orbit for a given energy E, nothing is gained by going from the trace formula to the spectral determinant. The spectral determinant is a real function for real energies, and its zeros are again the Bohr-Sommerfeld quantized eigenenergies (36.16).

36.4 Two-dof systems

For flows in two configuration dimensions the monodromy matrix M_p has two eigenvalues Λ_p and $1/\Lambda_p$, as explained in sect. 5.2. Isolated periodic orbits can be elliptic or hyperbolic. Here we discuss only the hyperbolic case, when the eigenvalues are real and their absolute value is not equal to one. The determinant appearing in the trace formulas can be written in terms of the expanding eigenvalue as

$$\left|\det\left(1-M_p^r\right)\right|^{1/2} = \left|\Lambda_p^r\right|^{1/2}\left(1-1/\Lambda_p^r\right) ,$$

and its inverse can be expanded as a geometric series

$$\frac{1}{\left|\det\left(1-M_p^r\right)\right|^{1/2}} = \sum_{k=0}^{\infty}\frac{1}{\left|\Lambda_p^r\right|^{1/2}\Lambda_p^{kr}} .$$

restore this section and exercises

With the 2-dof expression for the average density of states (36.9) the spectral determinant becomes

$$\begin{aligned}\det\left(\hat{H}-E\right)_{sc} &= e^{i\frac{m\mathcal{A}E}{2\hbar^2}}\exp\left(-\sum_p\sum_{r=1}^{\infty}\sum_{k=0}^{\infty}\frac{e^{ir(S_p/\hbar - m_p\pi/2)}}{r\left|\Lambda_p^r\right|^{1/2}\Lambda_p^{kr}}\right) \\ &= e^{i\frac{m\mathcal{A}E}{2\hbar^2}}\prod_p\prod_{k=0}^{\infty}\left(1-\frac{e^{\frac{i}{\hbar}S_p - \frac{i\pi}{2}m_p}}{\left|\Lambda_p\right|^{1/2}\Lambda_p^k}\right) . \quad (36.19)\end{aligned}$$

⇓PRIVATE

36.5 Semiclassical zeta function

a section on the 0 zeta function

Green's function!time dependent

36.6 Noisy trace formula

⇓PRIVATE

In fact I'm Vattay Gábor, just these Indo-Europeans mix up the right order.

⇑PRIVATE

(G. Vattay and P. Cvitanović)

The Fokker-Planck equation (35.14) can be viewed as the 'Schrödinger' problem of the 'quantized' Hamiltonian. The quantization means the introduction of operators $\hat{x} = x$ and $\hat{p} = -D\nabla$. D plays the role of $i\hbar$. The noisy commutators fulfill

$$[\hat{x}, \hat{p}] = D. \tag{36.20}$$

The Schrödinger equation is then

$$D\partial_t \psi = \hat{H}\psi = -D\nabla v\psi + D^2\nabla^2\psi. \tag{36.21}$$

The noise Hamilton operator is not a hermitian one, therefore the eigenenergies E_n defined as

$$\hat{H}\psi_n = E_n\psi_n \tag{36.22}$$

are complex numbers and their conjugates. Another special feature is that the eigenenergies of the Hamilton operator are proportional with D, due to the absence of a D independent potential term. It is then convenient to absorb the D dependence into $s_n = E_n/D$, which is then the eigenvalue of the Fokker-Planck equation.

not Feynman? this is Wiener path integral?

The Feynman path integral formalism can now be extended for this case. The time domain Green's function or in other words the evolution operator in Feynman formalism reads

$$\mathcal{L}^t(x, x') = \int \mathcal{D}x \exp\left(-\frac{1}{D}\int_0^t L(t')dt'\right), \tag{36.23}$$

where $\mathcal{D}x$ denotes the continuous limit of the usual discretized path summation for all possible paths connecting x with x' in time t and the integral in the exponent is the noise action computed for the path.

The analog of the Gutzwiller trace formula in this case is easy to write down:

$$Tr\mathcal{L}(E) = \int_0^\infty dt e^{Et/D} \int dx \mathcal{L}^t(x, x')$$

$$= \frac{1}{D}\sum_{p,r=1}^{\infty}\frac{e^{-\frac{r}{D}\int_0^{T_p}dt(L_p(t)-E)-ir\nu_p\pi}}{|\det\left(M_p^r-1\right)|^{1/2}}, \tag{36.24}$$

where the summation is over over all repaeats of the prime periodic orbits of Hamilton's equations. The action in the exponent, the monodromy matrix, and the topological index are the analogs of those in the Gutzwiller trace formula, with $i\hbar \to 2D$. The periodic orbits of the underlying noiseless dynamics are also the periodic orbits of the Hamilton's equations, with zero momentum $p = 0$. Other periodic orbits are possible. The monodromy matrix, action and topological index for the old periodic orbits have some nice features. [2] The monodromy matrix M_p then has two separate diagonal blocks, each of which is the fundamental matrix J_p of the orbit in the noiseless dynamics. Using this, we can express the semiclassical amplitude as

link gutz. trace

how do you know this: "if the original dynamics is not uniformly hyperbolic"?

$$\frac{1}{|\det\left(M_p^r-1\right)|^{1/2}} = \frac{1}{|\det\left(J_p^r-1\right)|}. \tag{36.25}$$

The topological index counts the number of conjugate points. They come in pairs due to the structure of the matrix, so no phase factor goes into the exponent. For the deterministic periodic orbits, the Lagrangian is zero and by using $s = E/D$, the exponent becomes e^{srT_p}. Each deterministic periodic orbit p contributes to the trace formula a term of form

$$\mathrm{tr}\,\mathcal{L}|_p \sim \frac{1}{D}\sum_r \frac{e^{srT_p}}{|\det\left(J_p^r-1\right)|},$$

eq link, CvitEck here

[3] This is exactly the classical trace formula.

local minima, where variational searches fail

On the new periodic orbits, which were not present in the noiseless case, these simplifications cannot be carried out.

In the exponent, an extra $-\frac{1}{D}\int_0^{T_p} L_p(t)dt$ term shows up and the monodromy matrix cannot be factorized as above. The quantity $R_p = \int_0^{T_p} L_p(t)dt$ is a positive number independent of D. In the weak noise limit, these orbits are strongly suppressed due to the small term $e^{-R_p/D}$.

⇑PRIVATE

We have shown the analogy of the quantum and noise problems. [4]

Commentary

⇓PRELIMINARY

Remark 36.1 Validity of the semiclassical quantization. For a scholarly discussion of the many puzzles that arise in the study of the validity and applicability of the semiclassical quantization developed above, see the review by Voros [**?**].

[2] Mason: define monodromy matrix, action and topological index

[3] Vattay: $1/D$ is just because the argument of the trace is E instead of s. In $Tr\mathcal{L}(s)$ the $1/D$ factor is not present.

[4] Mason: you have not

The main problem is that the semiclassical Van Vleck propagators are not multiplicative - the more appropriate term for the operation of joining them by evaluating saddlepoints is Mather's *conjunction* that plays the same role in the variational theory of area preserving twist maps.

conjunction

Remark 36.2 Where does the symplectic structure come from? The Hamiltonian or symplectic structure of the equations describing the most probable path was not present in the original deterministic equation $\dot{x} = v(x)$. It is a property of the approximation we made. Instead of x and p, one can introduce other canonical coordinates via a canonical transformation. But then their 'quantization' will not reproduce the Fokker-Planck equation. We get the Fokker-Planck equation only if the system is quantized in Cartesian coordinates. We can say that the symplectic symmetry is present only on the first level of the approximation. Thinking about the correspondence between classical and quantum mechanics, we see that the Hamilton equations of motion are the first approximation of quantum mechanics. However, there is no way to quantize systems in general canonical coordinates. In this line of thought, the symplectic structure is not a deep symmetry of nature, but an artifact of a semiclassical approximation to quantum dynamics. (Gábor Vattay)

⇑PRELIMINARY

Remark 36.3 Zeta functions. For "zeta function" nomenclature, see remark 15.4 on page 282.

Résumé

to "Why does it work"?

Spectral determinants and dynamical zeta functions arise both in classical and quantum mechanics because in both the dynamical evolution can be described by the action of linear evolution operators on infinite-dimensional vector spaces. In quantum mechanics the periodic orbit theory arose from studies of semi-conductors, and the unstable periodic orbits have been measured in experiments on the very paradigm of Bohr's atom, the hydrogen atom, this time in strong external fields.

In practice, most "quantum chaos" calculations take the stationary phase approximation to quantum mechanics (the Gutzwiller trace formula, possibly improved by including tunneling periodic trajectories, diffraction corrections, etc.) as the point of departure. Once the stationary phase approximation is made, what follows is *classical* in the sense that all quantities used in periodic orbit calculations - actions, stabilities, geometrical phases - are classical quantities. The problem is then to understand and control the convergence of classical periodic orbit formulas.

While various periodic orbit formulas are formally equivalent, practice shows that some are preferable to others. Three classes of periodic orbit formulas are frequently used:

Trace formulas. The trace of the semiclassical Green's function

$$\operatorname{tr} G_{sc}(E) = \int dq\, G_{sc}(q,q,E)$$

is given by a sum over the periodic orbits (36.12). While easiest to derive, in calculations the trace formulas are inconvenient for anything other than the leading eigenvalue estimates, as they tend to be divergent in the region of physical interest. In classical dynamics trace formulas hide under a variety of appelations such as the f–α or multifractal formalism; in quantum mechanics they are known as the Gutzwiller trace formulas.

refeq 7.19

refeq ??

Zeros of *Ruelle or dynamical zeta functions*

$$1/\zeta(s) = \prod_p (1-t_p), \quad t_p = \frac{1}{|\Lambda_p|^{1/2}} e^{\frac{i}{\hbar}S_p - i\pi m_p/2}$$

yield, in combination with cycle expansions, the semiclassical estimates of *quantum* resonances. For hyperbolic systems the dynamical zeta functions have good convergence and are a useful tool for determination of classical and quantum mechanical averages.

Spectral determinants, Selberg-type zeta functions, Fredholm determinants, functional determinants are the natural objects for spectral calculations, with convergence better than for dynamical zeta functions, but with less transparent cycle expansions. The 2-dof semiclassical spectral determinant (36.19)

$$\det(\hat{H}-E)_{sc} = e^{i\pi N_{sc}(E)} \prod_p \prod_{k=0}^{\infty} \left(1 - \frac{e^{iS_p/\hbar - i\pi m_p/2}}{|\Lambda_p|^{1/2}\Lambda_p^k}\right)$$

is a typical example. Most periodic orbit calculations are based on cycle expansions of such determinants.

As we have assumed repeatedly during the derivation of the trace formula that the periodic orbits are isolated, and do not form families (as is the case for integrable systems or in KAM tori of systems with mixed phase space), the formulas discussed so far are valid only for hyperbolic and elliptic periodic orbits.

For deterministic dynamical flows and number theory, spectral determinants and zeta functions are exact. The quantum-mechanical ones, derived by the Gutzwiller approach, are at best only the stationary phase approximations to the exact quantum spectral determinants, and for quantum mechanics an important conceptual problem arises already at the level of derivation of the semiclassical formulas; how accurate are they, and can the periodic orbit theory be systematically improved?

References

[36.1] R.G. Littlejohn, *J. Stat. Phys.* **68**, 7 (1992).

[36.2] L.D. Landau and E.M. Lifshitz, *Mechanics* (Pergamon, London, 1959).

[36.3] R.G. Littlejohn, *"Semiclassical structure of trace formulas"*, in G. Casati and B. Chirikov, eds., *Quantum Chaos*, (Cambridge University Press, Cambridge 1994).

[36.4] M.C. Gutzwiller, *J. Math. Phys.* **8**, 1979 (1967); **10**, 1004 (1969); **11**, 1791 (1970); **12**, 343 (1971).

[36.5] M.C. Gutzwiller, *J. Math. Phys.* **12**, 343 (1971)

[36.6] M.C. Gutzwiller, *Physica* **D5**, 183 (1982)

[36.7] M.C. Gutzwiller, *J. Phys. Chem.* **92**, 3154 (1984).

[36.8] A. Voros, *J. Phys.* **A 21**, 685 (1988).

[36.9] A. Voros, *Aspects of semiclassical theory in the presence of classical chaos*, *Prog. Theor. Phys. Suppl.* **116**, 17 (1994).

[36.10] P. Cvitanović and P.E. Rosenqvist, in G.F. Dell'Antonio, S. Fantoni and V.R. Manfredi, eds., *From Classical to Quantum Chaos, Soc. Italiana di Fisica Conf. Proceed.* **41**, pp. 57-64 (Ed. Compositori, Bologna 1993).

[36.11] A. Wirzba, *CHAOS* **2**, 77 (1992).

[36.12] P. Cvitanović, G. Vattay and A. Wirzba, *"Quantum fluids and classical determinants"*, in H. Friedrich and B. Eckhardt., eds., *Classical, Semiclassical and Quantum Dynamics in Atoms – in Memory of Dieter Wintgen*, *Lecture Notes in Physics* **485** (Springer, New York 1997), `chao-dyn/9608012`.

[36.13] E.B. Bogomolny, CHAOS **2**, 5 (1992).

[36.14] E.B. Bogomolny, *Nonlinearity* **5**, 805 (1992).

⇓PRELIMINARY

[36.15] E.A. Spiegel

Ed will supply the reference

⇑PRELIMINARY

[36.16] M. Kline, *Mathematical Thought from Ancient to Modern Times* (Oxford Univ. Press, Oxford 1972); on Monge and theory of characteristics - chapter 22.7.

[36.17] E.T. Bell, *Men of Mathematics* (Penguin, London 1937).

[36.18] R.P. Feynman, *Statistical Physics* (Addison Wesley, New York 1990).

[36.19] H. Goldstein, *Classical Mechanics* (Addison-Wesley, Reading, 1980); chapter 9.

[36.20] G. Tanner and D. Wintgen, *CHAOS* **2**, 53 (1992).

[36.21] P. Cvitanović and F. Christiansen, *CHAOS* **2**, 61 (1992).

[36.22] M.V. Berry and J.P. Keating, *J. Phys.* **A 23**, 4839 (1990).

[36.23] H.H. Rugh, *"Generalized Fredholm determinants and Selberg zeta functions for Axiom A dynamical systems"*, *Ergodic Theory Dynamical Systems* **16**, 805 (1996).

[36.24] B. Eckhard and G. Russberg, Phys. Rev. **E 47**, 1578 (1993).

[36.25] D. Ruelle, *Statistical Mechanics, Thermodynamical Formalism* (Addison-Wesley, Reading MA, 1987).

[36.26] P. Szépfalusy, T. Tél, A. Csordás and Z. Kovács, Phys. Rev. **A 36**, 3525 (1987).

[36.27] H.H. Rugh, Nonlinearity **5**, 1237 (1992) and H.H. Rugh, *Ph.D. Thesis* (Niels Bohr Institute, 1993).

[36.28] P. Cvitanović, P.E. Rosenqvist, H.H. Rugh and G. Vattay, *Scattering Theory - special issue*, CHAOS (1993).

[36.29] E.J. Heller, S. Tomsovic and A. Sepúlveda CHAOS **2**, *Periodic Orbit Theory - special issue*, 105, (1992).

[36.30] V.I. Arnold, *Geometrical Methods in the Theory of Ordinary Differential Equations*, (Springer, New York 1983).

[36.31] R. Dashen, B. Hasslacher and A. Neveu , "Nonperturbative methods and extended hadron models in field theory. 1. Semiclassical functional methods.", *Phys. Rev.* **D10**, 4114 (1974).

never referred to?:

[36.32] V.I. Arnold, *Geometrical Methods in the Theory of Ordinary Differential Equations* (Springer, New York 1983).

Exercises

Exercise 36.1 Monodromy matrix from second variations of the action. *Show that*

$$D_{\perp j}/D'_{\perp j} = (\mathbf{1} - M) \tag{36.26}$$

Exercise 36.2 Jacobi gymnastics. *Prove that the ratio of determinants in (R.70) can be expressed as*

$$\frac{\det D'_{\perp j}(q_\parallel, 0, E)}{\det D_{\perp j}(q_\parallel, 0, E)} = \det \begin{pmatrix} I - M_{qq} & -M_{qp} \\ -M_{pq} & I - M_{pp} \end{pmatrix} = \det\left(1 - M_j\right), \tag{36.27}$$

where M_j is the monodromy matrix of the periodic orbit.

Exercise 36.3 Volume of d-dimensional sphere. *Show that the volume of a d-dimensional sphere of radius r equals $\pi^{d/2} r^d / \Gamma(1 + d/2)$. Show that $\Gamma(1 + d/2) = \Gamma(d/2) d/2$.*

Exercise 36.4 Average density of states in 1 dimension. *Show that in one dimension the average density of states is given by (36.8)*

$$\bar{d}(E) = \frac{T(E)}{2\pi\hbar},$$

where $T(E)$ is the time period of the 1-dimensional motion and show that

$$\bar{N}(E) = \frac{S(E)}{2\pi\hbar}, \tag{36.28}$$

where $S(E) = \oint p(q, E)\, dq$ is the action of the orbit.

Exercise 36.5 Average density of states in 2 dimensions. *Show that in 2 dimensions the average density of states is given by (36.9)*

$$\bar{d}(E) = \frac{m\mathcal{A}(E)}{2\pi\hbar^2},$$

where $\mathcal{A}(E)$ is the classically allowed area of configuration space for which $U(q) < E$.

[5] Dorte: not sure how to appendix this - and the fax not very clear, so you are on your own!! ⇓PRELIMINARY

Exercise 36.6 2-d Hamiltonian flows. *The simplest application of (??) is to 2-dimensional hyperbolic Hamiltonian flows. In this case the derivation of the quasiclassical trace formula is very simple. The [2 × 2]-dimensional phase space fundamental matrix is*

$$\begin{pmatrix} \delta q' \\ \delta p' \end{pmatrix} = M \begin{pmatrix} \delta q \\ \delta p \end{pmatrix} .$$

In 2-d phase space the curvature matrix $\mathbf{M}$ *is* $[1 \times 1]$*, ie. the scalar* $\kappa := \partial p/\partial q$*. Divide through with* δq*.*

$$\frac{dq'}{dq} \begin{pmatrix} 1 \\ \kappa' \end{pmatrix} = M \begin{pmatrix} 1 \\ \kappa \end{pmatrix} . \tag{36.29}$$

Writing $M = \begin{pmatrix} A & B \\ C & D \end{pmatrix}$ *we have*

$$\frac{dq'}{dq} = A + B\kappa\,, \qquad \kappa' = M(\kappa) = \frac{A + B\kappa}{C + D\kappa}\,.$$

For a periodic orbit there are two solutions

$$M \begin{pmatrix} 1 \\ \kappa_\pm \end{pmatrix} = \Lambda_\pm \begin{pmatrix} 1 \\ \kappa_\pm \end{pmatrix}$$

so the configuration volume ratio $\frac{dq'}{dq}$ *is for a periodic orbit simply the eigenvalue of the phase space Jacobian. The* κ *part of the trace is*

$$\int d\kappa\, \delta(\kappa - M(\kappa)) = \frac{1}{\left|1 - \frac{\partial M}{\partial \kappa}\right|}\,. \qquad \frac{\partial M}{\partial \kappa} = \frac{1}{(A + B\kappa)^2} = \frac{1}{\Lambda_\pm^2}$$

so the curvature matrix contribution to the trace is

$$\int d\kappa\, \delta(\kappa - M(\kappa)) \left|\frac{dq'}{dq}\right|^{1/2} = \frac{|\Lambda_+|^{1/2}}{\left|1 - 1/\Lambda_+^2\right|} + \frac{|\Lambda_-|^{1/2}}{\left|1 - 1/\Lambda_-^2\right|}$$

Substituting into (15.7) yields the spectral determinant

$$\begin{aligned} \det(\mathbf{1} - \mathcal{L}) &= \exp\left(-\sum_{p,r} \frac{1}{r\,|\,\Lambda_p^r\,|} \frac{e^{irS_p(E) + i\,topological p\pi}}{(1 - 1/\Lambda_p^r)^2} \Delta_{p,r}\right) \\ \Delta_{p,r} &= \frac{|\,\Lambda_p^r\,|^{1/2}}{1 - 1/\Lambda_p^{2r}} + \frac{|\,\Lambda_p^r\,|^{-5/2}}{1 - 1/\Lambda_p^{2r}}\,, \end{aligned} \tag{36.30}$$

⇑PRELIMINARY

periodic!orbit extraction—(
periodic!orbit condition
super-stable fixed point
super-exponential!convergence
convergence!super-exponential

Chapter 37

Relaxation for cyclists

Cycles, i.e., solutions of the periodic orbit condition (17.1)

$$f^{t+T}(x) = f^t(x)\,, \qquad T > 0 \tag{37.1}$$

are prerequisite to chapters 14 and 15 evaluation of spectra of classical evolution operators, and, as we shall see in chapter 36, the semiclassical approximations to quantum evolution operators. Chapter 17 offered an introductory, hands-on guide to extraction of periodic orbits by means of the Newton-Raphson method. Here we take a very different tack, drawing inspiration from variational principles of classical mechanics, and path integrals of quantum mechanics.

emphasize importance of equilibrium points!

In sect. 17.2.1 we converted orbits unstable forward in time into orbits stable backwards in time. Indeed, all methods for finding unstable cycles are based on the idea of constructing a new dynamical system such that (*i*) the position of the cycle is the same for the original system and the transformed one, (*ii*) the unstable cycle in the original system is a stable cycle of the transformed system.

The Newton-Raphson method for determining a fixed point x_* for a map $x' = f(x)$ is an example. The method replaces iteration of $f(x)$ by iteration of the Newton-Raphson map (17.5)

$$x'_i = g_i(x) = x_i - \left(\frac{1}{M(x) - \mathbf{1}}\right)_{ij} (f(x) - x)_j\,. \tag{37.2}$$

A fixed point x_* for a map $f(x)$ is also a fixed point of $g(x)$, indeed a super-stable fixed point since $\partial g_i(x_*)/\partial x_j = 0$. This makes the convergence to the fixed point super-exponential.

We also learned in chapter 17 that methods that start with initial guesses for a number of points along a cycle are considerably more robust

cost function
periodic!orbit extraction!relaxation algorithm
relaxation algorithm
gradient algorithm
Henon@H"enon!map
map!H"enon

and safer than searches based on direct solution of the fixed-point condition (37.1). The relaxation (or variational) methods that we shall now describe take this multipoint approach to its logical extreme, and start by a guess of not a few points along a periodic orbit, but a guess of the entire orbit.

The idea is to make an informed rough guess of what the desired periodic orbit looks like globally, and then use variational methods to drive the initial guess toward the exact solution. Sacrificing computer memory for robustness of the method, we replace a guess that a *point* is on the periodic orbit by a guess of the *entire orbit*. And, sacrificing speed for safety, in sect. 37.1 we replace the Newton-Raphson *iteration* by a fictitious time *flow* that minimizes a cost function computed as deviation of the approximate flow from the true flow along a loop approximation to a periodic orbit.

If you have some insight into the topology of the flow and its symbolic dynamics, or have already found a set of short cycles, you might be able to construct an initial approximation to a longer cycle p as a sequence of N points $(\tilde{x}_1^{(0)}, \tilde{x}_2^{(0)}, \cdots, \tilde{x}_N^{(0)})$ with the periodic boundary condition $\tilde{x}_{N+1} = \tilde{x}_1$. Suppose you have an iterative method for improving your guess; after k iterations the cost function

normalize to take account of a continuous time limit?

$$F^2(\tilde{x}^{(k)}) = \sum_i^N \left(\tilde{x}_{i+1}^{(k)} - f(\tilde{x}_i^{(k)})\right)^2 \tag{37.3}$$

or some other more cleverly constructed function (for classical mechanics - action) is a measure of the deviation of the kth approximate cycle from the true cycle. This observation motivates variational approaches to determining cycles.

We give here three examples of such methods, two for maps, and one for billiards. In sect. 37.1 we start out by converting a problem of finding an unstable fixed point of a map into a problem of constructing a differential flow for which the desired fixed point is an attracting equilibrium point. Solving differential equations can be time intensive, so in sect. 37.2 we replace such flows by discrete iterations. In sect. 37.3 we show that for $2D$-dimensional billiard flows variation of D coordinates (where D is the number of Hamiltonian degrees of freedom) suffices to determine cycles in the full $2D$-dimensional phase space.

preface with crete02.tex?

37.1 Fictitious time relaxation

(O. Biham, C. Chandre and P. Cvitanović)

The relaxation (or gradient) algorithm for finding cycles is based on the observation that a trajectory of a map such as the Hénon map (3.15),

$$\begin{aligned} x_{i+1} &= 1 - ax_i^2 + by_i \\ y_{i+1} &= x_i\,, \end{aligned} \tag{37.4}$$

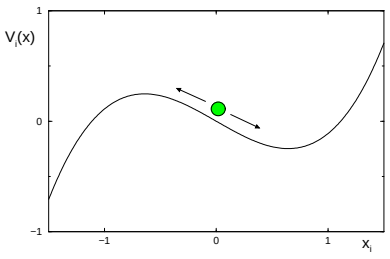

Figure 37.1: "Potential" $V_i(x)$ (37.7) for a typical point along an inital guess trajectory. For $\sigma_i = +1$ the flow is toward the local maximum of $V_i(x)$, and for $\sigma_i = -1$ toward the local minimum. A large deviation of x_i's is needed to destabilize a trajectory passing through such local extremum of $V_i(x)$, hence the basin of attraction is expected to be large.

is a stationary solution of the relaxation dynamics defined by the flow

$$\frac{dx_i}{d\tau} = v_i, \quad i = 1, \ldots, n \tag{37.5}$$

for any vector field $v_i = v_i(x)$ which vanishes on the trajectory. Here τ is a "fictitious time" variable, unrelated to the dynamical time (in this example, the discrete time of map iteration). As the simplest example, take v_i to be the deviation of an approximate trajectory from the exact 2-step recurrence form of the Hénon map (3.16)

$$v_i = x_{i+1} - 1 + ax_i^2 - bx_{i-1}. \tag{37.6}$$

For fixed x_{i-1}, x_{i+1} there are two values of x_i satisfying $v_i = 0$. These solutions are the two extremal points of a local "potential" function (no sum on i)

cannot write a global potential function $V(x) = \sum_i V_i(x)$!

$$v_i = \frac{\partial}{\partial x_i} V_i(x)\,, \qquad V_i(x) = x_i(x_{i+1} - bx_{i-1} - 1) + \frac{a}{3}x_i^3\,. \tag{37.7}$$

Assuming that the two extremal points are real, one is a local minimum of $V_i(x)$ and the other is a local maximum. Now here is the idea; replace (37.5) by

$$\frac{dx_i}{d\tau} = \sigma_i v_i, \quad i = 1, \ldots, n, \tag{37.8}$$

where $\sigma_i = \pm 1$.

The modified flow will be in the direction of the extremal point given by the local maximum of $V_i(x)$ if $\sigma_i = +1$ is chosen, or in the direction of the one corresponding to the local minimum if we take $\sigma_i = -1$. This is not quite what happens in solving (37.8) - all x_i and $V_i(x)$ change at each integration step - but this is the observation that motivates the method. The differential equations (37.8) then drive an approximate initial guess toward the exact trajectory. A sketch of the landscape in which x_i converges towards the proper fixed point is given in figure 37.1. As the "potential" function (37.7) is not bounded for a large $|x_i|$, the flow diverges for initial

Henon@Hénon!map!transient
Henon@Hénon!map!prime cycles
map!Hénon!prime cycles
prime cycle!Hénon map
cycle!prime!Hénon map
Henon@Hénon!map!prime cycles

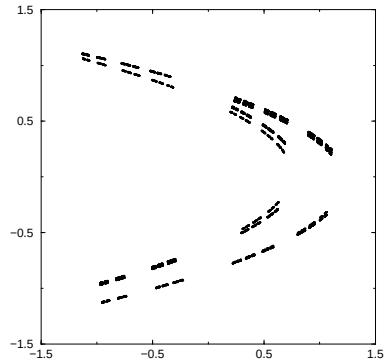

Figure 37.2: The repeller for the Hénon map at $a = 1.8$, $b = 0.3$.

guesses which are too distant from the true trajectory. However, the basin of attraction of initial guesses that converge to a given cycle is nevertheless very large, with the spread in acceptable initial guesses for figure 37.1 of order 1, in contrast to the exponential precision required of initial guesses by the Newton-Raphson method.

Example 37.1 Hénon map cycles. *Our aim in this calculation is to find all periodic orbits of period n for the Hénon map (37.4), in principle at most 2^n orbits. We start by choosing an initial guess trajectory $(x_1, x_2, \cdots, x_n)$ and impose the periodic boundary condition $x_{n+1} = x_1$. The simplest and a rather crude choice of the initial condition in the Hénon map example is $x_i = 0$ for all i. In order to find a given orbit one sets $\sigma_i = -1$ for all iterates i which are local minima of $V_i(x)$, and $\sigma_i = 1$ for iterates which are local maxima. In practice one runs through a complete list of prime cycles, such as the table 11.1. The real issue for all searches for periodic orbits, this one included, is how large is the basin of attraction of the desired periodic orbit? There is no easy answer to this question, but empirically it turns out that for the Hénon map such initial guess almost always converges to the desired trajectory as long as the initial $|x|$ is not too large compared to $1/\sqrt{a}$. Figure 37.1 gives some indication of a typical basin of attraction of the method (see also figure 37.3).*

⇓PRELIMINARY
find this? for table 37.1
⇑PRELIMINARY

(Work through exercise ??). The calculation is carried out by solving the set of n ordinary differential equations (37.8) using a simple Runge-Kutta method with a relatively large step size ($h = 0.1$) until $|v|$ becomes smaller than a given value ε (in a typical calculation $\varepsilon \sim 10^{-7}$). Empirically, in the case that an orbit corresponding to the desired itinerary does not exist, the initial guess escapes to infinity since the "potential" $V_i(x)$ grows without bound.

37.3
page 707

Applied to the Hénon map at the Hénon's parameters choice $a = 1.4$, $b = 0.3$, the method has yielded all periodic orbits to periods as long as $n = 28$, as well as selected orbits up to period $n = 1000$. All prime cycles up to period 10 for the Hénon map, $a = 1.4$ and $b = 0.3$, are listed in table 37.1. The number of unstable periodic orbits for periods $n \leq 28$ is given in table 37.2. Comparing this with the list of all possible 2-symbol alphabet prime cycles, table 11.1, we see that the pruning is quite extensive, with the number of cycle points of period n growing as $e^{0.4645 \cdot n} = (1.592)^n$ rather than as 2^n.

recheck 0.4645, 1.592

contruct grammar

As another example we plot all unstable periodic points up to period $n = 14$ for $a = 1.8$, $b = 0.3$ in figure 37.2. Comparing this repelling set with the strange attractor for the Hénon's parameters figure 3.5, we note the existence of gaps in the set, cut out by the preimages of the escaping regions.

replot figure 37.2 with the correct scale for (37.4), with x_{t-1} horizontally, x_t vertically (so it looks like a parabola, becomes on in the $b \to 0$ limit)

☞ remark 37.2

In practice, the relaxation flow (37.8) finds (almost) all periodic orbits which exist and indicates which ones do not. For the Hénon map the method enables us to calculate almost all unstable cycles of essentially any desired length and accuracy.

n	p	(y_p , x_p)	λ_p
1	0	(-1.13135447 , -1.13135447)	1.18167262
	1	(0.63135447 , 0.63135447)	0.65427061
2	01	(0.97580005 , -0.47580005)	0.55098676
4	0111	(-0.70676677 , 0.63819399)	0.53908457
6	010111	(-0.41515894 , 1.07011813)	0.55610982
	011111	(-0.80421990 , 0.44190995)	0.55245341
7	0011101	(-1.04667757 , -0.17877958)	0.40998559
	0011111	(-1.08728604 , -0.28539206)	0.46539757
	0101111	(-0.34267842 , 1.14123046)	0.41283650
	0111111	(-0.88050537 , 0.26827759)	0.51090634
8	00011101	(-1.25487963 , -0.82745422)	0.43876727
	00011111	(-1.25872451 , -0.83714168)	0.43942101
	00111101	(-1.14931330 , -0.48368863)	0.47834615
	00111111	(-1.14078564 , -0.44837319)	0.49353764
	01010111	(-0.52309999 , 0.93830866)	0.54805453
	01011111	(-0.38817041 , 1.09945313)	0.55972495
	01111111	(-0.83680827 , 0.36978609)	0.56236493
9	000111101	(-1.27793296 , -0.90626780)	0.38732115
	000111111	(-1.27771933 , -0.90378859)	0.39621864
	001111101	(-1.10392601 , -0.34524675)	0.51112950
	001111111	(-1.11352304 , -0.36427104)	0.51757012
	010111111	(-0.36894919 , 1.11803210)	0.54264571
	011111111	(-0.85789748 , 0.32147653)	0.56016658
10	0001111101	(-1.26640530 , -0.86684837)	0.47738235
	0001111111	(-1.26782752 , -0.86878943)	0.47745508
	0011111101	(-1.12796804 , -0.41787432)	0.52544529
	0011111111	(-1.12760083 , -0.40742737)	0.53063973
	0101010111	(-0.48815908 , 0.98458725)	0.54989554
	0101011111	(-0.53496022 , 0.92336925)	0.54960607
	0101110111	(-0.42726915 , 1.05695851)	0.54836764
	0101111111	(-0.37947780 , 1.10801373)	0.56915950
	0111011111	(-0.69555680 , 0.66088560)	0.54443884
	0111111111	(-0.84660200 , 0.34750875)	0.57591048
13	1110011101000	(-1.2085766485 , -0.6729999948)	0.19882434
	1110011101001	(-1.0598110494 , -0.2056310390)	0.21072511

Table 37.1: All prime cycles up to period 10 for the Hénon map, $a = 1.4$ and $b = 0.3$. The columns list the period n_p, the itinerary (defined in remark 37.4), a cycle point (y_p, x_p), and the cycle Lyapunov exponent $\lambda_p = \ln|\Lambda_p|/n_p$. While most of the cycles have $\lambda_p \approx 0.5$, several significantly do not. The $\overline{0}$ cycle point is very unstable, isolated and transient fixed point, with no other cycles returning close to it. At period 13 one finds a pair of cycles with exceptionally low Lyapunov exponents. The cycles are close for most of the trajectory, differing only in the one symbol corresponding to two cycle points straddle the (partition) fold of the attractor. As the system is not hyperbolic, there is no known lower bound on cycle Lyapunov exponents, and the Hénon's strange "attractor" might some day turn out to be nothing but a transient on the way to a periodic attractor of some long period.

equilibrium!point

n	M_n	N_n	n	M_n	N_n	n	M_n	N_n
11	14	156	17	166	2824	23	1930	44392
12	19	248	18	233	4264	24	2902	69952
13	32	418	19	364	6918	25	4498	112452
14	44	648	20	535	10808	26	6806	177376
15	72	1082	21	834	17544	27	10518	284042
16	102	1696	22	1225	27108	28	16031	449520

Table 37.2: The number of unstable periodic orbits of the Hénon map for $a = 1.4$, $b = 0.3$, of all periods $n \leq 28$. M_n is the number of prime cycles of length n, and N_n is the total number of periodic points of period n (including repeats of shorter prime cycles).

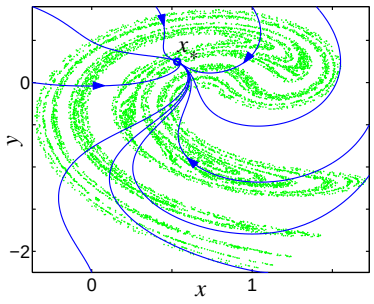

Figure 37.3: Typical trajectories of the vector field (37.9) for the stabilization of a hyperbolic fixed point of the Ikeda map (37.11) located at $(x, y) \approx (0.53275, 0.24689)$. The circle indicates the position of the fixed point. Note that the basin of attraction of this fixed point is large, larger than the entire Ikeda attractor.

The idea of the relaxation algorithm illustrated by the above Hénon map example is that instead of searching for an unstable periodic orbit of a map, one searches for a stable attractor of a vector field. More generally, consider a d-dimensional map $x' = f(x)$ with a hyperbolic fixed point x_*. Any fixed point x_* is by construction an equilibrium point of the fictitious time flow

$$\frac{dx}{d\tau} = f(x) - x. \tag{37.9}$$

If all eigenvalues of the fundamental matrix $J(x_*) = Df(x_*)$ have real parts smaller than unity, then x_* is a stable equilibrium point of the flow.

If some of the eigenvalues have real parts larger than unity, then one needs to modify the vector field so that the corresponding directions of the flow are turned into stable directions in a neighborhood of the fixed point. In the spirit of (37.8), modify the flow by

$$\frac{dx}{d\tau} = \mathbf{C}\,(f(x) - x)\ , \tag{37.10}$$

where $\mathbf{C}$ is a $[d \times d]$ invertible matrix. The aim is to turn x_* into a stable equilibrium point of the flow by an appropriate choice of $\mathbf{C}$. It can be shown that a set of permutation / reflection matrices with one and only one non-vanishing entry ± 1 per row or column (for d-dimensional systems, there are $d!2^d$ such matrices) suffices to stabilize any fixed point. In practice, one chooses a particular matrix $\mathbf{C}$, and the flow is integrated. For each choice of $\mathbf{C}$, one or more hyperbolic fixed points of the map may turn into stable equilibria of the flow.

☞ appendix H.2

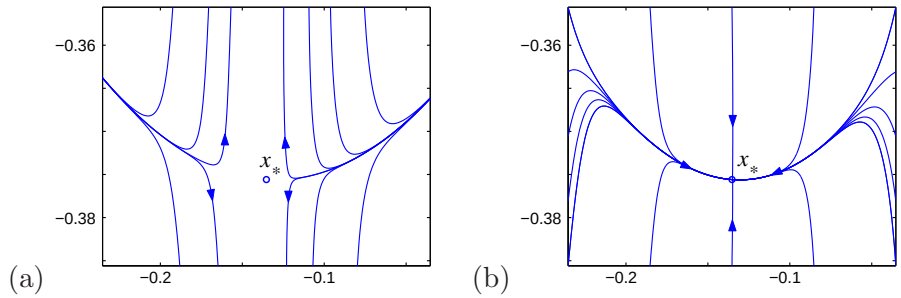

Figure 37.4: Typical trajectories of the vector field (37.10) for a hyperbolic fixed point $(x, y) \approx (-0.13529, -0.37559)$ of f^3, where f is the Ikeda map (37.11). The circle indicates the position of the fixed point. For the vector field corresponding to (a) $\mathbf{C} = \mathbf{1}$, x_* is a hyperbolic equilibrium point of the flow, while for (b) $\mathbf{C} = \left(\begin{smallmatrix} 1 & 0 \\ 0 & -1 \end{smallmatrix}\right)$, x_* is an attracting equilibrium point.

Example 37.2 Ikeda map: *We illustrate the method with the determination of the periodic orbits of the Ikeda map:*

$$\begin{aligned} x' &= 1 + a(x\cos w - y\sin w) \\ y' &= a(x\sin w + y\cos w) \\ \text{where}\quad w &= b - \frac{c}{1+x^2+y^2}\,, \end{aligned} \tag{37.11}$$

with $a = 0.9$, $b = 0.4$, $c = 6$. The fixed point x_* is located at $(x, y) \approx (0.53275, 0.24689)$, with eigenvalues of the fundamental matrix $(\Lambda_1, \Lambda_2) \approx (-2.3897, -0.3389)$, so the flow is already stabilized with $\mathbf{C} = \mathbf{1}$. Figure 37.3 depicts the flow of the vector field around the fixed point x_*.

In order to determine x_*, one needs to integrate the vector field (37.9) forward in time (the convergence is exponential in time), using a fourth order Runge-Kutta or any other integration routine.

In contrast, determination of the 3-cycles of the Ikeda map requires nontrivial $\mathbf{C}$ matrices, different from the identity. Consider for example the hyperbolic fixed point $(x, y) \approx (-0.13529, -0.37559)$ of the third iterate f^3 of the Ikeda map. The flow of the vector field for $\mathbf{C} = \mathbf{1}$, Figure 37.4 (a), indicates a hyperbolic equilibrium point, while for $\mathbf{C} = \left(\begin{smallmatrix} 1 & 0 \\ 0 & -1 \end{smallmatrix}\right)$ the flow of the vector field, figure 37.4 (b) indicates that x_* is an attracting equilibrium point, reached at exponential speed by integration forward in time.

The generalization from searches for fixed points to searches for cycles is straightforward. In order to determine a prime cycle $x = (x_1, x_2, \ldots, x_n)$ of a d-dimensional map $x' = f(x)$, we modify the multipoint shooting method of sect. 17.4.1, and consider the nd-dimensional vector field

$$\frac{dx}{d\tau} = \mathbf{C}\,(f(x) - x)\ , \tag{37.12}$$

where $f(x) = (f(x_n), f(x_1), f(x_2), \ldots, f(x_{n-1}))$, and $\mathbf{C}$ is an invertible $[nd \times nd]$ matrix. For the Hénon map, it is sufficient to consider a set of 2^n diagonal matrices with eigenvalues ± 1. Risking a bit of confusion, we denote by x, $f(x)$ both the d-dimensional vectors in (37.10), and nd-dimensional vectors in (37.12), as the structure of the equations is the same.

37.2 Discrete iteration relaxation method

add to the coauthors list

(C. Chandre, F.K. Diakonos and P. Schmelcher)

The problem with the Newton-Raphson iteration (37.2) is that it requires very precise initial guesses. For example, the nth iterate of a unimodal map has as many as 2^n periodic points crammed into the unit interval, so determination of all cycles of length n requires that the initial guess for each one of them has to be accurate to roughly 2^{-n}. This is not much of a problem for 1-dimensional maps, but making a good initial guess for where a cycle might lie in a d-dimensional state space can be a challenge.

Emboldened by the success of the cyclist relaxation trick (37.8) of manually turning instability into stability by a sign change, we now (*i*) abandon the Newton-Raphson method altogether, (*ii*) abandon the continuous fictitious time flow (37.9) with its time-consuming integration, replacing it by a map g with a larger basin of attraction (not restricted to a linear neighborhood of the fixed point). The idea is to construct a very simple map g, a linear transformation of the original f, for which the fixed point is stable. We replace the fundamental matrix prefactor in (37.2) (whose inversion can be time-consuming) by a constant matrix prefactor

$$x' = g(x) = x + \Delta\tau \mathbf{C}(f(x) - x), \tag{37.13}$$

where $\Delta\tau$ is a positive real number, and $\mathbf{C}$ is a $[d\times d]$ permutation and reflection matrix with one and only one non-vanishing entry ± 1 per row or column. A fixed point of f is also a fixed point of g. Since $\mathbf{C}$ is invertible, the inverse is also true.

This construction is motivated by the observation that for small $\Delta\tau \to d\tau$ the map (37.13) is the Euler method for integrating the modified flow (37.10), with the integration step $\Delta\tau$.

The argument why a suitable choice of matrix $\mathbf{C}$ can lead to the stabilization of an unstable periodic orbit is similar to the one used to motivate the construction of the modified vector field in sect. 37.1. Indeed, the flow (37.8) is the simplest example of this method, with the infinitesimal fictitious time increment $\Delta\tau \to d\tau$, the infinitesimal coordinate correction $(x - x') \to dx_i$, and the $[n\times n]$ diagonal matrix $\mathbf{C} \to \sigma_i = \pm 1$.

For a given fixed point of $f(x)$ we again chose a $\mathbf{C}$ such that the flow in the expanding directions of $M(x_*)$ is turned into a contracting flow. The aim is to stabilize x_* by a suitable choice of $\mathbf{C}$. In the case where the map has multiple fixed points, the set of fixed points is obtained by changing the matrix $\mathbf{C}$ (in general different for each unstable fixed point) and varying initial conditions for the map g. For example, for 2-dimensional dissipative maps it can be shown that the 3 matrices

☞ remark 37.3

$$\mathbf{C} \in \left\{ \begin{pmatrix} 1 & 0 \\ 0 & 1 \end{pmatrix}, \begin{pmatrix} -1 & 0 \\ 0 & 1 \end{pmatrix}, \begin{pmatrix} 1 & 0 \\ 0 & -1 \end{pmatrix} \right\}$$

appendix H.2

suffice to stabilize all kinds of possible hyperbolic fixed points.

If $\Delta\tau$ is chosen sufficiently small, the magnitude of the eigenvalues of the fixed point x_* in the transformed system are smaller than one, and one has a stable fixed point. However, $\Delta\tau$ should not be chosen too small: Since the convergence is geometrical with a ratio $1-\alpha\Delta\tau$ (where the value of constant α depends on the stability of the fixed point in the original system), small $\Delta\tau$ can slow down the speed of convergence. The critical value of $\Delta\tau$, which just suffices to make the fixed point stable, can be read off from the quadratic equations relating the stability coefficients of the original system and those of the transformed system. In practice, one can find the optimal $\Delta\tau$ by iterating the dynamical system stabilized with a given $\mathbf{C}$ and $\Delta\tau$. In general, all starting points converge on the attractor provided $\Delta\tau$ is small enough. If this is not the case, the trajectory either diverges (if $\Delta\tau$ is far too large) or it oscillates in a small section of the state space (if $\Delta\tau$ is close to its stabilizing value).

The search for the fixed points is now straightforward: A starting point chosen in the global neighborhood of the fixed point iterated with the transformed dynamical system g converges to the fixed point due to its stability. Numerical investigations show that the domain of attraction of a stabilized fixed point is a rather extended connected area, by no means confined to a linear neighborhood. At times the basin of attraction encompasses the complete state space of the attractor, so one can be sure to be within the attracting basin of a fixed point regardless of where on the on the attractor on picks the initial condition.

The step size $|g(x)-x|$ decreases exponentially when the trajectory approaches the fixed point. To get the coordinates of the fixed points with a high precision, one therefore needs a large number of iterations for the trajectory which is already in the linear neighborhood of the fixed point. To speed up the convergence of the final part of the approach to a fixed point we recommend a combination of the above approach with the Newton-Raphson method (37.2).

The fixed points of the nth iterate f^n are cycle points of a cycle of period n. If we consider the map

$$x' = g(x) = x + \Delta\tau\mathbf{C}(f^n(x) - x)\,, \tag{37.14}$$

the iterates of g converge to a fixed point provided that $\Delta\tau$ is sufficiently small and $\mathbf{C}$ is a $[d\times d]$ constant matrix chosen such that it stabilizes the flow. As n grows, $\Delta\tau$ has to be chosen smaller and smaller. In the case of the Ikeda map example 37.2 the method works well for $n \leq 20$. As in (37.12), the multipoint shooting method is the method of preference for determining longer cycles. Consider $x = (x_1, x_2, \ldots, x_n)$ and the nd-dimensional map

$$x' = f(x) = (f(x_n), f(x_1), \ldots, f(x_{n-1}))\,.$$

Maupertuis, P.L.M. de
least action principle

Determining cycles with period n for the d-dimensional f is equivalent to determining fixed points of the multipoint dn-dimensional f. The idea is to construct a matrix $\mathbf{C}$ such that the fixed point of f becomes stable for the map:

$$x' = x + \Delta\tau \mathbf{C}(f(x) - x),$$

where $\mathbf{C}$ is now a $[nd \times nd]$ permutation/reflection matrix with only one non-zero matrix element ± 1 per row or column. For any given matrix $\mathbf{C}$, a certain fraction of the cycles becomes stable and can be found by iterating the transformed map which is now a nd dimensional map.

From a practical point of view, the main advantage of this method compared to the Newton-Raphson method is twofold: (*i*) the stability matrix of the flow need not be computed, so there is no large matrix to invert, simplifying considerably the implementation, and (*ii*) empirical basins of attractions for individual $\mathbf{C}$ are much larger than for the Newton-Raphson method. The price is a reduction in the speed of convergence.

37.3 Least action method

(P. Dahlqvist)

The methods of sects. 37.1 and 37.2 are somewhat *ad hoc*, as for general flows and iterated maps there is no fundamental principle to guide us in chosing the cost function, such as (37.3), to vary.

include Per's section 5.5.

For Hamiltonian dynamics, we are on much firmer ground; Maupertuis least action principle. You yawn your way through it in every mechanics course - Maupertuis believed that the principle provided a proof of the existence of God - but as we shall now see, it is a very hands-on numerical method for finding cycles.

Indeed, the simplest and numerically most robust method for determining cycles of planar billiards is given by the principle of least action, or equivalently, by extremizing the length of an approximate orbit that visits a given sequence of disks. In contrast to the multipoint shooting method of sect. 17.4.1 which requires variation of $2N$ phase space points, extremization of a cycle length requires variation of only N bounce positions s_i.

The problem is to find the extremum values of cycle length $L(s)$ where $s = (s_1, \ldots, s_N)$, that is find the roots of $\partial_i L(s) = 0$. Expand to first order

$$\partial_i L(s_0 + \delta s) = \partial_i L(s_0) + \sum_j \partial_i \partial_j L(s_0) \delta s_j + \ldots$$

37.1
page 707

p	Λ_p	T_p
0	9.898979485566	4.000000000000
1	-1.177145519638$\times 10^{1}$	4.267949192431
01	-1.240948019921$\times 10^{2}$	8.316529485168
001	-1.240542557041$\times 10^{3}$	12.321746616182
011	1.449545074956$\times 10^{3}$	12.580807741032
0001	-1.229570686196$\times 10^{4}$	16.322276474382
0011	1.445997591902$\times 10^{4}$	16.585242906081
0111	-1.707901900894$\times 10^{4}$	16.849071859224
00001	-1.217338387051$\times 10^{5}$	20.322330025739
00011	1.432820951544$\times 10^{5}$	20.585689671758
00101	1.539257907420$\times 10^{5}$	20.638238386018
00111	-1.704107155425$\times 10^{5}$	20.853571517227
01011	-1.799019479426$\times 10^{5}$	20.897369388186
01111	2.010247347433$\times 10^{5}$	21.116994322373
000001	-1.205062923819$\times 10^{6}$	24.322335435738
000011	1.418521622814$\times 10^{6}$	24.585734788507
000101	1.525597448217$\times 10^{6}$	24.638760250323
000111	-1.688624934257$\times 10^{6}$	24.854025100071
001011	-1.796354939785$\times 10^{6}$	24.902167001066
001101	-1.796354939785$\times 10^{6}$	24.902167001066
001111	2.005733106218$\times 10^{6}$	25.121488488111
010111	2.119615015369$\times 10^{6}$	25.165628236279
011111	-2.366378254801$\times 10^{6}$	25.384945785676

three-disk@3-disk!prime cycles
prime cycle!3-disk
cycle!prime!3-disk

Table 37.3: All prime cycles up to 6 bounces for the 3-disk fundamental domain, center-to-center separation $R = 6$, disk radius $a = 1$. The columns list the cycle itinerary, its expanding eigenvalue Λ_p, and the length of the orbit (if the velocity=1 this is the same as its period or the action). Note that the two 6 cycles $\overline{001011}$ and $\overline{001101}$ are degenerate due to the time reversal symmetry, but are not related by any discrete spatial symmetry. (Computed by P.E. Rosenqvist.)

and use $M_{ij}(s_0) = \partial_i \partial_j L(s_0)$ in the N-dimensional Newton-Raphson iteration scheme of sect. 17.2.2

$$s_i \mapsto s_i - \sum_j \left(\frac{1}{M(s)} \right)_{ij} \partial_j L(s) \tag{37.15}$$

The extremization is achieved by recursive implementation of the above algorithm, with proviso that if the dynamics is pruned, one also has to check that the final extremal length orbit does not penetrate a billiard wall.

As an example, the short periods and stabilities of 3-disk cycles computed this way are listed table 37.3.

37.2
page 707
17.11
page 334

Explain the fundamental domain reflections signs in table 37.3; link it to a 3-disk figure

37.4 Newton Descent in Loop Space

⇓PRELIMINARY

For a flow described by a set of ODEs, multipoint shooting method of ?? can be quite efficient. However, multipoint shooting requires a set of state space Poincaré sections such that an orbit leaving one section reaches

link refsects:MultDimDescent

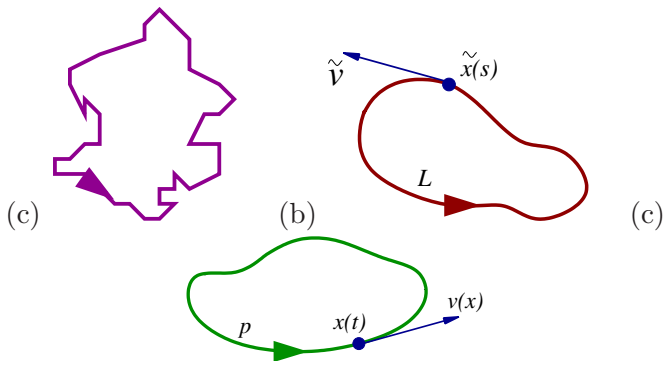

Figure 37.5: (a) A continuous path; (b) a loop L with its tangent velocity vector $\tilde{v}$; (c) a periodic orbit p defined by the vector field $v(x)$.

the next one in a qualitatively predictable manner, without traversing other sections along the way. In turbulent, high-dimensional flows such sequences of sections are hard to come by. One cure for this ill might be a large set of Poincaré sections, with the intervening flight segments short and controllable. Here we shall take another path, and discard fixed Poincaré sections altogether.

Emboldened by success of methods such as the multipoint shooting (which eliminates the long-time exponential instability by splitting an orbit into a number of short segments, each with a controllable expansion rate) and the cyclist relaxation methods of sect.?! (which replace map iteration by a contracting flow whose attractor is the desired periodic orbit of the original iterative dynamics), we now describe a method in which the initial guess is not a finite set of points, but an entire smooth, differentiable closed loop.

A general flow (**??**) has no extremal principle associated with it, the simplification of so there is a great deal of arbitrariness in constructing a flow in a loop space. We shall introduce here several simplest conceivable cost functions which penalize mis-orientation of the local loop tangent vector $\tilde{v}(\tilde{x})$ relative to the dynamical velocity field $v(\tilde{x})$ of (**??**), and construct a flow in the loop space which minimizes this function. This flow is corralled by general topological features of the dynamics, with rather distant initial guesses converging to the desired orbit. Once the loop is sufficiently close to the periodic orbit, faster numerical algorithms can be employed to pin it down.

In order to set the notation, we shall distinguish between (see figure 37.5):

closed path: any closed (not necessarily differentiable) continuous curve $J \subset \mathcal{M}$.

loop: a smooth, differentiable closed curve $\tilde{x}(s) \in L \subset \mathcal{M}$, parametrized by $s \in [0, 2\pi]$ with $\tilde{x}(s) = \tilde{x}(s+2\pi)$, with the magnitude of the loop tangent

vector fixed by the (so far arbitrary) parametrization of the loop,

$$\tilde{v}(\tilde{x}) = \frac{d\tilde{x}}{ds}\,, \quad \tilde{x} = \tilde{x}(s) \in L\,.$$

annulus: a smooth, differentiable surface $\tilde{x}(s,\tau) \in L(\tau)$ swept by a family of loops $L(\tau)$, by integration along a fictitious time flow (see figure 37.6 (a))

$$\dot{\tilde{x}} = \frac{\partial \tilde{x}}{\partial \tau}\,.$$

periodic orbit: given a smooth vector field $v = v(x)$, $(x,v) \in \mathbf{T}\mathcal{M}$, periodic orbit $x(t) \in p$ is a solution of

$$\frac{dx}{dt} = v(x)\,, \quad \text{such that } x(t) = x(t+T_p),$$

where T_p is the shortest period of p.

37.4.1 Loop parametrizations

Euclidean length

$$d^2 s = \sum_i dx_i^2$$

then

$$\tilde{v}(\tilde{x}) = \frac{d\tilde{x}}{ds} = \hat{n}\,.$$

is the unit tnagent vector: geometrically intrinsic, dimensionless and geometrically natural - but dynamically unnutural, knows nothing about the flow v.

Some immediate choices of the metric

$$d^2 s = g^{ij} dx_i dx_j$$

Euclidean

$$g^{ij} = \delta^{ij}$$

Parallel velocity (1-dimensional)

$$g^{ij} = \frac{v^i v^j}{v^2}$$

time!ordered integration

Transverse velocity ($(d$-1)-dimensional)

$$g^{ij} = \delta^{ij} - \frac{v^i v^j}{v^2}$$

Local shear (too local to be appealing)

$$g^{ij} = \left(A^T A\right)^{ij}$$

where

$$A_{ij}(x) = \frac{\partial v_i(x)}{\partial x_j}$$

from (37.21).

The deformation after a finite time t is described by the fundamental matrix

$$M^t(x_0) = \mathbf{T} e^{\oint_L \frac{dx_\parallel}{v_\parallel} \mathbf{A}(x(\tau))} ,$$

where $\mathbf{T}$ stands for the *time-ordered* integration. Its eigenvalues and eigendirections describe the deformation of an initial infinitesimal sphere of neighboring trajectories into an ellipsoid a finite time t later.

Symmetric and diagonalizable matrix $\mathbf{M} = (M^t)^T M^t$, with real positive eigenvalues $\{|\Lambda_1|^2 \geq \ldots \geq |\Lambda_d|^2\}$, and a complete orthonormal set of eigenvectors of $\{\mathbf{e}^1, \ldots, \mathbf{e}^d\}$. In the $\mathbf{M}\mathbf{e}^i = |\Lambda_i|\mathbf{e}^i$ eigenbasis, we have (37.32)

$$\mathbf{e}^{iT} \cdot \mathbf{M} \cdot \mathbf{e}^j = \delta^{ij} |\Lambda_i|^2 , \tag{37.16}$$

Prefereable, as intrinsic to the loop (prove: Λ_i smooth conjugacy invariants), and the eigendirections describe the invariant unstable/stable manifolds. The cost functional now measures the growth of an error along the loop

$$F^2[\tilde{x}] = \oint_L ds\, (\tilde{v} - v)_i |\Lambda_i|^2 , \tag{37.17}$$

penalizing errors in unstable directions, and ignoring the errors in the strongly contarcting directions (as the flow anyway takes care of them).

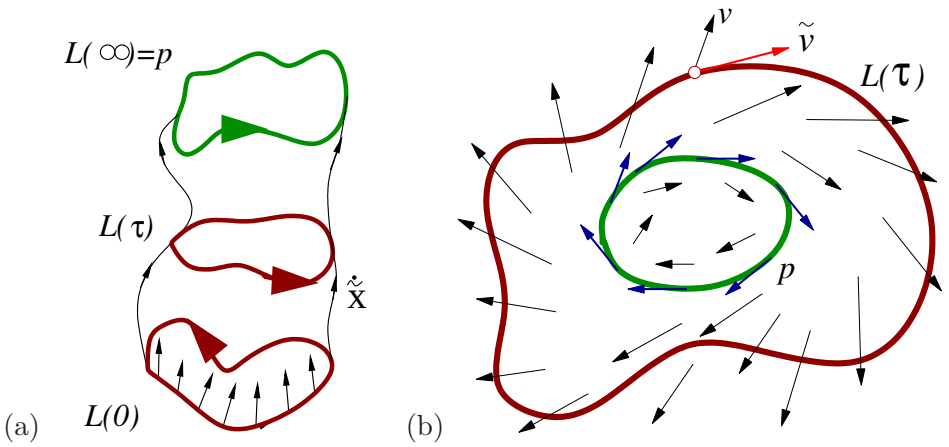

Figure 37.6: (a) An annulus $L(\tau)$ with vector field $\dot{\tilde{x}}$ connecting smoothly the initial loop $L(0)$ to a periodic orbit p. (b) In general the orientation of the loop tangent $\tilde{v}(\tilde{x})$ does not coincide with the orientation of the velocity field $v(\tilde{x})$; for a periodic orbit p it does so at every $x \in p$.

37.4.2 Newton Descent in the Loop Space

In the spirit of (**??**), we now define a cost functional for a loop and the associated fictitious time τ flow which sends an initial loop $L(0)$ via a loop family $L(\tau)$ into the periodic orbit $p = L(\infty)$, see figure 37.6 (a). The only thing that we are given is the velocity field $v(x)$, and we want to "comb" the loop $L(\tau)$ in such a way that its tangent field $\tilde{v}$ aligns with v everywhere, see figure 37.6 (b). The simplest cost functional for the job is

$$F^2[\tilde{x}] = \frac{1}{2\pi} \oint_L ds\, (\tilde{v} - v)^2\,, \quad \tilde{v} = \tilde{v}(\tilde{x}(s,\tau))\,, \quad v = v(\tilde{x}(s,\tau))\,. \tag{37.18}$$

Need to match the magnitude of the tangent field $\tilde{v}$ (measured in the loop parametrization units s) to the velocity field v (measured in the dynamical time units t). $|v|$ cannot vanish anywhere along the loop $L(\tau)$, as in that case the loop would be passing through an equilibrium point, and have infinite period.

Take a derivative of the cost functional $F^2[\tilde{x}]$ with respect to the (yet undetermined) fictitious time τ,

$$\frac{dF^2}{d\tau} = \frac{1}{\pi} \oint_L ds\, (\tilde{v} - v)\, \frac{d}{d\tau}(\tilde{v} - v)\,.$$

The simplest, exponentially decreasing cost functional is obtained by taking the $\tilde{x}(s,\tau)$ dependence on τ to be point-wise proportional to the deviation of the two vector fields

$$\frac{d}{d\tau}(\tilde{v} - v) = -(\tilde{v} - v)\,, \tag{37.19}$$

so the fictitious time flow drives the loop to $L(\infty) = p$, see figure 37.6 (a):

$$\tilde{v} - v = e^{-\tau}(\tilde{v} - v)|_{\tau=0}\,. \tag{37.20}$$

Making the $\tilde{x}$ dependence in (37.19) explicit we obtain our main result, the Newton descent PDE which evolves the initial loop $L(0)$ into the desired periodic orbit p

$$\frac{\partial^2 \tilde{x}}{\partial s \partial \tau} - A\frac{\partial \tilde{x}}{\partial \tau} - \frac{\partial}{\partial \tau} v = v - \tilde{v}\,, \qquad A_{ij}(x) = \frac{\partial v_i(x)}{\partial x_j} \tag{37.21}$$

in the fictitious time $\tau \to \infty$. Here A is the stability matrix of the flow (its integral around p yields the linearized stability matrix for the periodic orbit p).

37.4.3 A metric for the fictitous time flow?

Ideas:
invariant manifold wiath a few unstable directions
∞ strongly contarcting directions.
"noise" should be uniform in the rescaled coordinates.

As any pair of nearby points on a cycle returns to itself exactly at each cycle period, the eigenvalue of the fundamental matrix corresponding to the eigenvector along the flow necessarily equals unity for all periodic orbits. Hence flows require a separate treatment for the longitudinal direction. To find an isolated prime cycle p of period T_p, restrict the search to an infinitesimally thin tube $\mathcal{M}_p$ enveloping the cycle (see figure 1.11), and choose a local coordinate system with a longitudinal coordinate $dx_\parallel$ along the direction of the flow, and d transverse coordinates $x_\perp$

$$\int_{\mathcal{M}_p} dx_\perp dx_\parallel\, \delta\big(x_\perp - f^t_\perp(x)\big)\, \delta\Big(x_\parallel - f^t_\parallel(x)\Big)\ . \tag{37.22}$$

Let $v(x)$ be the magnitude of the velocity at the point x along the flow. $v(x)$ is strictly positive, as otherwise the orbit would stagnate for infinite time at $v(x) = 0$ points, and that would get us nowhere. Therefore we can
change $\sigma \to \tau'$ here
parametrize the longitudinal coordinate $x_\parallel$ by the flight time

$$x_\parallel(\tau) \;=\; \int_0^\tau d\sigma\, v(\sigma)$$

where $v(\sigma) = v(x_\parallel(\sigma))$, and L_p is the length of the circuit on which the periodic orbit lies, $\tau \in [0, T_p]$).

$$\Big(f^t_\parallel(x) - x_\parallel\Big) = \int_\tau^{t+\tau} d\sigma\, v(\sigma)\Big|_{mod\, L_p}$$

so that the integral around the longitudinal coordinate is rewritten as

time!ordered integration

$$\int_0^{L_p} dx_\parallel \, \delta\Big(x_\parallel - f_\parallel^t(x)\Big) \tag{37.23}$$

For the remaining transverse integration variables the fundamental matrix is defined in a reduced Poincaré surface of section $\mathcal{P}$ of constant $x_\parallel$. Linearization of the periodic flow transverse to the orbit yields

$$\int_{\mathcal{P}} dx_\perp \delta\Big(x_\perp - f_\perp^{rT_p}(x)\Big) = \frac{1}{\left|\det\left(\mathbf{1} - M_p^r\right)\right|} \,, \tag{37.24}$$

where M_p is the p-cycle $[d\times d]$ *transverse* fundamental matrix, and as in (14.5) we have to assume hyperbolicity, i.e., that the magnitudes of all transverse eigenvalues are bounded away from unity.

37.4.4 Cycle stabilities are cycle invariants

A neighborhood of a trajectory deforms as it is transported by a flow. In the linear approximation, the stability matrix $\mathbf{A}$ describes the shearing/compression/expansion of an infinitesimal neighborhood in an infinitesimal time step. The deformation after a finite time t is described by the fundamental matrix

$$M^t(x_0) = \mathbf{T} e^{\int_0^t d\tau \mathbf{A}(x(\tau))} \,,$$

where $\mathbf{T}$ stands for the *time-ordered* integration. Its eigenvalues and eigendirections describe the deformation of an initial infinitesimal sphere of neighboring trajectories into an ellipsoid a finite time t later. Nearby trajectories separate exponentially along unstable directions, approach each other along stable directions, and change slowly (algebraically) their distance along marginal directions. The fundamental matrix M^t is in general neither symmetric, nor diagonalizable by a rotation, nor do its (left or right) eigenvectors define an orthonormal coordinate frame. Furthermore, although the stability matrices are multiplicative along the flow, in dimensions higher than one their eigenvalues in general are not. This lack of multiplicativity has important repercussions for both classical and quantum dynamics.

☞ appendix I.1

⇓PRIVATE

☞ chapter 40

⇑PRIVATE

The 1-dimensional map cycle stability Λ_p is a product of derivatives over all points around the cycle, and is therefore independent of which periodic point is chosen as the initial one. In higher dimensions the form of the fundamental matrix $M_p(x_0)$ in (8.1) does depend on the choice of coordinates and the initial point $x_0 \in p$. Nevertheless, as we shall now show, the cycle stability *eigenvalues* are intrinsic property of a cycle also for multi-dimensional flows. Consider the ith eigenvalue, eigenvector pair $(\Lambda_{p,i}, \mathbf{e}_i)$ computed from M_p evaluated at a cycle point,

$$M_p(x)\mathbf{e}_i(x) = \Lambda_{p,i}\mathbf{e}_i(x) \,, \quad x \in p \,. \tag{37.25}$$

invariance!of flows
nonhyperbolic!flow

Consider another point on the cycle at time t later, $x' = f^t(x)$ whose fundamental matrix is $M_p(x')$. By the group property (4.33), $M^{T_p+t} = M^{t+T_p}$, and the fundamental matrix at x' can be written either as

$$M^{T_p+t}(x) = M^{T_p}(x')M^t(x) = M_p(x')M^t(x)\,, \quad \text{or} \quad M^{t+T_p}(x) = M^t(x)M_p(x)\,.$$

Multiplying (8.9) by $M^t(x)$, we find that the fundamental matrix evaluated at x' has the same eigenvalue,

$$M_p(x')\mathbf{e}_i(x') = \Lambda_{p,i}\mathbf{e}_i(x')\,, \quad \mathbf{e}_i(x') = M^t(x)\mathbf{e}_i(x)\,, \tag{37.26}$$

but with the eigenvector $\mathbf{e}_i$ transported along the flow $x \to x'$ to $\mathbf{e}_i(x') = M^t(x)\mathbf{e}_i(x)$. Hence, M_p evaluated anywhere along the cycle has the same set of stability eigenvalues $\{\Lambda_{p,1}, \Lambda_{p,2}, \cdots \Lambda_{p,d}\}$. As quantities such as $\operatorname{tr} M_p(x)$, $\det M_p(x)$ depend only on the eigenvalues of $M_p(x)$ and not on the starting point x, in expressions such as $\det\left(\mathbf{1} - M_p^r(x)\right)$ we may omit reference to any particular cycle point x:

YL: elaborate!

$$\det\left(\mathbf{1} - M_p^r\right) = \det\left(\mathbf{1} - M_p^r(x)\right) \quad \text{for any } x \in p\,. \tag{37.27}$$

We postpone the proof that the cycle stability eigenvalues are smooth conjugacy invariants of the flow to sect. 8.5.

37.4.5 Marginal eigenvalues

The presence of marginal eigenvalues signals either an invariance of the flow (which one should immediately exploit to simplify the problem), or a non-hyperbolicity of a flow (a source of much pain, hard to avoid).

chapter 21

A periodic orbit of a continuous flow always has at least one marginal eigenvalue. As $M^t(x)$ transports the velocity field $v(x)$ by (4.7), after a complete period

$$M_p(x)v(x) = v(x)\,, \tag{37.28}$$

so a periodic orbit of a *flow* always has an eigenvector $\mathbf{e}_{\|}(x) = v(x)$ parallel to the local velocity field with the unit eigenvalue

$$\Lambda_{p,\|} = 1\,. \tag{37.29}$$

7.2
page 118

The continuous invariance that gives rise to this marginal eigenvalues is the invariance of a cycle under a translation of its points along the cycle. As we shall see in sect. 14.3, this marginal stability direction can be eliminated by cutting the cycle by a Poincaré section and eliminating the continuous flow fundamental matrix in favor of the fundamental matrix of the Poincaré return map.

say "momodromy"?

37.4.6 Lyapunov exponents

Lyapunov exponent
time!average

The mean growth rate of the distance $|\delta x(t)|/|\delta x(0)|$ between neighboring trajectories (10.27) is given by the *Lyapunov exponent*

$$\lambda = \lim_{t\to\infty} \frac{1}{t} \ln |\delta x(t)|/|\delta x(0)| \tag{37.30}$$

(For notational brevity we shall often suppress the dependence of quantities such as $\lambda = \lambda(x_0)$, $\delta x(t) = \delta x(x_0, t)$ on the initial point x_0 and the time t). For infinitesimal δx we know the $\delta x_i(t)/\delta x_j(0)$ ratio exactly, as this is by definition the fundamental matrix (4.32)

$$\lim_{\delta x\to 0} \frac{\delta x_i(t)}{\delta x_j(0)} = \frac{\partial x_i(t)}{\partial x_j(0)} = M^t_{ij}(x_0)\,,$$

so the leading Lyapunov exponent can be computed from the linear approximation (4.25)

$$\lambda = \lim_{t\to\infty} \frac{1}{t} \ln \frac{\left|M^t(x_0)\delta x(0)\right|}{|\delta x(0)|} = \lim_{t\to\infty} \frac{1}{2t} \ln \left|\hat{n}^T (M^t)^T M^t \hat{n}\right| . \tag{37.31}$$

In this formula the scale of the initial separation drops out, only its orientation given by the unit vector $\hat{n} = \delta x/|\delta x|$ matters. The eigenvalues of M are either real or come in complex conjugate pairs. As M is in general not symmetric and not diagonalizable, it is more convenient to work with the symmetric and diagonalizable matrix $\mathbf{M} = (M^t)^T M^t$, with real positive eigenvalues $\{|\Lambda_1|^2 \geq \ldots \geq |\Lambda_d|^2\}$, and a complete orthonormal set of eigenvectors of $\{u_1, \ldots, u_d\}$. Expanding the initial orientation $\hat{n} = \sum(\hat{n}\cdot u_i)u_i$ in the $\mathbf{M}u_i = |\Lambda_i|u_i$ eigenbasis, we have

⇓PRELIMINARY
☞ remark 4.2
⇑PRELIMINARY

$$\hat{n}^T \mathbf{M} \hat{n} = \sum_{i=1}^{d} (\hat{n}\cdot u_i)^2 |\Lambda_i|^2 = (\hat{n}\cdot u_1)^2 e^{2\lambda_1 t} \left(1 + O(e^{-2(\lambda_1-\lambda_2)t})\right) , \tag{37.32}$$

where $t\lambda_i = \ln|\Lambda_i(x_0, t)|$, and we assume that $\lambda_1 > \lambda_2 \geq \lambda_3 \cdots$. For long times the largest Lyapunov exponent dominates exponentially (10.29), provided the orientation $\hat{n}$ of the initial separation was not chosen perpendicular to the dominant expanding eigendirection u_1. The Lyapunov exponent is the time average

$$\begin{aligned} \overline{\lambda(x_0)} &= \lim_{t\to\infty} \frac{1}{t} \left\{ \ln|\hat{n}\cdot u_1| + \ln|\Lambda_1(x_0, t)| + O(e^{-2(\lambda_1-\lambda_2)t}) \right\} \\ &= \lim_{t\to\infty} \frac{1}{t} \ln|\Lambda_1(x_0, t)|\,, \end{aligned} \tag{37.33}$$

where $\Lambda_1(x_0,t)$ is the leading eigenvalue of $M^t(x_0)$. By choosing the initial displacement such that $\hat{n}$ is normal to the first (i-1) eigendirections we can define not only the leading, but all Lyapunov exponents as well:

$$\overline{\lambda_i(x_0)} = \lim_{t\to\infty} \frac{1}{t} \ln |\Lambda_i(x_0,t)| \,, \qquad i = 1, 2, \cdots, d \,. \tag{37.34}$$

edit figure 10.5

The leading Lyapunov exponent now follows from the fundamental matrix by numerical integration of (4.34). The equations can be integrated accurately for a finite time.

make problem set, mention rescaling to avoid overflows

37.4.7 Evolution operator for Lyapunov exponents

The key idea is to extending the dynamical system by the tangent space of the flow, suggested by the standard numerical methods for evaluation of Lyapunov exponents: start at x_0 with an initial infinitesimal tangent space vector $\eta(0) \in \mathbf{T}\mathcal{M}_x$, and let the flow transport it along the trajectory $x(t) = f^t(x_0)$.

The dynamics in the $(x,\eta) \in U \times TU_x$ space is governed by the system of equations of variations [7.1]:

$$\dot{x} = \mathbf{v}(x) \,, \quad \dot{\eta} = \mathbf{D}\mathbf{v}(x)\eta \,.$$

Here $\mathbf{D}\mathbf{v}(x)$ is the derivative matrix of the flow. We write the solution as

$$x(t) = f^t(x_0) \,, \quad \eta(t) = M^t(x_0)\cdot\eta_0 \,, \tag{37.35}$$

with the tangent space vector η transported by the stability matrix $M^t(x_0) = \partial x(t)/\partial x_0$.

As explained in sect. 4.1, the growth rate of this vector is multiplicative along the trajectory and can be represented as $\eta(t) = |\eta(t)|/|\eta(0)|\mathbf{u}(t)$ where $\mathbf{u}(t)$ is a "unit" vector in some norm $||.||$. For asymptotic times and for almost every initial $(x_0,\eta(0))$, this factor converges to the leading eigenvalue of the linearized stability matrix of the flow.

We implement this multiplicative evaluation of stability eigenvalues by adjoining the d-dimensional transverse tangent space $\eta \in \mathbf{T}\mathcal{M}_x$; $\eta(x)\mathbf{v}(x) = 0$ to the (d+1)-dimensional dynamical evolution space $x \in \mathcal{M} \subset \mathbb{R}^{d+1}$. In order to determine the length of the vector η we introduce a homogeneous differentiable scalar function $g(\eta) = ||\eta||$. It has the property $g(\Lambda\eta) = |\Lambda|g(\eta)$ for any Λ. An example is the projection of a vector to its dth component

$$g\begin{pmatrix} \eta_1 \\ \eta_2 \\ \cdots \\ \eta_d \end{pmatrix} = |\eta_d| \,.$$

Any vector $\eta \in TU_x$ can now be represented by the product $\eta = \Lambda \mathbf{u}$, where $\mathbf{u}$ is a "unit" vector in the sense that its norm is $||\mathbf{u}|| = 1$, and the factor

$$\Lambda^t(x_0, \mathbf{u}_0) = g(\eta(t)) = g(M^t(x_0) \cdot \mathbf{u}_0) \tag{37.36}$$

is the multiplicative "stretching" factor.

Unlike the leading eigenvalue of the Jacobian the stretching factor is multiplicative along the trajectory:

$$\Lambda^{t'+t}(x_0, \mathbf{u}_0) = \Lambda^{t'}(x(t), \mathbf{u}(t))\, \Lambda^t(x_0, \mathbf{u}_0).$$

I.1 page 956

The $\mathbf{u}$ evolution constrained to $E\mathbf{T}_{g,x}$, the space of unit transverse tangent vectors, is given by rescaling of (37.35):

$$\mathbf{u}' = R^t(x, \mathbf{u}) = \frac{1}{\Lambda^t(x, \mathbf{u})} M^t(x) \cdot \mathbf{u}\,. \tag{37.37}$$

Eqs. (37.35), (37.36) and (37.37) enable us to define a *multiplicative* evolution operator on the extended space $U \times E\mathbf{T}_{g,x}$

$$\mathcal{L}^t(x', \mathbf{u}'; x, \mathbf{u}) = \delta\big(x' - f^t(x)\big)\, \frac{\delta\big(\mathbf{u}' - R^t(x, \mathbf{u})\big)}{|\Lambda^t(x, \mathbf{u})|^{\beta-1}}\,, \tag{37.38}$$

where β is a variable.

We note next that if the trajectory $f^t(x)$ is periodic with period T, the tangent space contains d periodic solutions

$$\mathbf{e}_i(x(T+t)) = \mathbf{e}_i(x(t))\,, \quad i = 1, ..., d,$$

corresponding to the d unit eigenvectors $\{\mathbf{e}_1, \mathbf{e}_2, \cdots, \mathbf{e}_d\}$ of the transverse stability matrix, with "stretching" factors (37.36) given by its eigenvalues

$$M_p(x) \cdot \mathbf{e}_i(x) = \Lambda_{p,i}\, \mathbf{e}_i(x)\,, \quad i = 1, ..., d. \qquad \text{(no summation on } i)$$

The $\int d\mathbf{u}$ integral in (**??**) picks up contributions from these periodic solutions. In order to compute the stability of the ith eigendirection solution, it is convenient to expand the variation around the eigenvector $\mathbf{e}_i$ in the stability matrix eigenbasis $\delta\mathbf{u} = \sum \delta u_\ell\, \mathbf{e}_\ell$. The variation of the map (37.37) at a complete period $t = T$ is then given by

$$\begin{aligned} \delta R^T(\mathbf{e}_i) &= \frac{M \cdot \delta\mathbf{u}}{g(M \cdot \mathbf{e}_i)} - \frac{M \cdot \mathbf{e}_i}{g(M \cdot \mathbf{e}_i)^2} \left(\frac{\partial g(\mathbf{e}_i)}{\partial \mathbf{u}} \cdot M \cdot \delta\mathbf{u} \right) \\ &= \sum_{k \neq i} \frac{\Lambda_{p,k}}{\Lambda_{p,i}} \left(\mathbf{e}_k - \mathbf{e}_i \frac{\partial g(\mathbf{e}_i)}{\partial u_k} \right) \delta u_k\,. \end{aligned} \tag{37.39}$$

periodic!orbit extraction—)

The δu_i component does not contribute to this sum since $g(\mathbf{e}_i + du_i\mathbf{e}_i) = 1 + du_i$ implies $\partial g(\mathbf{e}_i)/\partial u_i = 1$. Indeed, infinitesimal variations $\delta\mathbf{u}$ must satisfy

$$g(\mathbf{u}+\delta\mathbf{u}) = g(\mathbf{u}) = 1 \quad \Longrightarrow \quad \sum_{\ell=1}^{d} \delta u_\ell \frac{\partial g(\mathbf{u})}{\partial u_\ell} = 0\,,$$

so the allowed variations are of form

$$\delta\mathbf{u} = \sum_{k\neq i} \left(\mathbf{e}_k - \mathbf{e}_i \frac{\partial g(\mathbf{e}_i)}{\partial u_k}\right) c_k\,, \quad |c_k| \ll 1\,,$$

and in the neighborhood of the $\mathbf{e}_i$ eigenvector the $\int d\mathbf{u}$ integral can be expressed as

$$\int_g d\mathbf{u} = \int \prod_{k\neq i} dc_k\,.$$

⇑PRELIMINARY

Commentary

Prepare Lozi map exercise

Remark 37.1 Piece-wise linear maps. The Lozi map (3.17) is linear, and 100,000's of cycles can be easily computed by [2x2] matrix multiplication and inversion.

Remark 37.2 Relaxation method. The relaxation (or gradient) algorithm is one of the methods for solving extremal problems [37.13]. The method described above was introduced by Biham and Wenzel [37.1], who have also generalized it (in the case of the Hénon map) to determination of *all* 2^n cycles of period n, real or complex [37.2]. The applicability and reliability of the method is discussed in detail by Grassberger, Kantz and Moening [37.5], who give examples of the ways in which the method fails: (a) it might reach a limit cycle rather than a equilibrium saddlepoint (that can be remedied by the complex Biham-Wenzel algorithm [37.2]) (b) different symbol sequences can converge to the same cycle (i.e., more refined initial conditions might be needed). Furthermore, Hansen (ref. [37.7] and chapter 4. of ref. [1.7]) has pointed out that the method cannot find certain cycles for specific values of the Hénon map parameters.

In practice, the relaxation method for determining periodic orbits of maps appears to be effective almost always, but not always. It is much slower than the multipoint shooting method of sect. 17.4.1, but also much quicker to program, as it does not require evaluation of stability matrices and their inversion. If the complete set of cycles is required, the method has to be supplemented by other methods.

Remark 37.3 Hybrid Newton-Raphson/relaxation methods. The method discussed in sect. 37.2 was introduced by Schmelcher *et al* [37.9]. The method was extended

to flows by means of the Poincaré surface of section technique in ref. [37.10]. It is also possible to combine the Newton-Raphson method and (37.13) in the construction of a transformed map [37.14]. In this approach, each step of the iteration scheme is a linear superposition of a step of the stability transformed system and a step of the Newton-Raphson algorithm. Far from the linear neighborhood the weight is dominantly on the globally acting stability transformation algorithm. Close to the fixed point, the steps of the iteration are dominated by the Newton-Raphson procedure.

Henon@Hénon!attractor!topological entropy
Henon@Hénon!attractor!Lyapunov exponent
Henon@Hénon!attractor!Hausdorff dimension
topological!entropy!Hénon attractor
Lyapunov exponent!Hénon attractor
Hausdorff dimension!Hénon attractor
dimension!Hénon attractor
this is not checked at all yet

Remark 37.4 Relation to the Smale horseshoe symbolic dynamics. For a complete horseshoe Hénon repeller (a sufficiently large), such as the one given in figure 37.2, the signs $\sigma_i \in \{1, -1\}$ are in a 1-to-1 correspondence with the Smale horsheshoe symbolic dynamics $s_i \in \{0, 1\}$:

$$s_i = \begin{cases} 0 & \text{if } \sigma_i = -1\,, \quad x_i < 0 \\ 1 & \text{if } \sigma_i = +1\,, \quad x_i > 0 \end{cases} \,. \tag{37.40}$$

For arbitrary parameter values with a finite subshift symbolic dynamics or with arbitrarily complicated pruning, the relation of sign sequences $\{\sigma_1, \sigma_2, \cdots, \sigma_n\}$ to the itineraries $\{s_1, s_2, \cdots, s_n\}$ can be much subtler; this is discussed in ref. [37.5].

⇓PRELIMINARY

Remark 37.5 A compilation of the Hénon map numerical results. For the record - the most accurate estimates of various averages for the Hénon map, Hénon's parameters choice $a = 1.4$, $b = 0.3$, known to the authors, are: the topological entropy (13.1) is $h = 0.4645??$, the Lyapunov exponent $= 0.463$, the Hausdorff dimension $D_H = 1.274(2)$.

recheck 0.4645, 0.463, 1.274
⇓PRIVATE
⇑PRIVATE
give references

Remark 37.6 Software for searching for periodic solutions. Bard Ermentrout's description of AUTO makes it look very much like our variational method [37.15, 37.16]: AUTO solves boundary value problems by solving

$$\frac{x_{n+1} - x_n}{\Delta t} - F(x_n) = 0 \tag{37.41}$$

as a big system of algebraic equations, $G(x) = 0$. One needs to fix marginal directions; that is called the *colocation* method.

⇑PRELIMINARY

Remark 37.7 Ikeda map. Ikeda map (37.11) was introduced in ref. [37.12] is a model which exhibits complex dynamics observed in nonlinear optical ring cavities.

Remark 37.8 Relaxation for continuous time flows. For a d-dimensional flow $\dot{x} = v(x)$, the method described above can be extended by considering a Poincaré surface of section. The Poincaré section yields a map f with dimension d-1, and the above discrete iterative maps procedures can be carried out. A method that keeps the trial orbit continuous throughout the calculation is the Newton descent, a variational method for finding periodic orbits of continuous time flows, is described in refs. [37.15, 37.16].

Frenkel-Kontorova model
Aubry-Mather theory
Mather—seeAubry-Mather theory
generating function
☞ sect. 18.6

Remark 37.9 Stability ordering. The parameter $\Delta\tau$ in (37.13) is a key quantity here. It is related to the stability of the desired cycle in the transformed system: The more unstable a fixed point is, the smaller $\Delta\tau$ has to be to stabilize it. With increasing cycle periods, the unstable eigenvalue of the stability matrix increases and therefore $\Delta\tau$ has to be reduced to achieve stabilization of all fixed points. In many cases the least unstable cycles of a given period n are of physically most important [37.11]. In this context $\Delta\tau$ operates as a stability filter. It allows the selective stabilization of only those cycles which posses Lyapunov exponents smaller than a cut-off value. If one starts the search for cycles within a given period n with a value $\Delta\tau \approx O(10^{-1})$, and gradually lowers $\Delta\tau$ one obtains the sequence of all unstable orbits of order n sorted with increasing values of their Lyapunov exponents. For the specific choice of $\mathbf{C}$ the relation between $\Delta\tau$ and the stability coefficients of the fixed points of the original system is strictly monotonous. Transformed dynamical systems with other $\mathbf{C}$'s do not obey such a strict behavior but show a rough ordering of the sequence of stability eigenvalues of the fixed points stabilized in the course of decreasing values for $\Delta\tau$. As explained in sect. 18.6, stability ordered cycles are needed to order cycle expansions of dynamical quantities of chaotic systems for which a symbolic dynamics is not known. For such systems, an ordering of cycles with respect to their stability has been proposed [18.13, 18.14, 18.12], and shown to yield good results in practical applications.

Remark 37.10 Action extremization method. The action extremization (sect. 37.3) as a numerical method for finding cycles has been introduced independently by many people. We have learned it from G. Russberg, and from M. Sieber's and F. Steiner's hyperbola billiard computations [37.17, 37.18]. The convergence rate is really impressive, for the Sinai billiard some 5000 cycles are computed within CPU seconds with rather bad initial guesses.

Variational methods are the key ingredient of the Aubry-Mather theory of area-preserving twist maps (known in the condensed matter literature as the Frenkel-Kontorova models of 1-dimensional crystals), discrete-time Hamiltonian dynamical systems particularly suited to explorations of the K.A.M. theorem. Proofs of the Aubry-Mather theorem [37.20] on existence of quasi-periodic solutions are variational. It was quickly realized that the variational methods can also yield reliable, high precision computations of long periodic orbits of twist map models in 2 or more dimensions, needed for K.A.M. renormalization studies [37.19].

A fictitious time gradient flow similar to the one discussed here in sect. 37.1 was introduced by Anegent [37.21] for twist maps, and used by Gole [37.22] in his proof of the Aubry-Mather theorem. Mathematical bounds on the regions of stability of K.A.M. tori are notoriously restrictive compared to the numerical indications, and de la Llave, Falcolini and Tompaidis [37.23, 37.24] have found the gradient flow formulation advantageous both in studies of the analyticity domains of the K.A.M. stability, as well as proving the Aubry-Mather theorem for extended systems (for a pedagogical introduction, see the lattice dynamics section of ref. [37.25]).

All of the twist-maps work is based on extremizing the discrete dynamics version of the action S (in this context sometimes called a "generating function"). However, in their investigations in the complex plane, Falcolini and de la Llave [37.23] do find it useful to minimize instead $S\bar{S}$, analogous to our cost function (37.3).

Résumé

fill in

Unlike the Newton-Raphson method, variational methods are very robust. As each step around a cycle is short, they do not suffer from exponential instabilities, and with rather coarse initial guesses one can determine cycles of arbitrary length.

"exercise" - formulate such method for flows

References

[37.1] O. Biham and W. Wenzel, "Characterization of unstable periodic orbits in chaotic attractors and repellers", *Phys. Rev. Lett.* **63**, 819 (1989).

[37.2] O. Biham and W. Wenzel, *Phys. Rev.* **A 42**, 4639 (1990).

[37.3] P. Grassberger and H. Kantz, "Generating partitions for the dissipative Hénon map", *Phys. Lett. A* **113**, 235 (1985).

[37.4] H. Kantz and P. Grassberger, *Physica* **17D**, 75 (1985).

[37.5] P. Grassberger, H. Kantz, and U. Moenig. "On the symbolic dynamics of the Hénon map", *J. Phys.* **A 43**, 5217 (1989).

[37.6] M. Eisele, "Comparison of several generating partitions of the Hnon map", *J. Phys.* **A 32**, 1533 (1999).

[37.7] K.T. Hansen, "Remarks on the symbolic dynamics for the Hénon map", *Phys. Lett.* **A 165**, 100 (1992).

[37.8] D. Sterling and J.D. Meiss, "Computing periodic orbits using the anti-integrable limit", *Phys. Lett. A* **241**, 46 (1998); `chao-dyn/9802014`.

[37.9] P. Schmelcher and F.K. Diakonos, *Phys. Rev. Lett.* **78**, 4733 (1997); *Phys. Rev. E* **57**, 2739 (1998).

[37.10] D. Pingel, P. Schmelcher and F.K. Diakonos, O. Biham, *Phys. Rev. E* **64**, 026214 (2001).

[37.11] F. K. Diakonos, P. Schmelcher, O. Biham, *Phys. Rev. Lett.* **81**, 4349 (1998).

[37.12] K. Ikeda, *Opt. Commun.* **30**, 257 (1979).

[37.13] F. Stummel and K. Hainer, *Praktische Mathematik* (Teubner, Stuttgart 1982).

[37.14] R.L. Davidchack and Y.C. Lai, *Phys. Rev. E* **60**, 6172 (1999).

[37.15] P. Cvitanović and Y. Lan, "Turbulent fields and their recurrences", in N. Antoniou, ed., *Proceed. of 10. Intern. Workshop on Multiparticle Production: Correlations and Fluctuations in QCD* (World Scientific, Singapore 2003). `nlin.CD/0308006`

[37.16] Y. Lan and P. Cvitanović, "Variational method for finding periodic orbits in a general flow", *Phys. Rev.* **E 69** 016217 (2004), `nlin.CD/0308008`

[37.17] M. Sieber and F. Steiner, " Quantum Chaos in the Hyperbola Billiard", *Phys. Lett.* **A 148**, 415 (1990).

[37.18] M. Sieber, *The Hyperbola Billiard: A Model for the Semiclassical Quantization of Chaotic Systems*, Ph.D. thesis (Hamburg 1991); DESY report 91-030.

[37.19] H. T. Kook and J. D. Meiss, "Periodic orbits for reversible symplectic mappings", *Physica D* **35**, 65 (1989).

[37.20] J.N. Mather, "Variational construction of orbits of twist difeomorphisms", J. Amer. Math. Soc. **4** 207 (1991).

[37.21] S. B. Angenent, "The periodic orbits of an area preserving twist-map", *Comm. Math. Phys.* **115**, 353 (1988).

[37.22] C. Golé, "A new proof of the Aubry-Mather's theorem", *Math. Z.* **210**, 441 (1992).

[37.23] C. Falcolini and R. de la Llave, "Numerical calculation of domains of analyticity for perturbation theories in the presence of small divisors", *J. Stat. Phys.* **67**, 645 (1992).

[37.24] S. Tompaidis, "Numerical Study of Invariant Sets of a Quasi-periodic Perturbation of a Symplectic Map", *Experimental Mathematics* **5**, 211 (1996).

[37.25] R. de la Llave, *Variational methods for quasiperiodic solutions of partial differential equations*, `mp_arc 00-56`.

Exercises

Henon@Hénon!map
Henon@Hénon!map!prime cycles

Exercise 37.1 Evaluation of cycles by minimization*. *Given a symbol sequence, you can construct a guess trajectory by taking a point on the boundary of each disk in the sequence, and connecting them by straight lines. If this were a rubber band wrapped through 3 rings, it would shrink into the physical trajectory, which minimizes the action (in this case, the length) of the trajectory.*

Write a program to find the periodic orbits for your billiard simulator. Use the least action principle to extremize the length of the periodic orbit, and reproduce the periods and stabilities of 3-disk cycles, table 37.3. After that check the accuracy of the computed orbits by iterating them forward with your simulator. What is $|f^{T_p}(x) - x|$*?*

Exercise 37.2 Tracking cycles adiabatically*. *Once a cycle has been found, orbits for different system parameters values may be obtained by varying slowly (adiabatically) the parameters, and using the old orbit points as starting guesses in the Newton method. Try this method out on the 3-disk system. It works well for* $R : a$ *sufficiently large. For smaller values, some orbits change rather quickly and require very small step sizes. In addition, for ratios below* $R : a = 2.04821419\ldots$ *families of cycles are pruned, i.e. some of the minimal length trajectories are blocked by intervening disks. (See sect. 12.8.)*

⇓PRELIMINARY
⇑PRELIMINARY

Exercise 37.3 Find cycles of the Hénon map. *Apply the method of sect. 37.1 to the Hénon map at the Hénon's parameters choice* $a = 1.4$, $b = 0.3$, *and compute all prime cycles for at least* $n \leq 6$. *Estimate the topological entropy, either from the definition (13.1), or as the zero of a truncated topological zeta function (13.21). Do your cycles agree with the cycles listed in table 37.1?*

scattering!elastic
elastic!scattering

Chapter 38

Quantum scattering

Scattering is easier than gathering.
Irish proverb

(A. Wirzba, P. Cvitanović and N. Whelan)

So far the trace formulas have been derived assuming that the system under consideration is bound. As we shall now see, we are in luck - the semiclassics of bound systems is all we need to understand the semiclassics for open, scattering systems as well. We start by a brief review of the quantum theory of elastic scattering of a point particle from a (repulsive) potential, and then develop the connection to the standard Gutzwiller theory for bound systems. We do this in two steps - first, a heuristic derivation which helps us understand in what sense density of states is "density", and then we sketch a general derivation of the central result of the spectral theory of quantum scattering, the Krein-Friedel-Lloyd formula. The end result is that we establish a connection between the scattering resonances (both positions and widths) of an open quantum system and the poles of the trace of the Green function, which we learned to analyze in earlier chapters. [1]

38.1 Density of states

For a scattering problem the density of states (32.18) appear ill defined since formulas such as (36.6) involve integration over infinite spatial extent. What we will now show is that a quantity that makes sense physically is the difference of two densities - the first with the scatterer present and the second with the scatterer absent.

In nonrelativistic dynamics the relative motion can be separated from the center-of-mass motion. Therefore the elastic scattering of two particles can be treated as the scattering of one particle from a static potential $V(q)$.

[1] Whelan: I think there needs to be something like the above sentence to motivate why we are bothering with this chapter at all.

scattering!matrix
Smatrix@S-matrix

We will study the scattering of a point-particle of (reduced) mass m by a short-range potential $V(q)$, excluding *inter alia* the Coulomb potential. (The Coulomb potential decays slowly as a function of q so that various asymptotic approximations which apply to general potentials fail for it.) Although we can choose the spatial coordinate frame freely, it is advisable to place its origin somewhere near the geometrical center of the potential. The scattering problem is solved, if a scattering solution to the time-independent Schrödinger equation (32.5)

$$\left(-\frac{\hbar^2}{2m}\frac{\partial^2}{\partial q^2}+V(q)\right)\phi_{\vec{k}}(q)=E\phi_{\vec{k}}(q) \tag{38.1}$$

can be constructed. Here E is the energy, $\vec{p}=\hbar\vec{k}$ the initial momentum of the particle, and $\vec{k}$ the corresponding wave vector.

When the argument $r=|q|$ of the wave function is large compared to the typical size a of the scattering region, the Schrödinger equation effectively becomes a free particle equation because of the short-range nature of the potential. In the asymptotic domain $r \gg a$, the solution $\phi_{\vec{k}}(q)$ of (38.1) can be written as superposition of ingoing and outgoing solutions of the free particle Schrödinger equation for fixed angular momentum:

$$\phi(q)=A\phi^{(-)}(q)+B\phi^{(+)}(q)\,, \qquad (+\text{ boundary conditions})\,,$$

where in 1-dimensional problems $\phi^{(-)}(q)$, $\phi^{(+)}(q)$ are the "left", "right" moving plane waves, and in higher-dimensional scattering problems the "incoming", "outgoing" radial waves, with the constant matrices A, B fixed by the boundary conditions. What are the boundary conditions? The scatterer can modify only the outgoing waves (see figure 38.1), since the incoming ones, by definition, have yet to encounter the scattering region. This defines the quantum mechanical scattering matrix, or the *S matrix*

- means incoming

$$\phi_m(r)=\phi^{(-)}_m(r)+S_{mm'}\phi^{(+)}_{m'}(r)\,. \tag{38.2}$$

All scattering effects are incorporated in the deviation of $\mathbf{S}$ from the unit matrix, the transition matrix $\mathbf{T}$

$$\mathbf{S}=\mathbf{1}-i\mathbf{T}\,. \tag{38.3}$$

For concreteness, we have specialized to two dimensions, although the final formula is true for arbitrary dimensions. The indices m and m' are the angular momenta quantum numbers for the incoming and outgoing state of the scattering wave function, labeling the S-matrix elements $S_{mm'}$. More generally, given a set of quantum numbers β, γ, the S matrix is a collection $S_{\beta\gamma}$ of transition amplitudes $\beta \to \gamma$ normalized such that $|S_{\beta\gamma}|^2$ is the

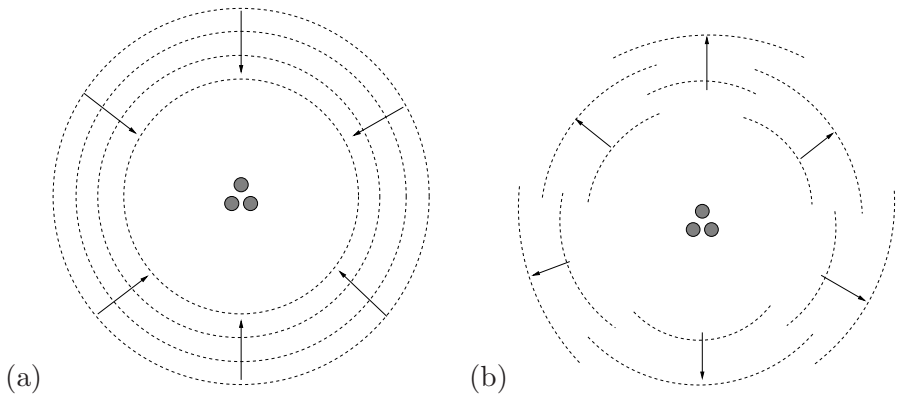

Figure 38.1: (a) *Incoming* spherical waves running into an obstacle. (b) Superposition of *outgoing* spherical waves scattered from an obstacle.

probability of the $\beta \to \gamma$ transition. The total probability that the ingoing state β ends up in some outgoing state must add up to unity

$$\sum_{\gamma} |S_{\beta\gamma}|^2 = 1\,, \tag{38.4}$$

so the S matrix is unitary: $\mathbf{S}^\dagger\mathbf{S} = \mathbf{S}\mathbf{S}^\dagger = \mathbf{1}$.

We have already encountered a solution to the 2-dimensional problem; free particle propagation Green's function (34.48) is a radial solution, given in terms of the Hankel function

$$G_0(r,0,E) = -\frac{im}{2\hbar^2} H_0^{(+)}(kr)\,,$$

where we have used $S_0(r,0,E)/\hbar = kr$ for the action. [2] The mth angular momentum eigenfunction is proportional to $\phi_m^{(\pm)}(q) \propto H_m^{(\pm)}(kr)$, and given a potential $V(q)$ we can in principle compute the infinity of matrix elements $S_{mm'}$. We will not need much information about $H_m^{(t)}(kr)$, other than that for large r its asymptotic form is

$$H^{\pm} \propto e^{\pm ikr}$$

In general, the potential $V(q)$ is not radially symmetric and (38.1) has to be solved numerically, by explicit integration, or by diagonalizing a large matrix in a specific basis. To simplify things a bit, we assume for the time being that a radially symmetric scatterer is centered at the origin; the final formula will be true for arbitrary asymmetric potentials. Then the solutions of the Schrödinger equation (32.5) are separable, $\phi_m(q) = \phi(r)e^{im\theta}$, $r = |q|$, the scattering matrix cannot mix different angular momentum eigenstates, and S is diagonal in the radial basis (38.2) with matrix elements given by

$$S_m(k) = e^{2i\delta_m(k)}. \tag{38.5}$$

[2] Whelan: inserted this to clarify that S_0 does not refer to the scattering matrix.

The matrix is unitary so in a diagonal basis all entries are pure phases. This means that an incoming state of the form $H_m^{(-)}(kr)e^{im\theta}$ gets scattered into an outgoing state of the form $S_m(k)H_m^{(+)}(kr)e^{im\theta}$, where $H_m^{(\mp)}(z)$ are incoming and outgoing Hankel functions respectively. We now embed the scatterer in a infinite cylindrical well of radius R, and will later take $R \to \infty$. Angular momentum is still conserved so that each eigenstate of this (now bound) problem corresponds to some value of m. For large $r \gg a$ each eigenstate is of the asymptotically free form

$$\begin{aligned} \phi_m(r) &\approx e^{im\theta}\left(S_m(k)H_m^{(+)}(kr) + H_m^{(-)}(kr)\right) \\ &\approx \cdots \cos(kr + \delta_m(k) - \chi_m)\,, \end{aligned} \tag{38.6}$$

where $\cdots$ is a common prefactor, and $\chi_m = m\pi/2 + \pi/4$ is an annoying phase factor from the asymptotic expansion of the Hankel functions that will play no role in what follows.

The state (38.6) must satisfy the external boundary condition that it vanish at $r = R$. This implies the quantization condition

$$k_n R + \delta_m(k_n) - \chi_m = \pi\,(n + 12)\ .$$

We now ask for the difference in the eigenvalues of two consecutive states of fixed m. Since R is large, the density of states is high, and the phase $\delta_m(k)$ does not change much over such a small interval. Therefore, to leading order we can include the effect of the change of the phase on state $n+1$ by Taylor expanding. is

$$k_{n+1}R + \delta_m(k_n) + (k_{n+1} - k_n)\delta_m'(k_n) - \chi_m \approx \pi + \pi(n + 12)\,.$$

Taking the difference of the two equations we obtain $\Delta k \approx \pi(R+\delta_m'(k))^{-1}$. This is the eigenvalue spacing which we now interpret as the inverse of the density of states within m angular momentum sbuspace

$$d_m(k) \approx \frac{1}{\pi}\left(R + \delta_m'(k)\right).$$

The R term is essentially the $1-d$ Weyl term (36.8), appropriate to $1-d$ radial quantization. For large R, the dominant behavior is given by the size of the circular enclosure with a correction in terms of the derivative of the scattering phase shift, approximation accurate to order $1/R$. However, not all is well: the area under consideration tends to infinity. We regularize this by subtracting from the result from the free particle density of states $d_0(k)$, for the same size container, but this time without any scatterer, figure 38.2. We also sum over all m values so that

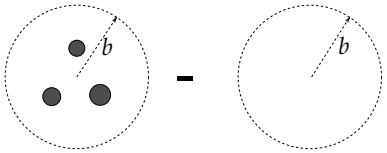

Figure 38.2: The "difference" of two bounded reference systems, one with and one without the scattering system.

$$d(k) - d_0(k) = \frac{1}{\pi}\sum_m \delta'_m(k) = \frac{1}{2\pi i}\sum_m \frac{d}{dk}\log S_m$$
$$= \frac{1}{2\pi i}\mathrm{Tr}\left(S^\dagger \frac{dS}{dk}\right). \qquad (38.7)$$

The first line follows from the definition of the phase shifts (38.5) while the second line follows from the unitarity of S so that $S^{-1} = S^\dagger$. We can now take the limit $R \to \infty$ since the R dependence has been cancelled away.

This is essentially what we want to prove since for the left hand side we already have the semiclassical theory for the trace of the difference of Green's functions,

$$d(k) - d_0(k) = -\frac{1}{2\pi k}\mathrm{Im}\left(\mathrm{tr}\left(G(k) - G_0(k)\right)\right). \qquad (38.8)$$

There are a number of generalizations. This can be done in any number of dimensions. It is also more common to do this as a function of energy and not wave number k. However, as the asymptotic dynamics is free wave dynamics labeled by the wavenumber k, we have adapted k as the natural variable in the above discussion.

Finally, we state without proof that the relation (38.7) applies even when there is no circular symmetry. The proof is more difficult since one cannot appeal to the phase shifts δ_m but must work directly with a non-diagonal S matrix.

38.2 Quantum mechanical scattering matrix

The results of the previous section indicate that there is a connection between the scattering matrix and the trace of the quantum Green's function (more formally between the difference of the Green's function with and without the scattering center.) We now show how this connection can be derived in a more rigorous manner. We will also work in terms of the energy E rather than the wavenumber k, since this is the more usual exposition. [3] Suppose particles interact via forces of sufficiently short range, so that in the remote past they were in a free particle state labeled β, and in the distant future they will likewise be free, in a state labeled γ. In the

[3] Whelan: I feel the various sections need to be glued together better than they were.

Heisenberg picture the S-matrix is defined as $\mathbf{S} = \Omega_- \Omega_+^\dagger$ in terms of the Møller operators

$$\Omega_\pm = \lim_{t \to \pm\infty} e^{iHt/\hbar} e^{-iH_0 t/\hbar} \,, \tag{38.9}$$

where H is the full Hamiltonian, whereas H_0 is the free Hamiltonian. In the interaction picture the S-matrix is given by

$$\begin{aligned} \mathbf{S} &= \Omega_+^\dagger \Omega_- = \lim_{t \to \infty} e^{iH_0 t/\hbar} e^{-2iHt/\hbar} e^{iH_0 t/\hbar} \\ &= T \exp\left(-i \int_{-\infty}^{+\infty} dt H'(t) \right) \,, \end{aligned} \tag{38.10}$$

where $H' = V = H - H_0$ is the interaction Hamiltonian and T is the time-ordering operator. In stationary scattering theory the S matrix has the following spectral representation

$$\begin{aligned} S &= \int_0^\infty dE\, S(E) \delta(H_0 - E) \\ S(E) &= Q_+(E) Q_-^{-1}(E), \qquad Q_\pm(E) = \mathbf{1} + (H_0 - E \pm i\epsilon)^{-1} V \end{aligned} \tag{38.11}$$

such that [4]

$$\mathrm{Tr}\left[S^\dagger(E) \frac{d}{dE} S(E) \right] = \mathrm{Tr}\left[\frac{1}{H_0 - E - i\epsilon} - \frac{1}{H - E - i\epsilon} - (\epsilon \leftrightarrow -\epsilon) \right] \,. \tag{38.12}$$

☞ appendix M

The manipulations leading to (38.12) are justified if the operators $Q_\pm(E)$ can be linked to trace-class operators.

We can now use this result to derive the Krein-Lloyd formula which is the central result of this chapter. The Krein-Lloyd formula provides the connection between the trace of the Green's function and the poles of the scattering matrix, implicit in all of the trace formulas for open quantum systems which will be presented in the subsequent chapters.

38.3 Krein-Friedel-Lloyd formula

The link between quantum mechanics and semiclassics for scattering problems is provided by the semiclassical limit of the Krein-Friedel-Lloyd sum for the spectral density which we now derive. This derivation builds on the results of the last section and extends the discussion of the opening section.

[4] Whelan: Are the above expressions just to be accepted or have we somehow derived them? If the former, we should at least cite somebody for the result. Also, how is S on the left side of the top equation distinct from $S(E)$; is it defined somewhere? I must admit that the step from (27.9) to (27.11) is vague in my mind.

In chapter 34 we linked the spectral density (see (32.18)) of a bounded system

Green's function!scattering
scattering!Green's function

$$d(E) \equiv \sum_n \delta(E_n - E) \tag{38.13}$$

via the identity

$$\begin{aligned}
\delta(E_n - E) &= -\lim_{\epsilon\to 0} \frac{1}{\pi} \mathrm{Im} \frac{1}{E - E_n + i\epsilon} \\
&= -\lim_{\epsilon\to 0} \frac{1}{\pi} \mathrm{Im} \langle E_n | \frac{1}{E - H + i\epsilon} | E_n \rangle \\
&= \frac{1}{2\pi\, i} \lim_{\epsilon\to 0} \left\langle E_n \left| \frac{1}{E - H - i\epsilon} - \frac{1}{E - H + i\epsilon} \right| E_n \right\rangle
\end{aligned} \tag{38.14}$$

to the trace of the Green's function (36.1.1). Furthermore, in the semiclassical approximation, the trace of the Green's function is given by the Gutzwiller trace formula (36.12) in terms of a smooth Weyl term and an oscillating contribution of periodic orbits.

Therefore, the task of constructing the semiclassics of a scattering system is completed, if we can find a connection between the spectral density $d(E)$ and the scattering matrix S. We will see that (38.12) provides the clue. Note that the right hand side of (38.12) has nearly the structure of (38.14) when the latter is inserted into (38.13). The principal difference between these two types of equations is that the S matrix refers to *outgoing* scattering wave functions which are not normalizable and which have a *continuous* spectrum, whereas the spectral density $d(E)$ refers to a bound system with normalizable wave functions with a discrete spectrum. Furthermore, the bound system is characterized by a *hermitian* operator, the Hamiltonian H, whereas the scattering system is characterized by a *unitary* operator, the S-matrix. How can we reconcile these completely different classes of wave functions, operators and spectra? The trick is to put our scattering system into a finite box as in the opening section. We choose a spherical conatiner with radius R and with its center at the center of our finite scattering system. Our scattering potential $V(\vec{r})$ will be unaltered within the box, whereas at the box walls we will choose an infinitely high potential, with the Dirichlet boundary conditions at the outside of the box:

$$\phi(\vec{r})|_{r=R} = 0 \ . \tag{38.15}$$

In this way, for any finite value of the radius R of the box, we have mapped our scattering system into a bound system with a spectral density $d(E;R)$ over discrete eigenenergies $E_n(R)$. It is therefore important that our scattering potential was chosen to be short-ranged to start with. (Which explains why the Coulomb potential requires special care.) The hope is that in the limit $R \to \infty$ we will recover the scattering system. But some

Krein-Friedel-Lloyd formula

care is required in implementing this. The smooth Weyl term $\bar{d}(E;R)$ belonging to our box with the enclosed potential V diverges for a spherical two-dimensional box of radius R quadratically, as $\pi R^2/(4\pi)$ or as R^3 in the three-dimensional case. This problem can easily be cured if the spectral density of an empty reference box of the *same* size (radius R) is subtracted (see figure 38.2). Then all the divergences linked to the increasing radius R in the limit $R \to \infty$ drop out of the difference. Furthermore, in the limit $R \to \infty$ the energy-eigenfunctions of the box are only normalizable as a delta distribution, similarly to a plane wave. So we seem to recover a continous spectrum. Still the problem remains that the wave functions do not discriminate between incoming and outgoing waves, whereas this symmetry, namely the hermiticity, is broken in the scattering problem. The last problem can be tackled if we replace the spectral density over discrete delta distributions by a smoothed spectral density with a small finite imaginary part η in the energy E:

$$d(E+i\eta;R) \equiv \frac{1}{i\,2\pi}\sum_n \left\{ \frac{1}{E-E_n(R)-i\eta} - \frac{1}{E-E_n(R)+i\eta} \right\} . \quad (38.16)$$

Note that $d(E+i\eta;R) \neq d(E-i\eta;R) = -d(E+i\eta;R)$. By the introduction of the positive *finite* imaginary part η the time-dependent behavior of the wave function has effectively been altered from an oscillating one to a decaying one and the hermiticity of the Hamiltonian is removed. Finally the limit $\eta \to 0$ can be carried out, respecting the order of the limiting procedures. First the limit $R \to \infty$ has to be performed for a *finite* value of η, only then the limit $\eta \to 0$ is allowed. In practice, one can try to work with a finite value of R, but then it will turn out (see below) that the scattering system is only recovered if $R\sqrt{\eta} \gg 1$.

Let us summarize the relation between the smoothed spectral densities $d(E+i\eta;R)$ of the boxed potential and $d^{(0)}(E+i\eta;R)$ of the empty reference system and the S matrix of the corresponding scattering system:

$$\begin{aligned} \lim_{\eta\to+0}\lim_{R\to\infty}\Big(d(E+i\eta;R) - d^{(0)}(E+i\eta;R)\Big) &= \frac{1}{2\pi i}\mathrm{Tr}\left[S^\dagger(E)\frac{d}{dE}S(E)\right] \\ = \frac{1}{2\pi i}\mathrm{Tr}\frac{d}{dE}\ln S(E) &= \frac{1}{2\pi i}\frac{d}{dE}\ln\det S(E) \end{aligned} \quad (38.17)$$

This is the *Krein-Friedel-Lloyd formula*. It replaces the scattering problem by the difference of two bounded reference billiards of the same radius R which finally will be taken to infinity. The first billiard contains the scattering region or potentials, whereas the other does not (see figure 38.2). Here $d(E+i\eta;R)$ and $d^{(0)}(E+i\eta;R)$ are the *smoothed* spectral densities in the presence or in the absence of the scatterers, respectively. In the semiclassical approximation, they are replaced by a Weyl term (36.11) and an oscillating sum over periodic orbits. As in (36.2), the trace formula (38.17) can be integrated to give a relation between the smoothed staircase

functions and the determinant of the S-matrix:

$$\lim_{\eta\to+0}\lim_{R\to\infty}\left(N(E+i\eta;R)-N^{(0)}(E+i\eta;R)\right) \;=\; \frac{1}{2\pi i}\,\ln\det S(E) \tag{38.18}$$

Furthermore, in both versions of the Krein-Friedel-Lloyd formulas the energy argument $E+i\eta$ can be replaced by the wavenumber argument $k+i\eta'$. These expressions only make sense for wavenumbers on or above the real k-axis. In particular, if k is chosen to be real, η' must be greater than zero. Otherwise, the exact left hand sides (38.18) and (38.17) would give discontinuous staircase or even delta function sums, respectively, whereas the right hand sides are continuous to start with, since they can be expressed by continuous phase shifts. Thus the order of the two limits in (38.18) and (38.17) is essential.

The necessity of the $+i\eta$ prescription can also be understood by purely phenomenological considerations in the semiclassical approximation: Without the $i\eta$ term there is no reason why one should be able to neglect spurious periodic orbits which are there solely because of the introduction of the confining boundary. The subtraction of the second (empty) reference system removes those spurious periodic orbits which never encounter the scattering region – in addition to the removal of the divergent Weyl term contributions in the limit $R\to\infty$. The periodic orbits that encounter both the scattering region and the external wall would still survive the first limit $R\to\infty$, if they were not exponentially suppressed by the $+i\eta$ term because of their

$$e^{iL(R)\sqrt{2m(E+i\eta)}} = e^{iL(R)k}\,e^{-L(R)\eta'}$$

behavior. As the length $L(R)$ of a spurious periodic orbit grows linearly with the radius R. The bound $R\eta'\gg 1$ is an essential precondition on the suppression of the unwanted spurious contributions of the container if the Krein-Friedel-Lloyd formulas (38.17) and (38.18) are evaluated at a finite value of R.

38.1 page 723

Finally, the semiclassical approximation can also help us in the interpretation of the Weyl term contributions for scattering problems. In scattering problems the Weyl term appears with a negative sign. The reason is the subtraction of the empty container from the container with the potential. If the potential is a dispersing billiard system (or a finite collection of dispersing billiards), we expect an excluded volume (or the sum of excluded volumes) relative to the empty container. In other words, the Weyl term contribution of the empty container is larger than of the filled one and therefore a negative net contribution is left over. Secondly, if the scattering potential is a collection of a finite number of non-overlapping scattering regions, the Krein-Friedel-Lloyd formulas show that the corresponding Weyl contributions are completely independent of the position of the single scatterers, as long as these do not overlap.

ask N. Søndergaard for premission to include this

5

[5] Whelan: Although this section does refer to scattering I am not sure how it fits into

time delay!Wigner
Wigner delay time
scattering!phase shift

38.4 Wigner time delay

The term $\frac{d}{dE}\ln\det S$ in the density formula (38.17) is dimensionally time. This suggests another, physically important interpretation of such formulas for scattering systems, the Wigner delay, defined as

$$\begin{aligned} d(k) &= \frac{d}{dk}\mathrm{Argdet}\left(\mathbf{S}(k)\right) \\ &= -i\frac{d}{dk}\log\det\left(\mathbf{S}(k)\right) \\ &= -i\,\mathrm{tr}\left(\mathbf{S}^\dagger(k)\frac{d\mathbf{S}}{dk}(k)\right) \end{aligned} \tag{38.19}$$

and can be shown to equal the total delay of a wave packet in a scattering system. We now review this fact.

A related quantity is the total scattering *phase shift* $\Theta(k)$ defined as

$$\det\mathbf{S}(k) = e^{+i\,\Theta(k)}\,,$$

so that $d(k) = \frac{d}{dk}\Theta(k)$.

The time delay may be both positive and negative, reflecting attractive respectively repulsive features of the scattering system. To elucidate the connection between the scattering determinant and the time delay we study a plane wave:

The phase of a wave packet will have the form:

$$\phi = \vec{k}\cdot\vec{x} - \omega\,t \;+\; \Theta\,.$$

Here the term in the parenthesis refers to the phase shift that will occur if scattering is present. [6] The center of the wave packet will be determined by the principle of stationary phase:

$$0 = d\phi = d\vec{k}\cdot\vec{x} - d\omega\,t \;+\; d\Theta\,.$$

Hence the packet is located at

$$\vec{x} = \frac{\partial\omega}{\partial\vec{k}}\,t \;-\frac{\partial\Theta}{\partial\vec{k}}\,.$$

the entire flow of the book. Are Wigner time delays used anywhere else in this course? If not, it might better be used as an appendix.

[6] Whelan: There are no parantheses. I might just kill the entire previous sentence.

The first term is just the group velocity times the given time t. Thus the the packet is retarded by a length given by the derivative of the phase shift with respect to the wave vector $\vec{k}$. The arrival of the wave packet at the position $\vec{x}$ will therefore be delayed. This *time delay* can similarly be found as

$$\tau(\omega) = \frac{\partial\Theta(\omega)}{\partial\omega}.$$

To show this we introduce the *slowness* of the phase $\vec{s} = \vec{k}/\omega$ for which $\vec{s}\cdot\vec{v}_g = 1$, where $\vec{v}_g$ is the group velocity to get

$$d\vec{k}\cdot\vec{x} = \vec{s}\cdot\vec{x}\,d\omega = \frac{x}{v_g}\,d\omega\,,$$

since we may assume $\vec{x}$ is parallel to the group velocity (consistent with the above). Hence the arrival time becomes

$$t = \frac{x}{v_g} + \frac{\partial\Theta(\omega)}{\partial\omega}\,.$$

If the scattering matrix is not diagonal, one interprets

$$\Delta t_{ij} = \mathrm{Re}\left(-i\,S_{ij}^{-1}\frac{\partial S_{ij}}{\partial\omega}\right) = \mathrm{Re}\left(\frac{\partial\Theta_{ij}}{\partial\omega}\right)$$

as the delay in the jth scattering channel after an injection in the ith. The probability for appearing in channel j goes as $|S_{ij}|^2$ and therefore the average delay for the incoming states in channel i is

$$\begin{aligned}\langle\Delta t_i\rangle &= \sum_j |S_{ij}|^2\Delta t_{ij} = \mathrm{Re}\,(-i\sum_j S_{ij}^*\frac{\partial S_{ij}}{\partial\omega}) = \mathrm{Re}\,(-i\,\mathbf{S}^\dagger\cdot\frac{\partial\mathbf{S}}{\partial\omega})_{ii}\\ &= -i\left(\mathbf{S}^\dagger\cdot\frac{\partial\mathbf{S}}{\partial\omega}\right)_{ii},\end{aligned}$$

where we have used the derivative, $\partial/\partial\omega$, of the unitarity relation $\mathbf{S}\cdot\mathbf{S}^\dagger = \mathbf{1}$ valid for real frequencies. This discussion can in particular be made for wave packets related to partial waves and superpositions of these like an incoming plane wave corresponding to free motion. The total Wigner delay therefore corresponds to the sum over all channel delays (38.19).

Commentary

Remark 38.1 Krein-Friedel-Lloyd formula. The third volume of Thirring [38.1], sections 3.6.14 (Levison Theorem) and 3.6.15 (the proof), or P. Scherer's thesis [38.15] (appendix) discusses the Levison Theorem.

It helps to start with a toy example or simplified example instead of the general theorem, namely for the radially symmetric potential in a symmetric cavity. Have a look at the book of K. Huang, chapter 10 (on the "second virial coefficient"), or Beth and Uhlenbeck [38.5], or Friedel [38.7]. These results for the correction to the density of states are particular cases of the Krein formula [38.3]. The Krein-Friedel-Lloyd formula (38.17) was derived in refs. [38.3, 38.7, 38.8, 38.9], see also refs. [38.11, 38.14, 38.15, 38.17, 38.18]. The original papers are by Krein and Birman [38.3, 38.4] but beware, they are mathematicans.

Also, have a look at pages 15-18 of Wirzba's talk on the Casimir effect [38.16]. Page 16 discusses the Beth-Uhlenbeck formula [38.5], the predecessor of the more general Krein formula for spherical cases.

Remark 38.2 Weyl term for empty container. For a discussion of why the Weyl term contribution of the empty container is larger than of the filled one and therefore a negative net contribution is left over, see ref. [38.15].

Remark 38.3 Wigner time delay. Wigner time delay and the Wigner-Smith time delay matrix, are powerful concepts for a statistical description of scattering. The diagonal elements Q_{aa} of the lifetime matrix $\mathbf{Q} = -i\mathbf{S}^{-1}\partial\mathbf{S}/\partial\omega$, where $\mathbf{S}$ is the $[2N\times 2N]$ scattering matrix, are interpreted in terms of the time spent in the scattering region by a wave packet incident in one channel. As shown by Smith [38.26], they are the sum over all ouput channels (both in reflection and transmission) of $\Delta t_{ab} = \mathrm{Re}\,[(-i/S_{ab})(\partial S_{ab}/\partial\omega)]$ weighted by the probability of emerging from that channel. The sum of the Q_{aa} over all $2N$ channels is the Wigner time delay $\tau_W = \sum_a Q_{aa}$, which is the trace of the lifetime matrix and is proportional to the density of states.

unsure about ref. [38.26] being the right one

⇓PRELIMINARY

Résumé

⇑PRELIMINARY

References

[38.1] W. Thirring, *Quantum mechanics of atoms and molecules*, *A course in mathematical physics* Vol. **3** (Springer, New York, 1979). (Springer, Wien 1979).

[38.2] A. Messiah, *Quantum Mechanics, Vol.* **I** (North-Holland, Amsterdam, 1961).

[38.3] M.G. Krein, *On the Trace Formula in Perturbation Theory*, Mat. Sborn. (N.S.) **33**, 597 (1953) ; *Perturbation Determinants and Formula for Traces of Unitary and Self-adjoint Operators*, Sov. Math.-Dokl. **3**, 707 (1962).

[38.4] M.Sh. Birman and M.G. Krein, *On the Theory of Wave Operators and Scattering Operators*, Sov. Math.-Dokl. **3**, 740 (1962); M.Sh. Birman and D.R. Yafaev, *St. Petersburg Math. J.* **4**, 833 (1993).

[38.5] E. Beth and G.E. Uhlenbeck, *Physica* **4**, 915 (1937).

[38.6] K. Huang, *Statistical Mechanics* (John Wiley & Sons, New York (1987).

[38.7] J. Friedel, *Phil. Mag.* **43**, 153 (1952); *Nuovo Cim. Ser. 10 Suppl.* **7**, 287 (1958).

[38.8] P. Lloyd, Wave propagation through an assembly of spheres. II. The density of single-particle eigenstates, *Proc. Phys. Soc.* **90**, 207 (1967).

[38.9] P. Lloyd and P.V. Smith, Multiple-scattering theory in condensed materials, *Adv. Phys.* **21**, 69 (1972), and references therein.

[38.10] R. Balian and C. Bloch, *Ann. Phys. (N.Y.)* **63**, 592 (1971)

[38.11] R. Balian and C. Bloch, *Solution of the Schrödinger Equation in Terms of Classical Paths Ann. Phys. (NY)* **85**, 514 (1974).

[38.12] R. Balian and C. Bloch, *Distribution of eigenfrequencies for the wave equation in a finite domain: III. Eigenfrequency density oscillations*, *Ann. Phys. (N.Y.)* **69**,76 (1972).

[38.13] J.S. Faulkner, "Scattering theory and cluster calculations", *J. Phys.* **C 10**, 4661 (1977).

[38.14] P. Gaspard and S.A. Rice, Semiclassical quantization of the scattering from a classically chaotic repellor, *J. Chem. Phys.* **90** (1989) 2242–2254.

[38.15] P. Scherer, *Quantenzustände eines klassisch chaotischen Billards*, Ph.D. thesis, Univ. Köln (Berichte des Forschungszentrums Jülich 2554, ISSN 0366-0885, Jülich, Nov. 1991).

[38.16] A. Wirzba, "A force from nothing into nothing: Casimir interactions" `ChaosBook.org/projects/Wirzba/openfull.ps.gz` (overheads, 2003).

[38.17] P. Gaspard, Scattering Resonances: Classical and Quantum Dynamics, in: *Proceedings of the Int. School of Physics "Enrico Fermi"*, Course CXIX, Varena, 23 July - 2 August 1991, eds G. Casati, I. Guarneri and U. Smilansky (North-Holland, Amsterdam, 1993).

[38.18] A. Norcliffe and I. C. Percival, J. Phys. B **1**, 774 (1968); L. Schulman, Phys. Rev. **176**, 1558 (1968).

[38.19] W. Franz, *Theorie der Beugung Elektromagnetischer Wellen* (Springer, Berlin 1957); "Über die Greenschen Funktionen des Zylinders und der Kugel", *Z. Naturforschung* **9a**, 705 (1954).

[38.20] G.N. Watson, *Proc. Roy. Soc. London Ser.* **A 95**, 83 (1918).

[38.21] M. Abramowitz and I.A. Stegun, *Handbook of Mathematical Functions with Formulas, Graphs and Mathematical Tables*, (Dover, New York, 1964).

[38.22] W. Franz and R. Galle, "Semiasymptotische Reihen für die Beugung einer ebenen Welle am Zylinder", *Z. Naturforschung* **10a**, 374 (1955).

[38.23] A. Wirzba, "Validity of the semiclassical periodic orbit approximation in the 2-and 3-disk problems", *CHAOS* **2**, 77 (1992).

[38.24] M.V. Berry, "Quantizing a Classically Ergodic System: Sinai's Billiard and the KKR Method", *Ann. Phys. (N.Y.)* **131**, 163 (1981).

add more Wirzba references

[38.25] E.P. Wigner, *Phys. Rev.* **98**, 145 (1955).

[38.26] F.T. Smith, *Phys. Rev.* **118**, 349 (1960).

[38.27] A. Wirzba, *Quantum Mechanics and Semiclassics of Hyperbolic n-Disk Scattering*, *Physics Reports* **309**, 1-116 (1999); chao-dyn/9712015.

[38.28] V. A. Gopar, P. A. Mello, and M. Buttiker, Phys. Rev. Lett. 77, 3005 (1996).

[38.29] P. W. Brouwer, K. M. Frahm, and C. W. J. Beenakker, Phys. Rev. Lett. 78, 4737 (1997).

unsure about ref. [38.26] being the right one

[38.30] Following the thesis of Eisenbud, the local delay time Dtab is defined in ref. [38.26] as the appearance of the peak in the outgoing signal in channel b after the injection of a wave packet in channel a. Our definition of the local delay time tab in Eq. (1) coincides with the definition of Dtab in the limit of narrow bandwidth pulses, as shown in Eq. (3).

[38.31] E. Doron and U. Smilansky, Phys. Rev. Lett. 68, 1255 (1992).

[38.32] G. Iannaccone, Phys. Rev. B 51, 4727 (1995).

[38.33] V. Gasparian, T. Christen, and M. Büttiker, Phys. Rev. A 54, 4022 (1996).

[38.34] For a complete and insightful review see Y. V. Fyodorv and H.-J. Sommers, J. Math. Phys. 38, 1918 (1997).

[38.35] R. Landauer and Th. Martin, Rev. Mod. Phys. 66, 217 (1994). j

Add here results on quantum 3-disk scattering?

[38.36] E. H. Hauge and J. A. Støveng, Rev. Mod. Phys. 61, 917 (1989).

Exercises

Exercise 38.1 Spurious orbits under the Krein-Friedel-Lloyd contruction. *Draw examples for the three types of period orbits under the Krein-Friedel-Lloyd construction: (a) the genuine periodic orbits of the scattering region, (b) spurious periodic orbits which can be removed by the subtraction of the reference system, (c) spurious periodic orbits which cannot be removed by this subtraction. What is the role of the double limit $\eta \to 0$, container size $b \to \infty$?*

Exercise 38.2 The one-disk scattering wave function. *Derive the one-disk scattering wave function.*

(Andreas Wirzba)

Exercise 38.3 Quantum two-disk scattering. *Compute the quasiclassical spectral determinant*

$$Z(\varepsilon) = \prod_{p,j,l} \left(1 - \frac{t_p}{\Lambda_p^{j+2l}}\right)^{j+1}$$

for the two disk problem. Use the geometry

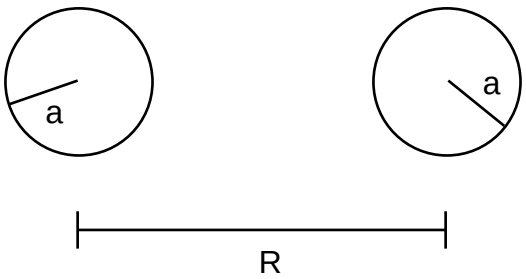

The full quantum mechanical version of this problem can be solved by finding the zeros in k for the determinant of the matrix

$$M_{m,n} = \delta_{m,n} + \frac{(-1)^n}{2} \frac{J_m(ka)}{H_n^{(1)}(ka)} \left(H_{m-n}^{(1)}(kR) + (-1)^n H_{m+n}^{(1)}(kR) \right) ,$$

where J_n is the nth Bessel function and $H_n^{(1)}$ is the Hankel function of the first kind. Find the zeros of the determinant closest to the origin by solving $\det M(k) = 0$. (Hints: notice the structure $M = I + A$ to approximate the determinant; or read Chaos **2**, *79 (1992))*

Exercise 38.4 Pinball topological index. *Upgrade your pinball simulator so that it computes the topological index for each orbit it finds.*

⇓PRELIMINARY

Exercise 38.5 Ghosts do not exist. *Prove the ghost cancellation rule (??).*

(Andreas Wirzba)

⇑PRELIMINARY

Chapter 39

Chaotic multiscattering

(A. Wirzba and P. Cvitanović)

We discuss here the semiclassics of scattering in open systems with a finite number of non-overlapping finite scattering regions. Why is this interesting at all? The semiclassics of scattering systems has five advantages compared to the bound-state problems such as the helium quantization discussed in chapter 41.

rigor, numerical accuracy, testbed for ideas

- For bound-state problem the semiclassical approximation does not respect quantum-mechanical unitarity, and the semi-classical eigenenergies are not real. Here we construct *a manifestly unitary* semiclassical scattering matrix.
- The Weyl-term contributions decouple from the multi-scattering system.
- The close relation to the classical escape processes discussed in chapter 1.

give a more precise section link

- For scattering systems the derivation of cycle expansions is more direct and controlled than in the bound-state case: the semiclassical cycle expansion is the saddle-point approximation to the cumulant expansion of the determinant of the exact quantum-mechanical multi-scattering matrix.
- The region of convergence of the semiclassical spectral function is larger than is the case for the bound-state case.

We start by a brief review of the elastic scattering of a point particle from finite collection of non-overlapping scattering regions in terms of the standard textbook scattering theory, and then develop the semiclassical scattering trace formulas and spectral determinants for scattering off N disks in a plane.

Helmholtz equation
Bessel function
Hankel function

39.1 Quantum mechanical scattering matrix

We now specialize to the elastic scattering of a point particle from finite collection of N non-overlapping reflecting disks in a 2-dimensional plane. As the point particle moves freely between the static scatterers, the time independent Schrödinger equation outside the scattering regions is the Helmholtz equation:

$$\left(\vec{\nabla}_r^2 + \vec{k}^2\right)\psi(\vec{r}) = 0\,, \qquad \vec{r}\,\text{outside the scattering regions.} \tag{39.1}$$

Here $\psi(\vec{r})$ is the wave function of the point particle at spatial position $\vec{r}$ and $E = \hbar^2\vec{k}^2/2m$ is its energy written in terms of its mass m and the wave vector $\vec{k}$ of the incident wave. For reflecting wall billiards the scattering problem is a boundary value problem with Dirichlet boundary conditions:

$$\psi(\vec{r}) = 0\,, \qquad \vec{r}\,\text{on the billiard perimeter} \tag{39.2}$$

As usual for scattering problems, we expand the wave function $\psi(\vec{r})$ in the (2-dimensional) angular momentum eigenfunctions basis

AW: changed Φ_r back to Φ_k. Note, ψ_m^k depends on $\vec{r}$.

$$\psi(\vec{r}) = \sum_{m=-\infty}^{\infty} \psi_m^k(\vec{r})e^{-im\Phi_k}\,, \tag{39.3}$$

where k and Φ_k are the length and angle of the wave vector, respectively. A plane wave in two dimensions expaned in the angular momentum basis is

AW: for consistency reasons one needs both Φ_k and Φ_r.

$$e^{i\vec{k}\cdot\vec{r}} = e^{ikr\cos(\Phi_r-\Phi_k)} = \sum_{m=-\infty}^{\infty} J_m(kr)e^{im(\Phi_r-\Phi_k)}\,, \tag{39.4}$$

where r and Φ_r denote the distance and angle of the spatial vector $\vec{r}$ as measured in the global 2-dimensional coordinate system.

The mth angular component $J_m(kr)e^{im\Phi_r}$ of a plane wave is split into a superposition of incoming and outgoing 2-dimensional spherical waves by decomposing the ordinary Bessel function $J_m(z)$ into the sum

$$J_m(z) = \frac{1}{2}\left(H_m^{(1)}(z) + H_m^{(2)}(z)\right) \tag{39.5}$$

of the Hankel functions $H_m^{(1)}(z)$ and $H_m^{(2)}(z)$ of the first and second kind. For $|z| \gg 1$ the Hankel functions behave asymptotically as:

$$\begin{aligned} H_m^{(2)}(z) &\sim \sqrt{\frac{2}{\pi z}}e^{-i(z-\frac{\pi}{2}m-\frac{\pi}{4})} \quad \text{incoming,} \\ H_m^{(1)}(z) &\sim \sqrt{\frac{2}{\pi z}}e^{+i(z-\frac{\pi}{2}m-\frac{\pi}{4})} \quad \text{outgoing.} \end{aligned} \tag{39.6}$$

Thus for $r \to \infty$ and k fixed, the mth angular component $J_m(kr)e^{im\Phi_r}$ of the plane wave can be written as superposition of incoming and outgoing 2-dimensional spherical waves:

one-disk@1-disk!scattering

$$J_m(kr)e^{im\Phi_r} \sim \frac{1}{\sqrt{2\pi kr}}\left[e^{-i(kr-\frac{\pi}{2}m-\frac{\pi}{4})} + e^{i(kr-\frac{\pi}{2}m-\frac{\pi}{4})}\right] e^{im\Phi_r} \ . \quad (39.7)$$

In terms of the asymptotic (angular momentum) components ψ_m^k of the wave function $\psi(\vec{r})$, the scattering matrix (38.3) is defined as

⇓PRELIMINARY

??
page ??

$$\psi_m^k \sim \frac{1}{\sqrt{2\pi kr}} \sum_{m'=-\infty}^{\infty} \left[\delta_{mm'} e^{-i(kr-\frac{\pi}{2}m'-\frac{\pi}{4})} + S_{mm'} e^{i(kr-\frac{\pi}{2}m'-\frac{\pi}{4})}\right] e^{im'\Phi_r} \quad (39.8)$$

⇑PRELIMINARY

The matrix element $S_{mm'}$ describes the scattering of an incoming wave with angular momentum m into an outgoing wave with angular momentum m'. If there are no scatterers, then $\mathbf{S} = \mathbf{1}$ and the asymptotic expression of the plane wave $e^{i\vec{k}\cdot\vec{r}}$ in two dimensions is recovered from $\psi(\vec{r})$.

39.1.1 1-disk scattering matrix

In general, $\mathbf{S}$ is nondiagonal and nonseparable. An exception is the 1-disk scatterer. If the origin of the coordinate system is placed at the center of the disk, by (39.5) the mth angular component of the time-independent scattering wave function is a superposition of incoming and outgoing 2-dimensional spherical waves

38.2
page 723

$$\begin{aligned} \psi_m^k &= \frac{1}{2}\left(H_m^{(2)}(kr) + S_{mm}H_m^{(1)}(kr)\right) e^{im\Phi_r} \\ &= \left(J_m(kr) - \frac{i}{2}T_{mm}H_m^{(1)}(kr)\right) e^{im\Phi_r} \ . \end{aligned}$$

The vanishing (39.2) of the wave function on the disk perimeter

$$0 = J_m(ka) - \frac{i}{2}T_{mm}H_m^{(1)}(ka)$$

yields the 1-disk scattering matrix in analytic form:

$$S^s_{mm'}(k) = \left(1 - \frac{2J_m(ka_s)}{H_m^{(1)}(ka_s)}\right)\delta_{mm'} = -\frac{H_m^{(2)}(ka_s)}{H_m^{(1)}(ka_s)}\delta_{mm'} \ , \quad (39.9)$$

where $a = a_s$ is radius of the disk and the suffix ^{s} indicates that we are dealing with a disk whose label is s. We shall derive a semiclassical approximation to this 1-disk $\mathbf{S}$-matrix in sect. 39.3.

Bessel function!addition theorem

multi-scattering matrix

39.1.2 Multi-scattering matrix

Consider next a scattering region consisting of N non-overlapping disks labeled $s \in \{1, 2, \cdots, N\}$, following the notational conventions of sect. 11.6. The strategy is to construct the full $\mathbf{T}$-matrix (38.3) from the exact 1-disk scattering matrix (39.9) by a succession of coordinate rotations and translations such that at each step the coordinate system is centered at the origin of a disk. Then the $\mathbf{T}$-matrix in $S_{mm'} = \delta_{mm'} - i\,T_{mm'}$ can be split into a product over three kinds of matrices,

Andreas, please recheck this equation

$$T_{mm'}(k) = \sum_{s,s'=1}^{N} \sum_{l_s, l_{s'}=-\infty}^{\infty} C_{ml_s}^{\ s}(k) \mathbf{M}^{-1}(k)_{l_s l_{s'}}^{s s'} D_{l_{s'} m'}^{s'}(k)\,.$$

The outgoing spherical wave scattered by the disk s is obtained by shifting the global coordinates origin distance R_s to the center of the disk s, and measuring the angle Φ_s with respect to direction $\mathbf{k}$ of the outgoing spherical wave. As in (39.9), the matrix $\mathbf{C}^s$ takes form

$$C_{ml_s}^{\ s} = \frac{2i}{\pi a_s} \frac{J_{m-l_s}(kR_s)}{H_{l_s}^{(1)}(ka_s)} e^{im\Phi_s}\,. \tag{39.10}$$

If we now describe the ingoing spherical wave in the disk s' coordinate frame by the matrix $\mathbf{D}^{s'}$

$$D_{l_{s'} m'}^{s'} = -\pi a_{s'} J_{m'-l_{s'}}(kR_{s'}) J_{l_{s'}}(ka_{s'}) e^{-im'\Phi_{s'}}\,, \tag{39.11}$$

edited to here 12jun06

looks wrong, redo!

and apply the Bessel function addition theorem

$$J_m(y+z) = \sum_{\ell=-\infty}^{\infty} J_{m-\ell}(y) J_\ell(z),$$

we recover the $\mathbf{T}$-matrix (39.9) for the single disk $s = s'$, $M = 1$ scattering. The Bessel function sum is a statement of the completness of the spherical wave basis; as we shift the origin from the disk s to the disk s' by distance $R_{s'}$, we have to reexpand all basis functions in the new coordinate frame.

The labels m and m' refer to the angular momentum quantum numbers of the ingoing and outgoing waves in the global coordinate system, and $l_s, l_{s'}$ refer to the (angular momentum) basis fixed at the sth and s'th scatterer, respectively. Thus, $\mathbf{C}^s$ and $\mathbf{D}^{s'}$ depend on the origin and orientation of the global coordinate system of the 2-dimensional plane as well as on the internal coordinates of the scatterers. As they can be made separable in the scatterer label s, they describe the single scatterer aspects of what, in general, is a multi-scattering problem.

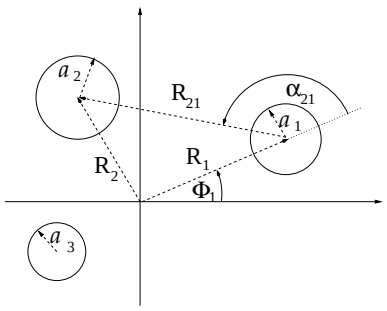

Figure 39.1: Global and local coordinates for a general 3-disk problem.

The matrix $\mathbf{M}$ is called the *multi-scattering matrix*. If the scattering problem consists only of one scatterer, $\mathbf{M}$ is simply the unit matrix $M^{ss'}_{l_s l_{s'}} = \delta^{ss'}\delta_{l_s l_{s'}}$. For scattering from more than one scatterer we separate out a "single traversal" matrix $\mathbf{A}$ which transports the scattered wave from a scattering region $\mathcal{M}_s$ to the scattering region $\mathcal{M}_{s'}$,

a multiscattered ctory illustrating expansion of $\mathbf{M}^{-1}$

Note that talk here about tum mechanics. rajectory is not ningful, yet. If wants to draw ething, it should avefront.

Changed the sign of $\mathbf{A}$ throughout, in deference to DasBuch notational conventions

$$M^{ss'}_{l_s l_{s'}} = \delta^{ss'}\delta_{l_s l_{s'}} - A^{ss'}_{l_s l_{s'}} \,. \tag{39.12}$$

The matrix $\mathbf{A}^{ss'}$ reads:

$$A^{ss'}_{l_s l_{s'}} = -(1-\delta^{ss'})\,\frac{a_s}{a_{s'}}\,\frac{J_{l_s}(ka_s)}{H^{(1)}_{l_{s'}}(ka_{s'})}\,H^{(1)}_{l_s - l_{s'}}(kR_{ss'})\,e^{i(l_s\alpha_{s's}-l_{s'}(\alpha_{ss'}-\pi))}\,. \tag{39.13}$$

Here, a_s is the radius of the sth disk. R_s and Φ_s are the distance and angle, respectively, of the ray from the origin in the 2-dimensional plane to the center of disk s as measured in the global coordinate system. Furthermore, $R_{ss'} = R_{s's}$ is the separation between the centers of the sth and s'th disk and $\alpha_{s's}$ of the ray from the center of disk s to the center of disk s' as measured in the local (body-fixed) coordinate system of disk s (see figure 39.1).

Expanded as a geometrical series about the unit matrix $\mathbf{1}$, the inverse matrix $\mathbf{M}^{-1}$ generates a multi-scattering series in powers of the single-traversal matrix $\mathbf{A}$. All genuine multi-scattering dynamics is contained in the matrix $\mathbf{A}$; by construction $\mathbf{A}$ vanishes for a single-scatterer system.

39.2 N-scatterer spectral determinant

In the following we limit ourselves to a study of the spectral properties of the $\mathbf{S}$-matrix: resonances, time delays and phase shifts. The resonances are given by the poles of the $\mathbf{S}$-matrix in the lower complex wave number (k) plane; more precisely, by the poles of the $\mathbf{S}$ on the second Riemann sheet of the complex energy plane. As the $\mathbf{S}$-matrix is unitary, it is also natural to focus on its total phase shift $\eta(k)$ defined by $\det \mathbf{S} = \exp^{2i\eta(k)}$. The

δ_m? see (38.5)

trace!-class operators

time-delay is proportional to the derivative of the phase shift with respect to the wave number k.

As we are only interested in spectral properties of the scattering problem, it suffices to study $\det \mathbf{S}$. This determinant is basis and coordinate-system independent, whereas the $\mathbf{S}$-matrix itself depends on the global coordinate system and on the choice of basis for the point particle wave function.

As the $\mathbf{S}$-matrix is, in general, an infinite dimensional matrix, it is not clear whether the corresponding determinant exists at all. If $\mathbf{T}$-matrix is trace-class, the determinant does exist. What does this mean?

39.2.1 Trace-class operators

An operator (an infinite-dimensional matrix) is called *trace-class* if and only if, for any choice of orthonormal basis, the sum of the diagonal matrix elements converges absolutely; it is called "Hilbert-Schmidt", if the sum of the absolute squared diagonal matrix elements converges. Once an operator is diagnosed as trace-class, we are allowed to manipulate it as we manipulate finite-dimensional matrices. We review the theory of trace-class operators in appendix M; here we will assume that the $\mathbf{T}$-matrix (38.3) is trace-class, and draw the conlusions.

If $\mathbf{A}$ is trace-class, the determinant $\det(\mathbf{1} - z\mathbf{A})$, as defined by the cumulant expansion, exists and is an entire function of z. Furthermore, the determinant is invariant under any unitary transformation.

add links to earlier materail, exercises

The cumulant expansion is the analytical continuation (as Taylor expansion in the book-keeping variable z) of the determinant

$$\det(\mathbf{1} - z\mathbf{A}) = \exp[\mathrm{tr}\,\ln(\mathbf{1} - z\mathbf{A})] = \exp\left(-\sum_{n=1}^{\infty}\frac{z^n}{z^n}\mathrm{tr}\,(\mathbf{A}^n)\right)\ .$$

That means

$$\det(\mathbf{1} - z\mathbf{A}) := \sum_{m=0}^{\infty} z^m Q_m(\mathbf{A})\ , \tag{39.14}$$

where the cumulants $Q_m(\mathbf{A})$ satisfy the Plemelj-Smithies recursion formula (M.26), a generalization of Newton's formula to determinants of infinite-dimensional matrices,

fix reference to (M.26) or d-cyc-exp?

$$\begin{aligned} Q_0(\mathbf{A}) &= 1 \\ Q_m(\mathbf{A}) &= -\frac{1}{m}\sum_{j=1}^{m} Q_{m-j}(\mathbf{A})\,\mathrm{tr}\,(\mathbf{A}^j) \quad \text{for } m \geq 1\,, \end{aligned} \tag{39.15}$$

in terms of cumulants of order $n < m$ and traces of order $n \leq m$. Because of the trace-class property of $\mathbf{A}$, all cumulants and traces exist separately.

For the general case of $N < \infty$ non-overlapping scatterers, the $\mathbf{T}$-matrix can be shown to be trace-class, so the determinant of the $\mathbf{S}$-matrix is well defined. What does trace-class property mean for the corresponding matrices $\mathbf{C}^s$, $\mathbf{D}^s$ and $\mathbf{A}^{ss'}$? Manipulating the operators as though they were finite matrices, we can perform the following transformations:

$$\begin{aligned} \det \mathbf{S} &= \det \left(\mathbf{1} - i\mathbf{C}\mathbf{M}^{-1}\mathbf{D}\right) \\ &= \mathrm{Det}\, \left(\mathbf{1} - i\mathbf{M}^{-1}\mathbf{D}\mathbf{C}\right) \,=\, \mathrm{Det}\, \left(\mathbf{M}^{-1}(\mathbf{M} - i\mathbf{D}\mathbf{C})\right) \\ &= \frac{\mathrm{Det}\,(\mathbf{M} - i\mathbf{D}\mathbf{C})}{\mathrm{Det}\,(\mathbf{M})} \,. \,. \end{aligned} \tag{39.16}$$

In the first line of (39.16) the determinant is taken over small ℓ (the angular momentum with respect to the global system). In the remainder of (39.16) the determinant is evaluated over the multiple indices $L_s = (s, l_s)$. In order to signal this difference we use the following notation: det ... and tr ... refer to the $|\ell\rangle$ space, Det ... and Tr ... refer to the multiple index space. The matrices in the multiple index space are expanded in the complete basis $\{|L_s\rangle\} = \{|s, \ell_s\rangle\}$ which refers for fixed index s to the origin of the sth scatterer and not any longer to the origin of the 2-dimensional plane.

Let us explicitly extract the product of the determinants of the subsystems from the determinant of the total system (39.16):

$$\begin{aligned} \det \mathbf{S} &= \frac{\mathrm{Det}\,(\mathbf{M} - i\mathbf{D}\mathbf{C})}{\mathrm{Det}\,(\mathbf{M})} \\ &= \frac{\mathrm{Det}\,(\mathbf{M} - i\mathbf{D}\mathbf{C})}{\mathrm{Det}\,\mathbf{M}} \frac{\prod_{s=1}^{N} \det \mathbf{S}^s}{\prod_{s=1}^{N} \det \mathbf{S}^s} \\ &= \left(\prod_{s=1}^{N} \det \mathbf{S}^s\right) \frac{\mathrm{Det}\,(\mathbf{M} - i\mathbf{D}\mathbf{C}) / \prod_{s=1}^{N} \det \mathbf{S}^s}{\mathrm{Det}\,\mathbf{M}} \,. \end{aligned} \tag{39.17}$$

The final step in the reformulation of the determinant of the $\mathbf{S}$-matrix of the N-scatterer problem follows from the unitarity of the $\mathbf{S}$-matrix. The unitarity of $\mathbf{S}^\dagger(k^*)$ implies for the determinant find refeq S-unitary

$$\det\left(\mathbf{S}(k^*)^\dagger\right) = 1/\det \mathbf{S}(k)\,, \tag{39.18}$$

where this manipulation is allowed because the $\mathbf{T}$-matrix is trace-class. The unitarity condition should apply for the $\mathbf{S}$-matrix of the total system, $\mathbf{S}$, as for the each of the single subsystems, $\mathbf{S}^s$, $s = 1, \cdots, N$. In terms of the result of (39.17), this implies

$$\frac{\mathrm{Det}\,(\mathbf{M}(k) - i\mathbf{D}(k)\mathbf{C}(k))}{\prod_{s=1}^{N} \det \mathbf{S}^s} = \mathrm{Det}\,(\mathbf{M}(k^*)^\dagger)$$

since all determinants in (39.17) exist separately and since the determinants $\det \mathbf{S}^s$ respect unitarity by themselves. Thus, we finally have

$$\det \mathbf{S}(k) = \left\{ \prod_{s=1}^{N} (\det \mathbf{S}^s(k)) \right\} \frac{\mathrm{Det}\, \mathbf{M}(k^*)^\dagger}{\mathrm{Det}\, \mathbf{M}(k)} \,, \tag{39.19}$$

where all determinants exist separately.

In summary: We assumed a scattering system of a *finite* number of *non-overlapping* scatterers which can be of different shape and size, but are all of finite extent. We assumed the trace-class character of the **T**-matrix belonging to the total system and of the single-traversal matrix **A** and finally unitarity of the **S**-matrices of the complete and all subsystems.

What can one say about the point-particle scattering from a finite number of scatterers of arbitrary shape and size? As long as each of $N < \infty$ single scatterers has a finite spatial extent, i.e., can be covered by a finite disk, the total system has a finite spatial extent as well. Therefore, it too can be put insided a circular domain of finite radius b, e.g., inside a single disk. If the impact parameter of the point particle measured with respect to the origin of this disk is larger than the disk size (actually larger than $(e/2) \times b$), then the **T** matrix elements of the N-scatterer problem become very small. If the wave number k is kept fixed, the modulus of the *diagonal* matrix elements, $|T_{mm}|$ with the angular momentum $m > (e/2)kb$, is bounded by the corresponding quantity of the covering disk.

39.2.2 Quantum cycle expansions

In formula (39.19) the genuine multi-scattering terms are separated from the single-scattering ones. We focus on the multi-scattering terms, i.e., on the ratio of the determinants of the multi-scattering matrix $\mathbf{M} = \mathbf{1} - \mathbf{A}$ in (39.19), since they are the origin of the periodic orbit sums in the semiclassical reduction. The resonances of the multi-scattering system are given by the zeros of $\mathrm{Det}\, \mathbf{M}(k)$ in the lower complex wave number plane.

In order to set up the problem for the semiclassical reduction, we express the determinant of the multi-scattering matrix in terms of the traces of the powers of the matrix **A**, by means of the cumulant expansion (39.14). Because of the finite number $N \geq 2$ of scatterers $\mathrm{tr}\,(\mathbf{A}^n)$ receives contributions corresponding to all periodic itineraries $s_1 s_2 s_3 \cdots s_{n-1} s_n$ of total symbol length n with an alphabet $s_i \in \{1, 2, \ldots, N\}$. of N symbols,

$$\begin{aligned} &\mathrm{tr}\, \mathbf{A}^{s_1 s_2} \mathbf{A}^{s_2 s_3} \cdots \mathbf{A}^{s_{n-1} s_n} \mathbf{A}^{s_n s_n} \\ &= \sum_{l_{s_1}=-\infty}^{+\infty} \sum_{l_{s_2}=-\infty}^{+\infty} \cdots \sum_{l_{s_n}=-\infty}^{+\infty} A^{s_1 s_2}_{l_{s_1} l_{s_2}} A^{s_2 s_3}_{l_{s_2} l_{s_3}} \cdots A^{s_{n-1} s_n}_{l_{s_{n-1}} l_{s_n}} A^{s_n s_1}_{l_{s_n} l_{s_1}} \,. \end{aligned} \tag{39.20}$$

Remember our notation that the trace $\mathrm{tr}\,(\cdots)$ refers only to the $|l\rangle$ space. By construction $\mathbf{A}$ describes only scatterer-to-scatterer transitions, so the symbolic dynamics has to respect the no-self-reflection pruning rule: for admissible itineraries the successive symbols have to be different. This rule is implemented by the factor $1-\delta^{ss'}$ in (39.13).

one-disk@1-disk!semiclassical scattering

The trace $\mathrm{tr}\,\mathbf{A}^n$ is the sum of all itineraries of length n,

$$\mathrm{tr}\,\mathbf{A}^n = \sum_{\{s_1 s_2 \cdots s_n\}} \mathrm{tr}\,\mathbf{A}^{s_1 s_2}\mathbf{A}^{s_2 s_3}\cdots\mathbf{A}^{s_{n-1}s_n}\mathbf{A}^{s_n s_1}\ . \tag{39.21}$$

We will show for the N-disk problem that these periodic itineraries correspond in the semiclassical limit, $ka_{s_i} \gg 1$, to *geometrical* periodic orbits with the same symbolic dynamics.

move this to a better place

For periodic orbits with creeping sections the symbolic alphabet has to be extended, see sect. 39.3.1. Furthermore, depending on the geometry, there might be nontrivial pruning rules based on the so called ghost orbits, see sect. 39.4.1.

39.2.3 Symmetry reductions

change to Det $\mathbf{M}$ in def.tex

The determinants over the multi-scattering matrices run over the multiple index L of the multiple index space. This is the proper form for the symmetry reduction (in the multiple index space), e.g., if the scatterer configuration is characterized by a discrete symmetry group G, we have

$$\mathrm{Det}\,\mathbf{M} = \prod_{\alpha} \left(\det \mathbf{M}_{\mathrm{D}_\alpha}(k)\right)^{d_\alpha}\ ,$$

where the index α runs over all conjugate classes of the symmetry group G and D_α is the αth representation of dimension d_α. The symmetry reduction on the exact quantum mechanical level is the same as for the classical evolution operators spectral determinant factorization (22.17) of sect. 22.4.2.

39.3 Semiclassical 1-disk scattering

We start by focusing on the single-scatterer problem. In order to be concrete, we will consider the semiclassical reduction of the scattering of a single disk in plane.

Instead of calculating the semiclassical approximation to the determinant of the one-disk system scattering matrix (39.9), we do so for

why boldface $\mathbf{d}(k)$?

$$\mathbf{d}(k) \equiv \frac{1}{2\pi i}\frac{d}{dk}\ln\det \mathbf{S}^1(ka) \ = \frac{1}{2\pi i}\frac{d}{dk}\mathrm{tr}\,\left(\ln \mathbf{S}^1(ka)\right) \tag{39.22}$$

might want to connect this to (18.21), the expection value of time

the so called *time delay*.

$$\begin{aligned}\mathbf{d}(k) &= \frac{1}{2\pi i}\frac{d}{dk}\mathrm{tr}\,\left(\ln\det \mathbf{S}^1(ka)\right) = \frac{1}{2\pi i}\sum_m \left(\frac{H_m^{(1)}(ka)}{H_m^{(2)}(ka)}\,\frac{d}{dk}\frac{H_m^{(2)}(ka)}{H_m^{(1)}(ka)}\right)\\ &= \frac{a}{2\pi i}\sum_m\left(\frac{H_m^{(2)\prime}(ka)}{H_m^{(2)}(ka)} - \frac{H_m^{(1)\prime}(ka)}{H_m^{(1)}(ka)}\right)\ .\end{aligned} \tag{39.23}$$

Here the prime denotes the derivative with respect to the argument of the Hankel functions. Let us introduce the abbreviation

$$\chi_\nu = \frac{H_\nu^{(2)\prime}(ka)}{H_\nu^{(2)}(ka)} - \frac{H_\nu^{(1)\prime}(ka)}{H_\nu^{(1)}(ka)}\ . \tag{39.24}$$

We apply the Watson contour method to (39.23)

$$\mathbf{d}(k) = \frac{a_j}{2\pi i}\sum_{m=-\infty}^{+\infty}\chi_m = \frac{a_j}{2\pi i}\,\frac{1}{2i}\oint_C \mathrm{d}\nu\,\frac{e^{-i\nu\pi}}{\sin(\nu\pi)}\chi_\nu\ . \tag{39.25}$$

Here the contour C encircles in a counter-clockwise manner a small semiinfinite strip D which completely covers the real ν-axis but which only has a small finite extent into the positive and negative imaginary ν direction. The contour C is then split up in the path above and below the real ν-axis such that

$$\mathbf{d}(k) = \frac{a}{4\pi i}\left\{\int_{-\infty+i\epsilon}^{+\infty+i\epsilon}\mathrm{d}\nu\,\frac{e^{-i\nu\pi}}{\sin(\nu\pi)}\chi_\nu - \int_{-\infty-i\epsilon}^{+\infty-i\epsilon}\mathrm{d}\nu\,\frac{e^{-i\nu\pi}}{\sin(\nu\pi)}\chi_\nu\right\}\ .$$

Then, we perform the substitution $\nu\to-\nu$ in the second integral so as to get

$$\begin{aligned}\mathbf{d}(k) &= \frac{a}{4\pi}\left\{\int_{-\infty+i\epsilon}^{+\infty+i\epsilon}\mathrm{d}\nu\,\frac{e^{-i\nu\pi}}{\sin(\nu\pi)}\chi_\nu + \mathrm{d}\nu\,\frac{e^{+i\nu\pi}}{\sin(\nu\pi)}\chi_{-\nu}\right\}\\ &= \frac{a}{2\pi i}\left\{2\int_{-\infty+i\epsilon}^{+\infty+i\epsilon}\mathrm{d}\nu\,\frac{e^{2i\nu\pi}}{1-e^{2i\nu\pi}}\,\chi_\nu + \int_{-\infty}^{+\infty}\mathrm{d}\nu\,\chi_\nu\right\}\ ,\end{aligned} \tag{39.26}$$

where we used the fact that $\chi_{-\nu}=\chi_\nu$. The contour in the last integral can be deformed to pass over the real ν-axis since its integrand has no Watson denominator.

Airy function
Airy function

We will now approximate the last expression semiclassically, i.e., under the assumption $ka \gg 1$. As the two contributions in the last line of (39.26) differ by the presence or absence of the Watson denominator, they will have to be handled semiclassically in different ways: the first will be closed in the upper complex plane and evaluated at the poles of χ_ν, the second integral will be evaluated on the real ν-axis under the Debye approximation for Hankel functions.

We will now work out the first term. The poles of χ_ν in the upper complex plane are given by the zeros of $H_\nu^{(1)}(ka)$ which will be denoted by $\nu_\ell(ka)$ and by the zeros of $H_\nu^{(2)}(ka)$ which we will denote by $-\bar\nu_\ell(ka)$, $\ell = 1, 2, 3, \cdots$. In the Airy approximation to the Hankel functions they are given by

$$\begin{aligned} \nu_\ell(ka) &= ka + i\alpha_\ell(ka)\ , && (39.27)\\ -\bar\nu_\ell(ka) &= -ka + i(\alpha_\ell(k^*a))^* = -\left(\nu_\ell(k^*a)\right)^*\ , && (39.28) \end{aligned}$$

with

refer to occurances of Airy fcts in simpler settings, such as in the $1-d$ WKB

$$\begin{aligned} i\alpha_\ell(ka) &= e^{i\frac{\pi}{3}}\left(\frac{ka}{6}\right)^{1/3} q_\ell \;-\; e^{-i\frac{\pi}{3}}\left(\frac{6}{ka}\right)^{1/3}\frac{q_\ell^2}{180} \;-\; \frac{1}{70ka}\left(1-\frac{q_\ell^3}{30}\right)\\ &+ e^{i\frac{\pi}{3}}\left(\frac{6}{ka}\right)^{\frac{5}{3}}\frac{1}{3150}\left(\frac{29q_\ell}{6^2}-\frac{281q_\ell^4}{180\cdot 6^3}\right) + \cdots . \qquad (39.29) \end{aligned}$$

Here q_ℓ labels the zeros of the Airy integral

$$A(q) \equiv \int_0^\infty \mathrm{d}\tau\ \cos(q\tau - \tau^3) = 3^{-1/3}\pi \mathrm{Ai}(-3^{-1/3}q)\ ,$$

with $\mathrm{Ai}(z)$ being the standard Airy function; approximately, $q_\ell \approx 6^{1/3}[3\pi(\ell - 1/4)]^{2/3}/2$. In order to keep the notation simple, we will abbreviate $\nu_\ell \equiv \nu_\ell(ka)$ and $\bar\nu_\ell \equiv \bar\nu_\ell(ka)$. Thus the first term of (39.26) becomes finally

$$\frac{a}{2\pi i}\left\{2\int_{-\infty+i\epsilon}^{+\infty+i\epsilon}\mathrm{d}\nu\ \frac{e^{2i\nu\pi}}{1-e^{2i\nu\pi}}\,\chi_\nu\right\} = 2a\sum_{\ell=1}^{\infty}\left(\frac{e^{2i\nu_\ell\pi}}{1-e^{2i\nu_\ell\pi}} + \frac{e^{-2i\bar\nu_\ell\pi}}{1-e^{-2i\bar\nu_\ell\pi}}\right).$$

In the second term of (39.26) we will insert the Debye approximations for the Hankel functions:

$$\begin{aligned} H_\nu^{(1/2)}(x) &\sim \sqrt{\frac{2}{\pi\sqrt{x^2-\nu^2}}}\exp\left(\pm i\sqrt{x^2-\nu^2} \mp i\nu\arccos\frac{\nu}{x} \mp i\frac{\pi}{4}\right) \quad \text{for } |x| > \nu \qquad (39.30)\\ H_\nu^{(1/2)}(x) &\sim \mp i\sqrt{\frac{2}{\pi\sqrt{\nu^2-x^2}}}\exp\left(-\sqrt{\nu^2-x^2} + \nu\,\mathrm{ArcCosh}\frac{\nu}{x}\right) \qquad \text{for } |x| < \nu\ . \end{aligned}$$

one-disk@1-disk!creeping
creeping!1-disk

Note that for $\nu > ka$ the contributions in χ_ν cancel. Thus the second integral of (39.26) becomes

$$\begin{aligned}\frac{a}{2\pi i}\int_{-\infty}^{+\infty} \mathrm{d}\nu\, \chi_\nu &= \frac{a}{2\pi i}\int_{-ka}^{+ka} \mathrm{d}\nu\, \frac{(-2i)}{a}\frac{d}{dk}\left(\sqrt{k^2a^2-\nu^2} - \nu \arccos\frac{\nu}{ka}\right) + \cdots \\ &= -\frac{1}{k\pi}\int_{-ka}^{ka} \mathrm{d}\nu \sqrt{k^2a^2-\nu^2} + \cdots = -\frac{a^2}{2}k + \cdots\ , \qquad (39.31)\end{aligned}$$

where $\cdots$ takes care of the polynomial corrections in the Debye approximation and the boundary correction terms in the ν integration.

In summary, the semiclassical approximation to $\mathbf{d}(k)$ reads

$$\mathbf{d}(k) = 2a\sum_{\ell=1}^{\infty}\left(\frac{e^{2i\nu_\ell\pi}}{1-e^{2i\nu_\ell\pi}} + \frac{e^{-2i\bar{\nu}_\ell\pi}}{1-e^{-2i\bar{\nu}_\ell\pi}}\right) - \frac{a^2}{2}k + \cdots\ .$$

Using the definition of the time delay (39.22), we get the following expression for $\det \mathbf{S}^1(ka)$:

$$\begin{aligned}&\ln\det\mathbf{S}^1(ka) - \lim_{k_0\to 0}\ln\det\mathbf{S}^1(k_0a) \qquad (39.32)\\ &= 2\pi i a\int_0^k \mathrm{d}\tilde{k}\left(-\frac{a\tilde{k}}{2} + 2\sum_{\ell=1}^{\infty}\left(\frac{e^{i2\pi\nu_\ell(\tilde{k}a)}}{1-e^{i2\pi\nu_\ell(\tilde{k}a)}} + \frac{e^{-i2\pi\bar{\nu}_\ell(\tilde{k}a)}}{1-e^{-i2\pi\bar{\nu}_\ell(\tilde{k}a)}}\right)\right) + \cdots \\ &\sim -2\pi i N(k) + 2\sum_{\ell=1}^{\infty}\int_0^k \mathrm{d}\tilde{k}\,\frac{d}{d\tilde{k}}\left\{-\ln\left(1-e^{i2\pi\nu_\ell(\tilde{k}a)}\right) + \ln\left(1-e^{-i2\pi\bar{\nu}_\ell(\tilde{k}a)}\right)\right\} + \cdots,\end{aligned}$$

where in the last expression it has been used that semiclassically $\frac{d}{dk}\nu_\ell(ka) \sim \frac{d}{dk}\bar{\nu}_\ell(ka) \sim a$ and that the Weyl term for a single disk of radius a goes like $N(k) = \pi a^2k^2/(4\pi) + \cdots$ (the next terms come from the boundary terms in the ν-integration in (39.31)). Note that for the lower limit, $k_0 \to 0$, we have two simplifications: First,

$$\begin{aligned}\lim_{k_0\to 0} S^1_{mm'}(k_0a) = \lim_{k_0\to 0}\frac{-H^{(2)}_m(k_0a)}{H^{(1)}_m(k_0a)}\delta_{mm'} &= 1\times\delta_{mm'} \qquad \forall m,m' \\ \to \lim_{k_0\to 0}\det\mathbf{S}^1(k_0a) &= 1\ .\end{aligned}$$

Secondly, for $k_0 \to 0$, the two terms in the curly bracket of (39.32) cancel.

39.3.1 1-disk spectrum interpreted; pure creeping

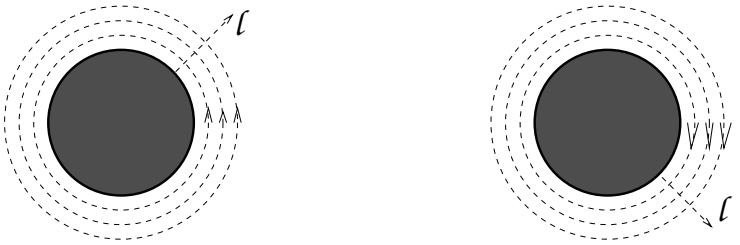

Figure 39.2: Right- and left-handed diffractive creeping paths of increasing mode number ℓ for a single disk.

To summarize: the semiclassical approximation to the determinant $\mathbf{S}^1(ka)$ is given by

$$\det \mathbf{S}^1(ka) \sim e^{-i2\pi N(k)} \frac{\prod_{\ell=1}^{\infty} \left(1 - e^{-2i\pi\bar{\nu}_\ell(ka)}\right)^2}{\prod_{\ell=1}^{\infty} \left(1 - e^{2i\pi\nu_\ell(ka)}\right)^2} , \tag{39.33}$$

with

$$\begin{array}{rclcl} \nu_\ell(ka) & = & ka + i\alpha_\ell(ka) & = & ka + e^{+i\pi/3}(ka/6)^{1/3} q_\ell + \cdots \\ \bar{\nu}_\ell(ka) & = & ka - i(\alpha_\ell(k^*a))^* & = & ka + e^{-i\pi/3}(ka/6)^{1/3} q_\ell + \cdots \\ & = & (\nu_\ell(k^*a))^* & & \end{array}$$

and $N(ka) = (\pi a^2 k^2)/4\pi + \cdots$ the leading term in the Weyl approximation for the staircase function of the wavenumber eigenvalues in the disk interior. From the point of view of the scattering particle, the interior domains of the disks are excluded relatively to the free evolution without scattering obstacles. Therefore the negative sign in front of the Weyl term. For the same reason, the subleading boundary term has here a Neumann structure, although the disks have Dirichlet boundary conditions.

Let us abbreviate the r.h.s. of (39.33) for a disk s as

$$\det \mathbf{S}^s(ka_s) \sim \left(e^{-i\pi N(ka_s)}\right)^2 \frac{\widetilde{Z}^s_\ell(k^*a_s)^*}{\widetilde{Z}^s_\ell(ka_s)} \frac{\widetilde{Z}^s_r(k^*a_s)^*}{\widetilde{Z}^s_r(ka_s)} , \tag{39.34}$$

where $\widetilde{Z}^s_\ell(ka_s)$ and $\widetilde{Z}^s_r(ka_s)$ are the *diffractional* zeta functions (here and in the following we will label semiclassical zeta functions *with* diffractive corrections by a tilde) for creeping orbits around the sth disk in the left-handed sense and the right-handed sense, respectively (see figure 39.2). The two orientations of the creeping orbits are the reason for the exponents 2 in (39.33). Equation (39.33) describes the semiclassical approximation to the incoherent part (= the curly bracket on the r.h.s.) of the exact expression (39.19) for the case that the scatterers are disks.

In the following we will discuss the semiclassical resonances in the 1-disk scattering problem with Dirichlet boundary conditions, i.e. the so-called

Airy function

shape resonances. The quantum mechanical resonances are the poles of the S-matrix in the complex k-plane. As the 1-disk scattering problem is separable, the S-matrix is already diagonalized in the angular momentum eigenbasis and takes the simple form (39.9). The exact quantummechanical poles of the scattering matrix are therefore given by the the zeros, $k^{\rm res}_{n\,m}$, of the Hankel functions $H^{(1)}_m(ka)$ in the lower complex k plane which can be labeled by two indices, m and n, where m denotes the angular quantum number of the Hankel function and n is a radial quantum number. As the Hankel functions have to vanish at specific k values, one cannot use the usual Debye approximation as semiclassical approximation for the Hankel function, since this approximation only works in case the Hankel function is dominated by only one saddle. However, for the vanishing of the Hankel function, one has to have the interplay of two saddles, thus an Airy approximation is needed as in the case of the creeping poles discussed above. The Airy approximation of the Hankel function $H^{(1)}_\nu(ka)$ of complex-valued index ν reads

$$H^{(1)}_\nu(ka) \sim \frac{2}{\pi} e^{-i\frac{\pi}{3}} \left(\frac{6}{ka}\right)^{1/3} A(q^{(1)}) \,,$$

with

$$q^{(1)} = e^{-i\frac{\pi}{3}} \left(\frac{6}{ka}\right)^{1/3} (\nu - ka) + \mathcal{O}\left((ka)^{-1}\right).$$

Hence the zeros ν_ℓ of the Hankel function in the complex ν plane follow from the zeros q_ℓ of the Airy integral $A(q)$ (see (39.3). Thus if we set $\nu_\ell = m$ (with m integer), we have the following semiclassical condition on $k^{\rm res}$

repeat of (39.29)?

$$\begin{aligned} m &\sim k^{\rm res}a + i\alpha_\ell(k^{\rm res}a) \\ &= e^{i\frac{\pi}{3}} \left(\frac{k^{\rm res}a}{6}\right)^{1/3} q_\ell \;-\; e^{-i\frac{\pi}{3}} \left(\frac{6}{k^{\rm res}a}\right)^{1/3} \frac{q_\ell^2}{180} \;-\; \frac{1}{70k^{\rm res}a} \Big(\\ &+ e^{i\frac{\pi}{3}} \left(\frac{6}{k^{\rm res}a}\right)^{\frac{5}{3}} \frac{1}{3150} \left(\frac{29q_\ell}{6^2} - \frac{281q_\ell^4}{180\cdot 6^3}\right) + \cdots, \end{aligned}$$

with $l = 1, 2, 3, \cdots$.

For a given index l this is equivalent to

$$0 \sim 1 - e^{(ik^{\rm res} - \alpha_\ell)2\pi a} \,,$$

the de-Broglie condition on the wave function that encircles the disk. Thus the semiclassical resonances of the 1-disk problem are given by the zeros of the following product

$$\prod_{l=1}^{\infty} \left(1 - e^{(ik - \alpha_\ell)2\pi a}\right),$$

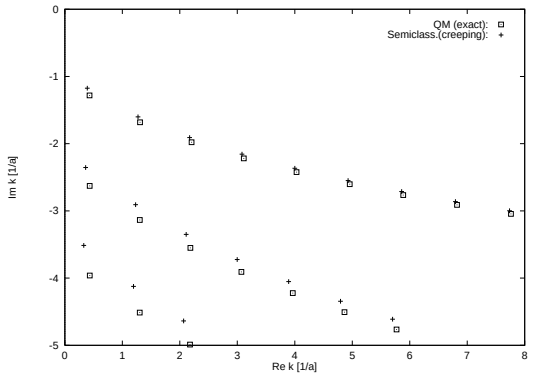

Figure 39.3: The shape resonances of the 1-disk system in the complex k plane in units of the disk radius a. The boxes label the exact quantum mechanical resonances (given by the zeros of $H_m^{(1)}(ka)$ for $m = 0, 1, 2$), the crosses label the diffractional semiclassical resonances (given by the zeros of the creeping formula in the Airy approximation (39.35) up to the order $\mathcal{O}([ka]^{1/3})$).

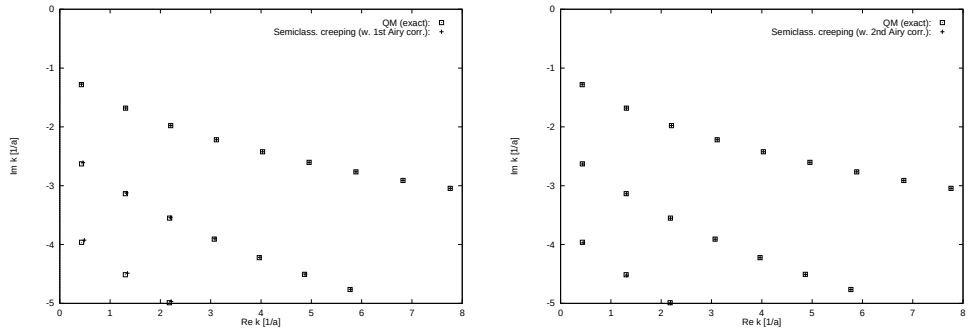

Figure 39.4: Same as in figure 39.3. However, the subleading terms in the Airy approximation (39.35) are taken into account up to the order $\mathcal{O}([ka]^{-1/3})$ (upper panel) and up to order $\mathcal{O}([ka]^{-1})$ (lower panel).

which is of course nothing else than $\widetilde{Z}_{\text{1-disk}}(k)$, the semiclassical diffraction zeta function of the 1-disk scattering problem, see (39.34). Note that this expression includes just the pure creeping contribution and no genuine geometrical parts. Because of

$$H_{-m}^{(1)}(ka) = (-1)^m H_m^{(1)}(ka)\,,$$

the zeros are doubly degenerate if $m \neq 0$, corresponding to right- and left handed creeping turns. The case $m = 0$ is unphysical, since all zeros of the Hankel function $H_0^{(1)}(ka)$ have negative real value.

From figure 39.3 one notes that the creeping terms in the Airy order $\mathcal{O}([ka]^{1/3})$, which are used in the Keller construction, systematically underestimate the magnitude of the imaginary parts of the exact data. However, the creeping data become better for increasing $\mathrm{Re}\, k$ and decreasing $|\mathrm{Im}\, k|$, as they should as semiclassical approximations.

explain Keller principle somewhere

In the upper panel of figure 39.4 one sees the change, when the next order in the Airy approximation (39.35) is taken into account. The approximation

is nearly perfect, especially for the leading row of resonances. The second Airy approximation using (39.35) up to order $\mathcal{O}([ka]^{-1})$ is perfect up to the drawing scale of figure 39.4 (lower panel).

⇓PRELIMINARY

We shall return to creeping contributions for $N > 1$ disk systems in chapter 42.

⇑PRELIMINARY

39.4 From quantum cycle to semiclassical cycle

The procedure for the semiclassical approximation of a general periodic itinerary (39.20) of length n is somewhat laborious, and we will only sketch the procedure here. It follows, in fact, rather closely the methods developed for the semiclassical reduction of the determinant of the 1-disk system.

The quantum cycle

$$\operatorname{tr} \mathbf{A}^{s_1 s_2} \cdots \mathbf{A}^{s_m s_1} = \sum_{l_{s_1}=-\infty}^{\infty} \cdots \sum_{l_{s_m}=-\infty}^{\infty} A^{s_1 s_2}_{l_{s_1} l_{s_2}} \cdots A^{s_m s_1}_{l_{s_m} l_{s_1}}$$

still has the structure of a "multi-trace" with respect to angular momentum.

Each of the sums $\sum_{l_{s_i}=-\infty}^{\infty}$ – as in the 1-disk case – is replaced by a *Watson contour* resummation in terms of complex angular momentum ν_{s_i}. Then the paths below the real ν_{s_i}-axes are transformed to paths above these axes, and the integrals split into expressions *with* and *without* an explicit Watson $\sin(\nu_{s_i}\pi)$ denominator.

1. In the $\sin(\nu_{s_i}\pi)$ -independent integrals we replace all Hankel and Bessel functions by Debye approximations. Then we evaluate the expression in the saddle point approximation: either left or right *specular reflection* at disk s_i or *ghost tunneling* through disk s_i result.

2. For the $\sin(\nu_{s_i}\pi)$ -dependent integrals, we close the contour in the upper ν_{s_i} plane and evaluate the integral at the residua $H^{(1)}_{\nu_{s_i}}(ka_{s_i})$=0. Then we use the Airy approximation for $J_{\nu_{s_i}}(ka_{s_i})$ and $H^{(1)}_{\nu_{s_i}}(ka_{s_i})$: left and right *creeping paths* around disk s_i result.

In the above we have assumed that no grazing geometrical paths appear. If they do show up, the analysis has to be extended to the case of coninciding saddles between the geometrical paths with $\pi/2$ angle reflection from the disk surface and paths with direct ghost tunneling through the disk.

There are three possibilities of "semiclassical" contact of the point particle with the disk s_i:

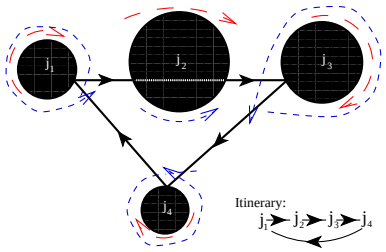

Figure 39.5: A 4-disk problem with three specular reflections, one ghost tunneling, and distinct creeping segments from which all associated creeping paths can be constructed.

1. either geometrical which in turn splits into three alternatives
   (a) *specular reflection* to the right,
   (b) *specular reflection* to the left,
   (c) or *'ghost tunneling'* where the latter induce the nontrivial pruning rules (as discussed above)
2. or *right-handed creeping turns*
3. or *left-handed creeping turns*,

see figure 39.5. The specular reflection to the right is linked to left-handed creeping paths with at least one knot. The specular reflection to the left matches a right-handed creeping paths with at least one knot, whereas the shortest left- and right-handed creeping paths in the ghost tunneling case are topologically trivial. In fact, the topology of the creeping paths encodes the choice between the three alternatives for the geometrical contact with the disk. This is the case for the simple reason that creeping sections have to be positive definite in length: the creeping amplitude has to decrease during the creeping process, as tangential rays are constantly emitted. In mathematical terms, it means that the creeping angle has to be positive. Thus, the positivity of the *two* creeping angles for the shortest left *and* right turn uniquely specifies the topology of the creeping sections which in turn specifies which of the three alternatives, either specular reflection to the right or to the left or straight "ghost" tunneling through disk j, is realized for the semiclassical geometrical path. Hence, the existence of a unique saddlepoint is guaranteed.

In order to be concrete, we will restrict ourselves in the following to the scattering from $N < \infty$ non-overlapping *disks* fixed in the 2-dimensional plane. The semiclassical approximation of the periodic itinerary

$$\mathrm{tr}\, \mathbf{A}^{s_1 s_2} \mathbf{A}^{s_2 s_3} \cdots \mathbf{A}^{s_{n-1} s_n} \mathbf{A}^{s_n s_1}$$

becomes a standard periodic orbit labeled by the symbol sequence $s_1 s_2 \cdots s_n$. Depending on the geometry, the individual legs $s_{i-1} \to s_i \to s_{i+1}$ result either from a standard specular reflection at disk s_i or from a ghost path passing straight through disk s_i. If furthermore creeping contributions are taken into account, the symbolic dynamics has to be generalized from single-letter symbols $\{s_i\}$ to triple-letter symbols $\{s_i, \sigma_i \times \ell_i\}$ with $\ell_i \geq 1$ integer

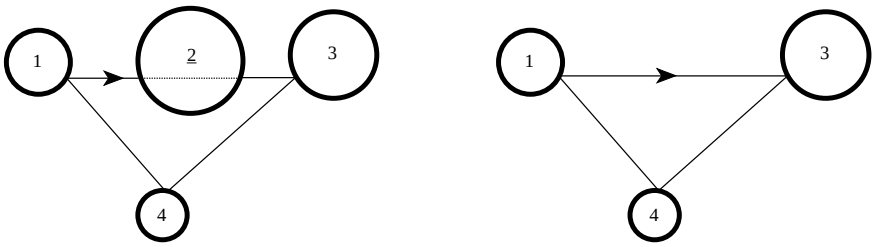

Figure 39.6: (a) The ghost itinerary $(1,\underline{2},3,4)$. (b) The parent itinerary $(1,3,4)$.

valued and $\sigma_i = 0, \pm 1$ [1] By definition, the value $\sigma_i = 0$ represents the non-creeping case, such that $\{s_i, 0 \times \ell_i\} = \{s_i, 0\} = \{s_i\}$ reduces to the old single-letter symbol. The magnitude of a nonzero ℓ_i corresponds to creeping sections of mode number $|\ell_i|$, whereas the sign $\sigma_i = \pm 1$ signals whether the creeping path turns around the disk s_i in the positive or negative sense. Additional full creeping turns around a disk s_i can be summed up as a geometrical series; therefore they do not lead to the introduction of a further symbol.

39.4.1 Ghost contributions

An itinerary with a semiclassical ghost section at, say, disk s_i can be shown to have the same weight as the corresponding itinerary without the s_i th symbol. Thus, semiclassically, they cancel each other in the tr $\ln(\mathbf{1} - \mathbf{A})$ expansion, where they are multiplied by the permutation factor n/r with the integer r counting the repeats. For example, let $(1,\underline{2},3,4)$ be a non-repeated periodic itinerary with a ghost section at disk 2 steming from the 4th-order trace tr A^4. By convention, an underlined disk index signals a ghost passage (as in figure 39.6a), with corresponding semiclassical ghost traversal matrices also underlined, $\underline{\mathbf{A}}^{i,\underline{i+1}}\underline{\mathbf{A}}^{\underline{i+1},i+2}$. Then its semiclassical, geometrical contribution to tr $\ln(\mathbf{1} - \mathbf{A})$ cancels exactly against the one of its "parent" itinerary $(1,3,4)$ (see figure 39.6b) resulting from the 3rd-order trace:

$$
\begin{aligned}
&-\frac{1}{4}\left(4\,\underline{\mathbf{A}}^{1,\underline{2}}\underline{\mathbf{A}}^{\underline{2},3}\mathbf{A}^{3,4}\mathbf{A}^{4,1}\right) - \frac{1}{3}\left(3\,\mathbf{A}^{1,3}\mathbf{A}^{3,4}\mathbf{A}^{4,1}\right) \\
&= \quad (+1-1)\,\mathbf{A}^{1,3}\mathbf{A}^{3,4}\mathbf{A}^{4,1} = 0\,.
\end{aligned}
$$

The prefactors $-1/3$ and $-1/4$ are due to the expansion of the logarithm, the factors 3 and 4 inside the brackets result from the cyclic permutation of the periodic itineraries, and the cancellation stems from the rule

⇓PRELIMINARY
38.5
page 723
⇑PRELIMINARY

$$
\cdots \underline{\mathbf{A}}^{i,\underline{i+1}}\underline{\mathbf{A}}^{\underline{i+1},i+2}\cdots = \cdots\left(-\mathbf{A}^{i,i+2}\right)\cdots\,. \tag{39.36}
$$

The reader might study more complicated examples and convince herself that the rule (39.36)(or (??) for the cases of adjacent ghost sections) is

⇓PRIVATE

IVATE

sufficient to cancel any primary or repeated periodic orbit with one or more ghost sections completely out of the expansion of $\mathrm{tr}\,\ln(\mathbf{1}-\mathbf{A})$ and therefore also out of the cumulant expansion in the semiclassical limit: Any periodic orbit of length m with $n(<m)$ ghost sections is cancelled by the sum of all 'parent' periodic orbits of length $m-i$ (with $1\le i\le n$ and i ghost sections removed) weighted by their cyclic permutation factor and by the prefactor resulting from the *trace-log* expansion. This is the way in which the nontrivial pruning for the N-disk billiards can be derived from the exact quantum mechanical expressions in the semiclassical limit. Note that there must exist at least one index i in any given *periodic* itinerary which corresponds to a non-ghost section, since otherwise the itinerary in the semiclassical limit could only be straight and therefore nonperiodic. Furthermore, the series in the ghost cancelation has to stop at the 2nd-order trace, $\mathrm{tr}\,\mathbf{A}^2$, as $\mathrm{tr}\,\mathbf{A}$ itself vanishes identically in the full domain which is considered here.

⇓PRELIMINARY

39.4.2 Semiclassical cycle weigth

AW: One of us has still to write these

regroup the terms in prime orbits (or refer to DasBuch section

write semiclassical cumulant expansion

truncated expansions

diffractive poles in 1-scatterer S-matrices

⇑PRELIMINARY

restore section3-disk system

39.5 Heisenberg uncertainty

Where is the boundary $ka\approx 2^{m-1}\bar{L}/a$ coming from?

This boundary follows from a combination of the uncertainty principle with ray optics and the non-vanishing value for the topological entropy of the 3-disk repeller. When the wave number k is fixed, quantum mechanics can only resolve the classical repelling set up to the critical topological order $n$given by (**??**). The quantum wave packet which explores the repelling set has to disentangle 2^n different sections of size $d\sim a/2^n$ on the "visible" part of the disk surface (which is of order a) between any two successive disk collisions. Successive collisions are separated spatially by the mean flight length $\bar{L}$, and the flux spreads with a factor $\bar{L}/a$. In other words, the uncertainty principle bounds the maximal sensible truncation in the cycle expansion order by the highest quantum resolution attainable for a given wavenumber k.

⇓PRIVATE
⇑PRIVATE

⇓PRELIMINARY

The upper limit n for which $c_m(k)$ with $m\le n$ approximates $Q_m(k)$ is increasing with increasing $\mathrm{Re}\,k$. For $n>m(\mathrm{Re}\,ka)$, defined in (**??**), the

[1] Actually, these are double-letter symbols as σ_i and l_i are only counted as a product.

cycle expansion terms and cumulant terms deviate so much from each other, that beyond this order the contributions of longer cycle expansions have nothing to do with quantum mechanics. The fact that $Z_{\rm GV}(k)|_n$ – even in its convergence regime – is a good approximation to quantum mechanics *only* up to a finite n is usually not noticed, as the terms in (**??**) are exponentially small on or close to the real axis and sum therefore to a tiny quantity. In other words, for $n > m(\mathrm{Re}\, ka)$ and close to the real k axis, the absolute error $|c_n(k) - Q_n(k)|$ is still small, the relative error $|c_n(k)/Q_n(k)|$ on the other hand is tremendous. With increasing negative $\mathrm{Im}\, k$, however, using the scaling rules (**??**) and (**??**), the deviations (**??**) are blown up, such that the relative errors $|c_n(k)/Q_n(k)|$ eventually become visible as absolute errors $|c_n(k) - Q_n(k)|$ (see e.g. the resonance calculation of ref. [M.1]). For $\mathrm{Im}\, k$ above the boundary of convergence these errors still sum up to a finite quantity which might, however, not be negligible any longer. Below the convergence line these errors sum up to infinity.

So, the value of Imk where — for a given n — the $Z_{\rm GV}(k)|_n$ sum deviates from $\det \mathbf{M}(k)|_n$ is governed by the real part of k and the scaling rules (**??**) and (**??**). It has nothing to do with the boundary of convergence of $Z_{GV}(k)$, as a good approximation is given by the *finite* sum of terms satisfying (**??**). Therefore, the truncated semiclassical expansion can describe the quantum mechanical resonance data even *below* the line of convergence of the infinite cycle expansion series, as we have already noted above.

On the other hand, the boundary line of the convergence regime of the semiclassical expansion is governed by $c_m(k)$, $m \to \infty$, terms which have nothing to do with the quantum analog $Q_m(k)$, i.e. solely by terms of type (**??**). The reason is that the convergence property of an infinite sum is governed by the *infinite* tail and not by the first few terms. Whether a semiclassical expansion converges or not is a separate issue from the question whether the quantum mechanical data are described well or not. The *convergence property* of a semiclassical zeta functions on the one hand and the *approximate description of quantum mechanics* by these zeta functions are therefore two different issues. It could happen that a zeta function is convergent, but not equivalent to quantum mechanics, as we have seen was the case with the extraneous resonances in the quasiclassical calculation. Or that it is not convergent in general, but its finite truncations nevertheless approximate well quantum mechanics, as is the case for the Gutzwiller-Voros zeta function

connect this to earlier text

$$Z_{\rm GV}(z;k) = \exp\left\{-\sum_p \sum_{r=1}^{\infty} \frac{1}{r} \frac{z^{rn_p}\, t_p^r}{1 - 1/\Lambda_p^r}\right\} = \prod_p \prod_{j=0}^{\infty} \left(1 - \frac{z^{n_p} t_p}{\Lambda_p^j}\right) , \quad (39.37)$$

where

$$t_p = e^{ikL_p - im_p\pi/2}/|\Lambda_p|^{\frac{1}{2}}$$

is the weight of the $p^{\rm th}$ prime cycle, n_p its topological length and z a

book-keeping variable for keeping track of the topological order in cycle expansions.

We conclude that the exponential rise of the number of cycles with increasing cycle expansion order n is the physical reason for the breakdown of the cycle expansion of the semiclassical zeta function(39.37) with respect to the exact quantum mechanical cumulant expansion.

Airy function
Debye approximation
Hankel function

⇑PRELIMINARY

Commentary

Remark 39.1 Sources. This chapter is based in its entirety on ref. [M.1]; the reader is referred to the full exposition for the proofs and discussion of details omitted here. sect. 39.3 is based on appendix E of ref. [M.1]. We follow Franz [38.19] in applying the Watson contour method [38.20] to (39.23). The Airy and Debye approximations to the Hankel functions are given in ref. [38.21], the Airy expansion of the 1-disk zeros can be found in ref. [38.22], see also ref. [**?**] for the expression of $\alpha_\ell(ka)$ to leading order. For details see refs. [38.19, 38.22, 38.23, M.1]. That the interior domains of the disks are excluded relatively to the free evolution without scattering obstacles was noted in refs. [38.24, 38.15].

change refs from Wirzba habilitation to Phys Reports throughout?

⇓PRIVATE

⇑PRIVATE

comment on Regge poles

The procedure for the semiclassical approximation of a general periodic itinerary (39.20) of length n can be found in ref. [M.1] for the case of the N-disk systems. The reader interested in the details of the semiclassical reduction is advised to consult this reference. For the case of grazing geometrical paths consult ref. [**?**]. In such cases we have coninciding saddles between the geometrical paths with $\pi/2$ angle reflection from the disk surface and paths with direct ghost tunneling through the disk.

⇓PRIVATE

⇑PRIVATE

The ghost orbits were introduced in refs. [38.12, 38.24].

merge with preceeding chapter?

Remark 39.2 Krein-Friedel-Lloyd formula. In the literature (see, e.g., refs. [38.14, 38.15] based on ref. [38.11] or ref. [38.1]) the transition from the quantum mechanics to the semiclassics of scattering problems has been performed via the semiclassical limit of the left hand sides of the Krein-Friedel-Lloyd sum for the (integrated) spectral density [M.5, M.6, 38.8, 38.9]. See also ref. [38.13] for a modern discussion of the Krein-Friedel-Lloyd formula and refs. [38.1, 38.17] for the connection of (38.17) to the the Wigner time delay.

find refref pinball

The order of the two limits in (38.18) and (38.17) is essential, see e.g. Balian and Bloch [38.11] who stress that smoothed level densities should be inserted into the Friedel sums.

The necessity of the $+i\epsilon$ in the semiclassical calculation can be understood by purely phenomenological considerations: Without the $i\epsilon$ term there is no reason why one should be able to neglect spurious periodic orbits which solely are there because of the introduction of the confining boundary. The subtraction of the second (empty) reference system helps just in the removal of those spurious periodic orbits which never encounter the scattering region. The ones that do would still survive the first limit $b \to \infty$, if they were not damped out by the $+i\epsilon$ term.

38.1
page 723

Remark 39.3 $\mathbf{T}$, $\mathbf{C}^s$, $\mathbf{D}^s$ and $\mathbf{A}^{ss'}$ matrices are trace-class In refs. [M.1] it has

find ref ,wh97

explicitly been shown that the $\mathbf{T}$-matrix as well as the $\mathbf{C}^s$, $\mathbf{D}^s$ and $\mathbf{A}^{ss'}$-matrices of the scattering problem from $N < \infty$ non-overlapping finite disks are all trace-class. The corresponding properties for the single-disk systems is particulary easy to prove.

⇓PRELIMINARY

??

page ??

Résumé

⇑PRELIMINARY

AW: still to add some more interesting exercises

create refsMultiscat

⇓PRIVATE

Chapter 40

Quantum pinball

Semiclassical periodic orbit expansions are applied to the dynamics of a point particle scattering elastically off several disks in a plane. Fredholm determinants, zeta functions, and convergence of their cycle expansions are tested and applied to evaluation of quantum resonances. We demonstrate the utility of the periodic orbit description of chaotic motion by computing from a few periodic orbits highly accurate estimates of a large number of quantum resonances for the classically chaotic 3-disk scattering problem. The symmetry decompositions of the eigenspectra are the same for the classical and the quantum problem, and good agreement between the periodic orbit estimates and the exact quantum poles is observed. make a remark here

We shall here focus on an ideal quantum system, scattering off three (or more) disks in the plane. The system that we shall discuss here is simple, yet physical and instructive.

PREDRAG'S REMARK:
What was really done in the introductory lecture on billiards: The subject was develop to detect a cylinder by waves (ie submarine, by radar): Frantz, Keller, Maslov.

That 1 disk scattering resonances are known analytically; 2-disk not, but there is no chaos; 3-disk first example of chaos, known by semi-analytic methods only recently.

That repellers clean as purelly hyperbolic, trivial symbolic dynamics.

I explained that for elastodynamics Mark found a quartz fortune teller's ball from Madagascar, measured 500.000 resonaces, and theorists are happy to compute 100.

That there are almost no analytic solutions known (square, circle, parallelopiped, perhaps sphere in isotropic case).

That numerics can barely do anything else but a potato.

That hard ceramics gas valves and MEMS need new quality control

techniques, perhaps in frequency rather than time domain.
- END PREDRAG'S REMARK -

Our classical pinball system consists of a point particle and three identical circular disks in the plane (fig. 40.5.4a). The point particle is scattered elastically off the disks and moves freely between collisions. The dynamics with one or two disks is simple (there is either no or one trapped trajectory), but with three or more disks there are infinitely many trapped trajectories, forming a repeller. This repeller can be in principle observed by measurements such as irregularly fluctuating outgoing angles *vs.* impact parameter, but such measurements are difficult and very sensitive to small perturbations. Much more robust are the global averages such as the mean trapping time; resonances and the delay times.

We shall apply here the expansion (31.2) to evaluation of repeller escape rates. The classical repeller escape rate γ is determined by the largest zero of $1/\zeta(s)$ (s real) with each prime cycle weighted by

$$t_p(s) = \Lambda_p^{-1} e^{-sT_p}. \tag{40.1}$$

Here T_p is the period of the prime cycle p and $\mu_p = \ln(\Lambda_p)$ is its stability exponent, where Λ_p is the leading eigenvalue of the cycle Jacobian. The associated *quantum* amplitude is essentially the square root of the classical weight.

The logarithmic derivative of the infinite product of ζ functions $\det(\hat{H} - E)_{sc} = \prod_{j=0}^{\infty} \zeta_j^{-1}(k)$, where the weights of the prime cycles for the different ζ_j's are

$$t_p^{(j)} = e^{-\mu_p(1/2+j)+\frac{i}{\hbar}S_p(k)+i\pi\nu_p/2}, \tag{40.2}$$

where $S_p(k)$ is the action and ν_p the Maslov index, and k is the quantum wavenumber. The zeros of $\det(\hat{H} - E)_{sc}$ in the complex k plane determine the eigenvalues or resonances of the quantum system; here we shall compute only those closest to the real energy axis, which are given by the zeros of $1/\zeta_0(k)$.

We have chosen here the 3-disk scattering system because it captures the essential topology, stability and phase space structure of cycles in 2-d non-integrable potentials without the complications typical of motions in generic smooth potentials (pruning of the symbolic dynamics mixed phase space, intermittency effects due to marginally stable orbits. The billiard cycles are faster to compute than for arbitrary smooth potentials, and we point to remark were aided much by the availability of the exact spectra in checking our results.

40.1 Spectral determinant for two-dimensional systems

spectral!determinant@“fd!2-dimensional

For Hamiltonian flows in two configuration dimensions the monodromy matrix M_p has two eigenvalues Λ_p and $1/\Lambda_p$, as explained in sect. 5.2. Isolated periodic orbits can be elliptic or hyperbolic. Here we discuss only the hyperbolic case, when the eigenvalues are real and not equal to one in magnitude. The determinant appearing in the trace formulas can be written in terms of the expanding eigenvalue as

$$|\det\left(1-M_p^r\right)|^{1/2} = |\Lambda_p^r|^{1/2}\left(1-1/\Lambda_p^r\right)\ ,$$

and its inverse can be expanded as a geometric series

$$\frac{1}{|\det\left(1-M_p^r\right)|^{1/2}} = \sum_{k=0}^{\infty}\frac{1}{|\Lambda_p^r|^{1/2}\Lambda_p^{kr}}.$$

restore links and exercises

With the 2-dimensional expression for the average density of states (36.9) the spectral determinant becomes

$$\begin{aligned}\det\left(\hat{H}-E\right)_{sc} &= e^{i\frac{mAE}{2\hbar^2}}\exp\left(-\sum_p\sum_{r=1}^{\infty}\sum_{k=0}^{\infty}\frac{e^{ir(S_p/\hbar-m_p\pi/2)}}{r|\Lambda_p^r|^{1/2}\Lambda_p^{kr}}\right)\\ &= e^{i\frac{mAE}{2\hbar^2}}\prod_p\prod_{k=0}^{\infty}\left(1-\frac{e^{\frac{i}{\hbar}S_p-\frac{i\pi}{2}m_p}}{|\Lambda_p|^{1/2}\Lambda_p^k}\right)\ . \qquad (40.3)\end{aligned}$$

⇓PRELIMINARY

40.2 Semiclassical zeta function

add a section on the $k=0$ zeta function part

40.3 Three-disk pinball

⇑PRELIMINARY

Here we shall illustrate the convergence of curvature expansions by computing the classical escape rates and quantum resonances for scattering off three disks. In this system the classical motion can be visualized as a pinball bouncing in a plane between three equally spaced disks of equal radius, and the quantum dynamics is described by wave functions which vanish on the boundaries of the disks. For billiard motion the momentum $vm = \hbar k = \sqrt{2E/m}$ is constant, the action $S_p(k)$ is given by $\hbar k L_p$, where L_p is the length of the cycle p, and the quantum amplitude (40.2) associated with the cycle p is simply $t_p = |\Lambda_p|^{-1/2}e^{ikL_p+in_p\pi}$. Here n_p is the number of bounces, and comes from the phase loss at every reflection (the boundary condition is $\psi|_{disk}=0$).

point to remark

replace by back reference

The prerequisite for efficient use of curvature expansions is firm control of the symbolic dynamics. For sufficiently separated disks, the symbolic

refer to earlier text, rather than to refs. [40.2, 6.3]

dynamics is a ternary dynamics with alphabet $\{1,2,3\}$ (the label of the disk the pinball bounces off) and a single pruning rule prohibiting consecutive repeats of the same symbol. The corresponding curvature expansion (31.2) is straightforward, and converges well. The C_{3v} point group invariance of the 3-disks problem simplifies and improves the curvature expansions in a rather beautiful way. The corresponding contributions to the Euler product (31.2) factorize as follows:

$$\begin{aligned}(1-t_p)^2 &= (1-t_p^{1/3})(1-t_p^{1/3})(1+t_p^{1/3}+t_p^{2/3})^2\\ (1-t_p)^3 &= (1-t_p^{1/2})(1+t_p^{1/2})(1-(t_p^{1/2})^2)^2\\ (1-t_p)^6 &= (1-t_p)(1-t_p)(1-t_p)^4. \end{aligned} \tag{40.4}$$

The three factors in this product contribute to the C_{3v} irreducible subclasses A_1, A_2 and E, respectively, and the 3-disk zeta function factorizes into $\zeta = \zeta_+\zeta_-\zeta_E^2$. Due to the symmetry, any 3-disk cycle can be pieced together from segments passing through the *fundamental domain* (see Fig. ?1?). The $t_p^{1/2}$, $t_p^{1/3}$ weights in (40.4) have direct physical meaning: they are the weights of the corresponding cycles restricted to the fundamental domain.

Restriction to the fundamental domain also simplifies the symbolic dynamics: it becomes binary, with no restrictions on allowed sequences [6.1, 40.31, 6.3]. The ternary 3-disk $\{1,2,3\}$ labels are converted into the binary fundamental domain labels $\{0,1\}$ by marking the backscatter by 0 and scatter to the third disk by 1. For ex., $\overline{23} = \ldots 232323\ldots$ maps into $\ldots 000\ldots = \overline{0}$ (and so do $\overline{12}$, $\overline{13}$), $\overline{123} = \ldots 12312\ldots$ maps into $\ldots 111\ldots = \overline{1}$, and so forth. (see Fig. ?1?).

The Euler product (31.2) on each irreducible subspace is easily evaluated using the factorization (40.4). On the symmetric A_1 and the antisymmetric A_2 subspaces, the ζ_+ and ζ_- are given by the standard curvature expansion for the binary dynamics:

$$\begin{aligned}1/\zeta_\mp &= (1\pm t_0)(1-t_1)(1\pm t_{10})(1-t_{100})(1\pm t_{101})(1\pm t_{1000})\ldots\\ &= 1\pm t_0 - t_1 \pm (t_{10}-t_1t_0) - (t_{100}-t_{10}t_0) \pm (t_{101}-t_{10}t_1)\\ &\quad -(t_{1001}-t_1t_{001}-t_{101}t_0+t_{10}t_0t_1) - \ldots\ldots \end{aligned} \tag{40.5}$$

while for the mixed-symmetry subspace E the curvature expansion is given by

$$\begin{aligned}1/\zeta_E &= (1+t_1+t_1^2)(1-t_0^2)(1+t_{100}+t_{100}^2)(1-t_{10}^2)\ldots\\ &= 1+t_1+(t_1^2-t_0^2)+(t_{100}-t_1t_0^2)+t_{1001}+(t_{100}-t_1t_0^2)t_1-t_{10}^2. \end{aligned} \tag{40.6}$$

Given the curvature expansions (40.5) and (40.6), the calculation is straightforward. We set the disk radius $a = 1$, fix the disk-disk center separation $R = 6$ (for the sample values listed here), compute the eigenvalues

and lengths of prime cycles up to 5 bounces (total of 14 cycles), substitute them into the curvature expansions, and determine the complex zeros; some hundred quantum resonances are easily determined, with accuracy as good as 7 significant digits for the resonances closest to the real axis. In Table ?1? we list a few typical results, illustrate their convergence by computing them with different maximal length cycles, and compare them to the numerical solutions for poles of the exact quantum scattering matrix. The convergence of the curvature expansions is striking; they are many orders of magnitude more accurate than the estimates by other methods, and the gain in efficiency is dramatic: while the quantum scattering matrix requires computation of large truncations (of order of (70×70)) of infinite matrices with Bessel functions entries, the curvature expansions require evaluation of some dozen complex exponentials and a couple of sums and differences. The judicious use of symmetry helps considerably; for example, going to the fundamental domain often *doubles* the number of significant digits for a given cycle length. The estimates can be further improved by extrapolations and knowledge of the analyticity properties of $1/\zeta$, e.g. the positions of poles.

No poles of the infinite product can occur within the half-plane of absolute convergence [40.16]. This also leads to an upper bound on the resonance lifetimes. The abscissa of absolute convergence can be determined as the leading zero of (40.5) with t_p replaced by $|t_p|$; $\mathrm{Im}(k)$ for all zeros of $1/\zeta$ must lie below k_c (for the present a:R=1:6 example, $k_c = -0.121557\ldots$). The convergence of the curvature expansion is best near k_c (the longest lived resonances) and deteriorates as one moves further in the imaginary k direction. As Re k grows, the density of resonances increases. Implications for the curvature expansion are that a certain number of terms have to be included before two resonances are distinguished; thereafter one again observes rapid convergence. This is illustrated in table ?1? for the resonances k_2 and k_3, which have the same n=1 approximation.

The explicit curvature expansions like (40.5) and (40.6) perhaps make it easier to explain our claims about the exponential convergence of curvature expansions. A typical curvature expansion term involves a long cycle $\{ab\}$ insert tosect{} here minus its shadowing approximation by shorter cycles $\{a\}$ and $\{b\}$:

$$t_{ab} - t_a t_b = t_{ab}(1 - t_a t_b/t_{ab}) = t_{ab}(1 - e^{-\Delta\mu_{ab}/2 + ik\Delta S_{ab}})$$

where $\Delta\mu_{ab} = \mu_a + \mu_b - \mu_{ab}$ and $\Delta S_{ab} = S_a + S_b - S_{ab}$. The exponential fall off of curvatures is a consequence of the smallness of the term in the brackets; $\Delta\mu$ and ΔS are exponentially small for long orbits, typically $O(e^{-\mu_{ab}})$. Therefore, to resolve some scale Δk, one has to keep all *difference* actions $> 1/\Delta k$. Their number increases like $(\Delta k)^{h/\lambda}$, i.e., roughly linearly (if the topological entropy h equals the average Lyapunov exponent λ), and not exponentially, as one might expect naively.

Figure caption

replace by link to exiting figure

1. The scattering geometry for the disk radius/separation ratio $a : R = 1 : 2.5$. (a) the three disks, with $\overline{12}$, $\overline{123}$ and $\overline{121232313}$ cycles indicated.

Table caption: Representative classical escape rate and quantum resonance results, illustrating the convergence of the curvature expansions. The calculations listed here are for disks with ratio radius to separation $a : R = 1 : 6$. The first column gives the maximal cycle length used, the second the estimate of the classical escape rate from the full 3-disk cycle expansion, the third from the fundamental domain expansion. For comparison, numerical simulation [6.2] yields $\gamma = .410\ldots$, and the $n = 2, 3$ approximations of ref. [6.2]. yield 0.3102, 0.4508 respectively. The remaining columns illustrate convergence of "typical" quantum resonances from the A_1 subspace. For comparison, the exact quantum values [6.2, 40.19] are given in the last row; the $n = 3$ approximation of ref. [6.2] gives $k_1 = 8.354 - i0.342$.

	quantum pole					
n	$\mathrm{Re}(k_1)$	$\mathrm{Im}(k_1)$	$\mathrm{Re}(k_2)$	$\mathrm{Im}(k_2)$	$\mathrm{Re}(k_3)$	$\mathrm{Im}(k_3)$
1	8.35954	−0.32103	27.36117	−0.15486	27.36117	−0.15486
2	8.26784	−0.28354	27.25948	−0.16044	27.68086	−0.36148
3	8.27549	−0.27576	27.25883	−0.15587	27.67331	−0.33837
4	8.27662	−0.27696	27.25922	−0.15561	27.67015	−0.33556
5	8.27640	−0.27712	27.25925	−0.15562	27.66956	−0.33531
exact	8.2611	-0.2749	27.2548	-0.1555	27.6661	-0.3340

40.4 Classical pinball

40.4.1 Symmetries of the system

We have already discussed the symmetries of the 3-disk pinball and its periodic orbits in sect. 22.1.1.

☞ sect. 22.1.1

40.4.2 Symbolic coding

We have already discussed the symbolic dynamics of the 3-disk pinball and its periodic orbits in sect. 1.4 and example 11.2.

☞ sect. 1.4
☞ example 11.2

40.4.3 Periodic orbits

There is only one length scale in the system, the ratio of the center-to-center separation to the disk radius $d : R$. The energy is a quadratic function of momenta, $H = p^2/2m$, so motion at different energies E and E_0 is related by the scaling $p_E \to p_0\sqrt{E/E_0}$ for momenta, $t_E \to t_0\sqrt{E_0/E}$ for times, and

$$S(E) = L\sqrt{2mE} = S(E_0)\sqrt{E/E_0} \tag{40.7}$$

for the actions, where L is the geometrical length of the orbit. The eigenvalues of the Jacobian transverse to a periodic orbit (see below) are invariant under the above energy rescaling. These observations will be useful below in the semiclassical context where the (34.15) will combine with $\hbar$ to the relevant quantum variable, the wavenumber $k = \sqrt{2mE}/\hbar$.

Each map has a fixed point, corresponding to the orbits $\overline{0}$ and $\overline{1}$. Longer periodic orbits are fixed points of sequences of maps, e.g.

$$T_0T_0T_1T_0T_1x_{10100} = x_{10100}\,, \tag{40.8}$$

check if incorporated?: (note that in our convention the maps are applied in reverse order compared to the symbolic sequence).

link

add pointer

The Jacobian of the single collision map is given by The sign of the eigenvalue depends of the number of collisions along the cycle. For the '0' symbol there are two bounces in the fundamental domain: one with the disk and one with the reflecting wall. Since the wall can be regarded as a disk of infinite radius, the trace changes sign two times and thus the eigenvalues are positive. Symbol '1' corresponds to one bounce with the disk but two wall bounces and hence the eigenvalues of the '1'-cycle are negative. For an arbitrary fundamental domain cycle, the eigenvalue sign is given by $(-1)^{n_1}$, where n_1 is the number of '1's in the binary string corresponding to the cycle.

8.1 page 129

The exact lengths and eigenvalues of $\overline{0}$, $\overline{1}$ and $\overline{10}$ cycles follow from elementary geometrical considerations, and are left to the reader as exercises. Longer cycles require numerical evaluation by methods such as the multipoint shooting or orbit length minimization. A typical set of the periodic orbit data, for $d : R = 6$ and length ≤ 6, is listed in table ?2?.

8.2 page 129

add pointers

40.5 Quantum pinball

For the three disk system, the explicit expressions of the outgoing waves in terms of the ingoing waves using the quantum scattering matrix S have been given by Gaspard and Rice. Resonances are related to complex zeros of $\mathrm{tr}\, S^\dagger \frac{dS}{dE}$, the generalization of the concept of the density of states to scattering systems. We shall first evaluate these complex zeros in the semiclassical approximation, and then compare them with the exact quantum-mechanical resonances.

40.5.1 The semiclassical density of states

The group theoretic weights associated with reducing the dynamics to irreducible representations of the discrete symmetry group can sometimes also be absorbed into the phase indices. In the A_1 representation, one has only reflections at the disks, none at the boundaries of the fundamental domain. Therefore, $\mu_p = 2n_p$, since the symbol string length counts the number of the disk collisions. For the A_2 representation, the wave function

is antisymmetric under reflections at the symmetry lines, and one can associate one additional reflection with each occurence of the symbol 0, and two reflections with each occurence of the symbol 1. The net effect is an additional overall minus sign, if the number of 0's in the symbol string of the orbit is odd. Furthermore, special attention should be paid to the orbits that run along the borders of the fundamental domain. The 3-disk system studied here does not have boundary orbits, but the 4-disk system, for example, does have such orbits.

link section

As mentioned above one can replace $S_p(E)/\hbar = L_p k$, where L_p is the geometric length of the orbit, and k is the wavenumber.

$$\rho(k) = -\mathrm{Im}\frac{1}{\pi}\frac{\partial}{\partial k}\log Z(k) \tag{40.9}$$

where $Z(k)$ is

$$Z(k) = \prod_{j=0}^{\infty}\prod_{p}(1 - e^{iL_p k - i\mu_p\pi/2}|\Lambda_p|^{-1/2}\Lambda_p^{-j})\,. \tag{40.10}$$

The quantum Selberg zeta function can also be expressed as a product over dynamical zeta functions,

$$Z(k) = \prod_{j=0}^{\infty} 1/\zeta_j\,, \tag{40.11}$$

this time with cycles weighted by semiclassical weights

$$t_p = z^{n_p} e^{iS_p/\hbar - i\mu_p\pi/2}/|\Lambda_p|^{1/2}\ . \tag{40.12}$$

Thousands of semiclassical and exact quantum resonances in the three symmetry subspaces A_1, A_2 and E have been computed; some of them are listed in table ?4? and plotted in fig. 40.5.4. The accuracy and numerical convergence of the semiclassical estimates cames as a surprise.

40.5.2 "Quantum escape rate"

The region of absolute convergence of the Gutzwiller trace formula in the $k = \kappa - is$ complex plane is determined by the convergence of the sum of absolute values of the terms in the series (**??**). The sum converges absolutely for $s < s_c$, where s_c is called the abscissa of absolute convergence. Since s_c is the value of s for which the sum

$$\tilde{\Omega}(s) = \sum_p \frac{T_p}{|\det(\mathbf{1} - \mathbf{J}_p)|^{1/2}} e^{sT_p}\,, \tag{40.13}$$

diverges, one can, by analogy to the determination of the classical escape rate by the divergence of the sum , interpret the abscissa of absolute convergence s_c as a "quantum escape rate". In fact, s_c is only a lower bound on the escape rate; the correct rate of a decay of a given initial wave function is given by a superposition of complex resonances evaluated below. Within the same short cycles truncations as in the classical case, one finds the s_c curves shown in the lower half of fig. 40.5.4.

ref

upper?

recheck?

Since the trace formulas are convergent in the domain of absolute convergence, one cannot have zeros of the zeta function or resonances of the S-matrix in that domain. In particular, for sufficiently large $d:R$, all resonances will stay a finite distance from the real axis. In contrast to the classical case, for $d:R$ less than about 2.8 the bound s_c actually becomes negative. As we shall see below, the semiclassical resonances do lie below the real axis, as they should; but this serves as a reminder that the resonances (and the energy eigenvalues for bound systems) are being evaluated in a region where cycle expansions are only conditionally convergent, and one has to be very careful in ordering terms in such expansions.

The same absolute convergence arguments can be applied to the dynamical zeta functions. Their logarithmic derivatives correspond to sums over orbits of form

$$-\frac{\partial}{\partial k}\ln\zeta_j = i\sum_p L_p \frac{e^{iL_pk-i\mu_p\pi/2}}{|\Lambda_p|^{1/2}\Lambda_p^j}\,. \tag{40.14}$$

Due to the extra powers of Λ_p's present in $1/\zeta_j$ cycle weigths, the corresponding abscissas of absolute convergence form an ordered sequence $s_j < s_{j-1} < \cdots < s_0$. The resonances closest to the real axis - which will be noticable as the sharpest resonances - should be due to zeros in $1/\zeta_0$ since the leading zeros of other $1/\zeta_j$ have larger imaginary parts. We find it often convenient to use this fact and restrict our numerical work to the leading zeros of $1/\zeta_0$ rather than the full Selberg zeta functions.

40.5.3 Quantum resonances

> If the same -Vedic mantra- is chanted loudly ("Vedaghosa") it will give divine joy to the listeners even if they do not understand its meaning. Such a sound has the power to make mankind happy.
> Guru Pujyasri Chandrasekharendra Sarasvati Svami, *"Hindu Dharma: The Universal Way of Life"*

We evaluate the exact quantum mechanical resonances by the method described in refsect{??}. A comparison of resonances obtained from cycle expansions truncated to the 14 cycles of periods ≤ 5 with the exact quantum values is given in table 5?. and in fig. 40.5.4, together with the difference between the semiclassical and quantum resonances $\delta = \sqrt{|k_{QM}-k_{sc}|}$.

Numerically this difference seems to decrease with increasing Re k, i.e., with approach to the semiclassical limit. As the semiclassical approximation ignores terms of higher order in $\hbar$, one expects on general grounds this difference to approach a non-zero constant. Our data are insufficient to estimate the asymptotic behaviour and to bound it away from zero.

Also shown in fig. 40.5.4 is the abscissa of absolute convergence s_c. No semiclassical resonance lies above it. Two of the lowest exact quantum resonances, for which the semiclassical approximation error is largest, do lie above s_c, but that is acceptable as the bound is semiclassical.

40.5.4 Poles of dynamical zeta functions

The exponential decay of the coefficients for $1/\zeta_0$ indicates the presence of a pole.

The double pole is not as surprising as it might seem at the first glance; indeed, the theorem that establishes that the classical Fredholm determinant (**??**) is entire implies that the poles in $1/\zeta_j$ must have right multiplicities in order that they be cancelled in the $F = \prod 1/\zeta_j$ product. More explicitely, $1/\zeta_j$ can be expressed in terms of weighted Fredholm determinants

$$F_j = \exp\left(-\sum_p \sum_{r=1}^{\infty} \frac{1}{r} \frac{(t_p/\Lambda_p^j)^r}{(1-1/\Lambda_p^r)^2}\right) \tag{40.15}$$

by inserting the identity

$$1 = \frac{1}{(1-1/\Lambda)^2} - \frac{2}{\Lambda}\frac{1}{(1-1/\Lambda)^2} + \frac{1}{\Lambda^2}\frac{1}{(1-1/\Lambda)^2}$$

into the exponential representation of $1/\zeta_j$. This yields

$$1/\zeta_j = \frac{F_j F_{j+2}}{F_{j+1}^2}\ , \tag{40.16}$$

and we conclude that for 2-dimensional Hamiltonian flows the dynamical zeta function $1/\zeta_j$ has a *double* leading pole coinciding with the leading zero of the F_{j+1} Fredholm determinant.

The effect of such convergence properties of the coefficients on the calculation of classical and quantum escape rates is demonstrated in table 5? and figure 40.5.4.

	n	. Z_{qm}	. $1/\zeta_0$
$d: R = 6$	1	0.11	0.119
	2	0.12153	0.12152
	3	0.1215574	0.121556
	4	0.121557625	0.12155760
	5	0.1215576283	0.121557627
	6	0.1215576284	0.1215576284
	7	0.1215576284	0.1215576284
$d: R = 3$	1	-0.076	0.019
	2	0.041	0.038
	3	0.04052	0.0403
	4	0.040575	0.04054
	5	0.0405789	0.040575
	6	0.04057935	0.040578
	7	0.040579405	0.0405793
	8	0.0405794102	0.04057940
	9	0.0405794108	0.0405794099
	10	0.0405794108	0.0405794107

Table 4?. Quantum escape rates computed from the Fredholm determinant F_{cl} (??), the quantum Selberg zeta function Z_{qm} (40.10), and the dynamical zeta function $1/\zeta_0$, as function of the maximal cycle length. Due to the presence of the same pole in both quantum zeta functions, the convergence of the quantum Selberg zeta function is not significantly better than the convergence of the dynamical zeta function. See also fig. 40.5.4.

The scattering geometry for the disk radius : separation ratio $R:d=1:2.5$. (a) the three disks, with $\overline{12}$, $\overline{123}$ and $\overline{121232313}$ cycles indicated. (PC: REFRE BACK TO THE FIGURE)

Some examples of 3-disk cycles: (a) $\overline{12123}$ and $\overline{13132}$ are mapped into each other by σ_{23}, the flip across 1 axis; this cycle has degeneracy 6 under C_{3v} symmetries. (PC: REFER BACK TO THE FIGURE)

	Re k_{QM}	Im k_{QM}	Re k_{zeta}	Im k_{zeta}
	0.69800	-0.07497	0.75831	-0.12282
	2.23960	-0.11880	2.27427	-0.13305
	3.76270	-0.14756	3.78787	-0.15412
	4.13165	-0.61702	4.15179	-0.66591
	5.27569	-0.18325	5.29607	-0.18678
	6.77609	-0.22750	6.79366	-0.22986
	8.26114	-0.27492	8.27663	-0.27698
	9.73452	-0.13880	9.74826	-0.32121
	10.33819	-0.37371	10.34656	-0.37834
	11.20210	-0.35823	11.21361	-0.36168
A_1	11.90760	-0.33223	11.91448	-0.33488
	12.66760	-0.39467	12.67500	-0.39841
	13.47692	-0.29412	13.48266	-0.29623
	14.13370	-0.42883	14.13680	-0.42956
	15.04170	-0.25552	15.04705	-0.25762
	16.59706	-0.21700	16.60244	-0.21889
	18.14115	-0.18280	18.14647	-0.18426
	19.67567	-0.15653	19.68084	-0.15761
	21.20308	-0.13958	21.20807	-0.14032
	22.72484	-0.13187	22.72966	-0.13235
	24.24120	-0.13284	24.24588	-0.13311
	25.75156	-0.14130	25.75605	-0.14153
	7.93363	-0.15129	7.94561	-0.15526
	9.45604	-0.13196	9.46661	-0.13458
	10.97616	-0.12325	10.98563	-0.12504
	12.49347	-0.12432	12.50215	-0.12550
	14.00693	-0.13468	14.01501	-0.13534
	15.51469	-0.15329	15.52229	-0.15368
A_2	17.01453	-0.17810	17.02178	-0.17836
	18.50574	-0.20544	18.51273	-0.20573
	19.99011	-0.23236	19.99681	-0.23275
	20.54565	-0.31325	20.54989	-0.31495
	21.46993	-0.25775	21.47596	-0.25817
	22.10098	-0.28557	22.95261	-0.28199
	22.94703	-0.28164	23.66203	-0.26365
	18.85038	-0.17271	18.56037	-0.17350
	19.44833	-0.25471	19.45385	-0.25454
E	20.37203	-0.17461	20.37745	-0.17502
	20.94214	-0.28849	20.94718	-0.28767
	21.88904	-0.19045	21.89438	-0.19059

turn this into a solution to a problem

Table 5. Several subsets of semiclassical and quantum resonances for $d:R=6$. The A_1 subspace resonances are plotted in Fig. 40.5.4.

Classical escape rates and bounds on quantum escape rates, *ie.* the zeros of the zeta functions (**??**) and (40.10) with absolute weights (40.13), as function of the disk-disk separation. The top two curves show the classical escape rate. Zeros computed from fixed points alone are shown as dotted lines, zeros from fixed points and period two orbits as full lines, and the Monte Carlo estimates of classical escape rates are marked by diamonds. The classical escape rate should approach 0 as $R:d \to 0.5$; in this limit cycle expansions are expected to converge poorly due to pruning and intermittency effects. The two lower curves show s_c, the abscissa of absolute convergence of the Gutzwiller trace formula, which serves as a crude lower bound on the imaginary part of the semiclassical quantum resonances. Though this bound becomes negative near $R:d \approx 0.33$, the semiclassical resonances do remain below the real energy axis, see fig. 40.5.4.

Semiclassical scattering resonances (diamonds) compared with the exact quantum scattering resonances (crosses). The lines in the upper half of the diagram indicate the (geometrical) difference between the semiclassical and quantum resonances for all resonances with $\mathrm{Im}\, k > -0.4$, magnified by a factor 10. The dotted line at $k_c = -0.121556$ indicates the semiclassical abscissa of convergence; all semiclassical resonances lie below this line, but the first two quantum resonances lie above it. For the semiclassical calculation, all orbits up to symbolic length 5 have been used in the cycle expansion for ζ_0^{-1}.

Energy dependence of the cycle expansion coefficients for $d:R=6$. Shown are (from top to bottom) the absolute values of the coefficients C_4, C_6, C_8, C_{10} and C_{12} (barely visible in the lower right corner) as a function of the wavenumber k.

The coefficients of the cycle expansion for the quantum Selberg zeta function $Z_{qm}(z)$ (connected with lines) and for $1/\zeta_0$ (not connected) for ratios $d:R=6$ (diamonds), 3 (squares) and 2.5 (triangles). Note that the asymptotic slope for the quantum Selberg zeta functions and the dynamical zeta functions is the same; the double pole present in the dynamical zeta function persists as a single pole in the Selberg product.

The coefficients of the cycle expansion for the quantum Selberg zeta function $Z_{qm}(z)$ after multiplication with $(1-z/z_1)$ where z_1 is the zero of $\zeta_1^{-1}(z)$. The coefficients still decay only exponentially but with much steeper slope, indicating the presence of yet another pole.

Convergence of zeros of zeta functions towards the asymptotic values as more and more orbits are included. Shown are the convergence of the classical Fredholm determinant escape rate estimates, the quantum Selberg zeta function lowest resonance estimates, and the quantum $1/\zeta_0$ lowest resonance estimates for ratios $d:R=6$ and $d:R=3$. The zero obtained for $n=14$ has been taken as the asymptotic value. Note the faster than exponential convergence for the classical Fredholm determinant, and the exponential approach for the quantum zeta functions.

inte remark: refs. [6.3, 18.11, 6.2, 6.4]

40.5.5 3-disk numerical resonances

We start by performing our numerical tests on the 3-disk repeller. The 3-disk repeller is the simplest physical realization of an Axiom A system, particularly convenient for numerical investigations. The methods that we use to extract periodic orbits, their periods and their stability eigenvalues are described in chapter 17. For billiards the cycle weight t_p required for evaluation of the classical escape rates and correlation spectra is given by (**??**). The action S_p is proportional to the cycle period T_p, and the Maslov index changes by $+2$ for each disk bounce, $m_p = 2n_p$, so the quantum weight (40.12) is given by

$$t_p = (-1)^{n_p} \frac{e^{-ikT_p}}{\sqrt{|\Lambda_p|}} z^{n_p} , \tag{40.17}$$

where $k = (\text{momentum})/2\pi$ is the wavenumber, and we take velocity $= 1$, mass $= 1$.

Cycle expansion (**??**) coefficients $|C_n|$ for different determinants and zeta functions are plotted in figs. 40.1 and 40.2 as function of the topological cycle length n. Zeta functions exhibit exponential falloff, implying a pole in the complex plane, while both the classical and the semiclassical spectral determinants appear to exhibit a faster than exponential falloff, with no indication of a finite radius of convergence within the numerical validity of our cycle expansion truncations.

In particular, the semiclassical spectral determinant enables us to uncover a larger part of the quantum resonances than what was hitherto accessible by means of the dynamical zeta functions. The eye is conveniently guided to the zeros by means of complex s plane contour plots, with different intervals of the absolute value of the function under investigation assigned different colors; zeros emerge as centers of elliptic neighborhoods of rapidly changing colors. Detailed scans of the whole area of the complex s plane under investigation and searches for the zeros of classical and semiclassical spectral determinants, fig. 40.3, reveal complicated patterns of resonances, with the classical and the semiclassical resonance patterns surprisingly similar. It is known [6.3] that the leading semiclassical resonances are very accurate approximations to the exact quantum resonances; the semiclassical resonances further down in the s complex plane in fig. 40.3 have not yet been compared with the exact quantum values. It would be of interest to check whether also all semiclassical spectral determinant resonances correspond to the true quantum resonances.

incorporate my notes

An interpretation of the resonance spectrum of the semiclassical spectral determinant is given in ref. [6.4], where the resonances are related to the oscillations in $N(t)$, the number of particles that have not escaped by the time t, with the basic frequency $\overline{\omega} = 2\pi/\overline{T}$ given by the inverse of $\overline{T}$, the mean flight time between the disks. $\overline{\omega}$ yields the mean spacing of the resonances along the imaginary k axis. In the 3-disk system there are two

fundamental frequencies, ω_0 and ω_1, determined by the inverse periods of the two fundamental cycles $\overline{0}$ and $\overline{1}$. Corresponding beat frequency [11.17] $f = 2\pi/(T_1 - T_0)$ is clearly visible in fig. 40.3. A rough measurement of the period of the beats in fig. 40.3 yields some 23.7 units along the real k axis, to be compared to $2\pi/(T_1 - T_0) = 23.4$.

defer this to diffraction

Effect of sub-dominant resonances on the measurable spectra are exponentially small, and presumably of little physical interest. We investigate them in detail here mostly in order to demonstrate that our determinants indeed exhibit better convergence than the semiclassical zeta function.

Contour plots are also helpful in comparing the domain of convergence of the spectral determinant to that of the semiclassical zeta function. As can be seen from fig. 40.4, the semiclassical spectral determinant can be continued considerably farther down in the complex k plane, in contrast to the dynamical zeta function scans. While the zeta functions clearly exhibit a finite radius of convergence, in agreement with the arguments of sect. ??, both the semiclassical spectral determinant and the semiclassical spectral determinant behave as entire functions. We compute the abscissa of absolute convergence for the semiclassical zeta function by means of (**??**); for the case at hand we obtain the leading zero at $k_{ac} = 0.0 - i\,0.699110157151\ldots$. Indeed, comparison of the contour plots of fig. 40.4 shows that no feature of the semiclassical zeta function countor plot below k_c is significant. Interestingly enough, the apparent border of semiclassical zeta function convergence in fig. 40.4 seems to coincide with $\mathrm{Re}(s) = 0$, $\mathrm{Im}(s) = -1.09653395\ldots$, the zero obtained from $F_{1/2}(k)$ by removing quantum phases, $t_p \to |t_p|$, but keeping the eigenvalue Λ_p sign. in eq. (**??**).

As discussed above, for 1-d systems the pole of ζ_0^{-1} coincides with the leading zero of ζ_1^{-1}, and the resulting product remains finite and has a zero close to the leading ζ_1^{-1} zero. In simple examples, such as the symmetric 1-dimensional tent map repeller, the non-leading / leading zeros of the classical F_0 / F_1 maps are identical. This suggests that some of the *non-leading* zeros of F are shadows of the ζ_1^{-1} zeros and hence likely to lie close to the *leading* zeros of F_1. For example, the non-leading resonance $k = 0.9915231008 + i\,12.5163342128$ of the semiclassical spectral determinant (see fig. 40.3), while distinct from the leading resonance of F_1 at $k = 0.99197582677 + i\,12.5029206443798$, belongs to a family of resonances that all lie very close to the leading F_1 resonances. We are confident that such resonances are distinct, as their cycle expansions converge super-exponentially to all digits listed above, in agreement with the general theory.

The F spectrum that is not echoed by the F_1 spectrum can be isolated by "subtracting" the F_1 spectrum, *ie.* removing those resonances from the F spectrum that lie closer than some ϵ to a F_1 resonance. The resulting spectrum is depicted in fig. **??**.

What is particularly interesting about this spectrum is that with the resonances associated with the F_1 spectrum removed, families that connect non-leading resonances at $\mathrm{Re}(k) = 0$ with the leading part of the resonance

spectrum for larger $\mathrm{Re}(k)$ are clearly visible in fig. **??**. This makes it rather clear that the evaluation of leading resonances for large $\mathrm{Re}(k)$ requires inclusion of longer cycles, the same that are required to control the spectrum for large negative $\mathrm{Im}(k)$ at $\mathrm{Re}(k) = 0$. This is the conundrum of semiclassical cycle expansions; while semiclassical intuition implies that the semiclassical zeta function should be applicable for large $\mathrm{Re}(k)$, in practice the semiclassical cycle expansions work best for the bottom of the spectrum.

In conclusion, we have tested numerically the semiclassical spectral determinant.

Note: Vattay *et al.* have succeeded in constructing a multiplicative evolution operator for semiclassical quantum mechanics, whose Fredholm determinant is

$$F(\beta, E) \;=\; \exp\left(-\sum_{p,r}\frac{1}{r}\frac{|\Lambda_p|^{-r\beta}e^{i(S_p(k)/\hbar+\nu_p\pi/2)r}}{(1-1/\Lambda_p^r)^2(1-1/\Lambda_p^{2r})}\right). \tag{40.18}$$

This determinant is entire for the Axiom A flows. In particular, the semiclassical spectral determinant can now be written as a ratio of two Vattay determinants

$$F_{qm}(k) = \frac{F(\frac{1}{2},k)}{F(\frac{5}{2},k)}.$$

As explained in sect. **??**, the abscissa of convergence for such ratio is given by the upper bound on the leading zeros of $F(\frac{5}{2},k)$. For example, for the 3-disk, $R:a=6:1$ system we find

$$\mathrm{Im}(k_{ac}) = -1.276625955\ldots$$

so the semiclassical spectral determinant can be continued almost a factor 2 down in the complex k plane beyond the region of applicability of the semiclassical zeta function. This explains why for all practical purposes the semiclassical spectral determinants behave as entire functions: only careful numerics reveals the difference between the semiclassical spectral determinant and the Vattay determinant in higher order terms in cycle expansions. The difference is illustrated by fig. 40.5; the suspicious straight section visible in the semiclassical spectral determinant ($\triangle$) in fig. 40.2 turns out to indeed indicate a pole, while the Vattay determinant converges super-exponentially.

Figure 40.1: $\log_{10}|C_n|$, the contribution of cycles of topological length n to the cycle expansion $\sum C_n z^n$ for 3-disk repeller. Shown are: ($\circ$) $1/\zeta_0$, (∇) the semiclassical zeta function, ($\Box$) $1/\zeta_0\zeta_1^2$, and ($\triangle$) the semiclassical spectral determinant. Exponential falloff implies that $1/\zeta_0$ and the semiclassical zeta function have the same leading pole, cancelled in the $1/\zeta_0\zeta_1^2$ product. For comparison, ($\Diamond$) the semiclassical spectral determinant coefficients are plotted as well; cycle expansions for both spectral determinants appear to follow the asymptotic estimate $C_n \approx \Lambda^{-n^{3/2}}$. A_1 symmetric subspace, with center spacing - disk radius ratio $R:a=3:1$, evaluated at the lowest resonance, wavenumber $k = 7.8727 - 0.3847\,i$, maximal cycle length $n = 8$.

Figure 40.2: Same as fig. 40.1, but with $R:a=6:1$. This illustrates possible pitfalls of numerical tests of asymptotics; the semiclassical spectral determinant appears to have the same pole as the quantum $1/\zeta_0\zeta_1^2$, but as we have no estimate on the size of pre-asymptotic oscillations in cycle expansions, it is difficult to draw reliable conclusions from such numerics. See fig. 13 for estimate of the semiclassical spectral determinant abscissa of absolute convergence.

Figure 40.3: Leading resonances in the 3-disk repeller A_1 subspace, (a) for the semiclassical spectral determinant, and (b) the 952 leading resonances of the semiclassical spectral determinant F_{qm}. Ratio $R:a=6:0$, cycle expansions truncated at cycle length $n = 8$.

Figure 40.4: Complex s plane countor plot comparison of (a) the semiclassical zeta function $\log|\det(\hat{H}-E)_{sc}(s)|$ with (b) the semiclassical spectral determinant $\log|F_{qm}(s)|$. The border of the convergence of the semiclassical zeta function agrees with the location of the abscissa of absolute convergence, given by the $\hat{F}_{1/2}$ leading eigenvalue at $\mathrm{Re}(s)=0$, $\mathrm{Im}(s) = -0.699110157151\ldots$. The semiclassical spectral determinant can be continued at least a factor 2 further down in the complex plane. 3-disk repeller, $R:a=6:1$, A_1 subspace, maximal cycle length $n = 8$.

Figure 40.5: Same parameter values 3-disk system as fig. 40.1: ($\circ$) the semiclassical spectral determinant compared with ($\Box$) the Vattay determinant. While the semiclassical spectral determinant is expected to have a pole at $\mathrm{Im}(k) = -1.276625955\ldots$, the Vattay determinant should be entire, and exhibits numerically faster than exponential convergence.

Table 40.1: The "quantum" eigenvalues obtained from the semiclassical zeta function $\det(\hat{H}-E)_{sc}(s)$ and the semiclassical spectral determinant $F_{qm}(s)$ for the baker's map. Only the leading eigenvalues are expected to coincide. The digits listed correspond to those unchanged between the cycle length $n = 23$ and $n = 24$ truncations.

	$\det(\hat{H}-E)_{sc}(s)$	$F_{qm}(s)$	
k	Real part	Real part	Im. part
1	0.34051779186	+0.3405177918632516	
2	-0.39	-0.3500689652275	
3		-0.7175716624	
4-5		-1.099684	$\pm$ 0.115118
6-7		-1.59	$\pm$ 0.227

Commentary

Remark 40.1 Our hopes. Quite generally, despite considerable progress (see for example the periodic orbit theory theme issue of CHAOS [11.18]), the semiclassical quantization of bounded systems is still not a routine calculation: all known bounded systems have either pruning, marginally stable periodic orbits and/or accumualting sequences of orbits, and the quantum Selberg zeta functions have poles that degrade the converegence of cycle expansions. We remain optimistic, and believe that not so long in the future many of these problems will be overcome.

Remark 40.2 Poles of dynamical zeta functions. Numerical investigations [40.21] of both the classical and the quantum dynamical $1/\zeta_j$ functions for 2-dimensional Hamiltonian flows indicate that a $1/\zeta_j$ function has a *double* pole coinciding with the leading zero of $1/\zeta_{j+1}$. Consequently $1/\zeta_0$, $1/\zeta_0\zeta_1$ and the quantum Selberg zeta function all have the same leading pole, and coefficients in their cycle expansions fall off exponentially with the same slope, fig. 40.5.4. Multiplying the quantum Selberg zeta function with $(1-z/z_1)$, where z_1 is the leading zero of $1/\zeta_1(z)$, one obtains faster, but still exponential decay in the coefficients, indicating further poles down in the complex plane (see fig. 40.5.4).

Résumé

To summarize, we have demonstrated that the curvature expansions are a very efficient way of evaluating the semiclassical periodic orbit sums. The essential ingredient for this success has been the physical insight that the dynamical zeta functions expanded this way utilize the shadowing of arbitrarily long orbits by shorter cycles; the technical prerequisite for implementing this shadowing is a good understanding of the symbolic dynamics of the classical dynamical system. Exploiting the symmetries of the problem, we are able to compute accurately a large number of resonances, using as input the actions and eigenvalues of as few as 2–14 prime cycles.

We conclude with three more general comments on the relation of classical and quantum chaotic dynamics:

1. The curvature expansion approach presented here applies to strongly chaotic (non-integrable) systems, and is thus a quantization scheme for a class of systems complementary to those amenable to torus quantization.

2. The symmetry factorization (40.4) of the dynamical zeta function is intrinsic to the classical dynamics, and not a special property of quantal spectra

3. For the strange sets studied in refs. [18.1, 40.2], the curvature expansion is believed to be the *exact* perturbation expansion for classical chaotic averages: even though each cycle carries with it only its linearized neighborhood (analogue of the stationary phase approximation in the derivation of the quantum Gutzwiller sum), the union of the periodic points captures the invariant content of the full underlying smoothly curved dynamics.

As we have shown in the above, the three disk system is an ideal system for tests of periodic orbit expansions in hyperbolic systems, not only in the classical but also in the semiclassical context. With a little bit of geometry one can obtain very good estimates for the classical and quantum escape rates as a function of the separation : radius ratio (fig. 40.5.4), demonstrating the accuracy of approximating the repeller by a few scales. With numerically obtained periodic orbits up to periods 14 one can test the analyticity properties of quantum Selberg zeta functions and Fredholm determinants; to our surprise we found that quantum Selberg zeta functions have poles. Their presence spoils the faster than exponential convergence typical of the classical Fredholm determinants; whether their analyticity can be improved is still being investigated. In the case of sufficiently separated three disks, this may not seem to be terribly important (one already has good exponential convergence), but also the more poorly converging cycle expansions for spectra of bounded systems also seem to have poles.

This success points to the most serious problem in classical chaos, namely the problem of Mandelbrot. (still with no solution in sight).

create problems for exerQuantPin.tex

References

[40.1] P. Cvitanović, *Phys. Rev. Lett.* **61**, 2729 (1988)

[40.2] R. Artuso, E. Aurell and P. Cvitanović, (to be published)

[40.3] R. Artuso, E. Aurell and P. Cvitanović, *Nonlinearity* **3**, 325 (1990).

[40.4] R. Artuso, E. Aurell and P. Cvitanović, *Nonlinearity* **3**, 361 (1990).

[40.5] P. Cvitanović and B. Eckhardt (in preparation)

[40.6] F. Christiansen, P. Cvitanović and H.H. Rugh, *J. Phys* **A 23**, L713 (1990).

[40.7] P. Cvitanović, ed., *Periodic Orbit Theory - theme issue*, *CHAOS* **2**, 1-158 (1992).

[40.8] P. Cvitanović and P.E. Rosenqvist, in G.F. Dell'Antonio, S. Fantoni and V.R. Manfredi, eds., *From Classical to Quantum Chaos, Soc. Italiana di Fisica Conf. Proceed.* **41**, pp. 57-64 (Ed. Compositori, Bologna 1993).

[40.9] P. Cvitanović and B. Eckhardt, *J. Phys.* **A 24**, L237 (1991).

[40.10] P. Cvitanović and B. Eckhardt, *Phys. Rev. Lett.* **63**, 823 (1989).

[40.11] P. Cvitanović and B. Eckhardt, *J. Phys.* **A 24**, L237 (1991)

[40.12] P. Cvitanović and B. Eckhardt, to appear in *Nonlinearity* (1993)

[40.13] P. Cvitanović, B. Eckhardt, P.E. Rosenqvist, G. Russberg and P. Scherer, in G. Casati and B. Chirikov, eds., *Quantum Chaos*, (Cambridge University Press, Cambridge 1993).

[40.14] P. Cvitanović, in J.H. Kim and J. Stringer, eds., *Applied Chaos*, (John Wiley & Sons, New York 1992).

[40.15] P. Cvitanović and P.E. Rosenqvist, *A new determinant for quantum chaos*, Proc. SISSA workshop "From Classical to Quantum Chaos", Trieste (July 1992)

[40.16] B. Eckhardt and E. Aurell, *Europhysics Letter* **9**, 509 (1989)

[40.17] B. Eckhardt and E. Aurell, *Europhys. Lett.* **9**, *509 (1989)*

[40.18] B. Eckhardt, *J. Phys.* **A 20**, 5971 (1987)

[40.19] P. Scherer and B. Eckhardt (in preparation)

[40.20] B. Eckhardt, *Physica* **D 33**, 89 (1988)

[40.21] B. Eckhardt and G. Russberg, *Phys. Rev.* **E 47**, 1578 (1993).

[40.22] B. Eckhardt and G. Russberg, *Phys. Rev.* **E 47**, 1578 (1993).

[40.23] M.C. Gutzwiller, *J. Math. Phys.* **8**, 1979 (1967), **10**, 1004 (1969), **11**, 1791 (1970), **12**, 343(1971)

[40.24] M.C. Gutzwiller, *J. Phys. Chem.* **92**, 3154 (1984)

[40.25] M.C. Gutzwiller, *Chaos in Classical and Quantum Mechanics* (Springer, New York 1990).

[40.26] M.C. Gutzwiller, *Chaos in Classical and Quantum Mechanics* (Springer, New York 1990)

[40.27] R. Balian and C. Bloch, *Ann. Phys. (NY)* **85**, 514 (1974)

[40.28] W.M. Miller, *Adv. Chem. Phys.* **30**, 77 (1975)

[40.29] A lucid introduction to escape from repellers is given in L.P. Kadanoff and C. Tang, *Proc. Natl. Acad. Sci.* **81**, 1276 (1984). The ζ–function formulation is given in D. Ruelle, *J. Stat. Phys* **44**, 281 (1986); W. Parry and M. Pollicott, *Ann. Math.* **118**, 573 (1983) and discussed in ref. [18.10].

[40.30] M. Hamermesh, *Group Theory and its Application to Physical Problems* (Addison-Wesley, Reading, 1962)

[40.31] P. Grassberger, F. Christiansen and H.H. Rugh (private communications)

[40.32] G.L. Da Silva Ritter, A.M. Ozorio de Almeida and R. Douady, *Physica* **D29**, 181 (1987)

[40.33] D. Ruelle, *Statistical Mechanics, Thermodynamic Formalism* (Addison-Wesley, Reading MA, 1978).

[40.34] A. Grothendieck, *"La théorie de Fredholm"*, Bull. Soc. Math. France **84**, 319 (1956).

[40.35] F. Christiansen, G. Paladin and H.H. Rugh, *Phys. Rev. Lett.* **65**, 2087 (1990).

[40.36] F. Christiansen, S. Isola, G. Paladin and H.H. Rugh, *J. Phys.* **A 23**, L1301 (1990).

[40.37] D. Ruelle, *Inventiones math.* **34**, 231 (1976).

[40.38] D. Fried, *Ann. Scient. Éc. Norm. Sup.* **19**, 491 (1986).

[40.39] S. Smale, *Bull. Am. Math. Soc.* **73**, 747 (1967).

[40.40] T.C. Halsey, M.H. Jensen, L.P. Kadanoff, I. Procaccia and B.I. Shraiman, *Phys. Rev.* **A107**, 1141 (1986).

[40.41] T. Prellberg and J. Slawny, *J. Stat. Phys.* **66**, 503 (1992).

[40.42] Ya.G. Sinai, *Russ. Math. Surveys* **166**, 21 (1972).

[40.43] L. Euler, *Opera Omnia* (Teubner, 1922).

[40.44] R. Bowen, *Equilibrium states and the ergodic theory of Anosov-diffeomorphisms*, Springer Lecture Notes in Math. **470** (1975).

[40.45] A. Selberg, *J. Ind. Math. Soc.* **20**, 47 (1956).

[40.46] P. Gaspard and S. Rice, *J. Chem. Phys.* **90**, 2225 (1989)

[40.47] P. Gaspard and S. Rice, *J. Chem. Phys.* **90**, 2242 (1989); **90**, 2255 (1989)

[40.48] F. Takens, "Detecting strange attractors in turbulence", *Springer Lecture Notes in Math.* **898**, 366(1981).

[40.49] M.V. Berry and J.P. Keating, *J. Phys.* **A 23**, 4839 (1990).

[40.50] P.E. Rosenqvist, Copenhagen University master's thesis (1991), unpublished.

[40.51] M.V. Berry and K.E. Mount, *Rep. Prog. Phys.* **35**, 315 (1972)

[40.52] D. Wintgen, *Phys. Rev. Lett.* **58**, 1589 (1987)

[40.53] D. Ruelle, *Statistical Mechanics, Thermodynamic Formalism* (Addison-Wesley, Reading 1978)

[40.54] F. Christiansen, G. Paladin and H.H. Rugh, *Phys. Rev. Lett.* **65**, 2087 (1990)

[40.55] R. Balian and C. Bloch, *Ann. Phys. (NY)* **85**, 514 (1974)

[40.56] A. Voros, *J. Phys.* **A 21**, 685 (1988)

[40.57] P.E. Rosenqvist (unpublished)

[40.58] H.H. Rugh, *Nonlinearity*,**5**, 1237 (1992)

[40.59] T. Harayama and A. Shudo, *J. Phys.* **A 25**, 4595 (1992)

[40.60] Ya.G. Sinai *Usp. Mat. Nauk* **25**, 141 (1970)

[40.61] L. Bunimovič, *Comm. Math. Phys.* **65**, 295 (1979)

⇑PRIVATE

Bohr!helium
Rutherford
helium
three body@3-body problem

Chapter 41

Helium atom

preceed this by a chapter on 3-disk quantum scattering

> "But," Bohr protested, "nobody will believe me unless I can explain every atom and every molecule." Rutherford was quick to reply, "Bohr, you explain hydrogen and you explain helium and everybody will believe the rest."
> John Archibald Wheeler (1986)

(G. Tanner)

So far much has been said about 1-dimensional maps, game of pinball and other curious but rather idealized dynamical systems. If you have become impatient and started wondering what good are the methods learned so far in solving real physical problems, we have good news for you. We will show in this chapter that the concepts of symbolic dynamics, unstable periodic orbits, and cycle expansions are essential tools to understand and calculate classical and quantum mechanical properties of nothing less than the helium, a dreaded three-body Coulomb problem.

This sounds almost like one step too much at a time; we all know how rich and complicated the dynamics of the three-body problem is – can we really jump from three static disks directly to three charged particles moving under the influence of their mutually attracting or repelling forces? It turns out, we can, but we have to do it with care. The full problem is indeed not accessible in all its detail, but we are able to analyze a somewhat simpler subsystem – collinear helium. This system plays an important role in the classical dynamics of the full three-body problem and its quantum spectrum.

The main work in reducing the quantum mechanics of helium to a semiclassical treatment of collinear helium lies in understanding why we are allowed to do so. We will not worry about this too much in the beginning; after all, 80 years and many failed attempts separate Heisenberg, Bohr and others in the 1920ties from the insights we have today on the role chaos plays for helium and its quantum spectrum. We have introduced collinear helium and learned how to integrate its trajectories in sect. 7.3.

action!helium
Kustaanheimo-Stiefel transformation

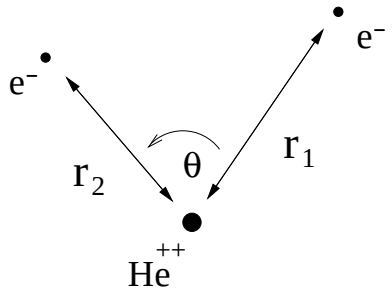

Figure 41.1: Coordinates for the helium three body problem in the plane.

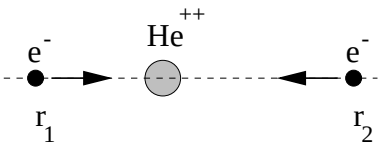

Figure 41.2: Collinear helium, with the two electrons on opposite sides of the nucleus.

Here we will find periodic orbits and determine the relevant eigenvalues of the fundamental matrix in sect. 41.1. We will explain in sect. 41.5 why a quantization of the collinear dynamics in helium will enable us to find parts of the full helium spectrum; we then set up the semiclassical spectral determinant and evaluate its cycle expansion. A full quantum justification of this treatment of helium is briefly discussed in sect. 41.5.1.

41.1 Classical dynamics of collinear helium

Recapitulating briefly what we learned in sect. 7.3: the collinear helium system consists of two electrons of mass m_e and charge $-e$ moving on a line with respect to a fixed positively charged nucleus of charge $+2e$, as in figure 41.2.

The Hamiltonian can be brought to a non–dimensionalized form

$$H = \frac{p_1^2}{2} + \frac{p_2^2}{2} - \frac{2}{r_1} - \frac{2}{r_2} + \frac{1}{r_1 + r_2} = -1\,. \tag{41.1}$$

The case of negative energies chosen here is the most interesting one for us. It exhibits chaos, unstable periodic orbits and is responsible for the bound states and resonances of the quantum problem treated in sect. 41.5.

There is another classical quantity important for a semiclassical treatment of quantum mechanics, and which will also feature prominently in the discussion in the next section; this is the classical action (34.15) which scales with energy as

$$S(E) = \oint \mathrm{d}\mathbf{q}(E)\cdot\mathbf{p}(E) = \frac{e^2 m_e^{1/2}}{(-E)^{1/2}}\, S, \tag{41.2}$$

with S being the action obtained from (41.1) for $E = -1$, and coordinates $\mathbf{q} = (r_1, r_2)$, $\mathbf{p} = (p_1, p_2)$. For the Hamiltonian (41.1), the period of a cycle and its action are related by (34.17), $T_p = \frac{1}{2} S_p$.

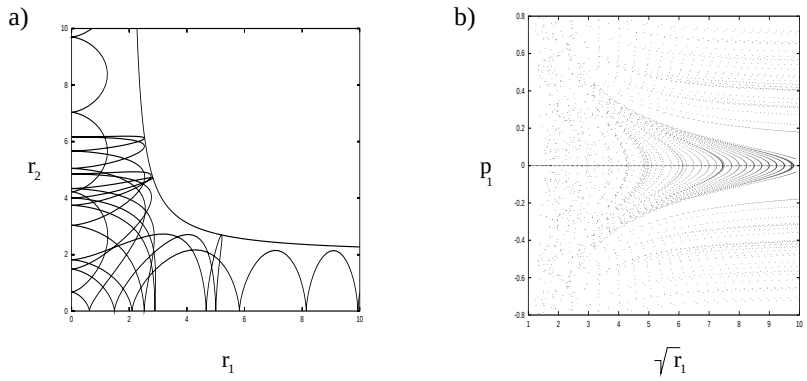

Figure 41.3: (a) A typical trajectory in the $r_1 - r_2$ plane; the trajectory enters here along the r_1 axis and escapes to infinity along the r_2 axis; (b) Poincaré map (r_2=0) for collinear helium. Strong chaos prevails for small r_1 near the nucleus.

After a Kustaanheimo–Stiefel transformation

$$r_1 = Q_1^2\,, \qquad r_2 = Q_2^2\,, \qquad p_1 = \frac{P_1}{2Q_1}\,, \qquad p_2 = \frac{P_2}{2Q_2}\,, \tag{41.3}$$

and reparametrization of time by $d\tau = dt/r_1 r_2$, the equations of motion take form (7.18)

41.1 page 794

$$\begin{aligned} \dot{P}_1 &= 2Q_1\left[2 - \frac{P_2^2}{8} - Q_2^2\left(1 + \frac{Q_2^2}{R_{12}^4}\right)\right]; \qquad \dot{Q}_1 = \frac{1}{4}P_1 Q_2^2 \\ \dot{P}_2 &= 2Q_2\left[2 - \frac{P_1^2}{8} - Q_1^2\left(1 + \frac{Q_1^2}{R_{12}^4}\right)\right]; \qquad \dot{Q}_2 = \frac{1}{4}P_2 Q_1^2. \end{aligned} \tag{41.4}$$

Individual electron–nucleus collisions at $r_1 = Q_1^2 = 0$ or $r_2 = Q_2^2 = 0$ no longer pose a problem to a numerical integration routine. The equations (7.18) are singular only at the triple collision $R_{12} = 0$, i.e., when both electrons hit the nucleus at the same time.

The new coordinates and the Hamiltonian (7.17) are very useful when calculating trajectories for collinear helium; they are, however, less intuitive as a visualization of the three-body dynamics. We will therefore refer to the old coordinates r_1, r_2 when discussing the dynamics and the periodic orbits.

41.2 Chaos, symbolic dynamics and periodic orbits

Let us have a closer look at the dynamics in collinear helium. The electrons are attracted by the nucleus. During an electron–nucleus collision momentum is transferred between the inner and outer electron. The inner electron has a maximal screening effect on the charge of the nucleus, diminishing the attractive force on the outer electron. This electron – electron interaction

fundamental!domain!collinear helium
helium!collinear!fundamental domain

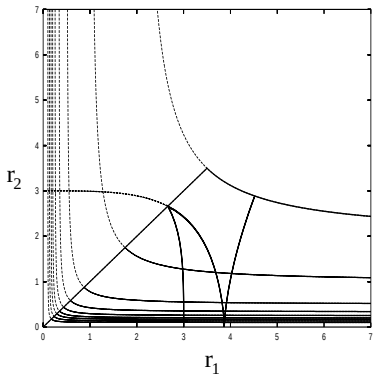

Figure 41.4: The cycle 011 in the fundamental domain $r_1 \geq r_2$ (full line) and in the full domain (dashed line).

is negligible if the outer electron is far from the nucleus at a collision and the overall dynamics is regular like in the 1-dimensional Kepler problem.

Things change drastically if both electrons approach the nucleus nearly simultaneously. The momentum transfer between the electrons depends now sensitively on how the particles approach the origin. Intuitively, these nearly missed triple collisions render the dynamics chaotic. A typical trajectory is plotted in figure 41.3 (a) where we used r_1 and r_2 as the relevant axis. The dynamics can also be visualized in a Poincaré surface of section, see figure 41.3 (b). We plot here the coordinate and momentum of the outer electron whenever the inner particle hits the nucleus, i.e., r_1 or $r_2 = 0$. As the unstructured gray region of the Poincaré section for small r_1 illustrates, the dynamics is chaotic whenever the outer electron is close to the origin during a collision. Conversely, regular motions dominate whenever the outer electron is far from the nucleus. As one of the electrons escapes for almost any starting condition, the system is unbounded: one electron (say electron 1) can escape, with an arbitrary amount of kinetic energy taken by the fugative. The remaining electron is trapped in a Kepler ellipse with total energy in the range $[-1, -\infty]$. There is no energy barrier which would separate the bound from the unbound regions of the phase space. From general kinematic arguments one deduces that the outer electron will not return when $p_1 > 0$, $r_2 \leq 2$ at $p_2 = 0$, the turning point of the inner electron. Only if the two electrons approach the nucleus almost symmetrically along the line $r_1 = r_2$, and pass close to the triple collision can the momentum transfer between the electrons be large enough to kick one of the particles out completely. In other words, the electron escape originates from the near triple collisions.

The collinear helium dynamics has some important properties which we now list.

41.2.1 Reflection symmetry

The Hamiltonian (7.9) is invariant with respect to electron–electron exchange; this symmetry corresponds to the mirror symmetry of the potential along the line $r_1 = r_2$, figure 41.4. As a consequence, we can restrict ourselves to the dynamics in the *fundamental domain* $r_1 \geq r_2$ and treat a crossing

of the diagonal $r_1 = r_2$ as a hard wall reflection. The dynamics in the full domain can then be reconstructed by unfolding the trajectory through back-reflections. As explained in chapter 22, the dynamics in the fundamental domain is the key to the factorization of spectral determinants, to be implemented here in (41.15). Note also the similarity between the fundamental domain of the collinear potential figure 41.4, and the fundamental domain figure 11.6 (b) in the 3–disk system, a simpler problem with the same binary symbolic dynamics.

collinear
helium!symbolic
dynamics
symbolic
dynamics!binary!collinear
helium
binary!symbolic
dynamics!collinear
helium

in depth:
sect. 22.6, p. 442

41.2.2 Symbolic dynamics

We have already made the claim that the triple collisions render the collinear helium fully chaotic. We have no proof of the assertion, but the analysis of the symbolic dynamics lends further credence to the claim.

The potential in (41.1) forms a ridge along the line $r_1 = r_2$. One can show that a trajectory passing the ridge must go through at least one two-body collision $r_1 = 0$ or $r_2 = 0$ before coming back to the diagonal $r_1 = r_2$. This suggests a *binary* symbolic dynamics corresponding to the dynamics in the fundamental domain $r_1 \geq r_2$; the symbolic dynamics is linked to the Poincaré map $r_2 = 0$ and the symbols 0 and 1 are defined as

0: if the trajectory is not reflected from the line $r_1 = r_2$ between two collisions with the nucleus $r_2 = 0$;

1: if a trajectory is reflected from the line $r_1 = r_2$ between two collisions with the nucleus $r_2 = 0$.

Empirically, the symbolic dynamics is complete for a Poincaré map in the fundamental domain, i.e., there exists a one-to-one correspondence between binary symbol sequences and collinear trajectories in the fundamental domain, with exception of the $\overline{0}$ cycle.

41.2.3 Periodic orbits

The existence of a binary symbolic dynamics makes it easy to count the number of periodic orbits in the fundamental domain, as in sect. 13.5.2. However, mere existence of these cycles does not suffice to calculate semiclassical spectral determinants. We need to determine their phase space trajectories and calculate their periods, topological indices and stabilities. A restriction of the periodic orbit search to a suitable Poincaré surface of section, e.g. $r_2 = 0$ or $r_1 = r_2$, leaves us in general with a 2-dimensional search. Methods to find periodic orbits in multi-dimensional spaces have been

libration orbit
self-retracing cycle

described in chapter 17. They depend sensitively on good starting guesses. A systematic search for all orbits can be achieved only after combining multi-dimensional Newton methods with interpolation algorithms based on the binary symbolic dynamics phase space partitioning(see sect. 17.6.3) . All cycles up to symbol length 16 (some 8000 primitive cycles) have been computed by such methods, with some examples shown in figure 41.5. All numerical evidence indicates that the dynamics of collinear helium is hyperbolic, and that all periodic orbits are unstable.

⇓PRELIMINARY
⇑PRELIMINARY
into remarks: cite Tanner

Note that the fixed point $\overline{0}$ cycle is not in this list. The $\overline{0}$ cycle would correspond to the situation where the outer electron sits at rest infinitely far from the nucleus while the inner electron bounces back and forth into the nucleus. The orbit is the limiting case of an electron escaping to infinity with zero kinetic energy. The orbit is in the regular (i.e., separable) limit of the dynamics and is thus marginally stable. The existence of this orbit is also related to intermittent behavior generating the quasi–regular dynamics for large r_1 that we have already noted in figure 41.3 (b).

Search algorithm for an arbitrary periodic orbit is quite cumbersome to program. There is, however, a class of periodic orbits, orbits with symmetries, which can be easily found by a one-parameter search. The only symmetry left for the dynamics in the fundamental domain is time reversal symmetry; a time reversal symmetric periodic orbit is an orbit whose trajectory in phase space is mapped onto itself when changing $(p_1, p_2) \to (-p_1, -p_2)$, by reversing the direction of the momentum of the orbit. Such an orbit must be a "libration" [1] or self-retracing cycle, an orbit that runs back and forth along the same path in the (r_1, r_2) plane. The cycles $\overline{1}$, $\overline{01}$ and $\overline{001}$ in figure 41.5 are examples of self-retracing cycles. Luckily, the shortest cycles that we desire most ardently have this symmetry.

buscar en la red: for example "Breve dictionario del argentino exquisito" Adolfo Bioy Cesares, for "capicua"

Why is this observation helpful? A self-retracing cycle must start perpendicular to the boundary of the fundamental domain, that is, on either of the axis $r_2 = 0$ or $r_1 = r_2$, or on the potential boundary $-\frac{2}{r_1}-\frac{2}{r_2}+\frac{1'}{r_1+r_2} = -1$. By shooting off trajectories perpendicular to the boundaries and monitoring the orbits returning to the boundary with the right symbol length we will find time reversal symmetric cycles by varying the starting point on the boundary as the only parameter. But how can we tell whether a given cycle is self-retracing or not? All the relevant information is contained in the itineraries; a cycle is self-retracing if its itinerary is invariant under time reversal symmetry (i.e., read backwards) and a suitable number of cyclic permutations. All binary strings up to length 5 fulfill this condition. The symbolic dynamics contains even more information; we can tell at which boundary the total reflection occurs. One finds that an orbit starts out perpendicular

- to the diagonal $r_1 = r_2$ if the itinerary is time reversal invariant and has an odd number of 1's; an example is the cycle $\overline{001}$ in figure 41.5;

[1] Tanner: Explain that much earlier

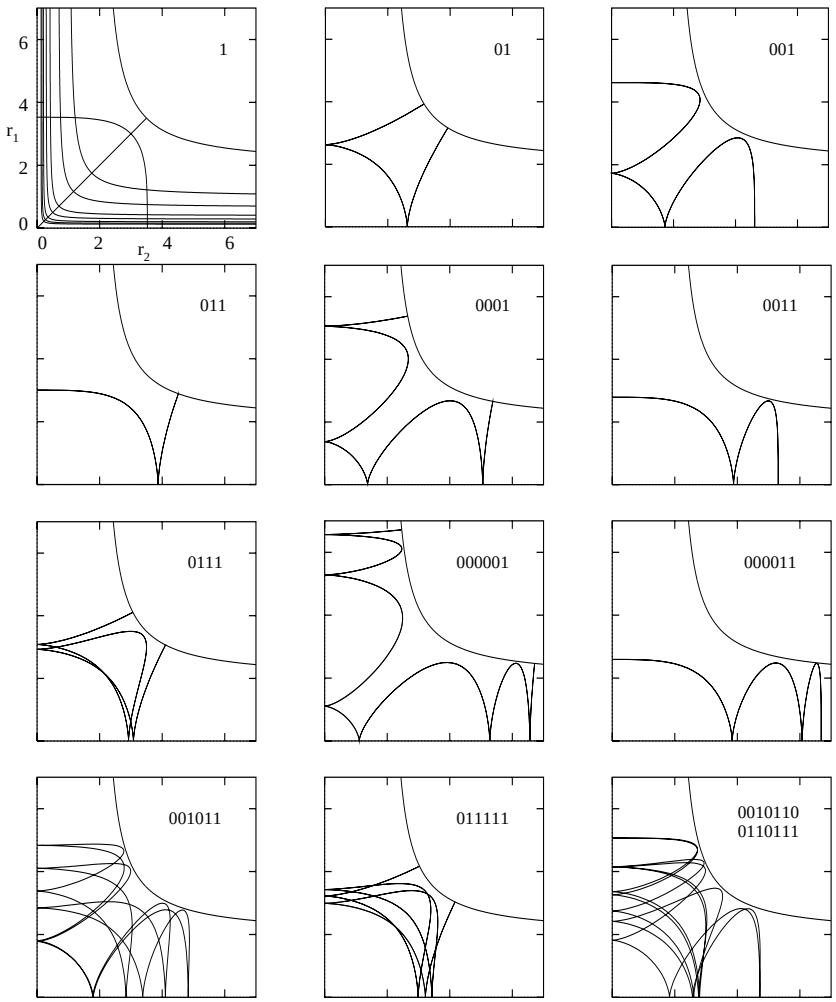

Figure 41.5: Some of the shortest cycles in collinear helium. The classical collinear electron motion is bounded by the potential barrier $-1 = -2/r_1 - 2/r_2 + 1/(r_1 + r_2)$ and the condition $r_i \geq 0$. The orbits are shown in the full r_1–r_2 domain, the itineraries refers to the dynamics in the $r_1 \geq r_2$ fundamental domain. The last figure, the 14-cycle 00101100110111, is an example of a typical cycle with no symmetry.

- to the axis $r_2 = 0$ if the itinerary is time reversal invariant and has an even number of symbols; an example is the cycle $\overline{0011}$ in figure 41.5;

- to the potential boundary if the itinerary is time reversal invariant and has an odd number of symbols; an example is the cycle $\overline{011}$ in figure 41.5.

where are these cycles in figure 41.5?

All cycles up to symbol length 5 are time reversal invariant, the first two non-time reversal symmetric cycles are cycles $\overline{001011}$ and $\overline{001101}$ in figure 41.5. Their determination would require a two-parameter search. The two cycles are mapped onto each other by time reversal symmetry, i.e., they have the same trace in the r_1–r_2 plane, but they trace out distinct cycles in the full phase space.

mention that 001101 is not in Fig. 25.5

We are ready to integrate trajectories for classical collinear helium with the help of the equations of motions (7.18) and to find all cycles up to length 5. There is only one thing not yet in place; we need the governing equations for the matrix elements of the fundamental matrix along a trajectory in order to calculate stability indices. We will provide the main equations in the next section, with the details of the derivation relegated to the appendix D.2. [2]

41.5
page 794

41.3 Local coordinates, fundamental matrix

In this section, we will derive the equations of motion for the fundamental matrix along a collinear helium trajectory. The fundamental matrix is 4-dimensional; the two trivial eigenvectors corresponding to the conservation of energy and displacements along a trajectory can, however, be projected out by suitable orthogonal coordinates transformations, see appendix D. We will give the transformation to local coordinates explicitly, here for the regularized coordinates (7.16), and state the resulting equations of motion for the reduced $[2 \times 2]$ fundamental matrix.

The vector locally parallel to the trajectory is pointing in the direction of the phase space velocity (5.7)

$$v_m = \dot{x}_m(t) = \omega_{mn} \frac{\partial H}{\partial x_n} = (H_{P_1}, H_{P_2}, -H_{Q_1}, -H_{Q_2})^T,$$

with $H_{Q_i} = \frac{\partial H}{\partial Q_i}$, and $H_{P_i} = \frac{\partial H}{\partial P_i}$, $i = 1,2$. The vector perpendicular to a trajectory $x(t) = (Q_1(t), Q_2(t), P_1(t), P_2(t))$ and to the energy manifold is given by the gradient of the Hamiltonian (7.17)

$$\gamma = \nabla H = (H_{Q_1}, H_{Q_2}, H_{P_1}, H_{P_2})^T .$$

[2] Tanner: Have a look at that appendix

By symmetry $v_m\gamma_m = \omega_{mn}\frac{\partial H}{\partial x_n}\frac{\partial H}{\partial x_m} = 0$, so the two vectors are orthogonal.

Next, we consider the orthogonal matrix

$$\begin{aligned}\mathbf{O} &= (\gamma_1, \gamma_2, \gamma/R, v) \qquad (41.5)\\ &= \begin{pmatrix} -H_{P_2}/R & H_{Q_2} & H_{Q_1}/R & H_{P_1} \\ H_{P_1}/R & -H_{Q_1} & H_{Q_2}/R & H_{P_2} \\ -H_{Q_2}/R & -H_{P_2} & H_{P_1}/R & -H_{Q_1} \\ H_{Q_1}/R & H_{P_1} & H_{P_2}/R & -H_{Q_2} \end{pmatrix}\end{aligned}$$

with $R = |\nabla H|^2 = (H_{Q_1}^2 + H_{Q_2}^2 + H_{P_1}^2 + H_{P_2}^2)$, which provides a transformation to local phase space coordinates centered on the trajectory $x(t)$ along the two vectors (γ, v). The vectors $\gamma_{1,2}$ are phase space vectors perpendicular to the trajectory and to the energy manifold in the 4-dimensional phase space of collinear helium. The fundamental matrix (4.6) rotated to the local coordinate system by $\mathbf{O}$ then has the form

41.6
page 795

Gregor had a σ here, maybe a symplectic form ω is missing, recheck

$$\mathbf{m} = \begin{pmatrix} m_{11} & m_{12} & * & 0 \\ m_{21} & m_{22} & * & 0 \\ 0 & 0 & 1 & 0 \\ * & * & * & 1 \end{pmatrix}, \quad M = \mathbf{O^T m O}$$

The linearized motion perpendicular to the trajectory on the energy manifold is described by the $[2 \times 2]$ matrix $\mathbf{m}$; the 'trivial' directions correspond to unit eigenvalues on the diagonal in the 3rd and 4th column and row.

The equations of motion for the reduced fundamental matrix $\mathbf{m}$ are given by

$$\dot{\mathbf{m}} = \mathbf{l}(t)\mathbf{m}(t), \qquad (41.6)$$

with $\mathbf{m}(0) = \mathbf{1}$. The matrix $\mathbf{l}$ depends on the trajectory in phase space and has the form

$$\mathbf{l} = \begin{pmatrix} l_{11} & l_{12} & * & 0 \\ l_{21} & l_{22} & * & 0 \\ 0 & 0 & 0 & 0 \\ * & * & * & 0 \end{pmatrix},$$

where the relevant matrix elements l_{ij} are given by

$$\begin{aligned} l_{11} &= \frac{1}{R}[2H_{Q_1Q_2}(H_{Q_2}H_{P_1} + H_{Q_1}H_{P_2}) \qquad (41.7)\\ &\quad +(H_{Q_1}H_{P_1} - H_{Q_2}H_{P_2})(H_{Q_1Q_1} - H_{Q_2Q_2} - H_{P_1P_1} + H_{P_2P_2})] \\ l_{12} &= -2H_{Q_1Q_2}(H_{Q_1}H_{Q_2} - H_{P_1}H_{P_2}) \\ &\quad +(H_{Q_1}^2 + H_{P_2}^2)(H_{Q_2Q_2} + H_{P_1P_1}) + (H_{Q_2}^2 + H_{P_1}^2)(H_{Q_1Q_1} + H_{P_2P_2}) \\ l_{21} &= \frac{1}{R^2}[2(H_{Q_1P_2} + H_{Q_2P_1})(H_{Q_2}H_{P_1} + H_{Q_1}H_{P_8}) \\ &\quad -(H_{P_1}^2 + H_{P_2}^2)(H_{Q_1Q_1} + H_{Q_2Q_2}) - (H_{Q_1}^2 + H_{Q_2}^2)(H_{P_1P_1} + H_{P_2P_2})] \\ l_{22} &= -l_{11}\,. \end{aligned}$$

action!relation to period
period!relation to action

p	$S_p/2\pi$	$\ln \lvert\Lambda_p\rvert$	σ_p	m_p
1	1.82900	0.6012	0.5393	2
01	3.61825	1.8622	1.0918	4
001	5.32615	3.4287	1.6402	6
011	5.39451	1.8603	1.6117	6
0001	6.96677	4.4378	2.1710	8
0011	7.04134	2.3417	2.1327	8
0111	7.25849	3.1124	2.1705	8
00001	8.56618	5.1100	2.6919	10
00011	8.64306	2.7207	2.6478	10
00101	8.93700	5.1562	2.7291	10
00111	8.94619	4.5932	2.7173	10
01011	9.02689	4.1765	2.7140	10
01111	9.07179	3.3424	2.6989	10
000001	10.13872	5.6047	3.2073	12
000011	10.21673	3.0323	3.1594	12
000101	10.57067	6.1393	3.2591	12
000111	10.57628	5.6766	3.2495	12
001011	10.70698	5.3251	3.2519	12
001101	10.70698	5.3251	3.2519	12
001111	10.74303	4.3317	3.2332	12
010111	10.87855	5.0002	3.2626	12
011111	10.91015	4.2408	3.2467	12

Table 41.1: Action S_p (in units of 2π), Lyapunov exponent $|\Lambda_p|/T_p$ for the motion in the collinear plane, winding number σ_p for the motion perpendicular to the collinear plane, and the topological index m_p for all fundamental domain cycles up to topological length 6.

Here $H_{Q_iQ_j}$, $H_{P_iP_j}$, i, $j = 1, 2$ are the second partial derivatives of H with respect to the coordinates Q_i, P_i, evaluated at the phase space coordinate of the classical trajectory. [3]

[4]

41.4 Getting ready

Now everything is in place: the regularized equations of motion can be implemented in a Runge–Kutta or any other integration scheme to calculate trajectories. We have a symbolic dynamics and know how many cycles there are and how to find them (at least up to symbol length 5). We know how to compute the fundamental matrix whose eigenvalues enter the semiclassical spectral determinant (36.13). By (34.17) the action S_p is proportional to the period of the orbit, $S_p = 2T_p$.

There is, however, still a slight complication. Collinear helium is an invariant 4-dimensional subspace of the full helium phase space. If we

[3] Dorte: uforstaaeligt!
[4] Tanner: Check if σ in table 41.3 in multiples of π or 2π.

Bohr!helium
Rydberg series

restrict the dynamics to angular momentum equal zero, we are left with 6 phase space coordinates. That is not a problem when computing periodic orbits, they are oblivious to the other dimensions. However, the fundamental matrix does pick up extra contributions. When we calculate the fundamental matrix for the full problem, we must also allow for displacements out of the collinear plane, so the full fundamental matrix for dynamics for $L = 0$ angular momentum is 6 dimensional. Fortunately, the linearized dynamics in and off the collinear helium subspace decouple, and the fundamental matrix can be written in terms of two distinct $[2 \times 2]$ matrices, with trivial eigendirections providing the remaining two dimensions. The submatrix related to displacements off the linear configuration characterizes the linearized dynamics in the additional degree of freedom, the Θ-coordinate in figure 41.1. It turns out that the linearized dynamics in the Θ coordinate is stable, corresponding to a bending type motion of the two electrons. We will need the stability exponents for all degrees of freedom in evaluating the semiclassical spectral determinant in sect. 41.5.

The numerical values of the actions, stability exponents, stability angles, and topological indices for the shortest cycles are listed in table 41.3. These numbers, needed for the semiclassical quantization implemented in the next section, an also be helpful in checking your own calculations.

41.5 Semiclassical quantization of collinear helium

Before we get down to a serious calculation of the helium quantum energy levels let us have a brief look at the overall structure of the spectrum. This will give us a preliminary feel for which parts of the helium spectrum are accessible with the help of our collinear model – and which are not. In order to keep the discussion as simple as possible and to concentrate on the semiclassical aspects of our calculations we offer here only a rough overview. For a guide to more detailed accounts see remark 41.4.

41.5.1 Structure of helium spectrum

We start by recalling Bohr's formula for the spectrum of hydrogen like one-electron atoms. The eigenenergies form a Rydberg series

$$E_N = -\frac{e^4 m_e}{\hbar^2}\frac{Z^2}{2N^2}\,, \tag{41.8}$$

where Ze is the charge of the nucleus and m_e is the mass of the electron. Through the rest of this chapter we adopt the atomic units $e = m_e = \hbar = 1$.

The simplest model for the helium spectrum is obtained by treating the two electrons as independent particles moving in the potential of the nucleus neglecting the electron–electron interaction. Both electrons are then bound

in hydrogen like states; the inner electron will see a charge $Z = 2$, screening at the same time the nucleus, the outer electron will move in a Coulomb potential with effective charge $Z-1 = 1$. In this way obtain a first estimate for the total energy

$$E_{N,n} = -\frac{2}{N^2} - \frac{1}{2n^2} \qquad \text{with} \quad n > N. \tag{41.9}$$

This double Rydberg formula contains already most of the information we need to understand the basic structure of the spectrum. The (correct) ionizations thresholds $E_N = -\frac{2}{N^2}$ are obtained in the limit $n \to \infty$, yielding the ground and excited states of the helium ion He^+. We will therefore refer to N as the principal quantum number. We also see that all states $E_{N,n}$ with $N \geq 2$ lie above the first ionization threshold for $N = 1$. As soon as we switch on electron-electron interaction these states are no longer bound states; they turn into resonant states which decay into a bound state of the helium ion and a free outer electron. This might not come as a big surprise if we have the classical analysis of the previous section in mind: we already found that one of the classical electrons will almost always escape after some finite time. More remarkable is the fact that the first, $N = 1$ series consists of true bound states for all n, an effect which can only be understood by quantum arguments.

The hydrogen-like quantum energies (41.8) are highly degenerate; states with different angular momentum but the same principal quantum number N share the same energy. We recall from basic quantum mechanics of hydrogen atom that the possible angular momenta for a given N span $l = 0, 1 \ldots N-1$. How does that affect the helium case? Total angular momentum L for the helium three-body problem is conserved. The collinear helium is a subspace of the classical phase space for $L = 0$; we thus expect that we can only quantize helium states corresponding to the total angular momentum zero, a subspectrum of the full helium spectrum. Going back to our crude estimate (41.9) we may now attribute angular momenta to the two independent electrons, l_1 and l_2 say. In order to obtain total angular momentum $L = 0$ we need $l_1 = l_2 = l$ and $l_{z1} = -l_{z2}$, that is, there are N different states corresponding to $L = 0$ for fixed quantum numbers N, n. That means that we expect N different Rydberg series converging to each ionization threshold $E_N = -2/N^2$. This is indeed the case and the N different series can be identified also in the exact helium quantum spectrum, see figure 41.6. The degeneracies between the different N Rydberg series corresponding to the same principal quantum number N, are removed by the electron-electron interaction. We thus already have a rather good idea of the coarse structure of the spectrum.

In the next step, we may even speculate which parts of the $L = 0$ spectrum can be reproduced by the semiclassical quantization of collinear helium. In the collinear helium, both classical electrons move back and forth along a common axis through the nucleus, so each has zero angular momentum. We therefore expect that collinear helium describes the Rydberg series with $l = l_1 = l_2 = 0$. These series are the energetically lowest states

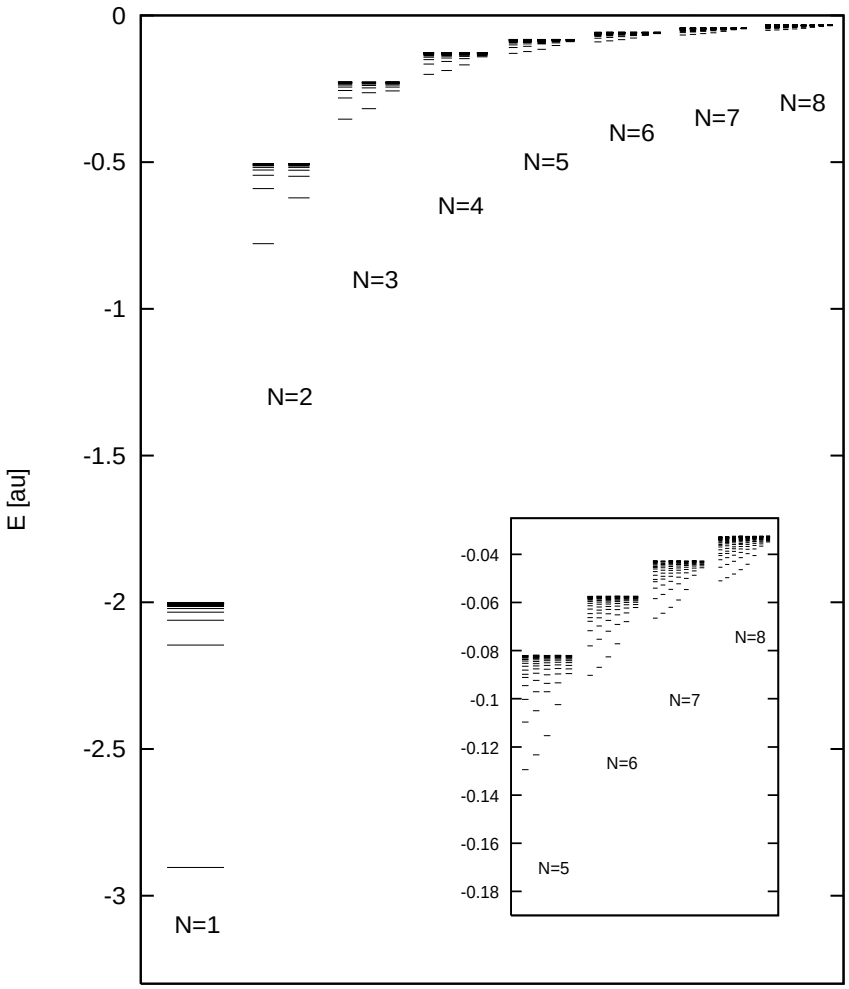

Figure 41.6: The exact quantum helium spectrum for $L = 0$. The energy levels denoted [5] by bars have been obtained from full 3-dimensional quantum calculations [41.3].

Dorte: ulaeseligt

semiclassical!spectral determinant!collinear helium
staircase!mean eigenvalue density

for fixed (N, n), corresponding to the Rydberg series on the outermost left side of the spectrum in figure 41.6. We will see in the next section that this is indeed the case and that the collinear model holds down to the $N = 1$ bound state series, including even the ground state of helium! We will also find a semiclassical quantum number corresponding to the angular momentum l and show that the collinear model describes states for moderate angular momentum l as long as $l \ll N$. .

☞ remark 41.4

41.5.2 Semiclassical spectral determinant for collinear helium

Nothing but lassitude can stop us now from calculating our first semiclassical eigenvalues. The only thing left to do is to set up the spectral determinant in terms of the periodic orbits of collinear helium and to write out the first few terms of its cycle expansion with the help of the binary symbolic dynamics. The semiclassical spectral determinant (36.13) has been written as product over all cycles of the classical systems. The energy dependence in collinear helium enters the classical dynamics only through simple scaling transformations described in sect. 7.3.1 which makes it possible to write the semiclassical spectral determinant in the form

$$\det\left(\hat{H}-E\right)_{sc} = \exp\left(-\sum_{p}\sum_{r=1}^{\infty}\frac{1}{r}\frac{e^{ir(sS_p-m_p\frac{\pi}{2})}}{(-\det\left(1-M_{p\perp}^{r}\right))^{1/2}|\det\left(1-M_{p\parallel}^{r}\right)|^{1/2}}\right), \quad (41.10)$$

replace by k? then $k \to \ell$ elsewhere

with the energy dependence absorbed into the variable

$$s = \frac{e^2}{\hbar}\sqrt{\frac{m_e}{-E}},$$

obtained by using the scaling relation (41.2) for the action. As explained in sect. 41.3, the fact that the $[4 \times 4]$ fundamental matrix decouples into two $[2 \times 2]$ submatrices corresponding to the dynamics *in* the collinear space and *perpendicular* to it makes it possible to write the denominator in terms of a product of two determinants. Stable and unstable degrees of freedom enter the trace formula in different ways, (see the discussion in sect. **??**) [6] [7] reflected by the absence of the modulus sign and the minus sign in front of $\det\left(1 - M_{\perp}\right)$. The topological index m_p corresponds to the unstable dynamics in the collinear plane. Note that the factor $e^{i\pi\bar{N}(E)}$ present in (36.13) is absent in (41.10). Collinear helium is an open system, i.e., the eigenenergies are resonances corresponding to the complex zeros of the semiclassical spectral determinant and the mean energy staircase $\bar{N}(E)$ not defined. [8] In order to obtain a spectral determinant as an infinite product of the form (36.19) we may proceed as in (15.10) by expanding the determinants in (41.10) in terms of the eigenvalues of the corresponding

⇓PRELIMINARY
⇑PRELIMINARY

[6] Dorte: sect. **??**hat??
[7] Tanner: reference
[8] Tanner: Make reference to Andreas chapter

fundamental matrices. The matrix representing displacements perpendicular to the collinear space has eigenvalues of the form $\exp(\pm 2\pi i\sigma)$, reflecting stable linearized dynamics. σ is the full winding number along the orbit in the stable degree of freedom, multiplicative under multiple repetitions of this orbit , see sect. **??**. [9] The eigenvalues corresponding to the unstable dynamics along the collinear axis are paired as $\{\Lambda, 1/\Lambda\}$ with $|\Lambda| > 1$ and real. As in (15.10) and (36.19) we may thus write

⇓PRIVATE
⇑PRIVATE

$$\begin{aligned}
&\left[-\det\left(1-M_\perp^r\right)\left|\det\left(1-M_\parallel^r\right)\right|\right]^{-1/2} \qquad (41.11)\\
&= \left[-(1-\Lambda^r)(1-\Lambda^{-r})|(1-e^{2\pi i r\sigma})(1-e^{-2\pi i r\sigma})\right]^{-1/2}\\
&= \sum_{k,\ell=0}^{\infty} \frac{1}{|\Lambda^r|^{1/2}\Lambda^{rk}} e^{-ir(\ell+1/2)\sigma}\,.
\end{aligned}$$

The $\pm$ sign corresponds to the hyperbolic/inverse hyperbolic periodic orbits with positive/negative eigenvalues Λ. [10] Using the relation (41.12) we see that the sum over r in (41.10) is the expansion of the logarithm, so the semiclassical spectral determinant can be rewritten as a product over dynamical zeta functions, as in (15.10): [11]

problem: same as Maslov

$$\det\left(\hat{H}-E\right)_{sc} = \prod_{k=0}^{\infty}\prod_{m=0}^{\infty}\zeta_{k,m}^{-1} = \prod_{k=0}^{\infty}\prod_{m=0}^{\infty}\prod_{p}(1-t_p^{(k,m)})\,, \qquad (41.12)$$

where the cycle weights are given by

$$t_p^{(k,m)} = \frac{1}{|\Lambda|^{1/2}\Lambda^k} e^{i\left(sS_p - m_p\frac{\pi}{2} - 4\pi(\ell+1/2)\sigma_p\right)}\,, \qquad (41.13)$$

and m_p is the topological index for the motion in the collinear plane which equals twice the topological length of the cycle. [12] The two independent directions perpendicular to the collinear axis lead to a twofold degeneracy in this degree of freedom which accounts for an additional factor 2 in front of the winding number σ. The values for the actions, winding numbers and stability indices of the shortest cycles in collinear helium are listed in table 41.3.

Gregor, I have changed to Lyapunov exponent $\lambda_p = \log|\Lambda_p|/T$, rather than stability exponent $\lambda_p = \log|\Lambda_p|$, for consistency with the rest of the text

The integer indices ℓ and k play very different roles in the semiclassical spectral determinant (41.12). A linearized approximation of the flow along a cycle corresponds to a harmonic approximation of the potential in the vicinity of the trajectory. Stable motion corresponds to a harmonic oscillator potential, unstable motion to an inverted harmonic oscillator.

[9] Tanner: Ref to section about isolated stable orbits.
[10] Tanner: Discuss invers/hyperbolic orbit, even/odd maslov; ref to gutzwiller chapter.
[11] Mason: It states, "Using the relation (25.19)" to get equation... (25.19). Most likely possibility is that the first 21.19 should be 21.xx for some other xx.
[12] Tanner: Explain why

The index ℓ which contributes as a phase to the cycle weights in the dynamical zeta functions can therefore be interpreted as a harmonic oscillator quantum number; it corresponds to vibrational modes in the Θ coordinate and can in our simplified picture developed in sect. 41.5.1 be related to the quantum number $l = l_1 = l_2$ representing the single particle angular momenta. Every distinct ℓ value corresponds to a full spectrum which we obtain from the zeros of the semiclassical spectral determinant $1/\zeta_\ell$ keeping ℓ fixed. The harmonic oscillator approximation will eventually break down with increasing off-line excitations and thus increasing ℓ. The index k corresponds to 'excitations' along the unstable direction and can be identified with local resonances of the inverted harmonic oscillator centered on the given orbit. [13] The cycle contributions $t_p^{(k,m)}$ decrease exponentially with increasing k. Higher k terms in an expansion of the determinant give corrections which become important only for large negative imaginary s values. As we are interested only in the leading zeros of (41.12), i.e., the zeros closest to the real energy axis, it is sufficient to take only the $k = 0$ terms into account.

cross reference

Next, let us have a look at the discrete symmetries discussed in sect. 41.2. Collinear helium has a C_2 symmetry as it is invariant under reflection across the $r_1 = r_2$ line corresponding to the electron-electron exchange symmetry. As explained in sects. 22.1.2 and 22.5, we may use this symmetry to factorize the semiclassical spectral determinant. The spectrum corresponding to the states symmetric or antisymmetric with respect to reflection can be obtained by writing the dynamical zeta functions in the symmetry factorized form

$$1/\zeta^{(\ell)} = \prod_a (1 - t_a)^2 \prod_{\tilde{s}} (1 - t_{\tilde{s}}^2)\,. \tag{41.14}$$

say m dependence implicit in $t_a = t_a^{(0,\ell)}$ as defined in (28.14a)

Here, the first product is taken over all asymmetric prime cycles, i.e., cycles that are not self-dual under the C_2 symmetry. Such cycles come in pairs, as two equivalent orbits are mapped into each other by the symmetry transformation. The second product runs over all self-dual cycles; these orbits cross the axis $r_1 = r_2$ twice at a right angle. The self-dual cycles close in the fundamental domain $r_1 \leq r_2$ already at half the period compared to the orbit in the full domain, and the cycle weights $t_{\tilde{s}}$ in (41.14) are the weights of fundamental domain cycles. The C_2 symmetry now leads to the factorization of (41.14) $1/\zeta = \zeta_+^{-1}\zeta_-^{-1}$, with

$$\begin{aligned} 1/\zeta_+^{(\ell)} &= \prod_a (1 - t_a) \prod_{\tilde{s}} (1 - t_{\tilde{s}})\,, \\ 1/\zeta_-^{(\ell)} &= \prod_a (1 - t_a) \prod_{\tilde{s}} (1 + t_{\tilde{s}})\,, \end{aligned} \tag{41.15}$$

setting $k = 0$ in what follows. The symmetric subspace resonances are given by the zeros of $1/\zeta_+^{(\ell)}$, antisymmetric resonances by the zeros of $1/\zeta_-^{(\ell)}$, with

[13] Tanner: Reference Gabor chapter

the two dynamical zeta functions defined as products over orbits in the fundamental domain. The symmetry properties of an orbit can be read off directly from its symbol sequence, as explained in sect. 41.2. An orbit with an odd number of 1's in the itinerary is self-dual under the C_2 symmetry and enters the spectral determinant in (41.15) with a negative or a positive sign, depending on the symmetry subspace under consideration.

41.5.3 Cycle expansion results

So far we have established a factorized form of the semiclassical spectral determinant and have thereby picked up two *good quantum numbers*; the quantum number m has been identified with an excitation of the bending vibrations, the exchange symmetry quantum number ± 1 corresponds to states being symmetric or antisymmetric with respect to the electron-electron exchange. We may now start writing down the binary cycle expansion (18.5) and determine the zeros of spectral determinant. There is, however, still another problem: there is no cycle 0 in the collinear helium. The symbol sequence $\overline{0}$ corresponds to the limit of an outer electron fixed with zero kinetic energy at $r_1 = \infty$, the inner electron bouncing back and forth into the singularity at the origin. This introduces intermittency in our system, a problem discussed in chapter 21. We note that the behavior of cycles going far out in the channel r_1 or $r_2 \to \infty$ is very different from those staying in the near core region. A cycle expansion using the binary alphabet reproduces states where both electrons are localized in the near core regions: these are the lowest states in each Rydberg series. The states converging to the various ionization thresholds $E_N = -2/N^2$ correspond to eigenfunctions where the wave function of the outer electron is stretched far out into the ionization channel $r_1, r_2 \to \infty$. To include those states, we have to deal with the dynamics in the limit of large r_1, r_2. This turns out to be equivalent to switching to a symbolic dynamics with an infinite alphabetdiscussed in sect. 21.3.1, a step beyond our ambition horizon right now. With this observation in mind, we may write the cycle expansion (....) for a binary alphabet without the $\overline{0}$ cycle as

⇓PRELIMINARY
⇑PRELIMINARY
☞ remark 41.5
replace by the intermittency table

$$
\begin{aligned}
1/\zeta^{\ell}(s) = \quad 1 \quad & -t_1^{(\ell)} - t_{01}^{(\ell)} - [t_{001}^{(\ell)} + t_{011}^{(\ell)} - t_{01}^{(\ell)} t_1^{(\ell)}] \\
& -[t_{0001}^{(\ell)} + t_{0011}^{(\ell)} - t_{001}^{(\ell)} t_1^{(\ell)} + t_{0111}^{(\ell)} - t_{011}^{(\ell)} t_1^{(\ell)}] - \ldots
\end{aligned} \tag{41.16}
$$

The weights $t_p^{(\ell)}$ are given in (41.12), with contributions of orbits and composite orbits of the same total symbol length collected within square brackets. The cycle expansion depends only on the classical actions, stability indices and winding numbers, given for orbits up to length 6 in table 41.3. To get reacquainted with the cycle expansion formula (41.16), consider a truncation of the series after the first term

$$
1/\zeta^{(\ell)}(s) \approx 1 - t_1 \,.
$$

N	n	$j=1$	$j=4$	$j=8$	$j=12$	$j=16$	$-E_{\rm qm}$
1	1	3.0970	2.9692	2.9001	2.9390	2.9248	2.9037
2	2	0.8044	0.7714	0.7744	0.7730	0.7727	0.7779
2	3	—	0.5698	0.5906	0.5916	0.5902	0.5899
2	4	—	—	—	0.5383	0.5429	0.5449
3	3	0.3622	0.3472	0.3543	0.3535	0.3503	0.3535
3	4	—	—	0.2812	0.2808	0.2808	0.2811
3	5	—	—	0.2550	0.2561	0.2559	0.2560
3	6	—	—	—	0.2416	0.2433	0.2438
4	4	0.2050	0.1962	0.1980	0.2004	0.2012	0.2010
4	5	—	0.1655	0.1650	0.1654	0.1657	0.1657
4	6	—	—	0.1508	0.1505	0.1507	0.1508
4	7	—	—	0.1413	0.1426	0.1426	0.1426

Table 41.2: Collinear helium, real part of the symmetric subspace resonances obtained by a cycle expansion (41.16) up to cycle length j. The exact quantum energies [41.3] are in the last column. The states are labeled by their principal quantum numbers. A dash as an entry indicates a missing zero at that level of approximation.

The quantization condition $1/\zeta^{(\ell)}(s)=0$ leads to

$$E_{m,N}=-\frac{(S_1/2\pi)^2}{[m+\frac{1}{2}+2(N+\frac{1}{2})\sigma_1]^2}, \qquad m,N=0,1,2,\dots\ , \tag{41.17}$$

with $S_1/2\pi = 1.8290$ for the action and $\sigma_1 = 0.5393$ for the winding number, see table 41.3, the 1 cycle in the fundamental domain. This cycle can be described as the *asymmetric stretch* orbit, see figure 41.5. The additional quantum number N in (41.17) corresponds to the principal quantum number defined in sect. 41.5.1. The states described by the quantization condition (41.17) are those centered closest to the nucleus and correspond therefore to the lowest states in each Rydberg series (for a fixed m and N values), in figure 41.6. The simple formula (41.17) gives already a rather good estimate for the ground state of helium! Results obtained from (41.17) are tabulated in table 41.2, see the 3rd column under $j=1$ and the comparison with the full quantum calculations.

In order to obtain higher excited quantum states, we need to include more orbits in the cycle expansion (41.16), covering more of the phase space dynamics further away from the center. Taking longer and longer cycles into account, we indeed reveal more and more states in each N-series for fixed m. This is illustrated by the data listed in table 41.2 for symmetric states obtained from truncations of the cycle expansion of $1/\zeta_+$.

41.7
page 795

Results of the same quality are obtained for antisymmetric states by calculating the zeros of [14] $1/\zeta_-^{(\ell)}$. Repeating the calculation with $\ell=1$ or higher in (41.15) reveals states in the Rydberg series which are to the right of the energetically lowest series in figure 41.6.

[14] Dorte: ulaesligt

Hopf, Heinz

Commentary

Remark 41.1 Sources. The full 3-dimensional Hamiltonian after elimination of the center of mass coordinates, and an account of the finite nucleus mass effects is given in ref. [41.2]. The general two–body collision regularizing Kustaanheimo–Stiefel transformation [41.5], a generalization of Levi-Civita's [41.13] Pauli matrix two–body collision regularization for motion in a plane, is due to Kustaanheimo [41.12] who realized that the correct higher-dimensional generalization of the "square root removal" trick (7.14), by introducing a vector Q with property $r = |Q|^2$, is the same as Dirac's trick of getting linear equation for spin 1/2 fermions by means of spinors. Vector spaces equipped with a product and a known satisfy $|Q \cdot Q| = |Q|^2$ define *normed algebras*. They appear in various physical applications - as quaternions, octonions, spinors. The technique was originally developed in celestial mechanics [41.6] to obtain numerically stable solutions for planetary motions. The basic idea was in place as early as 1931, when H. Hopf [41.14] used a KS transformation in order to illustrate a Hopf's invariant. The KS transformation for the collinear helium was introduced in ref. [41.2].

Remark 41.2 Complete binary symbolic dynamics. No stable periodic orbit and no exception to the binary symbolic dynamics of the collinear helium cycles have been found in numerical investigations. A proof that all cycles are unstable, that they are uniquely labeled by the binary symbolic dynamcis, and that this dynamics is complete is, however, still missing. The conjectured Markov partition of the phase space is given by the triple collision manifold, i.e., by those trajectories which start in or end at the singular point $r_1 = r_2 = 0$. See also ref. [41.2].

Remark 41.3 Spin and particle exchange symmetry. In our presentation of collinear helium we have completely ignored all dynamical effects due to the spin of the particles involved, such as the electronic spin-orbit coupling. Electrons are fermions and that determines the symmetry properties of the quantum states. The total wave function, including the spin degrees of freedom, must be antisymmetric under the electron-electron exchange transformation. That means that a quantum state symmetric in the position variables must have an antisymmetric spin wave function, i.e., the spins are antiparallel and the total spin is zero (singletstate). Antisymmetric states have symmetric spin wave function with total spin 1 (tripletstates). The threefold degeneracy of spin 1 states is lifted by the spin-orbit coupling.

Remark 41.4 Helium quantum numbers. The classification of the helium states in terms of single electron quantum numbers, sketched in sect. 41.5.1, prevailed until the 1960's; a growing discrepancy between experimental results and theoretical predictions made it necessary to refine this picture. In particular, the different Rydberg series sharing a given N-quantum number correspond, roughly speaking, to a quantization of the inter electronic angle Θ, see figure 41.1, and can not be described in terms of single electron quantum numbers l_1, l_2. The fact that

something is slightly wrong with the single electron picture laid out in sect. 41.5.1 is highlighted when considering the collinear configuration where both electrons are on the *same* side of the nucleus. As both electrons again have angular momentum equal to zero, the corresponding quantum states should also belong to single electron quantum numbers $(l_1, l_2) = (0, 0)$. However, the single electron picture breaks down completely in the limit $\Theta = 0$ where electron-electron interaction becomes the dominant effect. The quantum states corresponding to this classical configuration are distinctively different from those obtained from the collinear dynamics with electrons on different sides of the nucleus. The Rydberg series related to the classical $\Theta = 0$ dynamics are on the outermost rigth side in each N subspectrum in figure 41.6, and contain the energetically highest states for given N, n quantum numbers, see also remark 41.5. A detailed account of the historical development as well as a modern interpretation of the spectrum can be found in ref. [41.1].

Remark 41.5 Beyond the unstable collinear helium subspace. The semiclassical quantization of the chaotic collinear helium subspace is discussed in refs. [41.7, 41.8, 41.9]. Classical and semiclassical considerations beyond what has been discussed in sect. 41.5 follow several other directions, all outside the main of this book.

A classical study of the dynamics of collinear helium where both electrons are on the same side of the nucleus reveals that this configuration is fully stable both in the collinear plane and perpendicular to it. The corresponding quantum states can be obtained with the help of an approximate EBK-quantization which reveals helium resonances with extremely long lifetimes (quasi - bound states in the continuum). These states form the energetically highest Rydberg series for a given principal quantum number N, see figure 41.6. Details can be found in refs. [41.10, 41.11].

In order to obtain the Rydberg series structure of the spectrum, i.e., the succession of states converging to various ionization thresholds, we need to take into account the dynamics of orbits which make large excursions along the r_1 or r_2 axis. In the chaotic collinear subspace these orbits are characterized by symbol sequences of form $(a0^n)$ where a stands for an arbitrary binary symbol sequence and 0^n is a succession of n 0's in a row. A summation of the form $\sum_{n=0}^{\infty} t_{a0^n}$, where t_p are the cycle weights in (41.12), and cycle expansion of indeed yield all Rydberg states up the various ionization thresholds, see ref. [41.4]. For a comprehensive overview on spectra of two-electron atoms and semiclassical treatments ref. [41.1].

Résumé

We have covered a lot of ground starting with considerations of the classical properties of a three-body Coulomb problem, and ending with the semiclassical helium spectrum. We saw that the three-body problem restricted to the dynamics on a collinear appears to be fully chaotic; this implies that traditional semiclassical methods such as *WKB*quantization discussed in chapter 33 will not work and that we needed the full periodic orbit theory to obtain leads to the semiclassical spectrum of helium. As a piece of unexpected

⇓PRIVATE
⇑PRIVATE

luck the symbolic dynamics is simple, and the semiclassical quantization of the collinear dynamics yields an important part of the helium spectrum, including the ground state, to a reasonable accuracy. A sceptic might say: "Why bother with all the semiclassical considerations? A straightforward numerical quantum calculation achieves the same goal with better precision." While this is true, the semiclassical analysis offers new insights into the *structure* of the spectrum. We discovered that the dynamics perpendicular to the collinear plane was stable, giving rise to an additional (approximate) quantum number ℓ. We thus understood the origin of the different Rydberg series depicted in figure 41.6, a fact which is not at all obvious from a numerical solution of the quantum problem.

Having traversed the long road from the classical game of pinball all the way to a credible helium spectrum computation, we could declare victory and fold down this enterprise. Nevertheless, there is still much to think about - what about such quintessentially quantum effects as diffraction, tunnelling, ...? As we shall now see, the periodic orbit theory has still much of interest to offer.

References

[41.1] G. Tanner, J-M. Rost and K. Richter, Rev. Mod. Phys. **72**, 497 (2000).

[41.2] K. Richter, G. Tanner, and D. Wintgen, Phys. Rev. A **48**, 4182 (1993).

[41.3] Bürgers A., Wintgen D. and Rost J. M., J. Phys. B **28**, 3163 (1995).

[41.4] G. Tanner and D. Wintgen Phys. Rev. Lett. **75** 2928 (1995).

[41.5] P. Kustaanheimo and E. Stiefel, *J. Reine Angew. Math.* **218**, 204 (1965).

[41.6] E.L. Steifel and G. Scheifele, *Linear and regular celestial mechanics* (Springer, New York 1971).

[41.7] G.S. Ezra, K. Richter, G. Tanner and D. Wintgen, J. Phys. B **24**, L413 (1991).

[41.8] D. Wintgen, K. Richter and G. Tanner, CHAOS **2**, 19 (1992).

[41.9] R. Blümel and W. P. Reinhardt, *Directions in Chaos Vol 4*, eds. D. H. Feng and J.-M. Yuan (World Scientific, Hongkong), 245 (1992).

[41.10] K. Richter and D. Wintgen, J. Phys. B **24**, L565 (1991).

[41.11] D. Wintgen and K. Richter, Comments At. Mol. Phys. **29**, 261 (1994). why no reference to D. Delande?

[41.12] P. Kustaanheimo, *Ann. Univ. Turku, Ser. AI.,* **73** (1964).

[41.13] T. Levi-Civita, *Opere mathematische* **2** (1956).

[41.14] H. Hopf, *Math. Ann.* **104** (1931).

Exercises

helium!collinear
helium!collinear!Poincaré section
helium!collinear!cycles

Exercise 41.1 **Kustaanheimo–Stiefel transformation.** *Check the Kustaanheimo–Stiefel regularization for collinear helium; derive the Hamiltonian (7.17) and the collinear helium equations of motion (7.18).*

Tanner should check this exercise

Exercise 41.2 **Helium in the plane.** *Starting with the helium Hamiltonian in the infinite nucleus mass approximation $m_{he} = \infty$, and angular momentum $L = 0$, show that the three body problem can be written in terms of three independent coordinates only, the electron-nucleus distances r_1 and r_2 and the inter-electron angle Θ, see figure 7.1.*

Exercise 41.3 **Helium trajectories.** *Do some trial integrations of the collinear helium equations of motion (7.18). Due to the energy conservation, only three of the phase space coordinates (Q_1, Q_2, P_1, P_2) are independent. Alternatively, you can integrate in 4 dimensions and use the energy conservation as a check on the quality of your integrator.*

The dynamics can be visualized as a motion in the original configuration space (r_1, r_2), $r_i \geq 0$ quadrant, or, better still, by an appropriately chosen 2-d Poincaré section, exercise 41.4. Most trajectories will run away, do not be surprised - the classical collinear helium is unbound. Try to guess approximately the shortest cycle of figure 41.4.

Exercise 41.4 **A Poincaré section for collinear Helium.** *Construct a Poincaré section of figure 41.3b that reduces the helium flow to a map. Try to delineate regions which correspond to finite symbol sequences, i.e. initial conditions that follow the same topological itinerary in the figure 41.3a space for a finite number of bounces. Such rough partition can be used to initiate 2–dimensional Newton-Raphson method searches for helium cycles, exercise 41.5.*

Exercise 41.5 **Collinear helium cycles.** *The motion in the (r_1, r_2) plane is topologically similar to the pinball motion in a 3-disk system, except that the motion is in the Coulomb potential.*

Just as in the 3-disk system the dynamics is simplified if viewed in the fundamental domain, *in this case the region between r_1 axis and the $r_1 = r_2$ diagonal. Modify your integration routine so the trajectory bounces off the diagonal as off a mirror. Miraculously, the symbolic dynamics for the survivors again turns out to be binary, with 0 symbol signifying a bounce off the r_1 axis, and 1 symbol for a bounce off the diagonal. Just as in the 3-disk game of pinball, we thus know what cycles need to be computed for the cycle expansion (41.16).*

Guess some short cycles by requiring that topologically they correspond to sequences of bounces either returning to the same r_i axis or reflecting off the diagonal. Now either Use special symmetries of orbits such as self-retracing to find all orbits up to length 5 by a 1-dimensional Newton search.

Exercise 41.6 **Collinear helium cycle stabilities.** *Compute the eigenvalues for the cycles you found in exercise 41.5, as described in sect. 41.3. You may either integrate the reduced 2×2 matrix using equations (41.6) together with the generating function $\mathbf{l}$ given in local coordinates by (41.7) or integrate the full 4×4 Jacobian matrix, see sect. 20.1.* [15] *Integration in 4 dimensions should give eigenvalues of the form $(1, 1, \Lambda_p, 1/\Lambda_p)$; The unit eigenvalues are due to the usual periodic orbit invariances; displacements along the orbit as well as perpendicular to the energy manifold are conserved; the latter one provides a check of the accuracy of your computation. Compare with table 41.3; you should get the actions and Lyapunov exponents right, but topological indices and stability angles we take on faith.*

helium!collinear!stabilities
helium!collinear!eigenenergies

Exercise 41.7 **Helium eigenenergies.** *Compute the lowest eigenenergies of singlet and triplet states of helium by substituting cycle data into the cycle expansion (41.16) for the symmetric and antisymmetric zeta functions (41.15). Probably the quickest way is to plot the magnitude of the zeta function as function of real energy and look for the minima. As the eigenenergies in general have a small imaginary part, a contour plot such as figure 18.1, can yield informed guesses. Better way would be to find the zeros by Newton method, sect. 18.2.3. How close are you to the cycle expansion and quantum results listed in table 41.2? You can find more quantum data in ref. [41.3].*

[15] Tanner: reference missing

⇓PRIVATE

Chapter 42

Periodic orbit theory of diffraction

> You know that love
> Will creep in service when it cannot go.
> William Shakespeare: Two Gentlemen of Verona, act iv. sc. 2.
>
> (Andreas Wirzba)

We will cast here the leading quantum diffraction effects in scattering into periodic orbit form, by including into the cycle expansions complex saddles as well.

We start by a brief review of the elastic scattering of a point particle from finite collection of non-overlapping scattering regions in terms of the standard textbook scattering theory, and then develop Keller's semiclassical diffraction theory for scattering off n disks in a plane.

42.1 Semiclassical creeping contributions

> Children learne to creepe ere they can learne to goe
> John Heywood, Proverbes 1546

For periodic orbits with creeping sections [38.23, ?, ?, ?, ?] the symbolic alphabet has to be extended. Furthermore, depending on the geometry, there might be nontrivial pruning rules based on the so called ghost orbits, see refs. [38.12, 38.24].

If the creeping contributions are taken into account, the symbolic dynamics has to be generalized from single-letter symbols $\{j_i\}$ to triple-letter symbols $\{j_i, s_i \times \ell_i\}$ with $\ell_i \geq 1$ integer valued and $s_i = 0, \pm 1$ [1] By definition, the

[1] Actually, these are double-letter symbols as s_i and l_i are only counted as a product.

value $s_i = 0$ represents the non-creeping case, such that $\{j_i, 0 \times \ell_i\} = \{j_i, 0\} = \{j_i\}$ reduces to the old single-letter symbol. The magnitude of a nonzero ℓ_i corresponds to creeping sections of mode number $|\ell_i|$, whereas the sign $s_i = \pm 1$ signals whether the creeping path turns around the disk j_i in the positive or negative sense. Additional full creeping turns around a disk j' can be summed up as a geometrical series; therefore they do not lead to the introduction of a further symbol.

Hence, we finally obtain the semiclassical result for the determinant of $\mathbf{S}^{(1)}(ka)$

$$\det \mathbf{S}^{(1)}(ka) \sim e^{-i2\pi N(k)} \frac{\prod_{\ell=1}^{\infty} \left(1 - e^{-2i\pi\bar{\nu}_\ell(ka)}\right)^2}{\prod_{\ell=1}^{\infty} \left(1 - e^{2i\pi\nu_\ell(ka)}\right)^2} \ , \tag{42.1}$$

with the creeping exponential

$$\begin{aligned} \nu_\ell(ka) &= ka + e^{+i\pi/3}(ka/6)^{1/3} q_\ell + \cdots = ka + i\alpha_\ell(ka) + \cdots & (42.2) \\ \bar{\nu}_\ell(ka) &= ka + e^{-i\pi/3}(ka/6)^{1/3} q_\ell + \cdots = ka - i(\alpha_\ell(k^* a))^* + \cdots \\ &= (\nu_\ell(k^* a))^* \ , & (42.3) \end{aligned}$$

Remark 42.1 Sources. This section is based on appendix E of ref. [M.1].

There are three possibilities of "semiclassical" contact of the point particle with the disk j_i:

1. either geometrical which in turn splits into three alternatives
   (a) *specular reflection* to the right,
   (b) *specular reflection* to the left,
   (c) or *'ghost tunneling'* where the latter induce the nontrivial pruning rules (as discussed above)
2. or *right-handed creeping turns*
3. or *left-handed creeping turns*.

See figure **??**. The specular reflection to the right is linked to a left-handed creeping path with a knot. The specular reflection to the left matches a right-handed creeping path with a knot, whereas the creeping paths in the ghost tunneling case are topologically trivial. In fact, the topology of the creeping paths encodes the choice between the three alternatives for the geometrical contact of the disk. This is the case for the simple reason that creeping sections have to be positive definite in length: the creeping amplitude has to decrease during the creeping process, as tangential rays are constantly emitted. In mathematical terms, it means that the creeping angle has to be positive. Thus, the positivity of the *two* creeping angles for

the left *and* right turn uniquely specifies which of the three alternatives, either specular reflection to the right or to the left or straight "ghost" tunneling through disk j, is realized for the semiclassical geometrical path. Hence, the existence of a saddlepoint is guaranteed.

References

[42.1] G. Vattay, A. Wirzba and P.E. Rosenqvist, *Phys. Rev. Lett.* **73**, 2304 (1994); *Proceedings of the International Conference on Dynamical Systems and Chaos: vol. 2*, Y. Aizawa, S. Saito and K. Shiraiwa eds. (World Scientific, Singapore, 1994).

[42.2] H. Bruus and N. D. Whelan, Nonlinearity, **9**, 1 (1996).

[42.3] P. E. Rosenqvist, N. D. Whelan and A. Wirzba, J. Phys. A **29**, 5441 (1996).

M. Berry recommends: Weyl formula for acoustics Balian and Bloch (1971)

⇑PRIVATE

Chapter 43

Diffraction distraction

(N. Whelan)

Diffraction effects characteristic to scattering off wedges are incorporated into the periodic orbit theory.

43.1 Quantum eavesdropping

As noted in chapter 41, the classical mechanics of the helium atom is undefined at the instant of a triple collision. This is a common phenomenon - there is often some singularity or discontinuity in the classical mechanics of physical systems. This discontinuity can even be helpful in classifying the dynamics. The points in phase space which have a past or future at the discontinuity form manifolds which divide the phase space and provide the symbolic dynamics. The general rule is that quantum mechanics smoothes over these discontinuities in a process we interpret as diffraction. We solve the local diffraction problem quantum mechanically and then incorporate this into our global solution. By doing so, we reconfirm the central leitmotif of this treatise: think locally - act globally.

While being a well-motivated physical example, the helium atom is somewhat involved. In fact, so involved that we do not have a clue how to do it. In its place we illustrate the concept of diffractive effects with a pinball game. There are various classes of discontinuities which a billiard can have. There may be a grazing condition such that some trajectories hit a smooth surface while others are unaffected - this leads to the creeping described in chapter 38. There may be a vertex such that trajectories to one side bounce differently from those to the other side. There may be a point scatterer or a magnetic flux line such that we do not know how to continue classical mechanics through the discontinuities. In what follows, we specialize the discussion to the second example - that of vertices or wedges. To further simplify the discussion, we consider the special case of a half line which can be thought of as a wedge of angle zero.

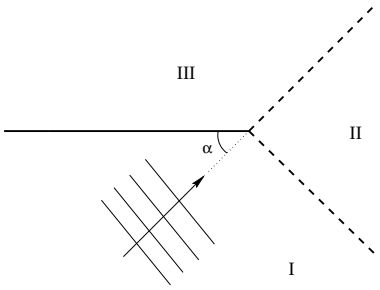

Figure 43.1: Scattering of a plane wave off a half line.

We start by solving the problem of the scattering of a plane wave off a half line (see figure 43.1). This is the local problem whose solution we will use to construct a global solution of more complicated geometries. We define the vertex to be the origin and launch a plane wave at it from an angle α. What is the total field? This is a problem solved by Sommerfeld in 1896 and our discussion closely follows his.

The total field consists of three parts - the incident field, the reflected field and the diffractive field. Ignoring the third of these for the moment, we see that the space is divided into three regions. In region I there is both an incident and a reflected wave. In region II there is only an incident field. In region III there is nothing so we call this the shadowed region. However, because of diffraction the field does enter this region. This accounts for why you can overhear a conversation if you are on the opposite side of a thick wall but with a door a few meters away. Traditionally such effects have been ignored in semiclassical calculations because they are relatively weak. However, they can be significant.

To solve this problem Sommerfeld worked by analogy with the full line case, so let us briefly consider that much simpler problem. There we know that the problem can be solved by images. An incident wave of amplitude A is of the form

$$v(r,\psi) = Ae^{-ikr\cos\psi} \tag{43.1}$$

where $\psi = \phi - \alpha$ and ϕ is the angular coordinate. The total field is then given by the method of images as

$$v_{\rm tot} = v(r,\phi-\alpha) - v(r,\phi+\alpha), \tag{43.2}$$

where the negative sign ensures that the boundary condition of zero field on the line is satisfied.

Sommerfeld then argued that $v(r,\psi)$ can also be given a complex integral representation

$$v(r,\psi) = A\int_C d\beta f(\beta,\psi)e^{-ikr\cos\beta}. \tag{43.3}$$

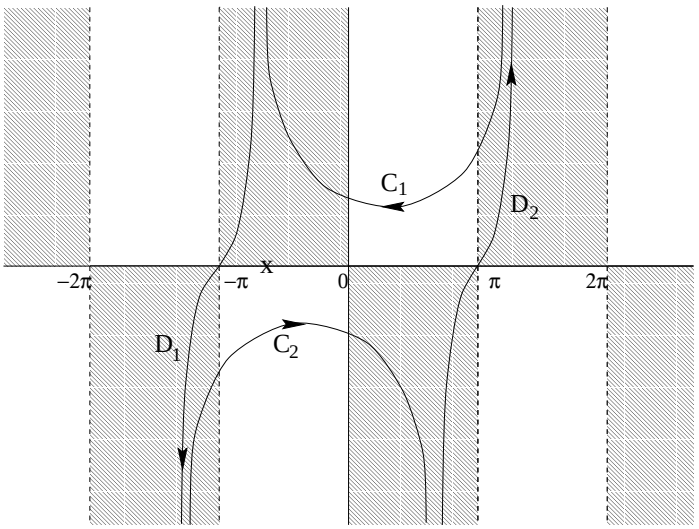

Figure 43.2: The contour in the complex β plane. The pole is at $\beta = -\psi$ (marked by $\times$ in the figure) and the integrand approaches zero in the shaded regions as the magnitude of the imaginary part of β approaches infinity.

This is certainly correct if the function $f(\beta, \psi)$ has a pole of residue $1/2\pi i$ at $\beta = -\psi$ and if the contour C encloses that pole. One choice is

$$f(\beta, \psi) = \frac{1}{2\pi} \frac{e^{i\beta}}{e^{i\beta} - e^{-i\psi}}. \tag{43.4}$$

(We choose the pole to be at $\beta = -\psi$ rather than $\beta = \psi$ for reasons discussed later.) One valid choice for the contour is shown in figure 43.2. This encloses the pole and vanishes as $|\mathrm{Im}\,\beta| \to \infty$ (as denoted by the shading). The sections D_1 and D_2 are congruent because they are displaced by 2π. However, they are traversed in an opposite sense and cancel, so our contour consists of just the sections C_1 and C_2. The motivation for expressing the solution in this complicated manner should become clear soon.

What have we done? We extended the space under consideration by a factor of two and then constructed a solution by assuming that there is also a source in the unphysical space. We superimpose the solutions from the two sources and at the end only consider the solution in the physical space to be meaningful. Furthermore, we expressed the solution as a contour integral which reflects the 2π periodicity of the problem. The half line scattering problem follows by analogy.

Whereas for the full line the field is periodic in 2π, for the half line it is periodic in 4π. This can be seen by the fact that the field can be expanded in a series of the form $\{\sin(\phi/2), \sin(\phi), \sin(3\phi/2), \cdots\}$. As above, we extend the space by thinking of it as two sheeted. The physical sheet is as shown in figure 43.1 and the unphysical sheet is congruent to it. The sheets are glued together along the half line so that a curve in the physical space which

intersects the half line is continued in the unphysical space and vice-versa. The boundary conditions are that the total field is zero on both faces of the half line (which are physically distinct boundary conditions) and that as $r \to \infty$ the field is composed solely of plane waves and outgoing circular waves of the form $g(\phi)\exp(ikr)/\sqrt{kr}$. This last condition is a result of Huygens' principle.

We assume that the complete solution is also given by the method of images as

$$v_{\rm tot} = u(r, \phi - \alpha) - u(r, \phi + \alpha). \tag{43.5}$$

where $u(r, \psi)$ is a 4π-periodic function to be determined. The second term is interpreted as an incident field from the unphysical space and the negative sign guarantees that the solution vanishes on both faces of the half line. Sommerfeld then made the ansatz that u is as given in equation (43.3) with the same contour $C_1 + C_2$ but with the 4π periodicity accounted for by replacing equation (43.4) with

$$f(\beta, \psi) = \frac{1}{4\pi} \frac{e^{i\beta/2}}{e^{i\beta/2} - e^{-i\psi/2}}. \tag{43.6}$$

(We divide by 4π rather than 2π so that the residue is properly normalized.) The integral (43.3) can be thought of as a linear superposition of an infinity of plane waves each of which satisfies the Helmholtz equation $(\nabla^2 + k^2)v = 0$, and so their combination also satisfies the Helmholtz equation. We will see that the diffracted field is an outgoing circular wave; this being a result of choosing the pole at $\beta = -\psi$ rather than $\beta = \psi$ in equation (43.4). Therefore, this ansatz is a solution of the equation and satisfies all boundary conditions and therefore constitutes a valid solution. By uniqueness this is the only solution.

In order to further understand this solution, it is useful to massage the contour. Depending on ϕ there may or may not be a pole between $\beta = -\pi$ and $\beta = \pi$. In region I, both functions $u(r, \phi \pm \alpha)$ have poles which correspond to the incident and reflected waves. In region II, only $u(r, \phi - \alpha)$ has a pole corresponding to the incident wave. In region III there are no poles because of the shadow. Once we have accounted for the geometrical waves (i.e., the poles), we extract the diffracted waves by saddle point analysis at $\beta = \pm\pi$. We do this by deforming the contours C so that they go through the saddles as shown in figure 43.2.

Contour C_1 becomes $E_2 + F$ while contour C_2 becomes $E_1 - F$ where the minus sign indicates that it is traversed in a negative sense. As a result, F has no net contribution and the contour consists of just E_1 and E_2.

As a result of these machinations, the curves E are simply the curves D of figure 43.2 but with a reversed sense. Since the integrand is no longer 2π

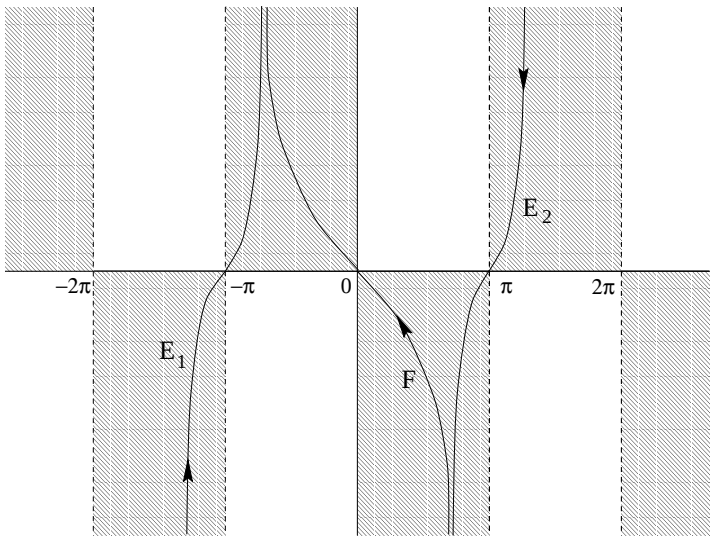

Figure 43.3: The contour used to evaluate the diffractive field after the contribution of possible poles has been explicitly evaluated. The curve F is traversed twice in opposite directions and has no net contribution.

stationary!phase approximation
Green's function!diffraction
diffraction!Green's function

periodic, the contributions from these curves no longer cancel. We evaluate both stationary phase integrals to obtain

$$u(r,\psi) \approx -A\frac{e^{i\pi/4}}{\sqrt{8\pi}}\sec(\psi/2)\frac{e^{ikr}}{\sqrt{kr}} \tag{43.7}$$

so that the total diffracted field is

$$v_{\rm diff} = -A\frac{e^{i\pi/4}}{\sqrt{8\pi}}\left(\sec\left(\frac{\phi-\alpha}{2}\right)-\sec\left(\frac{\phi+\alpha}{2}\right)\right)\frac{e^{ikr}}{\sqrt{kr}}. \tag{43.8}$$

Note that this expression breaks down when $\phi \pm \alpha = \pi$. These angles correspond to the borders among the three regions of figure 43.1 and must be handled more carefully - we can not do a stationary phase integral in the vicinity of a pole. However, the integral representation (43.3) and (43.6) is uniformly valid.

43.1
page 816

We now turn to the simple task of translating this result into the language of semiclassical Green's functions. Instead of an incident plane wave, we assume a source at point x' and then compute the resulting field at the receiver position x. If x is in region I, there is both a direct term, and a reflected term, if x is in region II there is only a direct term and if x is in region III there is neither. In any event these contributions to the semiclassical Green's function are known since the free space Green's function between two points x_2 and x_1 is

$$G_{\rm f}(x_2,x_1,k) = -\frac{i}{4}H_0^{(+)}(kd) \approx -\frac{1}{\sqrt{8\pi kd}}\exp\{i(kd+\pi/4)\}, \tag{43.9}$$

where d is the distance between the points. For a reflection, we need to multiply by -1 and the distance is the length of the path via the reflection point. Most interesting for us, there is also a diffractive contribution to the Green's function. In equation (43.8), we recognize that the coefficient A is simply the intensity at the origin if there were no scatterer. This is therefore replaced by the Green's function to go from the source to the vertex which we label x_V. Furthermore, we recognize that $\exp(ikr)/\sqrt{kr}$ is, within a proportionality constant, the semiclassical Green's function to go from the vertex to the receiver.

Collecting these facts, we say

$$G_{\rm diff}(x,x',k) = G_{\rm f}(x,x_V,k)d(\theta,\theta')G_{\rm f}(x_V,x',k), \tag{43.10}$$

where, by comparison with equations (43.8) and (43.9), we have

$$d(\theta,\theta') = \sec\left(\frac{\theta-\theta'}{2}\right) - \sec\left(\frac{\theta+\theta'}{2}\right). \tag{43.11}$$

Here θ' is the angle to the source as measured from the vertex and θ is the angle to the receiver. They were denoted as α and ϕ previously. Note that there is a symmetry between the source and receiver as we expect for a time-reversal invariant process. Also the diffraction coefficient d does not depend on which face of the half line we use to measure the angles. As we will see, a very important property of $G_{\rm diff}$ is that it is a simple multiplicative combination of other semiclassical Green's functions.

43.2
page 816

We now recover our classical perspective by realizing that we can still think of classical trajectories. In calculating the quantum Green's function, we sum over the contributions of various paths. These include the classical trajectories which connect the points and also paths which connect the points via the vertex. These have different weights as given by equations (43.9) and (43.10) but the concept of summing over classical paths is preserved.

For completeness, we remark that there is an exact integral representation for the Green's function in the presence of a wedge of arbitrary opening angle [43.15]. It can be written as

$$G(x,x',k) = g(r,r',k,\theta'-\theta) - g(r,r',k,\theta'+\theta) \tag{43.12}$$

where (r,θ) and (r',θ') are the polar coordinates of the points x and x' as measured from the vertex and the angles are measured from either face of the wedge. The function g is given by

$$g(r,r',k,\psi) = \frac{i}{8\pi\nu}\int_{C_1+C_2} d\beta \frac{H_0^+(k\sqrt{r^2+r'^2-2rr'\cos\beta})}{1-\exp\left(i\frac{\beta+\psi}{\nu}\right)} \tag{43.13}$$

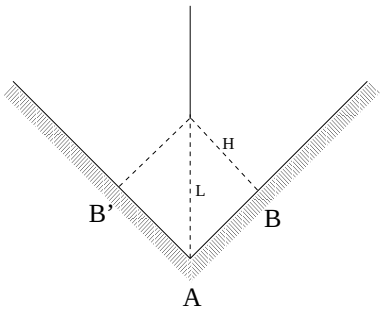

Figure 43.4: The billiard considered here. The dynamics consists of free motion followed by specular reflections off the faces. The top vertex induces diffraction while the bottom one is a right angle and induces two specular geometric reflections.

where $\nu = \gamma/\pi$ and γ is the opening angle of the wedge. (ie $\gamma = 2\pi$ in the case of the half plane). The contour $C_1 + C_2$ is the same as shown in figure 43.2.

The poles of this integral give contributions which can be identified with the geometric paths connecting x and x'. The saddle points at $\beta = \pm\pi$ give contributions which can be identified with the diffractive path connecting x and x'. The saddle point analysis allows us to identify the diffraction constant as

$$d(\theta,\theta') = -\frac{4\sin\frac{\pi}{\nu}}{\nu}\frac{\sin\frac{\theta}{\nu}\sin\frac{\theta'}{\nu}}{\left(\cos\frac{\pi}{\nu}-\cos\frac{\theta+\theta'}{\nu}\right)\left(\cos\frac{\pi}{\nu}-\cos\frac{\theta-\theta'}{\nu}\right)}, \qquad (43.14)$$

which reduces to (43.11) when $\nu = 2$. Note that the diffraction coefficient vanishes identically if $\nu = 1/n$ where n is any integer. This corresponds to wedge angles of $\gamma = \pi/n$ (eg. n=1 corresponds to a full line and n=2 corresponds to a right angle). This demonstration is limited by the fact that it came from a leading order asymptotic expansion but the result is quite general. For such wedge angles, we can use the method of images (we will require $2n-1$ images in addition to the actual source point) to obtain the Green's function and there is no diffractive contribution to any order. Classically this corresponds to the fact that for such angles, there is no discontinuity in the dynamics. Trajectories going into the vertex can be continued out of them unambiguously. This meshes with the discussion in the introduction where we argued that diffractive effects are intimately linked with classical discontinuities.

The integral representation is also useful because it allows us to consider geometries such that the angles are near the optical boundaries or the wedge angle is close to π/n. For these geometries the saddle point analysis leading to (43.14) is invalid due to the existence of a nearby pole. In that event, we require a more sophisticated asymptotic analysis of the full integral representation.

43.2 An application

Although we introduced diffraction as a correction to the purely classical effects; it is instructive to consider a system which can be quantized solely

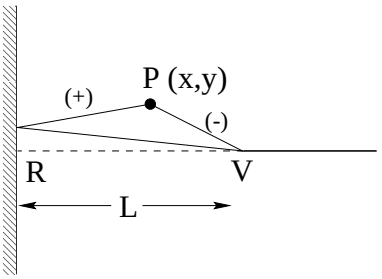

Figure 43.5: The dashed line shows a simple periodic diffractive orbit γ. Between the vertex V and a point P close to the orbit there are two geometric legs labeled $\pm$. The origin of the coordinate system is chosen to be at R.

in terms of periodic diffractive orbits. Consider the geometry shown in figure 43.4 The classical mechanics consists of free motion followed by specular reflections off faces. The upper vertex is a source of diffraction while the lower one is a right angle and induces no diffraction. This is an open system, there are no bound states - only scattering resonances. However, we can still test the effectiveness of the theory in predicting them. Formally, scattering resonances are the poles of the scattering S matrix and by an identity of Balian and Bloch are also poles of the quantum Green's function. We demonstrate this fact in chapter 38 for 2-dimensional scatterers. The poles have complex wavenumber k, as for the 3-disk problem.

Let us first consider how diffractive orbits arise in evaluating the trace of G which we call $g(k)$. Specifying the trace means that we must consider all paths which close on themselves in the configuration space while stationary phase arguments for large wavenumber k extract those which are periodic - just as for classical trajectories. In general, $g(k)$ is given by the sum over all diffractive and geometric orbits. The contribution of the simple diffractive orbit labeled γ shown in figure 43.5 to $g(k)$ is determined as follows.

We consider a point P just a little off the path and determine the semiclassical Green's function to return to P via the vertex using (43.9) and (43.10). To leading order in y the lengths of the two geometric paths connecting P and V are $d_\pm = (L \pm x) + y^2/(L \pm x)^2/2$ so that the phase factor $ik(d_+ + d_-)$ equals $2ikL + iky^2/(L^2 - x^2)$. The trace integral involves integrating over all points P and is

$$g_\gamma(k) \approx -2d_\gamma \frac{e^{i(2kL+\pi/2)}}{8\pi k} \int_0^L \frac{dx}{\sqrt{L^2-x^2}} \int_{-\infty}^{\infty} dy e^{\left(iky^2 \frac{L}{L^2-x^2}\right)} . \quad (43.15)$$

We introduced an overall negative sign to account for the reflection at the hard wall and multiplied by 2 to account for the two traversal senses, $VRPV$ and $VPRV$. In the spirit of stationary phase integrals, we have neglected the y dependence everywhere except in the exponential. The diffraction constant d_γ is the one corresponding to the diffractive periodic orbit. To evaluate the y integral, we use the identity

$$\int_{-\infty}^{\infty} d\xi e^{ia\xi^2} = e^{i\pi/4}\sqrt{\frac{\pi}{a}}, \quad (43.16)$$

and thus obtain a factor which precisely cancels the x dependence in the x

integral. This leads to the rather simple result

$$g_\gamma \approx -\frac{il_\gamma}{2k}\left\{\frac{d_\gamma}{\sqrt{8\pi k l_\gamma}}\right\} e^{i(kl_\gamma+\pi/4)} \tag{43.17}$$

where $l_\gamma = 2L$ is the length of the periodic diffractive orbit. A more sophisticated analysis of the trace integral has been done [43.6] using the integral representation (43.13). It is valid in the vicinity of an optical boundary and also for wedges with opening angles close to π/n.

Consider a periodic diffractive orbit with n_γ reflections off straight hard walls and μ_γ diffractions each with a diffraction constant $d_{\gamma,j}$. The total length of the orbit $L_\gamma = \sum l_{\gamma,j}$ is the sum of the various diffractive legs and l_γ is the length of the corresponding prime orbit. For such an orbit, (43.17) generalizes to

$$g_\gamma(k) = -\frac{il_\gamma}{2k}\left\{\prod_{j=1}^{\mu_\gamma}\frac{d_{\gamma,j}}{\sqrt{8\pi k l_{\gamma,j}}}\right\}\exp\left\{i(kL_\gamma + n_\gamma\pi - 3\mu_\gamma\pi/4)\right\}. \tag{43.18}$$

Each diffraction introduces a factor of $1/\sqrt{k}$ and multi-diffractive orbits are thereby suppressed.

43.3 page 816

If the orbit γ is prime then $L_\gamma = l_\gamma$. If γ is the r'th repeat of a prime orbit β we have $L_\gamma = rl_\beta$, $n_\gamma = rp_\beta$ and $\mu_\gamma = r\sigma_\beta$, where l_β, p_β and σ_β all refer to the prime orbit. We can then write

$$g_\gamma = g_{\beta,r} = -\frac{il_\beta}{2k}t_\beta^r \tag{43.19}$$

where

$$t_\beta = \left\{\prod_{j=1}^{\sigma_\beta}\frac{d_{\beta,j}}{\sqrt{8\pi k l_{\beta,j}}}\right\}\exp\left\{i(kl_\beta + p_\beta\pi - 3\sigma_\beta\pi/4)\right\}. \tag{43.20}$$

It then makes sense to organize the sum over diffractive orbits as a sum over the prime diffractive orbits and a sum over the repetitions

$$g_{\rm diff}(k) = \sum_\beta\sum_{r=1}^{\infty} g_{\beta,r} = -\frac{i}{2k}\sum_\beta l_\beta\frac{t_\beta}{1-t_\beta}. \tag{43.21}$$

We cast this as a logarithmic derivative (15.8) by noting that $\frac{dt_\beta}{dk} = il_\beta t_\beta - \sigma_\beta t_\beta/2k$ and recognizing that the first term dominates in the semiclassical limit. It follows that

$$g_{\rm diff}(k) \approx \frac{1}{2k}\frac{d}{dk}\left\{\ln\prod_\beta(1-t_\beta)\right\}. \tag{43.22}$$

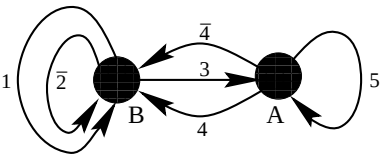

Figure 43.6: The two-node Markov graph with all the diffractive processes connecting the nodes.

In the case that there are only diffractive periodic orbits - as in the geometry of figure 43.4 - the poles of $g(k)$ are the zeros of a dynamical zeta function

$$1/\zeta(k) = \prod_{\beta}(1 - t_\beta). \tag{43.23}$$

For geometric orbits, this function would be evaluated with a cycle expansion as discussed in chapter 18. However, here we can use the multiplicative nature of the weights t_β to find a closed form representation of the function using a Markov graph, as in sect. 11.5.1. This multiplicative property of the weights follows from the fact that the diffractive Green's function (43.10) is multiplicative in segment semiclassical Green's functions, unlike the geometric case.

There is a reflection symmetry in the problem which means that all resonances can be classified as even or odd. Because of this, the dynamical zeta function factorizes as $1/\zeta = 1/\zeta_+\zeta_-$ (as explained in sects. 22.5 and 22.1.2) and we determine $1/\zeta_+$ and $1/\zeta_-$ separately using the ideas of symmetry decomposition of chapter 22.

In the Markov graph shown in figure 43.6, we enumerate all processes. We start by identifying the fundamental domain as just the right half of figure 43.4. There are two nodes which we call A and B. To get to another node from B, we can diffract (always via the vertex) in one of three directions. We can diffract back to B which we denote as process 1. We can diffract to B's image point B' and then follow this by a reflection. This process we denote as $\bar{2}$ where the bar indicates that it involves a reflection. Thirdly, we can diffract to node A. Starting at A we can also diffract to a node in three ways. We can diffract to B which we denote as 4. We can diffract to B' followed by a reflection which we denote as $\bar{4}$. Finally, we can diffract back to A which we denote as process 5. Each of these processes has its own weight which we can determine from the earlier discussion. First though, we construct the dynamical zeta functions.

The dynamical zeta functions are determined by enumerating all closed loops which do not intersect themselves in figure 43.6. We do it first for $1/\zeta_+$ because that is simpler. In that case, the processes with bars are treated on an equal footing as the others. Appealing back to sect. 22.5 we find

$$\begin{aligned} 1/\zeta_+ &= 1 - t_1 - t_{\bar{2}} - t_5 - t_3t_4 - t_3t_{\bar{4}} + t_5t_1 + t_5t_{\bar{2}}\,, \\ &= 1 - (t_1 + t_{\bar{2}} + t_5) - 2t_3t_4 + t_5(t_1 + t_{\bar{2}}) \end{aligned} \tag{43.24}$$

where we have used the fact that $t_4 = t_{\bar{4}}$ by symmetry. The last term has a positive sign because it involves the product of shorter closed loops. To calculate $1/\zeta_-$, we note that the processes with bars have a relative negative sign due to the group theoretic weight. Furthermore, process 5 is a boundary orbit (see sect. 22.3.1) and only affects the even resonances - the terms involving t_5 are absent from $1/\zeta_-$. The result is

$$\begin{aligned} 1/\zeta_- &= 1 - t_1 + t_{\bar{2}} - t_3 t_4 + t_3 t_{\bar{4}}\,, \\ &= 1 - (t_1 - t_{\bar{2}}). \end{aligned} \tag{43.25}$$

Note that these expressions have a finite number of terms and are not in the form of a curvature expansion, as for the 3-disk problem.

43.4 page 816

It now just remains to fix the weights. We use equation (43.20) but note that each weight involves just one diffraction constant. It is then convenient to define the quantities

$$u_A^2 = \frac{\exp\{i(2kL + 2\pi)\}}{\sqrt{16\pi kL}} \qquad u_B^2 = \frac{\exp\{i(2kH + \pi)\}}{\sqrt{16\pi kH}}. \tag{43.26}$$

The lengths L and $H = L/\sqrt{2}$ are defined in figure 43.4; we set $L = 1$ throughout. Bouncing inside the right angle at A corresponds to two specular reflections so that $p = 2$. We therefore explicitly include the factor $\exp(i2\pi)$ in (43.26) although it is trivially equal to one. Similarly, there is one specular reflection at point B giving $p = 1$ and therefore a factor of $\exp(i\pi)$. We have defined u_A and u_B because, together with some diffraction constants, they can be used to construct all of the weights. Altogether we define four diffraction coefficients: d_{AB} is the constant corresponding to diffracting from B to A and is found from (43.11) with $\theta' = 3\pi/4$ and $\theta = \pi$ and equals $2\sec(\pi/8) \approx 2.165$. With analogous notation, we have d_{AA} and $d_{BB} = d_{B'B}$ which equal 2 and $1 + \sqrt{2}$ respectively. $d_{ij} = d_{ji}$ due to the Green's function symmetry between source and receiver referred to earlier. Finally, there is the diffractive phase factor $s = \exp(-i3\pi/4)$ each time there is a diffraction. The weights are then as follows:

$$\begin{aligned} t_1 = sd_{BB}u_B^2 \quad t_{\bar{2}} &= sd_{B'B}u_B^2 \quad t_3 = t_4 = t_{\bar{4}} = sd_{AB}u_A u_B \\ t_5 &= sd_{AA}u_A^2. \end{aligned} \tag{43.27}$$

Each weight involves two u's and one d. The u's represent the contribution to the weight from the paths connecting the nodes to the vertex and the d gives the diffraction constant connecting the two paths.

The equality of d_{BB} and $d_{B'B}$ implies that $t_1 = t_{\bar{2}}$. From (43.25) this means that there are no odd resonances because 1 can never equal 0. For the even resonances equation (43.24) is an implicit equation for k which has zeros shown in figure 43.7.

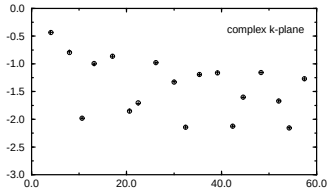

Figure 43.7: The even resonances of the wedge scatterer of figure 43.4 plotted in the complex $k-$plane, with $L = 1$. The exact resonances are represented as circles and their semiclassical approximations as crosses.

For comparison we also show the result from an exact quantum calculation. The agreement is very good right down to the ground state - as is so often the case with semiclassical calculations. In addition we can use our dynamical zeta function to find arbitrarily high resonances and the results actually improve in that limit. In the same limit, the exact numerical solution becomes more difficult to find so the dynamical zeta function approximation is particularly useful in that case.

43.5
page 816

In general a system will consist of both geometric and diffractive orbits. In that case, the full dynamical zeta function is the product of the geometric zeta function and the diffractive one. The diffractive weights are typically smaller by order $O(1/\sqrt{k})$ but for small k they can be numerically competitive so that there is a significant diffractive effect on the low-lying spectrum. It might be expected that higher in the spectrum, the effect of diffraction is weaker due to the decreasing weights. However, it should be pointed out that an analysis of the situation for creeping diffraction [43.7] concluded that the diffraction is actually *more* important higher in the spectrum due to the fact that an ever greater fraction of the orbits need to be corrected for diffractive effects. The equivalent analysis has not been done for edge diffraction but a similar conclusion can probably be expected.

To conclude this chapter, we return to the opening paragraph and discuss the possibility of doing such an analysis for helium. The important point which allowed us to successfully analyze the geometry of figure 43.4 is that when a trajectory is near the vertex, we can extract its diffraction constant without reference to the other facets of the problem. We say, therefore, that this is a "local" analysis for the purposes of which we have "turned off" the other aspects of the problem, namely sides AB and AB'. By analogy, for helium, we would look for some simpler description of the problem which applies near the three body collision. However, there is nothing to "turn off". The local problem is just as difficult as the global one since they are precisely the same problem, just related by scaling. Therefore, it is not at all clear that such an analysis is possible for helium.

Commentary

Remark 43.1 Classical discontinuities. Various classes of discontinuities for billiard and potential problems discussed in the literature:

- a grazing condition such that some trajectories hit a smooth surface while others are unaffected, refs. [43.1, 43.2, 43.3, 43.7]

- a vertex such that trajectories to one side bounce differently from those to the other side, refs. [43.2, 43.4, 43.5, 43.8, 43.9].
- a point scatterer [43.10, 43.11] or a magnetic flux line [43.12, 43.13] such that we do not know how to continue classical mechanics through the discontinuities.

diffraction!Sommerfeld
Sommerfeld!diffraction
diffraction!Keller
Keller!diffraction

Remark 43.2 Geometrical theory of diffraction. In the above discussion we borrowed heavily from the ideas of Keller who was interested in extending the geometrical ray picture of optics to cases where there is a discontinuity. He maintained that we could hang onto that ray-tracing picture by allowing rays to strike the vertex and then leave at any angle with amplitude (43.8). Both he and Sommerfeld were thinking of optics and not quantum mechanics and they did not phrase the results in terms of semiclassical Green's functions but the essential idea is the same.

Remark 43.3 Generalizations Consider the effect of replacing our half line by a wedge of angle γ_1 and the right angle by an arbitrary angle γ_2. If $\gamma_2 > \gamma_1$ and $\gamma_2 \geq \pi/2$ this is an open problem whose solution is given by equations (43.24) and (43.25) (there will then be odd resonances) but with modified weights reflecting the changed geometry [43.8]. (For $\gamma_2 < \pi/2$, more diffractive periodic orbits appear and the dynamical zeta functions are more complicated but can be calculated with the same machinery.) When $\gamma_2 = \gamma_1$, the problem in fact has bound states [43.21, 43.22]. This last case has been of interest in studying electron transport in mesoscopic devices and in microwave waveguides. However we can not use our formalism as it stands because the diffractive periodic orbits for this geometry lie right on the border between illuminated and shadowed regions so that equation (43.7) is invalid. Even the more uniform derivation of [43.6] fails for that particular geometry, the problem being that the diffractive orbit actually lives on the edge of a family of geometric orbits and this makes the analysis still more difficult.

Remark 43.4 Diffractive Green's functions. The result (43.17) is proportional to the length of the orbit times the semiclassical Green's function (43.9) to go from the vertex back to itself along the classical path. The multi-diffractive formula (43.18) is proportional to the total length of the orbit times the product of the semiclassical Green's functions to go from one vertex to the next along classical paths. This result generalizes to any system — either a pinball or a potential — which contains point singularities such that we can define a diffraction constant as above. The contribution to the trace of the semiclassical Green's function coming from a diffractive orbit which hits the singularities is proportional to the total length (or period) of the orbit times the product of semiclassical Green's functions in going from one singularity to the next. This result first appeared in reference [43.2] and a derivation can be found in reference [43.9]. A similar structure also exists for creeping [43.2].

Remark 43.5 Diffractive orbits for hydrogenic atoms. An analysis in terms of diffractive orbits has been made in a different atomic physics system, the response of hydrogenic atoms to strong magnetic fields [43.23]. In these systems, a single electron is highly excited and takes long traversals far from the nucleus. Upon returning to a hydrogen nucleus, it is re-ejected with the reversed momentum as

discussed in chapter 41. However, if the atom is not hydrogen but sodium or some other atom with one valence electron, the returning electron feels the charge distribution of the core electrons and not just the charge of the nucleus. This so-called quantum defect induces scattering in addition to the classical re-ejection present in the hydrogen atom. (In this case the local analysis consists of neglecting the magnetic field when the trajectory is near the nucleus.) This is formally similar to the vertex which causes both specular reflection and diffraction. There is then additional structure in the Fourier transform of the quantum spectrum corresponding to the induced diffractive orbits, and this has been observed experimentally [43.24].

Résumé

In this chapter we have discovered new types of periodic orbits contributing to the semiclassical traces and determinants. Unlike the periodic orbits we had seen so far, these are not true classical orbits. They are generated by singularities of the scattering potential. In these singular points the classical dynamics has no unique definition, and the classical orbits hitting the singularities can be continued in many different directions. While the classical mechanics does not know which way to go, quantum mechanics solves the dilemma by allowing us to continue in all possible directions. The likelihoods of different paths are given by the quantum mechanical weights called diffraction constants. The total contribution to a trace from such orbit is given by the product of transmission amplitudes between singularities and diffraction constants of singularities. The weights of diffractive periodic orbits are at least of order $1/\sqrt{k}$ weaker than the weights associated with classically realizable orbits, and their contribution at large energies is therefore negligible. Nevertheless, they can strongly influence the low lying resonances or energy levels. In some systems, such as the N disk scattering the diffraction effects do not only perturb semiclassical resonances, but can also create new low energy resonances. Therefore it is always important to include the contributions of diffractive periodic orbits when semiclassical methods are applied at low energies.

References

[43.1] A. Wirzba, CHAOS **2**, 77 (1992);

[43.2] G. Vattay, A. Wirzba and P. E. Rosenqvist, Phys. Rev. Lett. **73**, 2304 (1994); G. Vattay, A. Wirzba and P. E. Rosenqvist in *Proceedings of the International Conference on Dynamical Systems and Chaos: vol. 2*, edited by Y.Aizawa, S.Saito and K.Shiraiwa (World Scientific, Singapore, 1994).

[43.3] H. Primack, H. Schanz, U. Smilansky and I. Ussishkin, Phys. Rev. Lett. **76**, 1615 (1996).

[43.4] N. D. Whelan, Phys. Rev. E **51**, 3778 (1995).

[43.5] N. Pavloff and C. Schmit, Phys. Rev. Lett. **75**, 61 (1995).

[43.6] M. Sieber, N. Pavloff, C. Schmit, Phys. Rev. E **55**, 2279 (1997).

[43.7] H. Primack et. al., J. Phys. A **30**, 6693 (1997).

[43.8] N. D. Whelan, Phys. Rev. Lett. **76**, 2605 (1996).

[43.9] H. Bruus and N. D. Whelan, Nonlinearity, **9**, 1 (1996).

[43.10] P. Seba, Phys. Rev. Lett. **64**, 1855 (1990).

[43.11] P. E. Rosenqvist, N. D. Whelan and A. Wirzba, J. Phys. A **29**, 5441 (1996).

[43.12] M. Brack et. al., Chaos **5**, 317 (1995).

[43.13] S. M. Reimann et. al., Phys. Rev. A **53**, 39 (1996).

[43.14] A. Sommerfeld, Mathem. Ann. **47**, 317 (1896); *Optics* (Academic Press, New York 1954).

[43.15] H. S. Carslaw, Proc. London Math. Soc. (Ser. 1) **30**, 121 (1989); H. S. Carslaw, Proc. London Math. Soc. (Ser. 2) **18**, 291 (1920).

[43.16] J. B. Keller, J. Appl. Phys. **28**, 426 (1957).

[43.17] A. Voros, J. Phys. A **21**. 685 (1988).

[43.18] see for example, D. Ruelle, *Statistical Mechanics, Thermodynamic Formalism* (Addison-Wesley, Reading MA, 1978).

[43.19] see for example, P. Grassberger, Z. Naturforsch. **43a**, 671 (1988).

[43.20] P. Cvitanović and B. Eckhardt, Nonlinearity **6**, 277 (1993).

[43.21] P. Exner, P. Seba and P. Stovicek, Czech J. Phys **B39**, 1181 (1989).

[43.22] Hua Wu and D. W. L. Sprung, J. Appl. Phys. **72**, 151 (1992).

[43.23] P. A. Dando, T. S. Monteiro, D. Delande and K. T. Taylor, Phys. Rev. Lett. **74**, 1099 (1995). P. A. Dando, T. S. Monteiro and S. M. Owen, preprint (1997).

[43.24] D. Delande et. al., J. Phys. B **27**, 2771 (1994); G. Raithel et. al., J. Phys. B **27**, 2849 (1994); M. Courtney et. al., Phys. Rev. Lett., **73**, 1340 (1994).

stationary!phase approximation
three-disk@3-disk!point scatterer
scattering!point
point!scatterer

Exercises

(N. Whelan)

Exercise 43.1 Stationary phase integral. *Evaluate the two stationary phase integrals corresponding to contours E_1 and E_2 of figure 43.3 and thereby verify (43.7).*

Exercise 43.2 Scattering from a small disk *Imagine that instead of a wedge, we have a disk whose radius a is much smaller than the typical wavelengths we are considering. In that limit, solve the quantum scattering problem - find the scattered wave which result from an incident plane wave. You can do this by the method of partial waves - the analogous three dimensional problem is discussed in most quantum textbooks. You should find that only the $m = 0$ partial wave contributes for small a. Following the discussion above, show that the diffraction constant is*

$$d = \frac{2\pi}{\log\left(\frac{2}{ka}\right) - \gamma_e + i\frac{\pi}{2}} \tag{43.28}$$

where $\gamma_e = 0.577\cdots$ is Euler's constant. Note that in this limit d depends weakly on k but not on the scattering angle.

Exercise 43.3 Several diffractive legs. *Derive equation (43.18). The calculation involves considering slight variations of the diffractive orbit as in the simple case discussed above. Here it is more complicated because there are more diffractive arcs - however you should convince yourself that a slight variation of the diffractive orbit only affects one leg at a time.*

Exercise 43.4 Unsymmetrized dynamical zeta function. *Assume you know nothing about symmetry decomposition. Construct the three node Markov diagram for figure 43.1 by considering A, B and B' to be physically distinct. Write down the corresponding dynamical zeta function and check explicitly that for $B = B'$ it factorizes into the product of the the even and odd dynamical zeta functions. Why is there no term $t_{\bar{2}}$ in the full dynamical zeta function?*

Exercise 43.5 Three point scatterers. *Consider the limiting case of the three disk game of pinball of figure 1.1 where the disks are very much smaller than their spacing R. Use the results of exercise 43.2 to construct the desymmetrized dynamical zeta functions, as in sect. 22.6. You should find $1/\zeta_{A_1} = 1 - 2t$ where $t = de^{i(kR-3\pi/4)}/\sqrt{8\pi kR}$. Compare this formula with that from chapter 11. By assuming that the real part of k is much greater than the imaginary part show that the positions of the resonances are $k_n R = \alpha_n - i\beta_n$ where $\alpha_n = 2\pi n + 3\pi/4$, $\beta_n = \log\left(\sqrt{2\pi\alpha_n}/d\right)$ and n is a non-negative integer. (See also reference [43.11].)*

crosscheck whether it is in chapter 11?

⇓PRIVATE

uniform
approximation
bifurcation!catastrophe
catastrophe

Chapter 44

Uniform approximations

(D. Lippolis)

So far, in dealing with chaotic systems we have always tacitly assumed that all periodic orbits are unstable and isolated. That is true in some open systems, such as scattering off 3 disks in a plane, but any physically interesting bound Hamiltonian system tends to have mixed phase space. In such systems a small parameter change can drive many periodic orbits (of a period shorter than some cutoff) through bifurcations, with orbits arbitrarily close to one another as they collide. Physical parameters, such as slow change of external electric or magnetic fields in atomic and solid state experiments play role of such bifurcation parameters, so study of such bifurcations cannot be avoided. As the classical orbits collide, the corresponding saddlepoints coalesce, and the quadratic, Gaussian stationary phase approximation (33.15) that leads to the Van Vleck propagator (34.30) and the Gutzwiller trace formula (36.3) fails. At the bifurcation point the Jacobian in (36.11) has unit eigenvalues, so the contribution of such periodic orbits to the Gutzwiller trace formula diverges. In this chapter we go beyond the Gaussian saddlepoint approximation, replacing it by approximations uniform in $\hbar$ and parameter/parameters a which describe/describes the distance to the nearest bifurcation.

44.1 Bifurcations and catastrophes

The method of stationary phase can be applied to an integral of the form

☞ sect. 33.2

$$I = \int A(x) \exp\left(is\Phi(x)\right) dx \tag{44.1}$$

by approximating the integrand

$$\Phi(x) \simeq \Phi(x_0) + \frac{1}{2}\Phi''(x_0)\delta x^2 \qquad A(x) \simeq A(x_0) \tag{44.2}$$

normal form
fold catastrophe
catastrophe!fold
cusp catastrophe
catastrophe!cusp

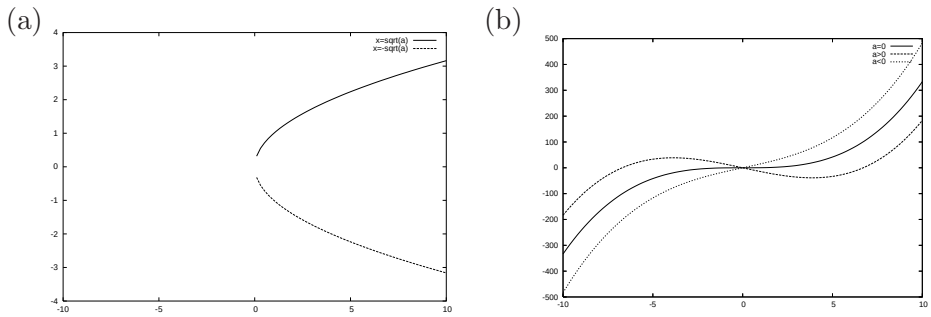

Figure 44.1: Stationary points of (a) the fold catastrophe and (b) the normal form (44.3) for different values of the parameter a.

give an estimat "sufficiently" far

in the neighborhood of the extremal point (stationary phase point) x_0. When the extremal points are not sufficiently far apart from one another, this approximation fails. Usually the "action" $\Phi(x)$ depends on one or more parameters, with the extremal points getting arbitrarily close to one another and eventually coalescing as the parameters vary. In the neighborhood of the bifurcation parameter values, the function is not well described by the quadratic approximation (44.2). The number of extremal points and their motion as a function of the parameters depends on the local symmetries of the bifurcation. The most robust bifurcation are of codimension one - variation of a single parameter suffices to drive the system through a bifurcation.

Example 44.1 Tangent, pitchfork bifurcation. *Consider the tangent bifurcation plotted in figure 44.1 whose normal form*

$$\Phi_a(x) \simeq \frac{1}{3}x^3 - ax\,, \tag{44.3}$$

is called fold catastrophe. *If the symmetry of the neighborhood of the bifurcation point is such that local map depends on even powers of x^2, the simplest bifurcation is the pitchfork bifurcation plotted in figure 44.2 whose normal form*

$$\Phi_a(x) \simeq \frac{1}{4}x^4 - \frac{1}{2}ax^2\,, \tag{44.4}$$

explain symmetry that forces cusp catstrph

is called cusp catastrophe.

What matters is that while the integral (44.1) can no longer be approximated by a Gaussian integral, it can still can be expressed in terms of special functions.

found many typos, please recheck this part

Example 44.2 Fold, cusp catastrophe. *If the local "action" $\Phi_a(x)$ starts with x^3, then in the neighborhood of the tangent bifurcation a slowly varying amplitude $A_a(x)$ can be approximated by a polynomial of first degree,*

$$\begin{aligned} I &= \int dx\, p(x) e^{i(x^3/3-ax)} = (p_0 + ip_1\, d/da)Ai(a) \\ A_a(x) &\simeq p(x) = p_0 + p_1 x\,, \end{aligned} \tag{44.5}$$

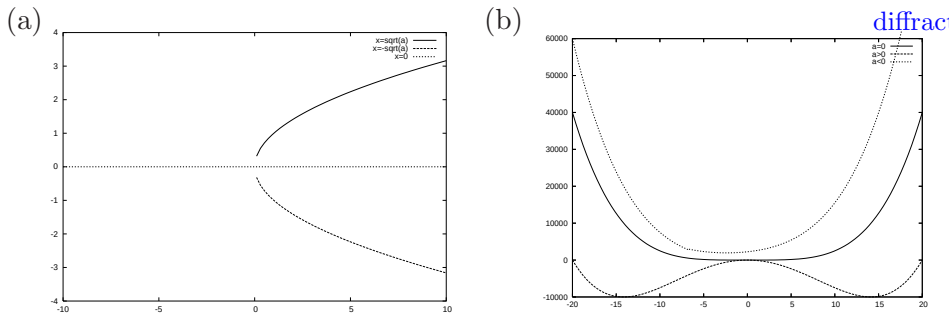

Figure 44.2: Stationary points of (a) the fold catastrophe and (b) the normal form (44.4) for different values of the parameter a.

where

$$Ai(a) = \int dx\, e^{i(x^3/3 - ax)} \tag{44.6}$$

is the Airy function. In the case of a cusp catastrophe, the normal form approximation to I requires $A_a(x) \simeq p(x) = p_0 + p_2 x^2$,

$$\begin{aligned} I &\simeq \int dx\, p(x) e^{i(x^4/4 - ax^2/2)} = \left(p_0 + 2ip_2 \frac{d}{da}\right) I(a) \\ I(a) &= \int dx\, e^{i(x^4/4 - ax^2/2)}\,, \end{aligned} \tag{44.7}$$

where the integral $I(a)$ can be expressed in terms of Bessel functions, [44.9]

no lit refs in the text, → remarks

$$I(a) = \frac{\pi |a|^{\frac{1}{2}}}{2} e^{-i(a^2 - \pi)/8} \left(J_{-\frac{1}{4}}(a^2/8) + \mathit{sign}(a) e^{-i\pi/4} J_{-\frac{1}{4}}(a^2/8) \right)\,. \tag{44.8}$$

formula wrong, fix Bessel indices

insert student HH Roux here

Of course, for simple examples such as a tangent or a pitchfork bifurcation no fancy theory of normal forms and catastrophes is needed, and you might wonder why are worrying about what happens at isolated points (measure zero!) in the classical state space? Doesn't $\hbar$ granularity of the quantum state space take care of that? Well, no. What happens in wave mechanics at manifolds of lower dimensionality is *diffraction*, the quintessentially wave-mechanical phenomenon important when diffracting singularities are of size comparable to the wavelength under study.

Our first example of diffraction, the turning point singularity in the 1-d WKB quantization of sect. 33.4 could be talked away with a bit of Fresnel/Maslov voodoo, so we did not even invoke the word "diffraction". In chapter 42 we saw that when the wavelength is comparable to the size of obstacles, diffraction significantly modifies and extends the original Gutzwiller theory. Similarly, in the scattering of wedges of chapter 43 diffraction became very important, because without it there would be no chaotic dynamics whatsoever.

⇓PRIVATE

⇑PRIVATE

Why should diffraction effects play a physically significant role here, where most of the state space is fraught with unstable periodic orbits,

Green's function!density of states
density of states!Green's function
closed orbit
splitting lemma

the potential is assumed smooth, and the diffraction is localized to a few orbits? Physical reason is that while individual strongly unstable orbits orbits contribute exponentially small terms to periodic orbits trace sums, marginally stable (intermittent) orbits are on the way to turning into elliptic islands, and their neighborhoods are disproportionally small. That is why, when you look at the bottom of a swimming pool, the main thing that you see is the web by caustics, even though such catastrophes are of much lower dimensionality than the full space.

44.2 Periodic orbits near bifurcations

Since the Gutzwiller trace formula derivation of sect. 36.1 no longer applies, let us start from the beginning: we would like to evaluate the right-hand side of (32.20) the quantum density of states in terms of the trace of the quantum Green's function, that is

$$\begin{aligned} d(E) &= \sum_n \delta(E-E_n) = -\lim_{\epsilon\to 0}\frac{1}{\pi}\mathrm{Im}\,\mathrm{tr}\,G(q,q',E+i\epsilon) \\ &= -\frac{1}{\pi}\mathrm{Im}\int d^2q d^2q' \delta(q-q')\,G(q,q',E) \end{aligned} \tag{44.9}$$

And here comes the first idea. In a codimension-one bifurcation embedded in a chaotic sea, almost all periodic orbit are unstable and isolated - at any given bifurcation parameter value, a set of only two or three periodic orbits are wed into the bifurcation. So we assume that the VanVleck semiclassical propagator (34.46) is good for q, q' separated by a small distance

$$G(q,q',E) = \frac{1}{i\hbar(2\pi\hbar)^{(D-1)/2}}\frac{1}{|\dot{q}\dot{q}'|^{1/2}}\,|\det D_\perp|^{1/2}\,e^{\frac{i}{\hbar}S-\frac{i\pi}{2}m}, \tag{44.10}$$

We have already evaluated an integral like this in sect. 36.1, and determined that the stationary phase condition enforces that the orbit is not only *closed orbit* returning in the spatial coordinate, but that it is *periodic* in the full state space.

In order to evaluate this in the neighborhood of a bifurcation we have to be bit more careful. While for isolated unstable orbit a Gaussian integral leads to the Gutzwiller trace formula, here we need to write the local action as the appropriate catastrophe normal form, such as the fold (44.3) or cusp (44.4) catastrophe.

And now the second idea: in the neighborhood of a codimension-one bifurcation, we can chose a natural Poincaré section such that the catastrophe dynamics occurs along one $[q,p]$ symplectic plane, and the rest is amenable to the usual Gaussian saddle-point analysis. More formally: the *splitting lemma* of catastrophe theory states that, given a function $f(x_1,...,x_n)$,

whose Hessian has rank $n-m$, a coordinate system $q_1, ..., q_n$ can be introduced
e Hessian in the neighborhood of a fixed point, such that
ewhere

$$f(q_1, ..., q_n) = g(q_1, ..., q_m) + h(q_{m+1}, ..., q_n)$$

where g has a extremal point degenerate at the origin and h is a non-degenerate quadratic form. In general, the number of parameters that participate in the bifurcation is called codimension of the bifurcation. The examples given in the previous section describe two different codimension-one bifurcations, since there is only one parameter – a – to tune. The splitting lemma tells us that the action (i.e., function f) can be split into a catastrophe polynomial plus a nondegenerate function that can hence be integrated with the saddle point approximation.

Example 44.3 2-dof system. *Let us show what happens in the simple case of a 2-dimensional system. First of all we choose a local frame of reference in the phase space with one coordinate along the orbit (called z) and the other one (y) perpendicular to it. The action is initially defined as a function of y, y', z, z', however, the Poincaré map (as well as the fundamental matrix matrix) is close to the identity near a bifurcation, so that it cannot be generated by a function of the initial and final coordinates ($y = y'$!). For this reason it is necessary to use a mixed coordinate-momentum representation of the action, by applying a Legendre transform*

$$S(z', y'z, y, E) = \tilde{S}(z', y', z, p_y, E) - yp_y$$

at the same time we replace one of the delta functions in (44.10) by

$$\delta(y - y') = \frac{1}{2\pi\hbar} \int dp_y e^{\frac{i}{\hbar} p_y (y - y')} .$$

That is because the function $\tilde{S}(p_y, y') - y'p_y$ is stationary at every fixed point of the Poincaré section defined by $z = const.$ and $E = const.$ The integral (44.10) is now proportional to

$$\int dz dy' dp_y \|\det D\|^{1/2} \exp\left(\frac{i}{\hbar}\hat{S}(z', y', z, p_y, E) - \frac{i}{\hbar}y'p_y - \frac{i\pi}{2}m\right)$$
$$z' = z + l \qquad (44.11)$$

where l is the length of the orbit. Finally, we switch to normal coordinates on the Poincaré section so that $\hat{S} = \hat{S}(p, q', E)$ at $z' = z + l$. The transformation produces a factor of $1/\dot{z}$ in the integral (44.11), that now reads

$$\int_0^l \frac{dz}{\dot{z}} \int dq' dp \left\| \frac{\partial \hat{S}}{\partial p \partial q'} \right\|^{1/2} \exp\left(\frac{i}{\hbar}\hat{S}(q', p, E) - \frac{i}{\hbar}q'p - \frac{i\pi}{2}m\right) . \qquad (44.12)$$

The first integral is just the period of the orbit. In the vicinity of the bifurcation, the action $S(q', p, E)$ can be expanded as a normal form. For simple examples such as a tangent or a pitchfork bifurcation no theory of normal forms is needed. It is enough to recall that a fixed point of the Poincaré map is a stationary point of the function $\hat{S}(q', p) - q'p$ in order to guess that a tangent bifurcation will yield

$$\hat{S}(q', p, E) = S_0(E) + q'p - \frac{1}{2}p^2 - aq' - q'^3$$

closed orbit

and a pitchfork bifurcation will give

$$\hat{S}(q',p,E) = S_0(E) + q'p - \frac{1}{2}p^2 - aq'^2 - q'^4 \,.$$

no lit refs in the text, → remarks

S_0 and a can be expressed in terms of the actions and amplitudes of the orbits involved in the bifurcation [44.5], so that the integrals (44.12) are now easy. The one over p is a Gaussian integral, while the one over q' can be expressed in terms of Airy or Bessel functions. More precisely, the determinant $|\det D|^{1/2}$ brings a polynomial of the first order in q', so that the whole integral can still be expressed in terms of the Airy function plus its first derivative with respect to the parameter a. Note that there exists a neighborhood $\Delta a \simeq \hbar$ around the bifurcation, necessitating inclusion of ghost orbits in the expansion, for the parameter values for which they participate in the bifurcation.

explain ghost orbits

44.1
page 830

44.3 Closed orbits

like having closed orbits here - another example of diffraction!

Closed orbit theory is used to study interactions of atoms with external static fields semiclassically. When an atom absorbs a photon, the electron goes into an outgoing Coulomb wave, which propagates away from the nucleus, until the wave fronts can be correlated with outgoing classical trajectories. Eventually the wave fronts are scattered back by the (electro)magnetic field, and interfere with the outgoing waves to produce the observed oscillations in the average-absorption spectrum. It turns out that the main contributions to the oscillating spectrum are given by the classical trajectories which start and end close to the nucleus, i.e. the closed orbits. Spectroscopic measurements do not give the density of states, but rather the oscillator strengths, defined as

$$f_n = 2(E_n - E_i)|\langle i|D|n\rangle|^2 \,, \tag{44.13}$$

where D is the component of the dipole operator describing the polarization of the exciting electromagnetic field. The density of oscillator strength

$$f(E) = \sum_n f_n \delta(E - E_n) \tag{44.14}$$

(and hence every single strength) can conveniently be expressed in terms of the quantum mechanical response function

$$g(E) \;=\; -\frac{1}{\pi}\sum_n \frac{|\langle i|D|n\rangle|^2}{E - E_n + i\epsilon} \;=\; -\frac{1}{\pi}\langle i|DG(E)D|i\rangle \tag{44.15}$$

by the relation

$$f(E) = 2(E - E_i)\,\mathrm{Im}\,[g(E)] \,. \tag{44.16}$$

Closed orbit!bifurcation

It is possible to compute $g(E)$ semiclassically, by using the Van Vleck approximation to the retarded Green's function $G(E)$. The result has the same form as the Gutzwiller trace formula:

$$g(E) = g_0(E) + g^{osc}(E)$$

where g_0 is a smooth contribution independent of the interaction with the external fields and

$$g^{osc}(E) = \sum_{co} \mathcal{A}_{co}(E) e^{i(S_{co}(E) - \frac{\pi}{2}\mu_{co})}\,, \tag{44.17}$$

is given as a sum over all the classical closed orbits. In the expression above, S_{co} is the action of the closed orbit, μ_{co} its topological index and

$$\mathcal{A}_{co} = 4\pi \frac{\mathcal{Y}^*(\theta_f, \phi_f)\mathcal{Y}(\theta_i, \phi_i)}{\sqrt{|M|}} \tag{44.18}$$

is a function of the initial and final angles (the $\mathcal{Y}$'s are linear combinations of spherical harmonics that characterize the initial or the final state) and

$$M = (\sin(\theta_i)\sin(\theta_f))^{-1} \det \frac{\partial(p_{\theta_f}, p_{\phi_f})}{\partial(\theta_i, \phi_i)} \tag{44.19}$$

is the ratio between the determinant of the fundamental matrix and the symmetric matrix of second derivatives of the action (that arises from the stationary phase approximation).

44.3.1 Closed orbits near bifurcations

The main point is that M vanishes at a bifurcation, that is why we need uniform approximations.

To that end, one starts with the results of the previous section for periodic orbits, and obtaines similar expressions in the case of bifurcations of closed orbits, by taking a reasonable ansatz for the uniform approximation of contribution to the response function

$$\Psi(E) = I(a) e^{iS_0(E)} \tag{44.20}$$

where

$$I(a) = \int dx\, p(x) e^{i\Phi_a(x)}\,. \tag{44.21}$$

Here $p(x)$ and $S_0(E)$ are unknown, while $\Phi_a(x)$ is a suitable normal form for the bifurcation in question, which we again assume to only depend on one parameter. The strategy is now to evaluate the unknowns from the limit of (44.20) far away from the bifurcation, where (44.21) can be computed by means of the stationary phase approximation to yield

$$\Psi(E) = \sum_{x_i} \frac{(2\pi i)^{1/2} p(x_i)}{\sqrt{|Hess\Phi_a(x_i)|}} \exp\left[i(S_0(E) + \Phi_a(x_i) - \pi\nu_i/2)\right], \quad (44.22)$$

where ν_i is the number of negative eigenvalues of the Hessian (5.9) and the sum is over all the extremal points x_i of $\Phi_a(x)$. Comparing the latter expression with the general form (44.17) of $\Psi(E)$, we can infer that

$$S_i(E) = S_0(E) + \Phi_a(x_i) \quad (44.23)$$

and hence find the values of $S_0(E)$ and the extremal points of $\Phi_a(x_i)$. As long as we are dealing with real orbits, ν_i corresponds to the topological index, otherwise it has to be determined so that $p(x_i)$ be continuous through the bifurcation [44.9]. However, that is not enough to determine $p(x)$ uniquely. Considering $p(x)$ is needed only in the neighborhood of $x = 0$, it is wise to Taylor-expand it about such point, so as to obtain a polynomial ansatz, with the coefficients to be determined from the values of the semiclassical amplitudes of (44.22) evaluated in the extremal points. Of course all that can be possible only if the polynomial has degree $k - 1$, where k is the number of orbits involved in the bifurcation. Everything is best explained by a simple example , such as

no lit refs in the text, → remarks

Example 44.4 Tangent bifurcation/fold catastrophe.

$$\Phi_a(x) = \frac{1}{3}x^3 - ax$$

which has extremal points at $x = \pm\sqrt{a}$, *real if* $a > 0$, *so that*

$$\Phi_a(\pm\sqrt{a}) = \mp\frac{2}{3}a^{2/3}$$

are its stationary values. Figure 44.3 illustrates the positions of extremal points, stationary values and second derivatives in the fold catastrophe. It is evident that both $\Phi_a(x_i)$ *and* $\Phi_a''(x_i)$ *are real even for* $a < 0$, *when the extremal points* x_i*'s are complex, that is they correspond to ghost orbits having real actions and stability determinants.*

Now we can evaluate $S_0(E)$ *and* a *as functions of* S_1, S_2, *by using (44.23):*

$$S_1 = S_0(E) - \frac{2}{3}a^{3/2}, \qquad S_2 = S_0(E) + \frac{2}{3}a^{3/2}$$

that leads to

$$S_0(E) = \frac{1}{2}(S_1 + S_2), \qquad |a| = \left(\frac{3}{4}|S_2 - S_1|\right)^{2/3}.$$

normal form

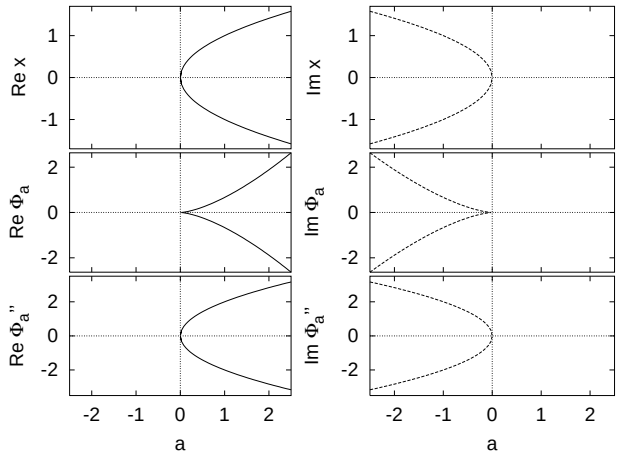

Figure 44.3: The positions of extremal points, stationary values and second derivatives in the fold catastrophe. Solid lines indicate extremal points, dashed lines complex extremal points. Dotted lines are coordinate axes. (T. Bartsch [44.9])

We also need an expression for the amplitudes, for which it is necessary to determine $p(x)$. *Equation (44.22) yields*

$$\mathcal{A}_1 = \frac{\sqrt{\pi}}{|a|^{1/4}} p(\sqrt{a}) e^{i\pi/4}\,, \qquad \mathcal{A}_2 = \frac{\sqrt{\pi}}{|a|^{1/4}} p(-\sqrt{a}) e^{-i\pi/4}\,. \tag{44.24}$$

If $p(x)$ *is a polynomial of the form*

$$p(x) = (p_0 + p_1 x)/2\pi$$

then the parameters p_0 *and* p_1 *read*

$$p_0 = \pi |a|^{1/4} e^{-i\pi/4} (\mathcal{A}_1 + i\mathcal{A}_2)\,, \qquad p_1 = \pi |a|^{-1/4} e^{-i\pi/4} (\mathcal{A}_1 - i\mathcal{A}_2)$$

so that now everything is known in the formula (44.21), which becomes

$$\int dx\, (p_0 + p_1 x) e^{i\Phi_a(x)}$$

and can be evaluated in terms of the Airy function and its derivative with respect to a

$$\int dx\, e^{i\Phi_a(x)} = Ai(-a)\,, \qquad \int dx\, x\, e^{i\Phi_a(x)} = -iAi'(-a)\,,$$

once S_1, S_2, $\mathcal{A}_1$ *and* $\mathcal{A}_2$ *have been computed, see figure 44.4.*

Commentary

Remark 44.1 Normal forms. The classification of all the possible bifurcation scenarios and corresponding normal forms is the realm of catastrophe theory [44.1], with higher co-dimension bifurcations requiring simultaneous fine tuning of more parameters and thus being less generic. The theory of normal forms is used to simplify nonlinear systems trough a near-identity change of variables. In the present context, it can be used to expand the action to a polynomial in the vicinity of a bifurcation [44.6].

uniform approximation
symmetry breaking
closed orbit
orbit!closed

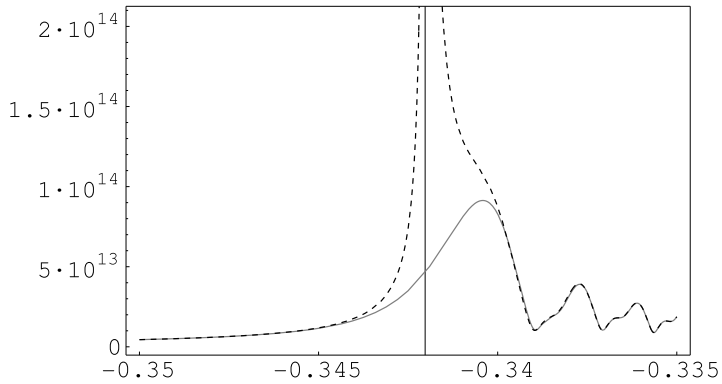

Figure 44.4: Magnitude of the contribution to the response function of the bifurcating orbits plotted versus the scaled energy [44.10]. The Gutzwiller trace formula (44.22) (dashed curve) diverges at the bifurcating point; the uniform approximation (44.20) (solid curve) interpolates smoothly between the values of the Gutzwiller trace formula on either side of the bifurcation.

Remark 44.2 Uniform approximations. Initially designed to include marginally stable orbits in the Gutzwiller trace formula, uniform approximations have found many applications in atomic physics. Work on diffraction integrals containing catastrophes was done in optics by Berry and Upstill [44.2]. Ozorio de Almeida and Hannay [44.3] and Schomerus and Sieber [44.5, 44.4] have developed uniform approximations near bifurcations of periodic orbits. Uniform approximations in closed orbit theory have been addressed by Gao and Delos [44.13] and Shaw and Robicheaux [44.12] for an atom in an electric field, and by Main and Wunner [44.11] and Bartsch [44.9] in for an atom in crossed electric and magnetic fields. When the change of a continous parameter causes the breaking of a symmetry of the system, a number of degenerate orbits may suddenly disappear. Uniform approximations for such bifurcations can be found in Creagh [44.14] and Brack *et al.* [44.15].

Remark 44.3 Closed orbits. Closed orbit theory was formulated in 1988 by Du, Delos [44.7] and Bogomolny [44.8], in order to explain the existence of oscillations in the average-absorption spectrum of an atom in a magnetic field.

give references: hydrogen in crossed electric and magnetic fields, if useful

Résumé

The method of (Gaussian) stationary phase approximation fails whenever two or more extremal points of the approximated function are too close to one another. In such cases higher order terms in expansion of classical action need to be kept, leading to uniform approximations in terms of functions of Airy or Bessel type that enables a smooth interpolation of trace formulas through bifurcation values. Coalescence of saddles occurs at bifurcation values of parameters of the classical dynamics. For periodic orbits close to bifurcations the Gutzwiller trace formula diverges, and the action needs to be expanded according to catastrophe/normal form theory. The method applies to bifurcations of closed orbits as well, since the contributions to the spectral density of the colliding orbits ultimately depend on their amplitudes and actions only.

not sure this explains it

References

[44.1] T. Poston and I. Stewart, *Catastrophe Theory and its applications* (Dover, 1996).

[44.2] M.V. Berry and C. Upstill, *Prog. in Optics* **18**, 257 (1980).

[44.3] A.M. Ozorio de Almeida and J.H. Hannay, *J. Phys. A* **20**,5873 (1987).

[44.4] M. Sieber, *J. Phys. A* **29**, 4715 (1996).

[44.5] H. Schomerus and M. Sieber, *J. Phys. A* **30**, 4537 (1997).

[44.6] P. Leboeuf and A. Mouchet, "Normal forms and complex periodic orbits in semiclassical expansions of Hamiltonian systems", *Ann. Phys.* **275**, 54 (1999); `chao-dyn/9809015`.

[44.7] M.L. Du and J.B. Delos, *Phys. Rev. A* **38**, 1896 (1988).

[44.8] E.B. Bogomolny, *Sov. Phys. JETP* **69**, 265 (1989).

[44.9] T. Bartsch, *The hydrogen atom in an electric field and in crossed electric and magnetic fields: Closed-orbit theory and semiclassical quantization*, Ph. D. thesis (Cuvillier Verlag, Göttingen 2002).

[44.10] T. Bartsch, J. Main, and G. Wunner, *Prog. Theor. Phys. Suppl.* **139**, 429 (2000).

[44.11] J. Main and G. Wunner, *Phys. Rev. A* **55**, 1743 (1997).

[44.12] J.A. Shaw and F. Robicheaux, *Phys. Rev. A* **58**, 1910 (1998).

[44.13] J. Gao and J.B. Delos, *Phys. Rev. A* **56**, 356 (1997).

[44.14] S.C. Creagh, *Ann. Phys.* **248**, 60 (1996).

[44.15] M. Brack *et al.*, *JPA* **32**, 331 (1999).

uniform approximation create more exercises...

Exercises

Exercise 44.1 Uniform approximation to a symmetric cusp catastrophe. *Consider the case of a pitchfork bifurcation described by the normal form (44.4). Keep in mind that at the bifurcation point the two orbits that bifurcate off the single orbit have both the same action and amplitude. Derive the uniform approximation for this bifurcation, using the general procedure given in sect. 44.3 and the computations of integral (44.1) in sect. 44.1 for a cusp catastrophe.*

(Domenico Lippolis)

⇑PRIVATE

Epilogue

> Nowadays, whatever the truth of the matter may be (and we will probably never know), the simplest solution is no longer emotionally satisfying. Everything we know about the world militates against it. The concepts of indeterminacy and chaos have filtered down to us from the higher sciences to confirm our nagging suspicions.
>
> L. Sante, "Review of 'American Tabloid' by James Ellroy", *New York Review of Books* (May 11, 1995)

A motion on a strange attractor can be approximated by shadowing long orbits by sequences of nearby shorter periodic orbits. This notion has here been made precise by approximating orbits by prime cycles, and evaluating associated curvatures. A curvature measures the deviation of a long cycle from its approximation by shorter cycles; the smoothness of the dynamical system implies exponential fall-off for (almost) all curvatures. We propose that the theoretical and experimental non–wandering sets be expressed in terms of the symbol sequences of short cycles (a topological characterization of the spatial layout of the non–wandering set) and their eigenvalues (metric structure) ; for example, plotted as fig. ?! or listed as in II, table 1?!. The cycle expansions then offer an efficient method for evaluating periodic orbit averages; accurate estimates can already be obtained from a few fundamental cycles.

⇓PRELIMINARY

For reasons of clarity we have here motivated the cycle expansions by a simple 1-d repeller of fig. ?!; detailed investigations of a series of low dimensional chaotic systems undertaken in the sequel paper II, as well as the classical and quantum pinball studies of refs. [O.18, 6.3, 1.6], give us some confidence in the general feasibility of the cycle analysis advocated here.

⇑PRELIMINARY

Cycles as the skeleton of chaos

We wind down this all-too-long treatise by asking: why cycle?

this paragraph is a repeat of parts of intro.tex, remove? rest into DasBuch summary?

We tend to think of a dynamical system as a smooth system whose evolution can be followed by integrating a set of differential equations.

Traditionally one used integrable motions as zeroth-order approximations to physical systems, and accounted for weak nonlinearities perturbatively. However, when the evolution is actually followed through to asymptotic times, one discovers that the strongly nonlinear systems show an amazingly rich structure which is not at all apparent in their formulation in terms of differential equations. In particular, the periodic orbits are important because they form the *skeleton* onto which all trajectories trapped for long times cling. This was already appreciated century ago by H. Poincaré, who, describing in *Les méthodes nouvelles de la méchanique céleste* his discovery of homoclinic tangles, mused that "the complexity of this figure will be striking, and I shall not even try to draw it". Today such drawings are cheap and plentiful; but Poincaré went a step further and, noting that hidden in this apparent chaos is a rigid skeleton, a tree of *cycles* (periodic orbits) of increasing lengths and self-similar structure, suggested that the cycles should be the key to chaotic dynamics.

The zeroth-order approximations to harshly chaotic dynamics are very different from those for the nearly integrable systems: a good starting approximation here is the stretching and kneading of a baker's map, rather than the winding of a harmonic oscillator.

For low dimensional deterministic dynamical systems description in terms of cycles has many virtues:

1. cycle symbol sequences are *topological* invariants: they give the spatial layout of a non–wandering set
2. cycle eigenvalues are *metric* invariants: they give the scale of each piece of a non–wandering set
3. cycles are *dense* on the asymptotic non–wandering set
4. cycles are ordered *hierarchically*: short cycles give good approximations to a non–wandering set, longer cycles only refinements. Errors due to neglecting long cycles can be bounded, and typically fall off exponentially or super-exponentially with the cutoff cycle length
5. cycles are *structurally robust*: for smooth flows eigenvalues of short cycles vary slowly with smooth parameter changes
6. asymptotic averages (such as correlations, escape rates, quantum mechanical eigenstates and other "thermodynamic" averages) can be efficiently computed from short cycles by means of *cycle expansions*

Points 1, 2: That the cycle topology and eigenvalues are invariant properties of dynamical systems follows from elementary considerations. If the same dynamics is given by a map f in one set of coordinates, and a map g in the next, then f and g (or any other good representation) are related by a reparametrization and a coordinate transformation $f = h^{-1} \circ g \circ h$. As both f and g are arbitrary representations of the dynamical system,

the explicit form of the conjugacy h is of no interest, only the properties invariant under any transformation h are of general import. The most obvious invariant properties are topological; a fixed point must be a fixed point in any representation, a trajectory which exactly returns to the initial point (a cycle) must do so in any representation. Furthermore, a good representation should not mutilate the data; h must be a smooth transformation which maps nearby cycle points of f into nearby cycle points of g. This smoothness guarantees that the cycles are not only topological invariants, but that their linearized neighborhoods are also metrically invariant. In particular, the cycle eigenvalues (eigenvalues of the fundamental matrixs $df^n(x)/dx$ of periodic orbits $f^n(x) = x$) are invariant.

Point 5: An important virtue of cycles is their *structural robustness*. Many quantities customarily associated with dynamical systems depend on the notion of "structural stability", i.e., robustness of non–wandering set to small parameter variations.

Still, the sufficiently short unstable cycles are structurally robust in the sense that they are only slightly distorted by such parameter changes, and averages computed using them as a skeleton are insensitive to small deformations of the non–wandering set. In contrast, lack of structural stability wreaks havoc with long time averages such as Lyapunov exponents (see sect. ??), for which there is no guarantee that they converge to the correct asymptotic value in any finite time numerical computation.

⇓PRELIMINARY
??
page ??
⇑PRELIMINARY
⇓PRELIMINARY
⇑PRELIMINARY

The main recent theoretical advance is **point 4:** we now know how to control the errors due to neglecting longer cycles. As we seen above, even though the number of invariants is infinite (unlike, for example, the number of Casimir invariants for a compact Lie group) the dynamics can be well approximated to any finite accuracy by a small finite set of invariants. The origin of this convergence is geometrical, as we shall see in appendix K.1.2, and for smooth flows the convergence of cycle expansions can even be super-exponential.

The cycle expansions such as (18.5) outperform the pedestrian methods such as extrapolations from the finite cover sums (19.2) for a number of reasons. The cycle expansion is a better averaging procedure than the naive box counting algorithms because the strange attractor is here pieced together in a topologically invariant way from neighborhoods ("space average") rather than explored by a long ergodic trajectory ("time average"). The cycle expansion is co-ordinate and reparametrization invariant - a finite nth level sum (19.2) is not. Cycles are of finite period but infinite duration, so the cycle eigenvalues are already evaluated in the $n \to \infty$ limit, but for the sum (19.2) the limit has to be estimated by numerical extrapolations. And, crucially, the higher terms in the cycle expansion (18.5) are deviations of longer prime cycles from their approximations by shorter cycles. Such combinations vanish exactly in piecewise linear approximations and fall off exponentially for smooth dynamical flows.

⇓PRELIMINARY

Perhaps it is worth emphasizing again that the Euler product formula (15.16) is an expression for the *exact* transfer operator T. We extract

its eigenvalues directly from (15.16) with no recourse to any explicit (and coordination dependent) eigenfunctions. Our cycle expansions are dominated by short cycles, but that does not mean that we are using finite covers to approximate the set: by resummation that led to (15.16) we have already been lifted to the topologically exact $k \to \infty$ non–wandering set. The approximation will consist in approximating the non–wandering set under investigation by "closeby" Cantor sets with a finite number of already asymptotically exact scales. The finite approximations $\tilde{T}^{(k)}$ were introduced only for reasons of pedagogy: our experience is that computations with the asymptotically exact cycles expression (15.16) are both quicker and of better convergence than computations that go through sequences of finite matrix estimates such as the Markov graph approximations.

However, the cycle expansions are not magic, and they will not converge any better than the more traditional thermodynamic sums *unless the following prerequisites are met*:

1. The essential prerequisite for implementing the above "shadowing" is a good understanding of the symbolic dynamics of the dynamical system; the present formulation requires that the symbolic dynamics be of a finite subshift type (see sect. 12.4). A generic dynamical system is *not* of that type: our strategy is to approach it by a sequence of finite subshift approximants, just as a generic number can be bracketed by a sequence of rational approximants.

2. The weight used in averaging must be multiplicative along the flow, and the flow should be smooth, so that nearby trajectories have nearby weights.

3. Cycle expansions converge only in the hyperbolic phase, i.e., only for averages dominated by the positive entropy of unstable cycles. Marginal fixed points show up indirectly, as power-law corrections and non-analyticities of the ζ functions. If a sequence of fundamental cycles t_f is infinite and accumulating toward marginal stability, the sequence must be summed up in order that the convergence of the cycle expansion be exponential (see sect. ?!).

4. As developed here, the cycle expansions are good only for extracting the leading eigenvalues of transfer operators. If more eigenvalues are needed, techniques for analytically continuing beyond the leading singularities must be developed.

When and if the cycles suffice for the complete characterization (and reconstruction) of a dynamical system is not known, but they do go further toward detailed invariant characterization of low dimensional chaotic dynamical systems than other current methods, and we hope that in the future the data will be presented in terms of cycles rather than "thermodynamic" averages.

We were guided here by the Axiom A intuition developed by Smale, Ruelle, and others: if the dynamical evolution can be cast in terms of an evolution operator multiplicative along the flow, if the corresponding mapping (for ex., return map for a Poincaré section of the flow) is analytic hyperbolic, and if the topology of the repeller is given by a finite Markov partition, then the spectral determinant (15.14) is entire.

The real life challenge are generic dynamical flows, which fit neither schematization. Unfortunately we know of no smooth potential which is both Axiom A, and has bound states. Most systems of interest are *not* of the "Axiom A" category; they are neither purely hyperbolic nor do they have a simple symbolic dynamics grammar. The crucial ingredient for nice analyticity properties of zeta functions is existence of finite grammar (coupled with uniform hyperbolicity). From the hyperbolic dynamics point of view, the Riemann zeta is perhaps the worst possible example; understanding the symbolic dynamics would amount to being able to give a finite grammar definition of all primes. Hyperbolic dynamics suggests that a generic "chaotic" dynamical system should be approached by a sequence of finite grammar approximations[18.2], pretty much as a "generic" number is approached by a sequence of continued fractions.

The procedure described above is one possible way of generating subshifts of finite type. One could have, for example, listed instead all non-vanishing elements of a $[2^4 \times 2^4]$ transition matrix; this yields a larger, non–minimal Markov graph. The Markov graph approach is more compact, but it is still not entirely natural in the context of the present problem: the graphs constructed by the algorithm outlined here are not necessarily minimal, the graphs associated with time reversed dynamics do not reflect this symmetry, and so on. Be it as it may, the method requires only simple string shifts and matches, and is easily implemented on a computer.

The above coarse approximations suffice for establishing the main result of this section, that the coefficients in the cycle expansions of Selberg products fall off faster than exponentially. The spectrum of $\mathcal{L}$ for the piecewise–linear approximate maps is only indicative of the spectrum for the exact nonlinear map; the details are subtle and the reader is referred to ref. [21.23, 16.17] for more careful convergence estimates. In particular, our estimates depended on the assumption that the symbolic dynamics is a subshift of finite type, that the cycle weight is multiplicative along the flow, and that the flow is smooth, so that nearby trajectories have nearby weights.

⇑PRELIMINARY

In the above we have reviewed the general properties of the cycle expansions; those have been applied to a series of examples of low-dimensional chaos: 1-d strange attractors, the period-doubling repeller, the Hénon-type maps and the mode locking intervals for circle maps. The cycle expansions have also been applied to the irrational windings set of critical circle maps, to the Hamiltonian period-doubling repeller, to a Hamiltonian three-disk game of pinball, to the three-disk quantum scattering resonances and to the extraction of correlation exponents, Feasibility of analysis of experimental

non–wandering set in terms of cycles is discussed in ref. [18.1].

Homework assignment

> "Lo! thy dread empire Chaos is restor'd, Light dies before thy uncreating word; Thy hand, great Anarch, lets the curtain fall, And universal darkness buries all."
>
> Alexander Pope, *The Dunciad*

We conclude cautiously with a homework assignment posed May 22, 1990 (the original due date was May 22, 2000, but alas...):

1. **Topology** Develop optimal sequences ("continued fraction approximants") of finite subshift approximations to generic dynamical systems. Apply to (a) the Hénon map, (b) the Lorenz flow and (c) the Hamiltonian standard map.

2. **Non-hyperbolicity** Incorporate power–law (marginal stability orbits, "intermittency" corrections into cycle expansions. Apply to long-time tails in the Hamiltonian diffusion problem.

3. **Phenomenology** Carry through a convincing analysis of a genuine experimentally extracted data set in terms of periodic orbits.

4. **Invariants** Prove that the scaling functions, or the cycles, or the spectrum of a transfer operator are the maximal set of invariants of an (physically interesting) dynamically generated non–wandering set.

5. **Field theory** Develop a periodic orbit theory of systems with many unstable degrees of freedom. Apply to (a) coupled lattices, (b) cellular automata, (c) neural networks.

6. **Tunneling** Add complex time orbits to quantum mechanical cycle expansions (WKB theory for chaotic systems).

7. **Unitarity** Evaluate corrections to the Gutzwiller semiclassical periodic orbit sums. (a) Show that the zeros (energy eigenvalues) of the appropriate Selberg products are real. (b) Find physically realistic systems for which the "semiclassical" periodic orbit expansions yield the exact quantization.

8. **Atomic spectra** Compute the helium spectrum from periodic orbit expansions (already accomplished by Wintgen and Tanner!).

9. **Symmetries** Include fermions, gauge fields into the periodic orbit theory.

10. **Quantum field theory** Develop quantum theory of systems with infinitely many classically unstable degrees of freedom. Apply to (a) quark confinement (b) early universe (c) the brain.

Conclusion

boredom
Borges, J.L.

> Good-bye. I am leaving because I am bored.
> George Saunders' dying words
>
> Nadie puede escribir un libro. Para Que un libro sea verdaderamente, Se requieren la aurora y el poniente Siglos, armas y el mar que une y separa.
> Jorge Luis Borges El Hacedor, *Ariosto y los arabes*

The buttler did it.

Index

Bunimovich!billiard—seestadium
chaology—seechaos
coding—seesymbolic dynamics
critical!point—seeequilibrium point
cycle—seeperiodic orbit
cycle point—seeperiodic point
Danish pastry—seesymbol plane
dof—seedegree of freedom
equivariant—seerelative
index!Maslov—seetopological index
Jacobian!matrix—seefundamental matrix
KS—seeKustaanheimo-Stiefel
libration orbit—seeself–retracing
logistic map—seeunimodal
Maslov index—seetopological index
Morse index—seetopological index
map!logistic—seeunimodal
eigenstate—seeeigenfunction
equilibrium!measure—seenatural measure
stability!exponent—seeFloquet exponent
stability eigenvalue—seeFloquet multiplier
Gauss!shift—seeGauss map
matrix!of variations—see“stabmat
neutral—seemarginal
ODE—seeordinary differential equations
PDE—seepartial differential equations
path integral!stochastic—seeWiener integral
pinball—see3-disk
primitive

abscissa
    absolute conv., 324
    conditional conv., 325
accelerator mode, 393
action, 468, 483, 493
    helium, 578
    relation to period, 587
admissible
    periodic points, 210
    trajectories, number of, 207
Airy
    equation, 474
    function, 474
Airy function, 474, 477, 567, 570, 575
    at a bifurcation, 477
Airy integral, 474
alphabet, 162
alternating
    binary ordering, 181
alternating binary tree, 204
analyticity
    domain, 247
anomalous diffusion, 401
Anosov flows, 195
antiharmonic extension, 668
arc, 180
area
    preserving map, 721
area preserving
    Hénon map, 84
Artin-Mazur zeta function, 217
attractor, 36
    basin, 36
    Hénon, 58
    strange, 36, 40, 150
Aubry-Mather theory, 539
autonomous flow, 39, 299
average
    space, 129
    time, 129
averages
    chaotic, 371
averaging, 29
    space, 144
    time, 142
Axiom A, 287
    systems, 281

baker's map, 96
Balmer spectrum, 456
basin of attraction, 36
BER
    approximation, 382
Bernoulli
    polynomials, 268
    shift, 268, 381
Bessel function, 558
    addition theorem, 560
bi-infinite itinerary, 178
bifurcation
    Airy function approximation, 477
    bizarre, 667
    generic, 96
    Hopf, 431
    saddle-node, 55
billiard
    map, 93
    stadium, 91
billiards, 91, 96, 796
    stability, 94, 116
binary
    prime cycles, 167
    symbolic dynamics
        collinear helium, 581
    tree, alternating, 204
binary ordering
    alternating, 181
Birkhoff
    ergodic theorem, 129
Birkhoff coordinates, 11
block
    finite sequence, 179
block, pruning, 180
Bohr
    – de Broglie picture, 456
    -Sommerfeld quantization, 456, 521, 647
    helium, 577, 588
    Uetli Schwur, 646
Bohr-Sommerfeld quantization, 474
Boltzmann
    equation, 407
Boltzmann, L, 24
boredom, 349, 621
Borges, J.L., 621

bounded operators, 735
Bourbaki, N., 54
Bowen, R., 26
brain, rat, 2, 27
branch cut, 365
  singularity, 367
Bunimovich
  billiard, *see* stadium
Burnett coefficient, 398

canonical
  transformation, 82
canonical transformation, 82
canonical transformations, 652
Cartwright M.L., 641
Cauchy criterion, 733
caustic, 487
ceiling function, 244, 287
center, 65
center manifold, 423
center of mass, 307
chain rule
  matrix, 731
change
  of coordinates, 102
chaology, *see* chaos
chaos, 5, 6
  caveats, 8
  deterministic, 25
  diagnostics, 42
  quantum, 25
  skeleton of, 11, 13
  spatiotemporal, 412
  successes, 8
character
  orthonormalitity, 713
  representation, 698
characteristic
  exponent, 64
  function, 124
  polynomial, 213
  value, 64
characteristic equation, 65
chicken heart palpitations, 5
circle map
  critical, 434
coarse-graining, 124
coding, *see* symbolic dynamics
collinear helium, 458
  symbolic dynamics, 581
combinatorics
  teaching, 172
complete
  N-ary dynamics, 163
complexity
  algorithmic, 226
confession
  C.N. Yang, 128
  Kepler, 638
  St. Augustine, 123
conjugacy, 103
  invariant, 120
  smooth, 102, 112, 120, 796
  topological, 173
connection formulas, 474
conservation
  equation, 504
  phase space volume, 83–85, 134
continuity
  equation, 134
continuity equation, 131, 485, 504, 507
contour integral, 252
contracting
  Floquet multipliers, 114
  flow, 36, 40, 70
  map, 77, 184
  stability eigenvalues, 236
contraction
  state space
    Rössler, 76
convergence
  abscissa of, 325
  mediocre, 726
  radius, 247
  super-exponential, 273, 527
convexity, 156
coordinate
  change, 102, 103, 796
  longitudinal, 495
  transformations, 112
Copenhagen School, xiv, 646
correlation
  decay
    power law, 360
  function, 284
  spectrum, 284
  time, 338
cost function, 528
covering
  symbolic dynamics, 178
creeping
  1-disk, 568
critical
  point, 116, 170, *see* equilibrium point
  value, 171, 396
cumulant
  expansion, 212, 215, 314
    Plemelj-Smithies, 739
curvature
  correction, 311

expansion, 28, 311
cycle, 11, *see* periodic orbit
expansion, 19, 311, 520
3-disk, 329
finite subshift, 319
Lyapunov exponent, 319
stability ordered, 321
fundamental, 213, 311, 724
limit, 150
Lyapunov exponent, 115
marginal stability, 61, 117
point, 179
prime, 179, 229, 238, 291
3-disk, 537
Hénon map, 530
pruning, 220
Rössler system, 292
stability, 113
Gauss map, 443
stable, 116
superstable, 116
unstable, 13
weigth, 250
cycle point, *see* periodic point
cycles
Rössler system, 305
cyclic
invariance, 292
symmetry, 210
cyclic group, 714

damped Newton's method, 295
Danish pastry, *see* symbol plane
de Broglie wavelength, 479
Debye approximation, 575
decay
rate, 257
rate of correlations, 284
degree of freedom, 8, 79, 428, 469
delta function
Dirac, 126, 463, 798, 821
density, 124, 504
evolution, 24
phase space, 134
density of states
average, 516
Green's function, 464
quantum, 464
determinant
Fredholm, 742
graph, 225
Hadamard, 247
spectral, 23, 212, 247
for flows, 249
trace relation, 212
trace-class operator, 736
deterministic
dynamics, 34
deterministic dynamics, 5
deterministic flow, 130
differential equations
ordinary
almost, 44, 791
diffraction
Green's function, 605
Keller, 613
Sommerfeld, 613
diffusion
anomalous, 401
constant, 146
equation, 505
Diffusion Limited Aggregates, 27
dihedral group, 714
dike map, 174, 185
dimension
box counting, 351
fractal, 351
generalized, 9
information, 351
intrisic, 8, 428
Dirac delta derivatives, 138
Dirac delta function, 21, 125, 126, 138, 148, 217, 238, 466, 488, 500, 505, 798, 821
Dirac path integral, 498
Dirichlet series, 324
dissipative
map, 77, 184
divergence rate
local, 153
divergence ultraviolet, 518
dof, *see* degree of freedom
doubling map, 280
Duffing
undamped, 80
Duffing oscillator, 38, 49
Duffing system, 41
dynamical
system, 33, 34
deterministic, 34
gradient, 44, 792
smooth, 34
systems
equivalent, 111
transitivity, 209
zeta function, 18, 251
Euler product rep., 251
dynamical system
infinite, 430
smooth, 19, 20, 28, 224, 641, 761, 763, 765
dynamics

deterministic, 5
hyperbolic, 165
irreversible, 37
reversible, 37
spatiotemporal, 25
stochastic, 5
symbolic, 10, 162, 178
symmetry, 712
topological, 162, 178, 179

edge, 180
eigen-direction, 61
eigenfunction
Perron-Frobenius operator, 266
energy, 461
eigenfunctions
Perron-Frobenius, 266
eigenstate, *see* eigenfunction
eigenvalue, 66, 257
Perron-Frobenius operator, 266
exponential spacing, 248
zero, 474, 492
Einstein
diffusion formula, 506
elastic
scattering, 543
elliptic
stability, 84
enemy
thy, 361
English
plain, 178
ensemble
microcanonical, 156
entire function, 266
entropy
barrier, 326
Gauss map, 452
topological, 6, 208, 222, 225
equation
of variations, 60
equilibria
Kuramoto-Sivashinsky, 419
equilibrium
measure, *see* natural measure
point, 39, 67, 128, 420, 532
Rössler system, 45, 67, 793
stability, 796
equivalence
of dynamical systems, 111
equivariant, *see* relative
ergodic
average, 129
theorem
multiplicative, 156
theory, 129
escape
intermittency, 370
rate, 13, 14, 147, 148, 269, 314, 319, 329, 335
rate, 3-disk, 318, 333
rate, vanishing, 318
rate,3-disk, 330
essential
spectral radius, 276
spectrum, 275
essential spectral radius, 285
Euler
formula, 63, 268, 810
limit, 68
product, 68, 255
product rep.
dynamical zeta function, 251
totient function, 436
Euler-MacLaurin
formula, 284
Eulerian
coordinates, 35, 61, 66
evolution
group, 44, 791
kernel
probabilistic, 130
operator, 21, 149
quantum, 463
semigroup, 150
expanding
Floquet multipliers, 114
stability eigenvalues, 236
expectation value, 144, 159
exponent
Floquet, 114
exponential
convergence, 247, 273
decay rate of correlations, 284
of a matrix, 63
exponential proliferation, 21, 226
extremal point, 470

false zeros, 255
Farey
map, 359, 382
mediant, 437
series, 435
tree, 437
Feynman path integral, 491, 498
Fick law, 505
finite subshift
cycle expansion, 319
first return function, 47
first return time, 379
fixed point, 292
maps, 58

marginally stable, 359
Floquet
exponents, 114
multiplier, metric invariants, 120
multipliers, 114
flow, 34, 37
autonomous, 39, 299
contracting, 36, 40, 70
deterministic, 130
elliptic, 115
generator of, 131, 656
Hamiltonian, 79, 721
hyperbolic, 84, 115, 257
incompressible, 70, 134
infinite-dimensional, 411–428
inverse hyperbolic, 84
linear, 62, 73
linearized, 60
nonhyperbolic, 115
spectral determinant, 249
stability, 66
stationary, 39
stochastic, 130
stretch&fold, 171
Fokker-Planck equation, 507
form
normal, 110
Fourier
mode
truncation, 414
fractal, 350
aggregates, 9
dimension, 351
geometry of nature, 9
probabilistic, 9
science, 9
Fredholm
determinant, 742
integral equations, 274
integral operator, 273
Fredholm theory, 273
Frenkel-Kontorova model, 539
frequency analysis, 42
Fresnel integral, 470, 477
function
space
piecewise constant, 239
functional, 129
Lyapunov, 36
functions
L^2 square-integrable, 285
analytic, 285
fundamental
cycle, 213
cycles, 724
domain, 168
collinear helium, 580
fundamental matrix, 15, 60, 659

Gälerkin truncation, 416
Galilean invariance, 414, 430
Gatto Nero
professor, 172
Gauss
shift, *see* Gauss map
Gauss map, 140, 382, 436, 447
cycle stability, 443
metric entropy, 452
Gaussian
integral, 138, 398, 500
integral, d-dimensional, 488, 500
noise, 773
probability density, 506
generating function, 238, 540
generating partition, 179
generator
of flow, 131, 656
golden mean
pruning, 214
gradient
system, 44, 792
gradient algorithm, 528
grammar
symbolic dynamics, 180
graph, 180
irreducible, 180
Markov, 180
Gray codes, 181
Green's function, 466
analogue of, 660
density of states, 464
diffraction, 605
energy dependent, 463
regularized, 518
scattering, 549
semiclassical, 499, 502
short distance, 496, 497
trace, 463
long orbits, 496
group, 697
cyclic, 714
dihedral, 714
dynamical, 37
evolution, 44, 791
finite, 697
integration, 713
matrix, 698
order of, 697
representation, 698
semi-, 131, 656
Gutzwiller
trace formula, 516

Gutzwiller path integral, 498

Hadamard determinant, 247
Hadamard product, 519
Hamilton
-Jacobi equation, 480
equations, 480
principal function, 483, 508
Hamiltonian, 461, 481
flow, 721
spectral determinant, 251
stability, 653
flows, stability, 81, 651
Hénon map, 84
repeller, periodic orbits, 306, 812
Hankel function, 497, 558, 575
Heaviside function, 465
Heisenberg, 647
picture, 733
Heisenberg, W, 655
Helfand moments, 398
helium, 577, 647
collinear, 46, 57, 80, 458, 598, 793
cycles, 306, 598
eigenenergies, 599
fundamental domain, 580
Poincaré section, 598
stabilities, 599
stability, 306
Helmholtz equation, 558
Hénon
attractor, 58, 130
Lyapunov exponent, 159, 802
map, 53, 55, 84, 190, 528, 542
fixed points, 58, 190
Hamiltonian, 84
inverse, 190
prime cycles, 530, 542
stability, 72, 116
symmetries, 721
transient, 530
Hénon, M., 55
heroes
unsung, xiv, xviii
Hessian matrix, 81
Hilbert
space, 462
Hilbert-Schmidt
condition, 274
operators, 735
Holmes, P., 427
Hopf
bifurcation, 431
Hopf, Ebehardt, 431
Hopf, Heinz, 595
horseshoe, 189
complete, 192
hydrodynamical
interpretation of QM, 498
hyperbolic
flow, 84, 115, 257
non-, 24
hyperbolicity assumption, 16, 237

in/out nodes, 65
inadmissible symbol sequence, 180
incommesurate, 36
incompressible flow, 70
indecomposability, 209
metric, 163
index
Maslov, *see* topological index
indifferent
stability, 61
induced map, 374
inertial manifold, 415, 427
infinite-dimensional flows, 411–428
inflection point, 432
information
dimension, 351
initial
conditions
sensitivity to, 6
point x_0, 15, 35, 60
state x_0, 15, 35
injective, 54
integrable system, 80, 101
integrated observable, 142
integration
group, 713
Runge-Kutta, 45
intermittency, 96, 279, 358
escape rate, 370
piecewise linear model, 361
resummation, 376
stability ordering, 322
invariance
cyclic, 292
Galilean, 414, 430
of flows, 117
symplectic, 81, 651
invariant
measure, 127
metric, 114, 120
topological, 113
invariant measure
Gauss map, 140
inverse
hyperbolic flow, 84
inverse iteration, 294
Hamiltonian repeller, 306, 812

involution, 714
inward/outward spirals, 65
irreducible
  graph, 180
irreversibility, 24
irreversible
  dynamics, 37
iteration, 34
  inverse, 294
    Hamiltonian repeller, 306, 812
  map, 52
itinerary, 10, 13, 162
  bi-infinite, 165, 178
  future, 172, 178
  past, 178

Jacobi, C.G.J., 73
Jacobian, 69, 125
  matrix, *see* fundamental matrix
Jonquière function, 363, 401, 407

KAM
  tori, 358
Keller
  diffraction, 613
Keller, J.B., 645
Keplerian orbit, 456
kernel
  resolving, 274
kneading
  determinant, 197
  sequence, 174, 185
  theory, 173
  value, 174, 185
kneading value
  unimodal, 185
Koopman operator, 655, 660
Kramers, 647
Krein-Friedel-Lloyd formula, 550
KS, *see* Kustaanheimo-Stiefel
Kuramoto, Y., 427
Kuramoto-Sivashinsky
  equilibria, 419, 422
  system, 417, 420, 423, 427
kurtosis, 159, 398
Kustaanheimo-Stiefel transformation, 106, 578

L^2 function space, 285
Lagrangian, 483
  coordinates, 35, 61, 66
  manifold, 484
laminar states, 358
Langevin equation, 506, 509
Laplace
  transform, 22, 132, 217, 240, 241, 246, 463, 499, 657
  transform, discrete, 211, 238, 381
Laplace, Pierre-Simon de, 4
least action principle, 536
Legendre transform, 483
Leibniz, Gottfried Wilhelm, 4
level set, 80
libration orbit, 582, *see* self–retracing
Lie algebra
  symplectic, 82
Lie group
  orthogonal, 82
lifetime, 14
limit
  cycle, 150
limit cycle
  stability, 797
linear
  flows, 62, 73
  stability, 59, 113, 420
linearized
  flow, 60
link, 180
Liouville
  equation, 134
  operator, 135
  theorem, 83–85, 134
Littlewood J.E., 641
local
  divergence rate, 153
  stability, 59, 113, 420
logistic map, *see* unimodal
longitudinal
  coordinate, 495
loop
  intersecting, 213
Lorentz gas, 358, 382
Lorenz, E.N., 55
loxodromic, 84, 653
Lozi map, 54, 55
Lyapunov exponent, 6, 70, 151
  cycle, 115
  cycle expansion, 319
  equilibrium, 420
  natural measure, 153
  numerical, 156
  numerically, 152
Lyapunov functional, 36
Lyapunov time, 6, 8, 37

$\mathcal{M}$ state space volume, 147
manifold
  stable, 188
map, 34, 47
  area preserving, 721
  contracting, 77, 184
  dike, 174, 185

dissipative, 77, 184
expanding, 164
fixed point, 58
Hénon, 53, 528, 721
Hamiltonian, 84
prime cycles, 530
Hamiltonian
Hénon, 84
iteration, 52
logistic, *see* unimodal
Lozi, 54, 55
once-folding, 190
order preserving, 173
orientation preserving, 721
orientation reversing, 721
quadratic, 54, 171
return, 11, 16, 47, 48, 190
stability, 71
stroboscopic, 796
tent, 171
unimodal, 170
marginal
stability, 16, 114, 279, 359
fixed point, 359
stability eigenvalues, 236
marginal stability
cycle, 61, 117
Markov
graph, 180
infinite, 215
partition, 398
finite, 164, 165
infinite, 198
not unique, 166
Maslov index, *see* topological index
material invariant, 504
Mather, *see* Aubry-Mather theory
matrix
exponential, 63, 658
group, 698
of variations, *see* stability matrix
stability, 60, 508
Maupertuis, P.L.M. de, 536
measure, 124
invariant, 127
natural, 128, 144
smooth, 143
mechanics
quantum, 461
statistical, 23
mediocre
convergence, 726
memory
finite, 177
metric
indecomposability, 163, 728
invariant, 114, 120
Floquet multiplier, 120
transitivity, 728
metric entropy
Gauss map, 452
microcanonical ensemble, 156
Mira, C., 55
Misiurewicz, M., 55
mixing, 6, 16, 129
Moebius inversion, 219
monodromy matrix, 71, 236, 652
Morse index, *see* topological index
multi-scattering matrix, 561
multifractals, 757
multiplicative ergodic theorem, 156
multipoint shooting method, 296

natural measure, 128, 144, 153, 282, 303
nature
geometry of, 9
Navier-Stokes equation, 411
neighborhood, 59, 120
Nero, G., 172
neutral, *see* marginal
stability, 61
Newton's method, 294
convergence, 295
damped, 295
flows, 299
optimal surface of section, 301
Newtonian dynamics, 79
node, 180
noise
Gaussian, 506, 510, 773
white, 506
non-wandering set, 36, 191
nonequilibrium, 389
nonhyperbolic
flow, 115, 117
norm, 733
normal form, 110

obscure
foundations, 646
jargon, 162
topology, 417, 422
observable, 129, 142
ODE, *see* ordinary differential equations
ODEs, 411
1-disk
creeping, 568
scattering, 559
semiclassical scattering, 565
Onsager-Machlup, 509
open systems, 13, 146

operator
evolution, 149
Hilbert-Schmidt, 735
Koopman, 655, 660
Liouville, 135
norm, 733
Perron-Frobenius, 126, 156
positive, 735
regularization, 741
resolvent, 132, 657
semigroup
bounded, 132, 657
shift, 178
trace-class, 734
orbit, 35, 52
inadmissible, 173
Keplerian, 456
periodic, 36, 179, 514, 515
returning, 513
order preserving map, 173
ordering
spatial, 172, 192
ordinary differential equations
almost, 44, 791
partial differential equations, 411
orientation
preserving map, 721
reversing map, 721
orthogonal
Lie group, 82
Oseledec multiplicative ergodic theorem, 156

palpitations, chicken heart, 5
paradise
this side of, 333
partial differential equations, 411
partition, 162, 179
generating, 179
infinite, 185, 222, 225
Markov, 164
state space, 124
partition function, 156
passive scalar, 504
past topological coordinate, 194
path integral
stochastic, *see* Wiener integral
PDE, *see* partial differential equations
PDEs, 411
period
relation to action, 587
periodic
orbit, 36, 179, 310, 514, 515
orbit condition, 291, 302, 527
orbit extraction, 291–303, 527–537
Hamiltonian repeller, 306, 812
inverse iteration, 294
multipoint shooting, 296
Newton's method, 294–295
relaxation algorithm, 528
point, 11, 21, 179
admissible, 210
count, 218
unstable, 13
periodic point, *see* cycle point
Perron-Frobenius
matrix, 208
operator, 126, 156, 266
theorem, 282, 287, 760
phase space, 34, *see* state space
3-disk, 728
density, 134
piecewise constant function, 239
piecewise linear map, 382
intermittency, 361
repeller, 147
pinball, *see* 3-disk
simulator, 99, 796
plain English, 178
Plemelj-Smithies cumulants, 739
Poincaré
invariants, 85
return map, 47, 48
cycle, 118
polynomial, 53
stability, 72
section, 11, 47, 91, 190
3-disk, 91
Hénon trick, 55
hyperplane, 48
Poincaré, H., 2, 7, 15
point
non-wandering, 36
periodic, 11, 179
scatterer, 616
wandering, 35
Poisson
bracket, 133–135, 651
resummation, 22, 377
Pollicott, M, 156, 380
polylogarithm, 363
polynomial
characteristic, 213
topological, 217
Pomeau, Y., 55
positive operators, 735
potential
problems, 44
power law
correlation decay, 360
pressure, 156

thermodynamic, 156
prime cycle, 179, 229, 238, 291
3-disk, 164, 229, 537
binary, 167
count, 219
Hénon map, 530
ternary, 168
primitive cycle, *see* prime cycle
probabilistic zeta function, 380
probability density
Gaussian, 506
profile
spatial, 35
propagator, 463
semiclassical, 487
short time, 489, 496
Van Vleck, 490
pruning, 10, 359
block, 180
front, 194
golden mean, 214
individual cycles, 220
primary interval, 175
rules, 165
symbolic dynamics, 180
pruning front
3-disk, 206
pseudocycle, 310

quadratic map, 54
quantization
Bohr-Sommerfeld, 456
semiclassical, 513
WKB, 467, 471
quantum
chaos, 459, 460, 518
evolution, 463
interference, 479
mechanics, 461
potential, 497
propagator, 463
resonances, 456
theory, old, 646
quantum chaology, *see* chaos, quantum
quasiperiodicity, 36

radius
of convergence, 247
random matrix theory, 460
recoding, 167, 180
rectangle, 192
rectification
flows, 103
maps, 109
recurrence, 36, 162
time, *see* return time
regularization, 106, 519
Green's function, 518
operator, 741
relative
solutions, 241
relaxation algorithm, 528
renormalization, 96
repeller, 13, 37, 146, 459
piecewise-linear, 147
single fixed point, 266
representation
character, 698
equivalent, 699
faithful, 699
matrix, 698
regular, 699
representative point, 34
residue
stability, 84
resolvent
kernel, 274
operator, 132, 657
resonance
Ruelle-Pollicott, 380
resonances
complex, 458
quantum, 456
Ruelle-Pollicott, 156
resummation
intermittency, 376
return map, 11, 16, 190
return time, 380
distribution, 380
returning orbit, 513
reversible
dynamics, 37
Riemann zeta function, 324, 382
Rössler system, 40, 41, 45, 49, 57, 76, 152, 161, 170, 189, 793
cycles, 292, 305
equilibria, 45, 67, 793
Roux
Henri, 24, 70
Ruelle
-Pollicott resonances, 156, 380
zeta function, *see* dynamical zeta function
Ruelle, D, 156, 380
Ruelle, D., 26
Runge-Kutta integration, 45
running orbits
Lorentz gas, 393
Rutherford, 577
Rydberg series, 588

saddle, 65

saddle point, *see* stationary phase
saddle-node
  bifurcation, 55
scattering
  3-dimensional spheres, 97
  elastic, 543
  Green's function, 549
  matrix, 544
  phase shift, 551
  point, 616
Schrödinger
  equation, 461
    time independent, 461
  picture, 733
Schrödinger, E, 655
section
  Poincaré, 11, 47, 91
self-retracing cycle, 582
self-similar, 21
semiclassical
  approximation, 480
  Green's function, 499, 502
  propagator, 487
  quantization, 513
  spectral determinant
    collinear helium, 590
  wave function, 486
  semiclassical zeta function, 519
semiclassical resonances
  3-disk, 786
semigroup, 131, 656
  dynamical, 37
  evolution, 150
  operator, 132, 657
Sensitivity
  initial conditions, 32, 789
sensitivity to initial conditions, 6, 150
set
  non-wandering, 191
shadowing, 19, 223
  3-disk, 318
shift, 178
  Bernoulli, 268, 381
  finite type, 180
  full, 178
  map, 432
  operator, 178
  sub-, 179
Sinai, Ya., 26
Sinai-Bowen-Ruelle measure, *see* natural measure
single fixed point
  repeller, 266
  spectral determinant, 267
singular value decomposition, 66
singularity
  branch cut, 367
Sivashinsky, G.I., 427
skeleton of chaos, 11, 13
Smale
  wild idea, 249, 258
Smale, S., 9, 26, 187, 197, 226, 259, 641
S-matrix, 544
smooth
  conjugacy, 102, 112, 120, 796
  dynamical system, 430
  dynamics, 19, 20, 28, 34, 224, 641, 761, 763, 765
    approximated, 723
    Spectral determinant, 287
  interaction, 767
  measure, 143
  potential, 97
Sommerfeld
  diffraction, 613
space
  analytic functions, 285
  average, 129
  averaging, 144
  density functions, 239
spatial
  profile, 35
spatiotemporal chaos, 412
spatiotemporal dynamics, 25
spectral
  determinant, 23, 212, 247
    1-d maps, 250
    2-d hyperbolic Hamiltonian flow, 251
    entire, 248, 272
    for flows, 249
    infinite product rep., 249
    single fixed point, 267
    weighted, 256
  spectral determinant
    1-dof, 521
    2-dof, 522
  radius, 267, 276
    essential, 285
  staircase, 464
spectral stability, 401
spectrum
  Balmer, 456
specular reflection, 91
SRB measure, *see* natural measure
St. Augustine, 123
stability
  billiards, 94, 116
  eigenvalue, 64
  eigenvalues, 236
  elliptic, 237

exact, 122, 796
exponent, 83, *see* Floquet exponent
flow, 66
Hamiltonian flow, 653
Hamiltonian flows, 81, 651
indifferent, 61
linear, 59, 113, 420
maps, 71
matrix, 60, 508
multiplier, *see* stability eigenvalue
neutral, 61, *see* marginal
ordering
cycle expansions, 321
intermittent flows, 322
Poincaré map cycle, 118
Poincaré return map, 72
residue, 84
spectral, 401
structural, 192, 195, 224, 401
window, 115
stability eigenvalue, *see* Floquet multiplier
stable
cycle, 116
manifold, 16, 188, 190
flow, 188
map, 188
stadium billiard, 91
stagnation point, *see* equilibrium point
staircase
mean eigenvalue density, 590
spectral, 464
standard map, 358
standing orbit
Lorentz gas, 393
state, 162, 180
set, 162
state space, 34
partition, 124
volume $\mathcal{M}$, 147
stationary
flow, 39
phase approximation, 470, 477, 490, 500, 514, 605, 616, 826, 827
point, *see* equilibrium point
state, 127
statistical mechanics, 23
steady state, *see* equilibrium point
Sterling formula, 477
stochastic
path integral, *see* Wiener integral
stochastic dynamics, 5
stochastic flow, 130
Stokes theorem, 85, 484
stosszahlansatz, 24, 407
strange
attractor, 36, 40
strange attractor, 150
stretch & fold dynamics, 53
stretch&fold flow, 171
strobe method, 47
stroboscopic map, 796
strongly connected graph, 180
structural stability, 192, 195, 224, 401
subshift, 179
finite type, 165, 180, 195
super-exponential
convergence, 527
super-stable fixed point, 527
superstable cycle, 116
surface of section
optimal, 301
surjective, 54
survival probability, 14, *see* escape rate
symbol
sequence
inadmissible, 180
square, 192
symbol square, 192, 193
symbolic
dynamics
at a bifurcation, 97
complete N-ary, 163
covering, 178
symbolic dynamics, 10, 162, 178
3-disk, 32, 164, 184, 802
binary
collinear helium, 581
coding, 180
Markov graph, 319
complete, 171, 192
grammar, 180
pruned, 180
recoding, 167, 180
unimodal, 172
symmetry
3-disk, 168
cyclic, 210
discrete, 166
dynamical system, 712
Hénon map, 721
symplectic
form, 81
group $Sp(2D)$, 652
Hénon map, 84
integrator, 659
invariance, 81, 651
Lie algebra, 82
map, 82
transformation, 82, 134, 197
systems

open, 146

tangent
bundle, 38, 60
space, 60
Tauberian theorem, 382
teaching
combinatorics, 172
template, 294
ternary
prime cycles, 168
tessalation
smooth dynamics, 723
thermodynamical
pressure, 156
3-body problem, 104, 458, 577, 638, 648
3-dimensional sphere
scattering, 97
3-disk
convergence, 278, 723
cycle
analytically, 122
count, 679
expansion, 329
escape rate, 160, 318, 330, 333
fractal dimension, 350
geometry, 91
hyperbolicity, 237
phase space, 728
pinball, 4, 93, 96, 97
point scatterer, 616
prime cycles, 17, 164, 229, 537
pruning front, 206
semiclassical resonances, 786
shadowing, 318
simulator, 99, 100
state space, 13, 350
symbolic dynamics, 11, 32, 164, 184, 802
symmetry, 168
transition matrix, 163
time
arrow of, 24
as parametrization, 102
average, 129, 152
averaging, 142
ceiling function, *see* ceiling function
ordered integration, 68, 74
time delay
Wigner, 551
topological
conjugacy, 173
dynamics, 162, 178–180
entropy, 6, 208, 222
future coordinate, 173
index, 487
invariant, 113
parameter, 175
polynomial, 217
trace formula, 211
transitivity, 209
zeta function, 217
topological index, 516, 647
torus, 36
totient function, 436
t_p
cycle weight, 250
trace
-class operators, 562
formula
classical, 22
flows, 240
Gutzwiller, 516
maps, 238, 267
topological, 211, 217
local, 210
trace-class operator, 734
determinant, 736
trajectory, 35, 63
discrete, 52
transfer
matrix, 127, 148
transfer operator, 258
spectrum, 248
transformation
canonical, 197
coordinate, 112
symplectic, 197
transient, 36, 163, 197
transition matrix, 163, 208, 210
3-disk, 163
transversality
condition, 48
transverse
stability, 496
Trotter product formula, 733
truncation
Gälerkin, 416
truncations
Fourier, 414
turbulence, 7, 8, 428
problem of, 411

Ulam map, 305
ultraviolet divergence, 518
unimodal
kneading value, 185
well ordered symbols, 185
unimodal map, 170
symbolic dynamics, 172
unstable

cycle, 13, 116
manifold, 16, 188, 190
map, 188
manifold, flow, 188
periodic point, 13
unsung
heroes, xiv, xviii
UPO (Unstable Periodic Orbit), *see* periodic orbit

van Kampen, N. G., 509
Van Vleck
propagator, 490
variational principle, 509
vector field, 38
vector fields
singularities, 103
vertex, 180
visitation frequency, 128
visitation sequence, *see* itinerary
volume preservation, 95
von Neumann
ergodicity, 660

wandering point, 35
wave function
semiclassical, 486
WKB, 487
weight
multiplicative, 29
well ordered symbols
unimodal, 185
Wentzel-Kramers-Brillouin, 467, *see* WKB
Wentzel-Kramers-Brillouin, 480
Weyl rule, 516
white noise, 506
Wiener integral, 509
Wigner delay time, 551
winding number, 432, 434
WKB, 480
connection formulas, 474
quantization, 467, 471
wave function, 487

Yang, C.N., 128
Young, L.-S., 55

zero eigenvalue, 474, 492
zeros
false, 255
zeta function
Artin-Mazur, 217
dynamical, 18, 251
probabilistic , 380
Ruelle, *see* dynamical
topological, 217

⇓PRIVATE

List of words

List of word used in DasBuch, derived from .glimpse_index, generated by

glimpseindex -S book/chapter/*tex book/Problems/*tex

The purpose of this list is to aid us in composing the index (and to catch a few misspellings here and there).

- abelian abscissa accelerated acceleration accelerator action adiabatic adjacency adjoint admissibility admissible advection alfalfa algebraic algorithmic algorithm alternating analytical angular. anharmonic anisotropic anomalous anosov antiharmonic antisymmetry anulus aperiodic appelation appelations appellation approximant approximants approximate approximation araki aristotle assignement assignements assignment asymmetric asymptotic asymptotics atomic attracting attractor autocorrelation automata automaton autonomous auxiliary auxilliary averaged average averages averaging averging
- backscatter ballistic balmer banach barrier basin bethe bilinear billards billiards binomial birkhoff block boson boundary bounded bourbaki bracket braids brain brains branchpoint breakdown bunimovich
- calculator cantor capacity carlsberg casimir ceiling celestial cellular chain chaology chaotic chaoticity characteristic characters chebyshev circle circulant circular classification class closure clouds cluster coarse coefficient coexisting collective colliding collinear collision combinatorial commensurate commutative commutator compact compactification competition complementary complete complexity complex compound computable computational concatenation concave conditional conductance cone configuration confinement conformal confussion conjecture conjugacy conjugating conservation conservative constrained constraint contour contracting control convergence convergent convexity convince cooperative copenhagen correlation correspondence couette coulomb countable counterterm coupled coupling covering creeping criterion critical cumulant curvature cutoff cycle cyclic cycling
- dada daughter decay decoding decoherence decomposition decouple defocusing degenerate dense density derivaties desymmetrization determinant determinism deterministic devil diagmanetic diagonalization diagram dicontinuous dictionary diffeomorphism differentiable diffraction diffusion dimension diophantine dipheomorphisms dipole dirac directed dirichlet discontinuous discovery discrete discretization dissociation disorder dispersing dissipation dissipative distance distinct distribution divergence divisibility dogma dominant doubling droplet dropolet dual duality duffing dylan dynamical dynamic dynamo

- eavesdropping egypt ehrenfest eigenbasis eigencondition eigendirection eigenenergy eigenequation eigenfunction eigenschaften eigensolution eigenspace eigenspectrum eigenstate eigenvalue eigenvector eignfunctions elastic elasticity electromagnetism electron ellipse elliptic embedding encoding endomorphism endpoint energy ensemble enthalpy entropy enumeration equilibrium equipartition equivalence ergodic ergodicity escape estimate euclidean eurostar evaluation evolution exceptional excitable exercises exhaustive existence expanding expansion expectation experimental experimentation experiments exponential exponent extended extensive extraction extrapolation extremal extremization
- factorial factorization factor farey feigenbaum fermat fermi fermion ferromagnetic feynman fibonacci field fingerprint fingertip finite finnish firmament fisher flame flow fluctuation fluid focusing folding foliation forced formalism forward fourier fractal fraction fractional fredholm freedom frequency fresnel friction frictionless frobenius front functional function functor fundamental
- gap gas gaussian gauss generalized generating generator generic geodesic geometrical geometry geophysical ghost gibbs global gluing god goe golden good gosts gradient graining grammar grandfather grandmother graph gravity grazing Green's greatest grothendick grothendieck group gutzwiller gymnastics
- hamiltonian hamlet hankel hannay hard harmonic harmonize hausdorff heaviside heisenberg helium henkel henon hermitian hermiticity hexagonal hierarchical hilbert historical homework homoclinic homogeneity homogeneous horizontal horocycle horseshoe human huygens hydrodynamics hydrogen hyperbolic hyperbolicity hyperion hyperplane hypersurface hypothesis
- ideal identity impact implicitly inadmissible incident incommunicable incomplete incompressible incremental indecomposable independence indeterminacy indifferent induced inducing inequality inequivalent inertial infinite infinitesimal infinity information ingredient ingredients inital innumerably instability instantaneous instanton integer integrability integral integration integrator intelligence interacting interfacial interference intermittency intermittent interpretation intersection interval intineraries intrinsic invalidating invariance invariant inverse inverted invertible ionization irrational irreducible irregular irrelevant irreversibility isolated isomorphic isotopy isotropic iterated iteration itinerary
- jacobian jacobi jonqui julia junction justification
- keller kepler keplerian kernel kierkegaard kinematic kinematics kinetic kink kneading knot kolmogorov krein kronecker kubo kuramoto kurtosis kustaanheimo
- label labo ladder lagrange lagrangian laminar landau langevin language laplace laplacian laser lattice lebesgue legendre leibniz length level lexical libration lifetim lifshitz light limbo limit linearity linearization linearizing linear linked liouville liouvillian literature localized local location locking logarithmic logistic longitudinal loop lorentz lorentzian lorenz lorenzian love loxodromic lozi lunar lyapunov

- macroscopic madelung magnetic magnetization magnification magnitude mandelbrot manifesto manifold mapping map marginal markov markovian maslov material mathematical mathematics matrix maupertuis maximal maximizing maxwell may mean measurable measurement measure mechanical mechanics mediant melancholy memory meromorphic mesoscopic method metric microcanonical microscopic microstate microwave minima minimal minimization minkowski miracle mirror misatributed misiurewicz mixing mixmaster model modeling modes modulus moebius molecular moment moments momentum monodromy monotone monotonicity moon morphism morse multidimensional multilinear multimodal multinomial multiplicative multiplicity multiplier multipoint

- naive natural nature necessary neigborhood neural neuronal neurosciences neuroscientist neutral newton newtonian nightmare nitpicking nodal node noise noiseless nonabelian noncanonical noncommuting nonequilibrium nonexponential nongeneric nonhyperbolic nonhyperbolicities nonhyperbolicity noninteger nonintegrable noninteracting noninvertible nonleading nonlinear nonmixing nonmonotone nonnegative nonoverlapping nonperturbative nonpositive nonscience nonselfadjoint nonseparable nonuniform nonuniqueness nonvanishing nonwandering normal normalizable normalization notation nuclear nucleus number numerical

- observable operatorial operator optical optimal orbital orbit ordering orientation origin ornestein orthogonal orthohelium orthonormal oscillating oscillator oscillatory overcounting overlapping overlayed overline

- pairing parabola parabolic paradigm paradox parahelium parallel parameter parametri parametric parametrized parititions parrique parrot partial particle particuli partilas partion partition partitons partner pascal passive past pastry path pattern pauli pendulum perceive percourse peregrination perfect perfro perhaphs peridoic periodcyc period periodic periodize permutation perpendicular perplexity persistent perturbation perturbative phase phasespace phenomenological philosophical photon physical physics physicsts piecewise pinbangles pinb pinoballo pitchfork plague planar planck plane planet planetary plausability plemelj plot poincare poincar pointlike point pointwise poison poisson polar polarization pole polygonal polynomial polynominal polytope position positive positivity postmodern potential powerlaw practise predicble predragese preexponential prefactor prepending preperiodic prerequisite prerequsites presentation preservation preserving pressue pressure primary prime primitive primo principal principle probabalistic probability process product program prohibited projectile projection projector proliferation promises proof propability propagation propagator proper prophet proportionality propreties pruning prunning pseudocycle pseudoorbit pseudos pseudospectral pseudosphere pseudow psudosphere ptolemy publised pump

- quadrant quadratic qualitative quantitative quantitive quantization quantizing quantum quantummechanics quark quarter quartic quasiclassical quasilinear quasiperiodic quientessentially quintessential quntum

- radial radical radii radius radons random randomization randomness rank rate rational rationals reactants reagents real reali realign realistic reality realizable realization realizing recoding recognition rectangle rectification recurrence recurrent recursion recursione recursive recycling redholm reducible reducing reduction redundant refine refinement refining reflecting reflection refraction region regular regularization reinjection relabeling relation relativi relativistic relavant relaxation relevant remeber renark renomarmalization renormalization renyi reparametrization repeated repeler repeller repelling repellor repertoire repetition representation representative reproducible repulsive rerens rescaling residue1 residue resistence resolution resolvent resolvop resonance response restor restricted resummation resurgence retification retracing return reversability reversibility reversible reversing revolution rieman riemann riemman rigorous rigourous rmark rmemebr robust roessler rossler rotational rotation route ruelle rule ruling runge

- saddle saddlepoint sanscrit sanskrit sawtooth saysthis scalar scale scaling scar scatterer scattering scenario schedlbauer schrodinger schroedinger scruffy search secretification section secular segment semicircle semiclasscial semiclassical semiclassics semigroup semiline sensitive separable separating sequence serapinski series shaded shading shadowing shadowning shakespeare shannon shear sheet shift sivashinsky shock shrinking siegel signal signifcant sign similarity simlar simpel simple simplicial simplified simulation simultaneous sina sinai singel single singlet singular singularity sink sistem sisters situating sivashinsky sixfold skarowsky skeleton skew slow Smale snell solar soliton solvable Sommerfeld sorrow sorting sould source space spatial spatiotemporal specchio speccolo spectral spectroscopy spectrum specular speed sphere spherical spiegel spike spin spiral spliting splitting square stabilit stability stab stacionarity stackr stadium stagnation staircase standard standart standing star start starting state static stationarity stationary statistical statistics steady sticking sticky stirling stirring stochastic stochasticity stokes stosszahlansatz straddle stradle straight strand strange stranges stream strength stress stretch strict string strip strobe strogatz stroke strong structural structure student subcritical subdeterminant subdivide subexponential subgroup subholes subinterval subleading submatrix subsequence subset subseteq subshift subspace subspectrum substitution substring substrips subsystem subtree sufficient summable sum supercritical superposition superstable suppore support suppression supress supression supset surreal survival suspension symbol symbolic symetrization symmetric symmetrization symmetr symmetry symplectic system

- takens tangency taylor technique tedious template temporal tensor tensoriels tent terminant terministes ternary tessellate tessellation test thare theorem theory therma thermodynamic thermodynamical thermostats threshold tiling time tool topolagical topological topologiques topology toral tori torus trace tracks trajectory transcendental transfer transfomation transform transformation transfrom transitional transition transitive transitivity transport transpose transversality transversal transverse trapped trapping trashendental traversal tree trellises treshold